UNIVERSITY OF SOUTHAMPTON

Faculty of Physical Sciences and Engineering

School of Electronics and Computer Science

Dielectric Behaviour of Silicon Nitride Epoxy Nanocomposites

by

Fuad N. F. Alhabill

Thesis for the degree of Doctor of Philosophy

August 2017

UNIVERSITY OF SOUTHAMPTON

ABSTRACT

FACULTY OF PHYSICAL SCIENCES & ENGINEERING

Electrical Engineering

Thesis for the degree of Doctor of Philosophy

DIELECTRIC BEHAVIOUR OF SILICON NITRIDE EPOXY NANOCOMPOSITES

by Fuad N. F. Alhabill

Nanodielectric materials have potential to meet the requirements of next generation insulation technology by offering attractive electrical, mechanical and/or thermal properties. A precise understanding of the factors and mechanisms that control the properties of nanocomposites could enable the tailoring and engineering of these composites to meet the requirements of a particular application. The surface chemistry of nanoparticles and their interactions with the base material are very important factors, among others, such as moisture adsorption and particle dispersion, which affect the electrical performance of nanodielectrics. This study examines factors that affect the electrical behaviour of silicon nitride/epoxy nanocomposites. First, a critical review of the models that have been proposed in the literature to describe the electrical behaviour of nanocomposites was conducted. Based on this review, a new model, namely the particle interphase model, was devised. The main proposition of this model is that nanoparticles contain a high concentration of defects close to their surfaces, which could be due to foreign atoms, surface geometrical irregularities or coordinative unsaturation, and these defects can perturb the electronic states in the outer layer of the particles which, consequently, may have a critical impact on the electrical behaviour of the bulk material. Therefore, unlike the existing models, which broadly are based on the proposition of a polymeric interphase layer around the nanoparticles, this model proposed the presence of a thin interphase layer inside the boundaries of the particles themselves that, from an electrical perspective, might have a more profound impact on the performance of nanodielectrics.

The experimental investigation started by characterising the surface chemistry of the nanofiller, where it was identified that the silicon nitride nanoparticles are covered with amine groups on their surface. Since these surface amine groups are the same as the amine groups in the hardener, this led to that these surface groups can react with the resin's epoxy groups and, thus, affect the resin/hardener stoichiometry. Consequently, the influence of the nanofiller on the epoxy matrix might be related to a commensurate change in the matrix stoichiometry, rather than being directly associated with the presence of the nanofiller. To

investigate this hypothesis, the effect of changing the resin/hardener stoichiometry was studied.

By changing the ratio of resin to hardener, a better understanding of the electrical behaviour and its relationship with the structure, dynamics and chemistry of the considered epoxy networks was achieved. Detailed electrical characterization showed that, in the glassy state, electrical properties of the studied epoxy networks are sensitive to the network's chemical content, rather than to variations in the network's structure or dynamics. Using formulations that contain an excess of hardener has a detrimental impact on DC conductivity, DC breakdown strength and water uptake of the resulting networks, whereas, decreasing the hardener content leads to enhancements in these properties. Conversely, AC breakdown results indicated that this parameter does not vary on changing the stoichiometry, which suggests that the AC and DC breakdown strengths are controlled by different mechanisms. A tentative explanation for the AC breakdown behaviour is suggested.

For silicon nitride filled systems, based on differential scanning calorimetry results, it was estimated that the inclusion of 2 wt% and 5 wt% of the silicon nitride nanofiller displaces the resin/hardener stoichiometry by ~6.5 % and ~18 %, respectively. This finding was further corroborated by dielectric spectroscopy and water absorption results. Therefore, this study renders conclusive evidence that nanofillers can directly and significantly affect the curing process of an epoxy network and, thus, this parameter should always be considered when introducing nanofillers into thermosetting matrices. Such a finding implies the presence of covalent bonding between the nanoparticles and the surrounding polymer and, therefore, offered an opportunity to question what is usually conjectured in literature that strong filler/polymer interactions can affect or confine the molecular dynamics of the polymer layer around the particles and also lead to better particle dispersion. The results indicate that while this chemical bonding leads to good nanoparticle dispersion, it does not have an appreciable influence on the segmental dynamics of the polymer. According to the uncertainties of the experimental technique used here, any affected polymeric layer around the particles should not have a thickness greater than 0.8 nm.

While the nanofiller stoichiometric effect explains many aspects of the electrical behaviour of the considered nanocomposites, it cannot account alone for the whole picture. The obtained data indicate the presence of additional effect that superimposes on the filler stoichiometric effect in influencing the electrical behaviour. Modifying the particle surface chemistry, via heat treatment at 1050 ^{o}C, showed that this additional effect is related to the particle interphase characteristics. The results demonstrate the crucial impact of the particle interphase and thus provide experimental credence to the proposed model.

Table of Contents

List of Tables

List of Figures

List of Abbreviations and Symbols

Abbreviations

AC	Alternating current
ASTM	American Society for Testing and Materials
DC	Direct current
DGEBA	Diglycidylether of bisphenol
DSC	Differential scanning calorimetry
FTIR	Fourier transform infrared
hBN	Hexagonal boron nitride
IR	Infrared
OH	Hydroxyl group
RH	Relative humidity
SEM	Scanning electron microscopy
Si_3N_4	Silicon nitride
SiN	Dried silicon nitride
SiN-C	Calcinated silicon nitride
SiO_2	Silicon dioxide
SiO-C	Calcinated silicon dioxide
vol%	Volume percentage
wt%	Weight percentage

Symbols

ϵ_r'	Real part of the relative permittivity
ϵ_r''	Imaginary part of the relative permittivity
ϵ_r^*	Complex relative permittivity
ΔC_p	Increase in the heat capacity over the glass transition
ΔT_g	Glass transition width
HP	Hardener percentage
HP_{eff}	Effective hardener percentage
M_c	Average molecular mass between crosslinks

T_g	Glass transition temperature
T_m	Melting temperature
α	Weibull scale parameter
β	Weibull shape parameter
τ	Dielectric relaxation time

Declaration of Authorship

I, Fuad N. F. Alhabill, declare that this thesis and the work presented in it are my own and has been generated by me as the result of my own original research.

Dielectric Behaviour of Silicon Nitride Epoxy Nanocomposites

I confirm that:

1. This work was done wholly or mainly while in candidature for a research degree at this University;
2. Where any part of this thesis has previously been submitted for a degree or any other qualification at this University or any other institution, this has been clearly stated;
3. Where I have consulted the published work of others, this is always clearly attributed;
4. Where I have quoted from the work of others, the source is always given. With the exception of such quotations, this thesis is entirely my own work;
5. I have acknowledged all main sources of help;
6. Where the thesis is based on work done by myself jointly with others, I have made clear exactly what was done by others and what I have contributed myself;
7. [Delete as appropriate] None of this work has been published before submission [or] Parts of this work have been published as: [please list references below]:

Signed: .....

Date: .....

Acknowledgements

I would like to express my deep gratitude to my supervisors, Dr Thomas Andritsch and Professor Alun S. Vaughan, for their continuous guidance, motivation, patience and invaluable discussions. I would like also to extent my gratitude to the internal examiners of the project over its different stages, Professor Neil White, Professor Gorge Chen and Professor Paul Lewin, who provided many helpful suggestions.

I am grateful to many of the members of the Tony Davies High Voltage Laboratory for their useful discussions over the years. Especially, I express my gratitude to Dr Suvi Virtanen and Dr Matt Praeger for their insightful ideas and also their training on many lab instruments. I am also grateful to Mr Nick White from the Optoelectronics Research Centre for his kind cooperation.

I am also indebted to many of my friends and colleagues in the University of Southampton, in particular to Dr Abdelrahman Attili, Dr Raed Ayoob, Mr Yan Wang, Mr Dayuan Qiang, Mr Omar Atiyeh and Mr Marios Theodosiou, for their constant help and support throughout my postgraduate studies.

I am very grateful to my family particularly, my honourable parents (Mr Nahid and Mrs Khitam) as no words can describe my gratitude to them for all what they have done for me since I was a little child. I would like to deeply thank my wife (Mrs Khadija) for her encouragement and patience and I want to share her any success, as she was always sharing with me all moments and challenges during my PhD journey. Additionally, I would like to thank my two daughters (Nour and Jana) for their love and to apologies for not spending with them the time they deserve during the last few years.

To the memory of my grandfather,

Mr Fuad bin Mohammed Alhabill,

may Allah be pleased with him, forgive and have mercy upon him,
and admit him into the Paradise.

Chapter 1

Introduction

1.1 Nanodielectrics: emergence and prospective

The utilization of nanotechnology for dielectric applications started relatively late compared with its applications in other arenas. In 1994, the potential of introducing nanoparticles into a dielectric material for electrical insulation applications were theoretically highlighted by Lewis [1]. However, nanodielectrics did not draw a lot of attention until 2002 when Nelson *et al.* had experimentally demonstrated some advantages for nanofilled materials over microfilled counterparts, such as reducing the space charge accumulation [2]. Since then, research interest in the nanodielectrics area has grown immensely. Many research groups worldwide have been conducting a great deal of research exploring the potential of the nanodielectrics and investigating the underlying mechanisms that control the behaviour of these material systems. However, a critical understanding of these mechanisms has not been achieved yet. Many of the proposed ideas and principles are still uncertain and they just qualitatively describe nanodielectrics.

While many published papers have reported some significant improvements in the dielectric properties that can be brought about through the incorporation of nanoparticles into a polymeric matrix, others have reported the opposite. This discrepancy in the reported results may reflect a lack of clear systematic methodology for, first, characterising the basic materials (the filler and the host polymer), second, processing these materials and producing the nanocomposites and, third, evaluating the electrical properties of the produced nanocomposites. As an example, nanofiller processing before and during the preparation of a nanocomposite may include exposure to humid environment or heat, which can change their water content [3, 4] or surface chemistry [5] and, consequently, the electrical properties of the produced nanocomposites. Therefore, a revision to the current approach, which is followed for designing and analysing the performance of nanodielectrics, may be needed. Since dielectric performance is concerned with the kinetics of small entities such as electrons, the prospective approach may need to consider the material characteristics at an electronic level; a level that may be neglected when designing and charactering nanocomposite systems for other applications, e.g. for mechanical applications.

1.2 Research motivation

The reliable production of electrical energy without causing adverse environmental consequences is of major global concern, since energy consumption is generally increasing and areas such as transport, which were previously the domain of fossil fuels, become increasingly electrified. This necessitates higher electric power transmission and distribution capacities, and consequently makes the need to improve insulation materials inevitable. Nanodielectric materials have the potential to meet the requirements of next generation of insulation technology, by offering attractive electrical, mechanical and/or thermal properties. A precise understanding of the physics and chemistry of the nanocomposites could enable tailoring and engineering these materials to meet the requirements of particular applications. The commercial impact of even incremental improvement in dielectric properties of insulation materials is potentially very large, since the quantity of electrical insulation in use is vast.

1.3 Objectives

It is widely accepted that the performance of nanodielectrics mainly depends on the interactions between the nanofiller and the matrix materials. These interactions rely on the surface chemistry of the nanofiller and the chemistry of the matrix. Other factors such as particle dispersion and water uptake, which can significantly affect the electrical performance of nanodielectrics, are also related to the surface chemistry of the nanoparticles. Additionally, the incorporation of the particles may alter the structure of the host polymeric matrix and, thus, influence the properties of the material that evolves. Each of the above factors should be investigated in order to determine the key factors that control the electrical behaviour of a specific nanocomposite. This study sets out to examine the key characteristics of a silicon nitride (filler) and an epoxy (matrix) which affect the electrical behaviour of silicon nitride/epoxy nanocomposites.

Epoxy resin is a technologically important thermosetting polymer used in a wide variety of applications. For electrical applications, it is used as an insulating dielectric in different applications including large power generators, switchgear, cast resin transformers, cable terminations and bushings. For nanodielectrics, the liquid state of the uncured epoxy resin is often considered as an advantage, since it allows better particle dispersion and also enables the particles effectively to interact with the reactive resin and hardener. Interestingly, the surface chemistry of silicon nitride is characterised by the existence of amine groups [7, 8] which, in principle, can chemically react with the epoxy groups in the resin. This makes silicon nitride inherently compatible with the matrix polymer, which should result in good particle dispersion and, therefore, minimize the effect of particle agglomeration. However, chemical reactions may influence the effective resin/hardener stoichiometry and consequently the structure of the epoxy network. Therefore, this study

will first investigate the impact of filler/matrix interactions on particle dispersion and resin/hardener stoichiometry in silicon nitride/epoxy nanocomposites. After that, the study will explore the consequences of these interactions and the potential chemical bonding between the filler and the polymer for molecular dynamics and electrical properties of the generated Si_3N_4/epoxy nanocomposites.

1.4 Thesis outline

Chapter 2 introduces the concept of a nanocomposite and critically reviews some of the models that have been proposed to describe the characteristics of the interphase region and to highlight the interactions that may occur in this region. Based on this review, a new model (particle interphase model) is proposed and then some of the already published experimental results are analysed in accordance with this hypothesised model. The main features of the epoxy resin and its curing process are detailed. The chapter then presents the nanofiller characteristics, which may affect the final performance of nanocomposites. Two nanofiller types, silicon nitride and silica, are mainly detailed. A literature review of epoxy-based nanocomposites is also included in the chapter.

Chapter 3 describes the techniques that are used to characterise and evaluate the performance of nanocomposites. The experimental settings for each technique are also covered.

Chapter 4 contains FTIR characterisation of the surface chemistry of the silicon nitride nanoparticles. The effect of heat treatment on water absorption and surface chemistry of the nanofiller is then investigated. The chapter then presents the preparation procedure used to prepare both the neat epoxy samples and the Si_3N_4 filled samples. The processing of the produced materials is also included.

Chapter 5 investigates the effect of changing resin/hardener stoichiometry on the electrical behaviour of the unfilled host matrix. By analysing the results, possible mechanisms that control the dielectric spectra, DC conductivity, DC breakdown strength, AC breakdown strength and water uptake of the matrix are proposed. The impact of water absorption on the electrical properties is also studied. In addition to characterising the electrical behaviour of the base matrix, this chapter provides a background for studying the effect of nanofillers on the network's resin/hardener stoichiometry.

Chapter 6 concentrates on studying the effect of adding silicon nitride nanofiller (and its consequent interactions with the epoxy matrix) on the resin/hardener stoichiometry, network structure and dynamics and particle dispersion. The results are analysed in the light of the data provided in chapter 5 and conclusions about the nanofiller effects are derived. The chapter then investigates the consequences of the nanofiller and its interactions with the matrix for the considered electrical properties. Water absorption is

used to probe any changes that may occur in the surface chemistry of the nanofiller inside the epoxy matrix. The impact of water inclusion on the considered electrical properties is then explored and the filled and unfilled samples are compared.

Chapter 7 focuses on the impact of modifying the particle interphase, via heat treatment, on the electrical properties of Si_3N_4/epoxy nanocomposites.

Chapter 8 summarises the main conclusions and includes suggestions for further research.

Chapter 2

Literature Review

2.1 Nanocomposites concept

A nanocomposite is composed from two materials, the base material and the filler material, where the filler has at least one dimension that falls within the nanoscale. In the dielectrics area, the base material is normally a polymer and these polymeric nanocomposites are often termed nanodielectrics. The nanophase filler may have three nanometric dimensions (nanoparticles), two nanometric dimensions (fibres), or one nanometric dimension (platelets) [6]. As the dimensions reach the nanoscale, they approach the atomic scale where the number of the atoms forming such dimensions comes to be relatively countable and hence the bulk properties gradually start to dilute or disappear [7]. For example, the electronic band structure, which consists of bands of energy states separated by band gaps, begins to convert into discrete energy levels when the particle size is less than 10 nm [7]. This may change the colour of materials with band gap energy that is comparable to the photon energy of visible light [7]. Other properties may behave in a similar way and become size-dependent [8, 9]. Even for larger dimensions, the outer layer atoms near the surface behave in a similar fashion. In fact, the classical macroscopic properties for a point in the bulk of a material are obtained by integrating over infinite (in an atomic scale) volumes around this point [10]. For example, point 1 in Figure 2.1 would give the macroscopic properties of the bulk of phase A if the dimensions of the particle A are considered atomically infinite. On the other hand, point 2 on the surface, in Figure 2.1, has a non-centro-symmetric nature and its properties will be affected by the existence of other atoms from phase B. Similarly, atoms located a few layers under the surface, i.e. point 3 in Figure 2.1, will be affected by the presence of phase B. The same thing is applicable to points 4 and 5 in phase B. The properties at these points are different from the properties of the bulk of both A and B and this region is what is meant by the terms interphase region or interaction zone. The thickness of the interphase depends on the property being considered and at what point the “infinite limit” is reached. In its turn, the infinite limit depends on the material molecules size or molecules mass. If phase A in Figure 2.1 represents the nanoparticle, which usually has small molecules, and phase B represents the polymer matrix, which has long molecules, then it is expected that the interphase extends into the phase A less than into the phase B. Thus, although the interphase is depicted in Figure 2.1 to extends in phase A and phase B similarly, the interphase inside the particle’s boundary (phase A) is expected to be less than the interphase in the surrounding polymer

(phase B). In this study, the interphase inside the particle is identified as the “the particle interphase” and the interphase in polymer matrix is called “the polymer interphase”. Additionally, the boundary surface between the particle and the matrix is called “the interface”.

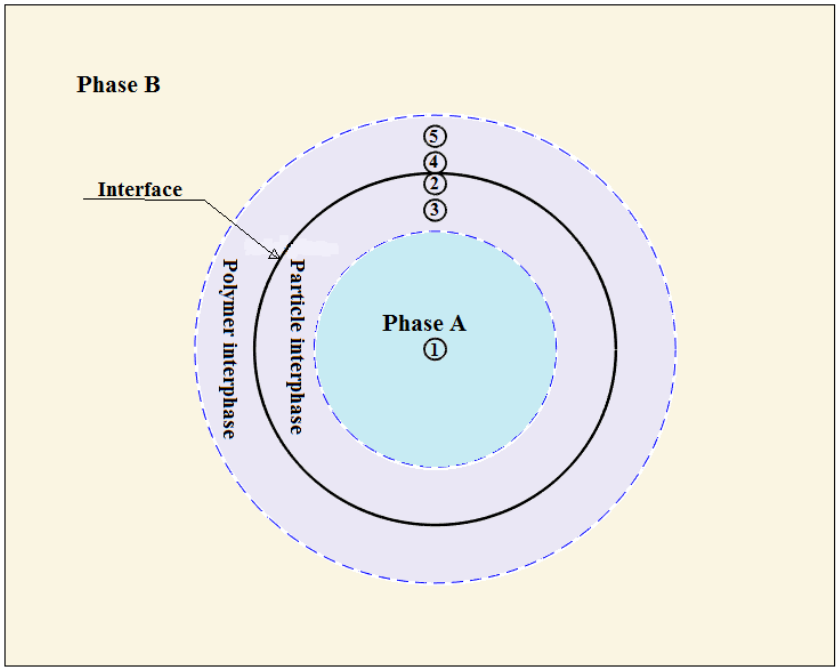

Figure 2.1: The interphase between two phases A and B (not to scale).

The main feature of nanoparticles is the large specific surface area compared with microparticles. Figure 2.2a illustrates the specific surface area per unit volume as a function of the particle diameter. The specific surface area increases sharply as the particle diameter becomes less than 100 nm [11]. As a consequence, the interphase regions will represent significantly increasing fractions of the nanocomposite volume as the particle diameter is reduced. Figure 2.2b shows the percentage volume of the interphases region as a function of nanoparticle loading for different particle diameters. As stated above, this interphase region may have its own characteristics, which are different from the bulk characteristics of both constituents of the nanocomposite, filler and matrix materials. Furthermore, modifying the surface of the nanoparticles can alter the interactions within the interphase regions and can achieve different properties. This can be accomplished by functionalization of the surface of the particles, which make them more compatible with the base material [12]. These features of nanocomposites hold a promise that such materials can be tailored and engineered to obtain multifunctional combinations of properties, where some properties can be improved without compromising others. Accordingly, a burgeoning interest in the subject has been shown during the last few years trying to maximize the utilization of these composites in the dielectric area.

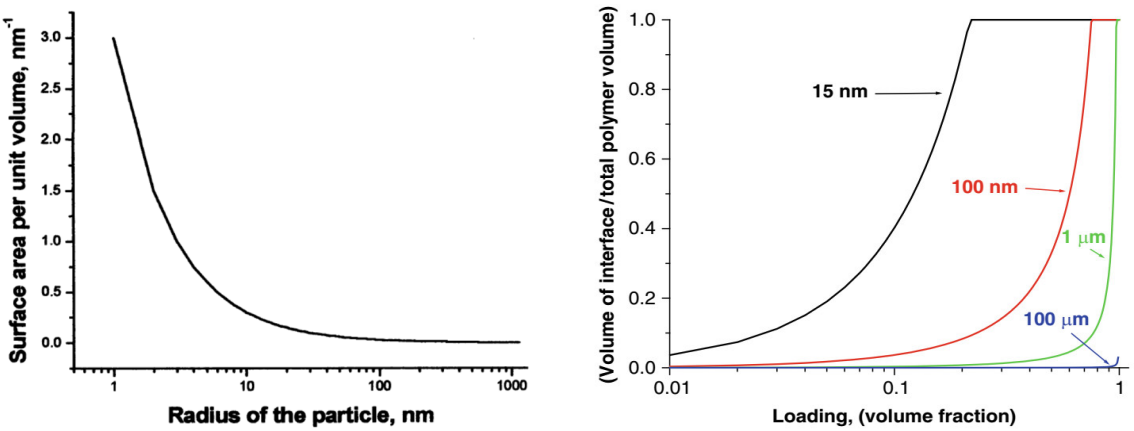

Figure 2.2: (a) The relationship between the surface area and the particle radius [11], (b) The interphase volume percentage as a function of nanoparticle loading for different particle diameters [13].

2.2 Electrical behaviour of nanocomposites

Over the last two decades, a great deal of research has been conducted trying to explore the potentials of nanodielectrics and investigate the underlying mechanisms that control the behaviour of these systems. Many of these factors have been empirically identified; however, detailed information about the underlying physics and chemistry behind these factors needs more research. In the following, some of the factors that are usually cited in the literature are discussed.

2.2.1 Particle dispersion

In order to activate the main characteristic of nanoparticles, which is their nanometre size, they should be effectively dispersed within the polymeric matrix. Considering their large specific surface area, the friction and surface tension forces between nanoparticles are dramatically higher than between microparticles, for example. This makes the nanoparticles stick together and complicates their dispersion [9]. Based on the theory of solubility between two phases, the nanoparticles can be efficiently dispersed in a matrix if the interactions between the particles and the matrix molecules are stronger than the cohesive forces between the particles themselves [14-16]. Hence the presence of strong interactions like the existence of chemical reactions between the surface of the particles and the polymer, should result in a better particle dispersion within the polymeric matrix. This urged many workers to treat the surface of the nanoparticles with matrix compatible functionalities for better particle dispersion [17-19]. In terms of dielectric performance, effective nanofiller dispersion can eliminate the negative consequences of nanoparticle clustering or aggregation. Nanoparticle agglomeration may result in a large enough particle to disturb and locally enhance the electric field due to the differences in the conductivity and permittivity between the filler and matrix materials, an analog to what occurs in the microcomposites [20, 21]. It is worth mentioning that treating the particles also implies

changing their surface chemistry, such as removing some of the hydroxyl groups on the surface, which can influence other factors, such as moisture adsorption and the interphase region (explained below). Therefore, the impact of treating the nanoparticles cannot be exclusively attributed to changes in particle dispersion. For example, although treating the particles in [18] resulted in worse particle dispersion compared with the untreated particles, the dielectric strength for nanocomposite containing the treated particles was higher. In this case, treating the particles might have a positive effect on other factors, which overwhelm the negative consequences of particle agglomeration.

2.2.2 Matrix morphology

Introducing nanoparticles into a polymeric matrix might alter its morphological structure, particularly for semicrystalline systems like polyethylene. Scanning electron microscope images reported in many studies have shown that the nanoparticles might act as nucleating centres, with the consequences of suppressing the size of spherulites and increasing their number [20, 22, 23]. Hosier [24] experimentally demonstrated that the breakdown strength can be affected by modifying the spherulitic morphology of an unfilled polyethylene matrix. A simulation study [25] considered the transport of an excess electron in the different structural phases of polyethylene (crystalline, lamellae and amorphous) and revealed that the electronic mobility is very sensitive to the local morphology and the distribution of the different phases throughout the material. Remarkably, this study indicated that the electron mobility in the lamellar phase is lower than that in the crystalline or the amorphous phases, where the inter-lamellar disordered regions offer deep electronic traps or localized states within the lamellar structure and, thus, increase the activation energy for the electrons to transit to higher energy extended states. Therefore, the changes in the dielectric performance of nanocomposites based on semicrystalline polymers might be greatly affected by perturbations to the crystalline morphology brought about by the addition of nanoparticles, rather than being associated directly with the particles themselves. Whilst this factor clearly should be considered when trying to explain the electrical behaviour of nanocomposites based on semicrystalline polymers, it should also be considered when comparing the impact of nanofillers on semicrystalline and amorphous base materials.

2.2.3 Water absorption

Many of the widely utilized nanoparticles, due to their surface chemistry, have the tendency to adsorb water molecules on their surface, which results in the formation of water shells surrounding the nanoparticles [3, 26-28]. The impact of such particle-associated water can be different from the water that is homogeneously absorbed throughout unfilled systems. For example, many investigations have reported that water uptake in silica nanocomposites results in a dielectric relaxation that does not appear in the corresponding unfilled systems [4, 19, 29]. Additionally, these water shells may form

percolation paths and, thus, drastically enhance charge transport in nanocomposite systems [26, 27].

Exposure to water is inevitable and, therefore, its effects should be considered when practically considering the potential of nanodielectrics. Furthermore, water content should be identified and taken into account as an important parameter in order better to analyse the electrical performance of nanocomposites.

2.2.4 Interphase region

As stated in the beginning of this chapter, the key idea that stimulated interest in nanodielectrics is that interfacial interactions between the nanofiller and the surrounding polymeric matrix may lead to the formation of interphase regions around the nanoparticles that have novel properties and which constitute a significant volume fraction of the whole nanodielectric material [6, 30, 31]. Many authors have tried to explain experimentally observed phenomena in nanocomposites based on the existence of such an interphase layer, where they consider nanocomposites as a tertiary system that consists of nanofiller, matrix and an interphase layer around the nanoparticles. For example, the dielectric permittivity of epoxy nanocomposites was found to be lower than that of both particle and polymer martials in [32-34] and this was explained by claiming that strong interfacial (filler/polymer) interactions results in a confined interphase layer around the particles with a lower permittivity than that of the unaffected matrix. Nevertheless, a critical understanding of the characteristics of the interphase region and how it affects electrical properties is not secured yet. The next section discusses, in details, some of the models that have been proposed to describe the interphase region in nanodielectrics.

All the above factors should be borne in mind when trying to design/analyse the dielectric behaviour of nanocomposites, as some of these factors may dominate others. For example, the negative dielectric consequences caused by particles' water absorption might dwarf any dielectric improvement caused by the introduction of the nanoparticles [35]. The relevance or the weight of each factor are functions of the matrix material, filler characteristics and the interactions between them.

2.3 Models for describing the interphase region in nanocomposites

Different models have been proposed to highlight the main characteristics of the interphase region and to describe the interactions that may occur in this region. In the following subsections three of these models are detailed.

2.3.1 Lewis intensity model

This model assumes that each atom and/or molecule in both phases A and B, Figure 2.3a, will interact with its surrounding via a combination of both short and long range forces.

The intensity of a property α will be the result of a certain combination of these forces; α could be any physical or chemical property. In an electrical context, it may be electron concentration, electrochemical potential, electric field or dielectric permittivity [7, 10].

Away from the surface of each phase, the forces that are responsible for any property may be considered constant, apart from spatial fluctuations on an atomic scale. This results in the mean macroscopic properties of phase A or B. Approaching the interface, these forces will change and thus the intensity of α will change as well. The interphase can be defined as the region over which the forces are different from both phases A and B. The thickness of the interphase depends on the range of the forces (if they are short or long range forces) responsible for the property in question. The profile of the property's intensity may be inconsistent with the traditional mixing rules. Typical examples for this model are illustrated in Figure 2.3b and c. The oxygen concentration at the interface between silicon and air is higher than in both silicon and air phases. Similarly, the electric field at the boundary between a conductor and n-type semiconductor is higher than in the conductor or the doped semiconductor. Other example from the nanocomposites area is the permittivity of titania/epoxy nanocomposites which appears less than the permittivity of either titania or epoxy [6].

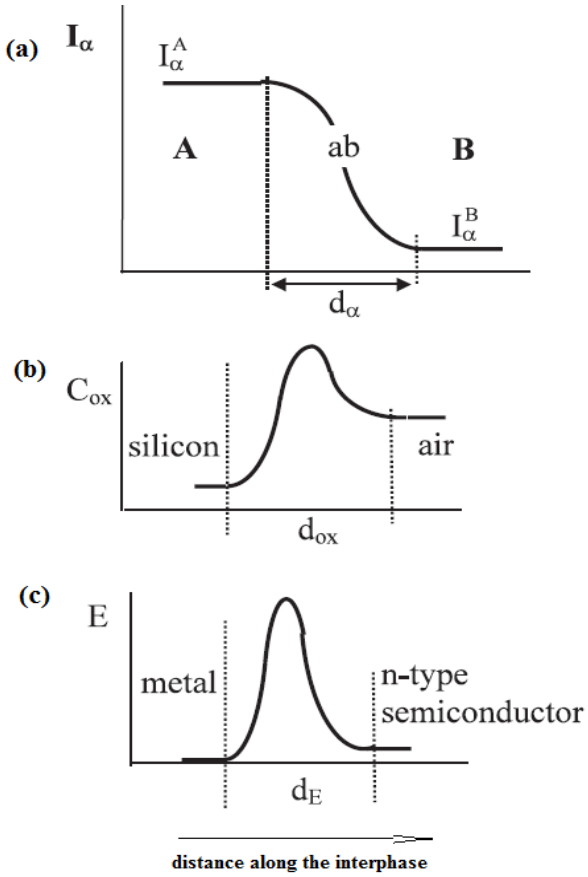

Figure 2.3: (a) Property α intensity (I_α) through the interphase between phases A and B, (b) Oxygen concentration at silicon air boundary, (c) Electric field at metal n-type semiconductor boundary. Adapted from [10].

2.3.2 Electrical double layer model

This model is based on a traditional model originally developed for colloidal systems. It assumes that introducing nanoparticles into a polymer matrix resembles putting them into a colloidal system, where an electrical double layer will be formed around the particles. The electrical double layer is formed because of the presence of electrically charged moieties on the surface of the particles, which may result from preferential dissociation or deposition of ions on the particle surface [36] or due to equalization of the Fermi levels of the particles and the solution [37]. Oppositely charged ions (counter ions) in the suspension will be attracted to the particle in order to screen the particle charge. This will result in forming a tightly attached layer of counter ions around the particle, which is called the Stern layer or Helmholtz double layer (indicating the original charges on the particle and the attracted counter ions). The Stern layer is of molecular thickness, ~1 nm, and may have high charge density. The Stern layer does not totally screen the original charge on the particle and hence extra counter-ions are still attracted by the particles, however, they will experience a repulsion from the similar charges in the Stern layer and they will not be strongly bound to the particle due to their thermal energy. In the equilibrium state a diffuse layer of counter ions, termed the Gouy-Chapman layer, is formed. As shown in Figure 2.4a, the Stern layer and the diffuse layer constitute what is called the electrical double layer and they will eventually balance the surface charge on the particle. The concentration of the co-ions and counter-ions as a function of the distance from the particle's surface is shown in Figure 2.4b. The thickness of the electric double layer depends on the type and concentration of the ions in the suspension [10, 38, 39].

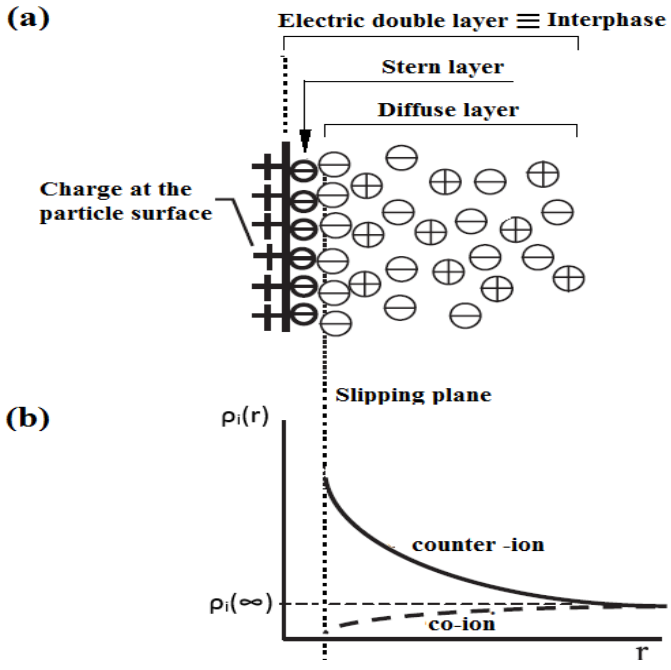

Figure 2.4: (a) Electric double layer model, (b) Co-ion and counter-ion concentrations, $\rho_i(r)$. Adapted from [10].

This model assumes that something similar occurs in nanocomposites and represents the interphase region by the electric double layer. In nanocomposites, the particles' surface

charge can be formed by mechanisms similar to that described above. The counter or screening charge can be established by forming a diffuse layer of mobile charges, similar to the Gouy-Chapman layer, in case the polymer contains mobile charges, or by inducing new dipoles and/or orientating of permanent dipoles [37]. This model qualitatively illustrates how the interphase can affect the charge mobility and dielectric permittivity of nanocomposites.

2.3.3 The multi-core model

The multi-core model proposed by Tanaka divides the interphase region into three layers surrounding the nanoparticles. In addition, an electric double layer is superimposed on these three layers as illustrated in Figure 2.5. The three layers are [37]:

1- The bonded layer: this consists of the polymer molecules that are bonded to the particles. This layer is of molecular thickness, and the bonding can be via covalent bonds, which may be induced by coupling agents, van der Waals or hydrogen bonds.
2- The bound layer: this corresponds to a region in which the polymer chains are strongly bound to the first layer. The chain mobility and the chain conformation are strongly affected by the presence of the particles. The thickness of this layer is between 2 and 9 nm depending on the strength of the interactions between the particle and the polymer.
3- The loose layer: this consists of polymer chains that are loosely connected to the second layer. The chains in this layer have different chain conformations from the rest of the polymer matrix.

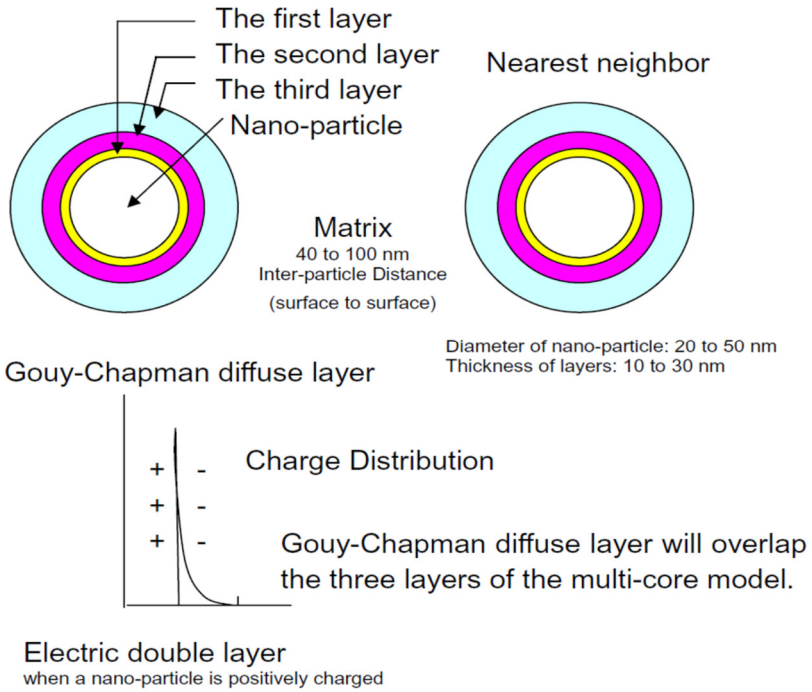

Figure 2.5: Multi-core model as proposed by Tanaka [37].

This model combines possible electrical, morphological and polymer dynamics effects of the interphase region in the nanocomposites. As an example for the chain dynamics effect, a study performed by Miwa [40] on poly(methyl acrylate)/clay nanocomposites showed that the mobility of the polymeric chains near the particles is constrained, which forms a rigid interphase region with thickness of 5 – 15 nm.

As can be seen from the above description, Lewis intensity model and electric double layer model do not offer a critical understanding of the interphase region, instead, they just conceptually describe it without distinct experimental or analytical evidence. The multicore model did present a more explicit mechanism for describing the potential influence of the nanoparticles on the molecular dynamics of the polymeric matrix, particularly when the particles are bonded to the polymer. Many experimental studies have investigated the effect of the nanofiller on the polymeric matrix by observing the molecular dynamics over the glass transition process using techniques such as differential scanning calorimetry or dielectric spectroscopy. Some of these studies did not detect any evidence for such effects, even where attractive interactions between the filler and the polymer, i.e. strong hydrogen bonding, are present [41, 42]. Therefore, the multicore model cannot be used fully to describe these nanocomposites. Other studies do detect an immobilised layer [43, 44], that does not contribute to the glass transition of the rest of the matrix, or a layer with different molecular dynamics around the particles [45, 46]. However these effects were marked at a high loading ratio, > 20 wt%, for nanoparticles less than 15 nm in diameter, and hence, the thickness of the confined layer was estimated to be less than ~2 nm [43, 44], much less than that anticipated by the multicore model. More importantly, direct linkage between molecular dynamics effects and the dielectric performance is neither clear nor experimentally proven. For example, even for nanocomposites where the filler has an impact on the cooperative relaxation at the glass transition process, the β relaxation, which is associated with smaller segmental dynamics, was not perturbed [43, 44]. For this relationship, the multicore model proposed that an electric double layer is superimposed on the multicore model. Additionally, the authors speculated that the strain on the confined polymeric segments around the nanoparticles affects the free volume content. No experimental evidence supports these claims. On the contrary, a recent study demonstrates that the free volume is little affected by the addition of nanoparticles, and cannot interpret the significant variations seen in the dielectric strength for many nanodielectrics [47]. As such, a mature understanding of the interphase region characteristics is not yet achieved.

A detailed model that can relate the macroscopic behaviour of nanodielectrics with the interactions between the particles and the encapsulating polymer is needed in order to open the potential of these composites to be tailored and designed and to meet our future demands on dielectrics. For underlying the dielectric behaviour, which is concerned with the mobility of as small species as electrons, the prospective model might need to

investigate the effect of the interactions at the microscopic level. For example, these interactions might affect the density of states in the interphase region, which consequently influences the overall electronic mobility in the system. Simulation studies of the interphase region would be powerful tool for tailoring the dielectric behaviour of the nanodielectrics and directing experimental exploration.

2.4 Proposal of particle interphase model (hypothesis)

Until now, the nanocomposites models proposed in the literature have concentrated on the interphase region inside the polymer, the "polymer interphase" in Figure 2.1, neglecting any interphase layer inside the boundaries of the particles themselves, "particles interphase" in Figure 2.1. This might be returned to that the molecules of the particles are very small compared with the polymer molecules or chains, thus, the particle interphase is expected to be much thinner than the polymer interphase. Nevertheless, the higher density of the particles implies denser electronic energy states and, consequently, any perturbations in the electronic states in the particles interphase, such as changing their energy levels or spatial extension, might have more profound impact on the dielectric performance.

Due to their large surface area, nanoparticles contain a high concentration of defects on their surfaces. These defects could be due to the presence of foreign atoms on the surface, surface geometrical irregularities or the non-centro-symmetry nature (coordinative unsaturation) of the molecules near the surface of the particle [8]. As a result of these defects, new *localized* energy levels in an otherwise forbidden band are generated. The generated energy levels may lie in the band gap between the valence and the conduction bands and represent charge traps (localized states in the band gap). Upon the availability of mobile charges, i.e. electrons/holes in the conduction/valence band, they prefer to fill these traps rather than staying in the conduction/valence band [48]. Once it filled the trap, it is difficult for the electron/hole to return to the conduction/valence band, particularly if the trap is deep enough, although it can move to similar traps around the particles, if these are close enough [48]. Through this mechanism, charges may move through the particle interphase and if the particles are not far from each other, they may move from one particle interphase to another, as depicted in Figure 2.6. This might facilitate charge mobility in nanocomposites and degrade the electrical insulation properties. Obviously, such conduction in the band gap relies on the inter-particle distance and the trap density in the particle interphase [49]. For example, if these traps are deep and/or far from each other, the reverse could occur, where the traps can capture the excited charge carriers and limit the charge conduction [50, 51].

Alternatively, if the above-mentioned defects generate energy states that are deeper in the conduction/valence band, this might widen the band gap in the particle interphase region and constitute an energy barrier for the charge movement. As a result, the charge carriers

will see the particle interphase, and consequently the whole particle, as an obstacle limiting their movement and increasing the length of their conduction paths as depicted in Figure 2.7. This might present a possible mechanism that results in improving the dielectric properties of the nanocomposites.

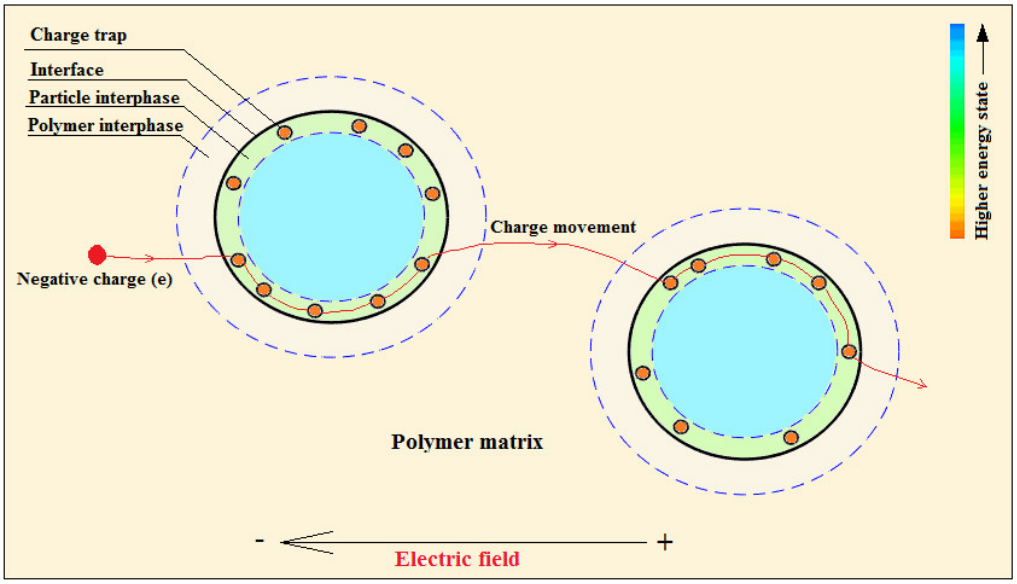

Figure 2.6: Possible mechanism for charge movement through the charge traps in the particle interphase (not to scale).

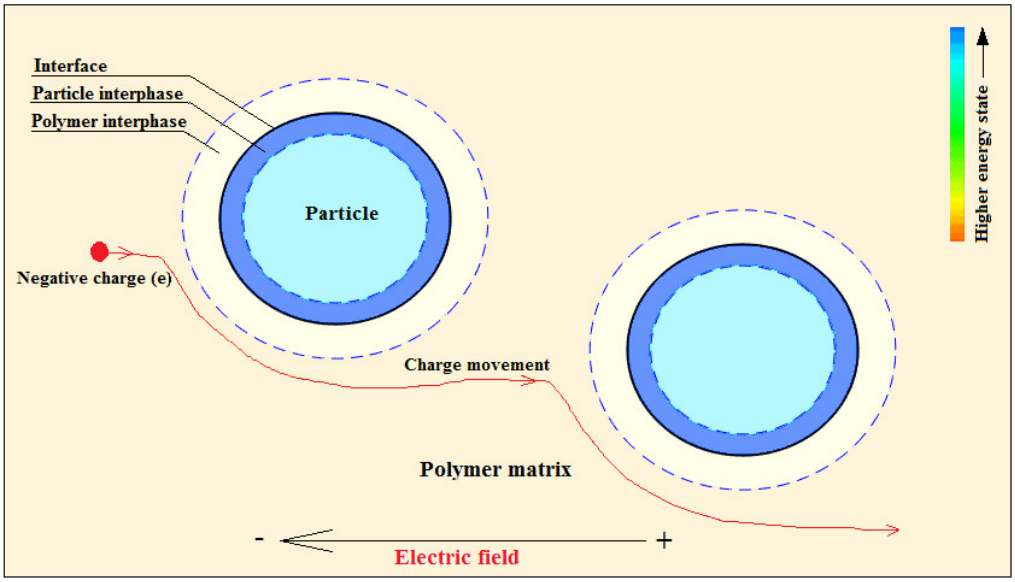

Figure 2.7: The particle interphase represents an energy barrier for charge movement (not to scale).

The crucial impact of the particle interphase on the dielectric behaviour could be pronounced in many experimental studies reported in the literature. The studies in [52, 53] investigate the effect of the addition of silica and hexagonal boron nitride (hBN) to an epoxy resin on the space charge dynamics and AC breakdown behaviour. The AC breakdown results correlate well with the space charge results, where the higher space charge accumulated in the silica epoxy nanocomposites leads to a lower AC breakdown

strength. The reverse was observed in the boron nitride filled composites. It is expected that the surface of the hBN, due to its uniform structure, does not contain as many defects as exist on the surface of the silica, which means that the silica might contain more charge traps, which leads to the development of more space charge. The study in [54] shows that treating nano-silica particles with a silane coupling agent before introducing them into a polyethylene matrix reduces the formation of the space charge and consequently increases the DC breakdown strength, compared with the untreated silica filled polyethylene. Complementary studies [23, 35] investigating the influence of varying the molecular length of the coupling agent, in an attempt to modify the polymer interphase, shows that increasing the chain length of the silane functionlizer has no appreciable impact on the electrical properties. This suggests that the mechanism by which the particle treatment affects the electrical behaviour is not merely related to the interactions that occur in the polymer interphase. Interestingly, heat treatment of nano-silica which leads to the removal of surface hydroxyl groups, replacing these with stable siloxane bridges, improves the dielectric performance of silica polyethylene nanocomposite [5]. These findings reveal that treating the nanoparticles in a way that modifies their surface chemistry (i.e. by replacing hydroxyl groups with silane molecules or removing hydroxyl groups thermally) can affect the localized states in the particle interphase region and that could be the reason behind the reduction in the space charge formulation, and subsequently, higher breakdown strength. A recent simulation study [55] considering the electronic density of states of magnesium oxide nanoparticles supports the above inference. The simulation predicts that electronic traps are generated near the surface of the particle with a depth of 1.3 eV when the particles are terminated with magnesium-oxygen bridges, 2.4 eV when the particles are terminated with hydroxyl groups and 0 eV (no traps) when the particles are terminated with a silane coupling agent. Although the simulation study is based on magnesium oxide, not silica, it is in line with the conclusion drawn from experimental observations that the electronic states near the surface of the particles are different from the states in the bulk and that they are very sensitive to the surface chemistry of the particles. Therefore, although the thickness of the particle interphase is expected to be very thin (the filler materials normally have small molecules), it might have a decisive impact on the electrical properties of the nanodielectrics.

2.5 Polymers

Polymers are widely used materials in every aspect of the life. Since the Second World War, polymeric materials research has captured more than one-third of the money raised for chemical research. Polymers consist of very long molecules, where the molar mass ranges from 10000 to tens of millions of g/mol [14]. These molecules, or chains, are composed of many repeated units called monomers. Within these molecules, the atoms are hold together by intramolecular bonds. On the other hand, intermolecular bonds are responsible for connecting polymeric chains within the polymeric material. Both the

intramolecular and intermolecular bonds could be one, or more, of the bonds listed in Table 2.1. This table also shows the dissociation energy of each bond, which refers to the strength of the bond. From Table 2.1, the covalent bond is approximately two orders of magnitude stronger than the other bonds.

The intramolecular bonds are chiefly covalent bonds, which connect the atoms together within the polymeric chain. However other bonds such as hydrogen bond may exist between the side atoms or groups along the backbone of the polymeric chain and influence the geometrical structure of the polymeric chain.

The intermolecular bonds determine if the polymer is thermoplastic or thermosetting. In a thermoplastic polymer, the intermolecular bonds are much weaker than the covalent bond. As a result, when the temperature is increased, the thermal energy will overcome the weak intermolecular bonds well before it will affect the covalent bonds (intramolecular bonds). Consequently, the polymer will melt or convert to the rubbery state (depending on its crystallinity, see appendix A.1). When the polymer is cooled down, it will go back to its solid state.

Table 2.1: Chemical bonds existing in polymers and their dissociation energy [14].

Bond type	Dissociation energy (kcal/mol)
Covalent bond	50 – 200
Hydrogen bond	3 – 7
Dipole interaction	1.5 – 3
Van der Waals bond	0.5 – 2
Ionic bond	10 – 20

In thermosetting polymers, the strength of the intermolecular bonds is comparable to the intramolecular bonds, i.e. they could be covalent bonds, as in cross-linked polymers. Thus, when the temperature is increased, the thermal energy will overcome the dissociation energy of both the intermolecular and intramolecular bonds at the same time. Consequently, the molecules of the polymer are separated to small pieces and degrade at the same time or before starting to melt and that is why such systems are called thermosetting. Unlike thermoplastic polymers, thermosetting polymers cannot be recycled. However, they are more thermally stable.

2.6 Epoxy resin

Epoxy resin is the generic name given to the prepolymer materials which contain two or more reactive epoxy (epoxide) groups in their molecules and are able to crosslink with a suitable curing agent (hardener) to form three dimensional networks [56]. In its initial state, an epoxy resin is an oligomeric material where its molecules are composed of a few

repeated units and have low molecular mass, when compared with polymeric molecules. The cured epoxy resin is also termed on epoxy [57]. In this study, to differentiate between the epoxy resin in its initial state and the cured epoxy, the term ‘epoxy resin’ is used to describe the former and ‘epoxy’ is used to represent the latter. Once it is cured, the epoxy resin converts into a crosslinked, thermosetting, amorphous polymer.

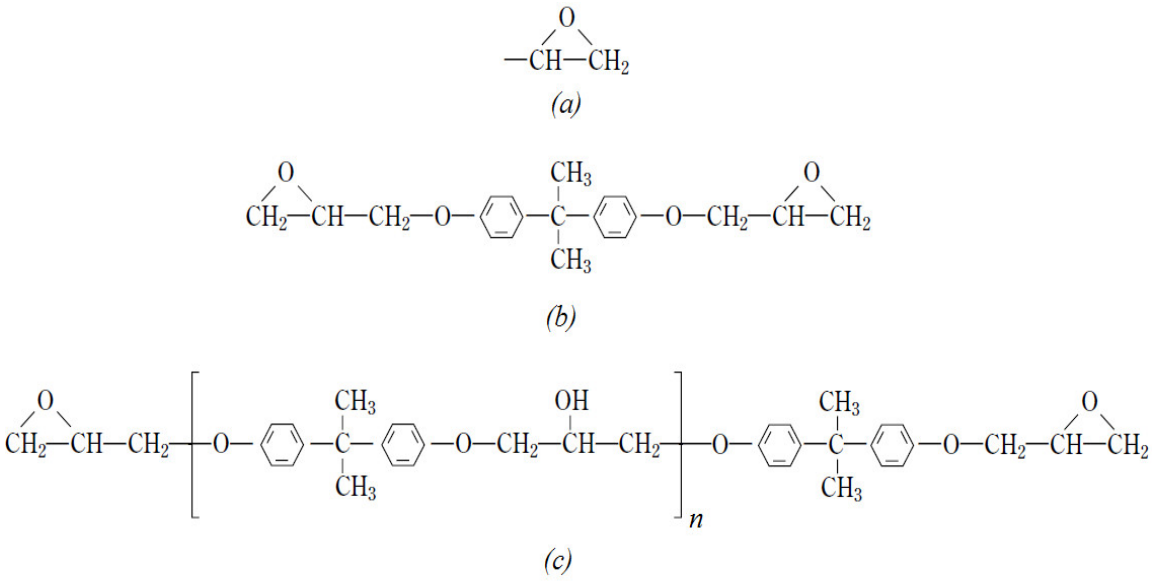

Figure 2.8: The chemical structure of (a) epoxy group, (b) DGEBA resin, and (c) DGEBA derivatives.

There is a wide variety of epoxy resins available for commercial use. This study concerns dyiglycidyl ether of bisphenol-A (DGEBA), one of the most widely used epoxy resins. The chemical structure of DGEBA and its derivatives are shown in Figure 2.8b and c, respectively. During manufacturing, the DGEBA molecules may homo-polymerize to produce longer molecules. Figure 2.8c shows the chemical structure of a homo-polymerized DGEBA molecule, where n indicates the number of homo-polymerizations, i.e. $n = 0$ means no homo-polymerization, $n = 1$ means one homo-polymerization and so on. Commercial DGEBA resins contain DGEBA with different molecular mass and the manufacturer normally gives the mean value of molar mass for its resin products. The pure DGEBA has the lowest molar mass equalling 340 g/mol, while the resin used in this study, DER 332 from Sigma-Aldrich, has a mean molar mass equalling 348 g/mol. This indicates that DER 332 has high purity and it is very close to being pure DGEBA. The molar mass affects the viscosity of the epoxy resin, where the higher the molecular mass, i.e. the higher the value of n in Figure 2.8c, the greater the viscosity of the resin [58]. The properties of the uncured epoxy resin, such as viscosity, are important for the processing of the resin to produce nanocomposites, for example, having the resin in a stable liquid phase is often considered to be advantage for such systems, where it is easier and more effective to disperse a filler material into the uncured liquid resin [52].

2.6.1 Epoxy curing

Epoxy resins can be cured by crosslinking with a curing agent, commonly known as a hardener, or by promoting homo polymerisation using a catalyst [59]. In the first method, the epoxy group tends to react with nucleophiles such as amine or hydroxyl groups. The hardener used in this study is Jeffamine D-230 from Huntsman. The chemical structure of Jeffamine D-230, Figure 2.9a, shows that it contains two primary amine groups in each molecule. Thus, each amine group can crosslink with two epoxy groups, as shown in Figure 2.9b. The reaction starts when the active amine hydrogen interacts with the epoxy oxygen, which results in opening of the epoxide ring, generating an hydroxyl group and connecting the two compounds together. The generated hydroxyl group may react with another epoxy group in the resin to form ether bonds. The rate of this reaction depends on the temperature during the curing process and the concentration of the hydroxyl group compared with the amine group [60, 61]. The curing temperature is a crucial factor, which can affect the rate and nature of the chemical reactions during the crosslinking process and hence produce networks with different architectures. For example, applying a curing temperature lower than the glass transition temperature (T_g) of the cured product, may result in an incompletely cured epoxy [62, 63].

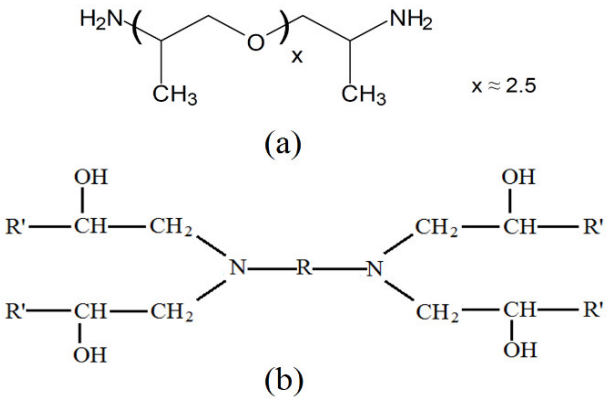

Figure 2.9: (a) The chemical structure of the Jeffamine D-230, (b) simple representation of a Jeffamine D-230 molecule crosslinks with four epoxy groups.

2.6.2 Resin/hardener ratio and its effects

The ratio between the epoxy and the amine groups affects the degree of crosslinking which, in turn, has an influence on the ultimate electrical and mechanical properties of the cured epoxy [63, 64]. The effect of changing the stoichiometry was investigated in [63-65] for resin and hardener systems that are similar to the system in the current study. These studies showed that an excess of hardener, beyond the stoichiometric ratio, leads to a slight decrease in the T_g, while an excess of the epoxy leads to a significant reduction in the T_g. This indicates that increasing the fraction of hardener does not markedly reduce the degree of crosslinking while increasing the fraction of epoxy does. This conclusion is supported

by the further experiments performed in [63], where the average molecular mass between crosslinks, deduced from measuring the rubbery state modulus has a similar trend, i.e. it increases slightly by increasing the hardener fraction and significantly by increasing the epoxy fraction. This asymmetrical behaviour of T_g is associated with the number of functionalities per resin molecule compared with the functionalities of the hardener molecule, as will be explained in section 5.2.

Interestingly, the electric breakdown results in [64] show the opposite trend, where the breakdown strength sharply decreases with an excess of hardener and slightly decreases with an excess of epoxy.

From these observations, it can be concluded that the stoichiometric formulation or the highest degree of crosslinking are not necessarily related to the best electrical performance. In fact, the degree of crosslinking controls the motion of polymer chains or polymer segments, whereas the charge mobility does not necessitate this. In the case of excess hardener or amine groups, the concentration of hydroxyl groups will increase because every time an epoxy group reacts, a hydroxyl group is generated, as shown in Figure 2.9b. On the other hand, in the case of excess epoxy, the concentration of the hydroxyl group will decrease since many epoxide groups will be left unreacted and thus without generating extra hydroxyl group, as proved by FTIR in [63]. Additionally, due to the shortage of amine groups, many of the epoxy groups may interact with the existing hydroxyl groups to form ether bonds, particularly at elevated temperatures near the end of the curing process. This conclusion about the hydroxyl groups is enhanced by testing the water absorption of cured samples, where samples with an excess of epoxy absorb less water, indicating that they have a reduced hydroxyl content [65]. Increasing hydroxyl group concentration seems to facilitate the charge mobility and this might be the reason behind the breakdown behaviour when changing the amine/epoxy ratio [53].

2.7 Nanofillers

As stated in section 2.1, the concept of nanocomposites is based upon the incorporation of a nanofiller, which has nanoscale dimensions and leads to the formation of interaction zones inside the polymeric matrix. Hence, understanding those characteristics of the nanofiller that affect their dispersion, interaction and compatibility with the polymer matrix is critical for understanding the behaviour of the produced nanocomposites. These characteristics include the synthesis method, the shape, the crystallinity and the surface chemistry of the nanoparticles. The nanoparticle synthesis method can affect the purity, aggregation tendency, size distribution and the surface functional groups of the nanoparticles [66-68]. Therefore, different synthesis techniques may lead to different nanoparticle behaviour. The shape of the nanoparticles, which can be quantified by the aspect ratio (the ratio between the longest and the shortest dimension of the particle), affects the specific surface area of the nanoparticles. The crystallinity of the particles can

affect the interaction between the particles and any other contacting material. For example, Fubini *et al*. [69] showed that α phase crystalline silicon nitride nanopowder retains most of the chemically adsorbed water (hydroxyl groups) on its surface when it is evacuated at 400 ^{o}C, while another study indicated that the amorphous counterpart loses most of the adsorbed hydroxyl groups when it is evacuated at 300 ^{o}C [70]. The surface chemistry and the functional groups existing on the surface of the nanoparticles determine the compatibility and the interactions that occur in the interphase region. The existence of matrix compatible functional groups on the particles surface may result in the formation of chemical bonds between the particles and the matrix, so increasing particle dispersibility [71]. This feature can be deliberately imparted by performing surface treatment of the particles, where matrix compatible functional groups are added to the surface of the particles. Any possible chemical reaction between the particles and the polymeric matrix is very important, particularly for thermosetting nanocomposites where the particles are mixed with the uncured resin and the possibility of forming chemical bonds between the particles and the uncured resin could change the nature of the produced network upon curing. The presence of hydroxyl groups, which are able to adsorb water molecules, is another characteristic that needs to be considered. This can increase the water absorption of the nanocomposite and could degrade the electrical performance of the material.

All these characteristics and their correlation with the base material should be considered in order better to understand the behaviour of nanocomposite. In the following sections, the characteristics of silicon nitride and silica nanoparticles are detailed. Although this study is mainly concerned with the silicon nitride, it is useful to study silica since it has historically been widely used in nanocomposite research. Furthermore, silicon nitride and silica have some similarities and some differences, as will be detailed below. Therefore, comparing the behaviour of silicon nitride and silica nanocomposites may provide us with useful information about the key characteristics that control the electrical performance of epoxy nanocomposites.

2.7.1 Silicon nitride nanoparticles

Silicon nitride (Si_3N_4) is an important ceramic material, which has excellent mechanical and electrical properties such as high breakdown strength, good oxidation and wear resistance and low thermal expansion coefficient both at room and elevated temperatures [72, 73]. However, nanoscale silicon nitride has received little attention as a filler material in polymeric nanodielectrics. Silicon nitride could have an amorphous structure, the α crystalline structure or the β crystalline structure [74].

Upon exposure to water vapour during its storage or processing, silicon nitride nanopowder dissociatively (chemically) adsorbs the water and forms silanol and secondary amine groups on its surface. A possible scheme for this process is depicted by Fubini [69], shown in Figure 2.10a, along with two possible arrangements illustrating how the silanol and the

amine groups can physically adsorb water molecules by forming hydrogen bonds, shown in Figure 2.10b. Water adsorption could be enhanced by the already existing amine groups that are formed during the synthesising of silicon nitride (for instance, synthesising Si_3N_4 by laser induced reaction between SiH_4 and NH_3 produces amine groups, -NH, on the surface) [75].

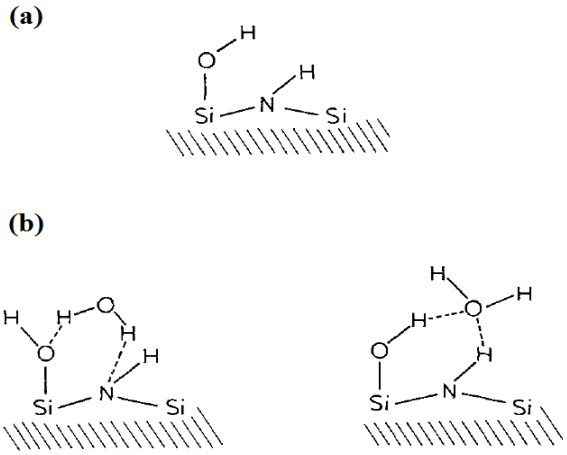

Figure 2.10: (a) Chemically adsorbed water forming silanol and amine groups, (b) Two possible schemes for hydrogen bonded water. Proposed by [69].

The effect of storing Si_3N_4 on the oxygen content on the surface was studied by [76, 77]. Samples of amorphous Si_3N_4 nanopowder produced by the vapour phase reaction of $SiCl_4$ and NH_3 were stored in three different environments, argon atmosphere, dry air and 80% relative humidity air, and the chemical composition of these samples was periodically examined using X-ray photoelectron spectrometer (XPS). The study showed that the surface composition of the sample stored in the argon atmosphere was not affected, whereas, for the sample stored in dry air, the surface oxygen content increased from 7.9% to 15.9% and the nitrogen content decreased from 31% to 28% after 90 days of storage. For the sample stored in 80% relative humidity air, the trend was more distinct, whereby, the oxygen content increased to 22.7% and 37.9% after 3 days and 90 days, respectively, and the nitrogen decreased to 23% and 11.9% over the same storage periods. This indicates that exposing Si_3N_4 to water increases the silanol groups at the expense of decreasing the amine groups. The decrease in the nitrogen (amine) content may be due to the hydrolysis of the amine groups following the reaction in Eq. 2.1 [75, 78]. Another possible explanation is that the physically adsorbed water layers cover the surface and prevent the XPS from detecting the amino groups.

$$Si_2{-}NH + 2H_2O = 2Si{-}OH + NH_3 \qquad \text{Eq. 2.1}$$

The hydrolytic instability of Si-N bonds and its affinity to react with water, lead to gradual oxidization of the surface of the Si_3N_4, so finally forming a layer of silica covering the surface of the silicon nitride [78] where the nitrogen content can gradually decrease

through a hydrolysis process releasing ammonia. The speed of this conversion depends on the storage conditions of the Si_3N_4.

The influence of heat treatment on the surface chemistry of crystalline Si_3N_4 was studied by [69]. The study showed that upon outgassing at 400 ^oC, the Si_3N_4 powder retains most of its hydroxyl and amine groups and when outgassing at 800 ^oC, it loses a significant amount of the surface hydroxyl and amine groups. However, in both cases, the surface remains hydrophilic. The authors claimed that the silanol and amine groups are condensed, upon heating at 800 ^oC in vacuum, to form water and Si-N bridges as illustrated in Figure 2.11. They assumed that the Si-N bridges are not stable and represent reactive sites that can easily adsorb water when exposed to it at room temperature, as indicated by the reverse reaction in Figure 2.11.

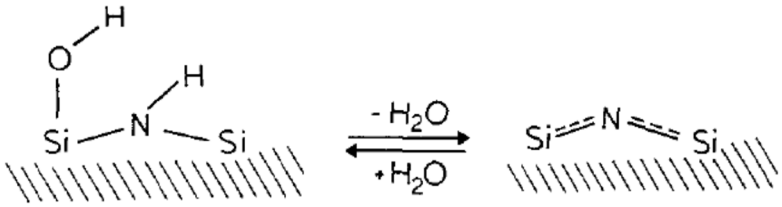

Figure 2.11: Hydration and dehydration of the silicon nitride as suggested by [69].

This conflicts with the study in [75], which claims that upon outgassing at 1500 ^oC, firstly, the amine groups are removed at temperature of 600 ^oC and then the silanol groups are condensed, subsequently the surface is covered by Si-O-Si bridges. This claim is supported by detecting ammonia released during the heat treatment, which means that part of surface nitrogen content is released in the form of ammonia. A possible equation describing this process is [79]:

$$Si\text{-}OH + Si\text{-}NH_2 \rightarrow Si_2O + NH_3 \uparrow \qquad \text{Eq. 2.2}$$

A possible compromise for these inconsistent studies is that both forms of losing the hydroxyl and the amine groups, illustrated by Figure 2.11 and Eq. 2.2, might occur on performing heat treatment at temperature above 800 ^oC, i.e. the Si_3N_4 surface will be covered by Si-N bridges and Si-O-Si bridges to different extents, depending on the oxidisation state of the studied silicon nitride. This conclusion is supported by the fact that Si_3N_4 did not show hydrophobicity as expected if its surface is completely covered by Si-O-Si bridges, as will be shown for silica.

2.7.2 Silica nanoparticles

Silica nanopowder is commonly used as a filler material in the nanodielectrics area. The surface of the silica is covered by silanol groups. The origin of the silanol groups is through the synthesis process of the silica or due to hydroxylation of the silica when it is exposed

to water. The number of the silanol groups could reach 5 OH/nm^2 upon completely hydroxylation [80]. The surface silanol groups can be in the form of isolated, germinal or bridged silanol as shown in Figure 2.12a. These groups have great ability physically to adsorb the water molecules by forming hydrogen bonds as illustrated in Figure 2.12b.

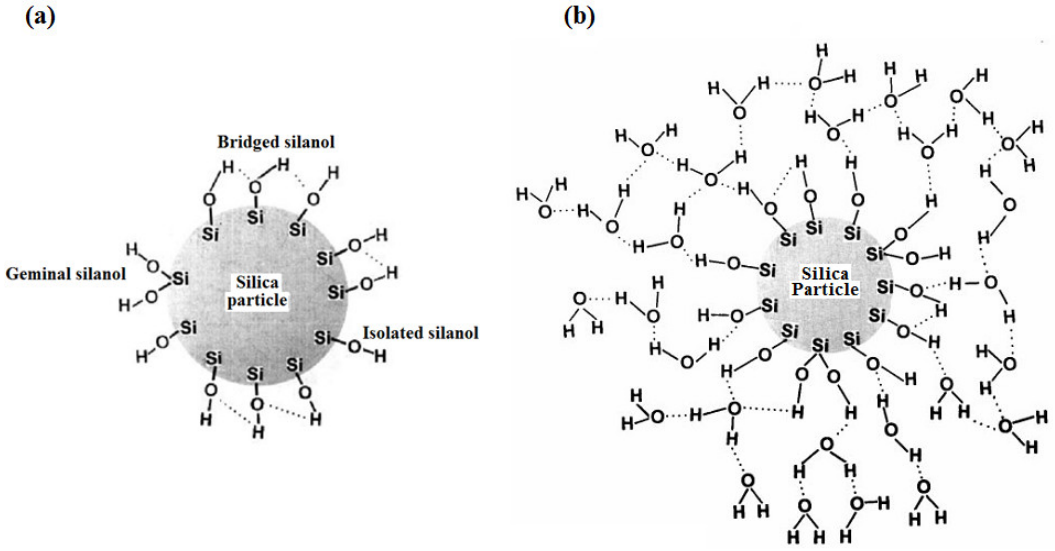

Figure 2.12: (a) Types of the silanol groups on the surface of the silica, (b) Layers of physically adsorbed water [81].

Heat treatment of the silica in vacuum at 190 ^oC completely removes the physically adsorbed water but does not affect the chemically adsorbed water (OH groups), Figure 2.13a. Increasing the heat treatment temperature will result in gradually desorption of the OH groups over a broad range of temperatures. This process follows the condensation reaction in Eq. 2.3.

$$\equiv Si\text{-}OH + \equiv Si\text{-}OH = Si\text{-}O\text{-}Si + H_2O \uparrow \qquad \text{Eq. 2.3}$$

As long as there is a significant amount of the silanol groups on the surface, the silica can easily re-adsorb the water upon exposure to it, as indicated by the reverse reaction between Figure 2.13b and a.

At temperatures around 1200 ^oC, most of the hydroxyl groups will be removed, such that the silica becomes covered by siloxane bridges (Si-O-Si) and hydrophobic (see Figure 2.13c). When the siloxane bridges are not surrounded by silanol groups, they are stable and react with water molecules at a slow rate. Therefore, at room temperature, the rehydroxylation process is very slow and takes a long time even on contact with liquid water. However, the rehydroxylation becomes easy and fast when in contact with water at 100 ^oC. The rehydroxylation starts near the remaining silanol groups, which act as centres of adsorption, and spreads slowly or fast depending on the temperature of the water [81].

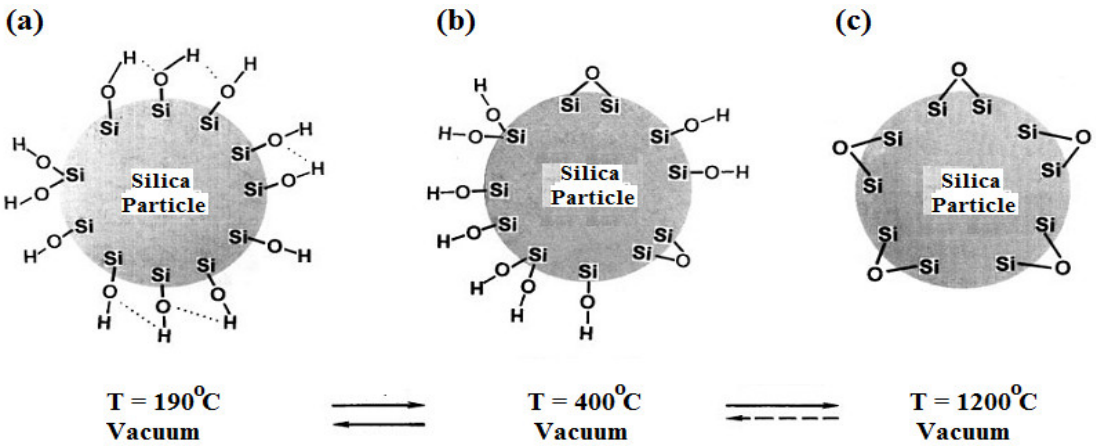

Figure 2.13: The effect of the heat treatment on the surface of the silica, adapted from [81].

2.8 Epoxy nanocomposites

Epoxy resin is a widely used material for dielectric applications. For nanodielectrics, the ease and effectiveness of dispersing a filler material into a liquid uncured resin make epoxies good candidates as host materials. Additionally, the actual filler loading for this system is not expected to deviate significantly from the nominal loading percentage, since there is no way for the nanoparticles to be lost. The results shown in the literature for the performance of the epoxy based nanocomposites vary between improving and degrading the performance, depending mainly on the filler material characteristics and if it is treated before use or not. Moreover, epoxies include many different chemical forms and this should be taken into account when comparing the results reported in literature.

2.8.1 Epoxy nanocomposites with untreated particles

The study in [52] investigated the effect of incorporating hexagonal boron nitride with particles ranging in size from 0.5 to 45 μm into an epoxy. The results show that the addition of 10 wt% of hBN considerably increased the thermal conductivity while maintaining or slightly increasing the breakdown strength. The sample which achieved the highest thermal conductivity also gave the highest breakdown strength. There is no clear trend connecting the results with the particles size. The authors claimed that the hBN particles increase the breakdown path length while work as bridges to conduct the heat.

The study in [29] compared the addition of 2.5 wt% hBN with a particle size of 0.5 μm, and 2.5 wt% silica with a particle sizes in the range 5 - 15 nm. The results point out that, while the nano-silica did not considerably change T_g, the addition of hBN reduced it by 4 °C. The authors ascribed this to impediment of reticulation by hBN particles, which act as obstacles. The study also showed that the hBN did not affect the relative permittivity, while the nano-silica increased the relative permittivity and induced a new relaxation peak at low frequencies near 1 Hz, which was ascribed by the authors to the existence of water

around the silica particles. The comparison between the influence of hBN and nano-silica is not too fair because of the large difference in particles size of hBN and silica. However, the conclusions drawn by the authors appear reasonable. An additional feature that merits investigation is that the surface of the silica might be more active and has more functional groups (silanol groups) than the hexagonal boron nitride, which may interfere with the chemical reactions occurred during the curing process. Even particles from the same material type could have different surface functionalities due to the variation in the purity, synthesis, and surface defects. The study in [82] utilized hBN particles with the same particle size used in [29], but indicated that the T_g increases for the filled epoxy. The authors state that the amine groups on the hBN particles interact with the epoxy and enhance the crosslinking of composite. This may indicate that the hBN powder used in this study has more surface amine groups than the one used in [29].

A comparison between the effects of nano- and micro-silica was conducted in [83]. This study shows that the micro-silica slightly decreased the T_g, particularly at the high loading percentage of 10 wt%, whereas the nano-silica increased the T_g with increasing filler loading. The AC breakdown data show that the nano-silica slightly decreased the breakdown strength and the micro-silica composites exhibited a greater reduction in the breakdown strength. The authors judged the dispersion level by the high Weibull shape parameter obtained for nanocomposites. This derivation may be not accurate since the macroscopic homogeneity (i.e. the breakdown measurements) does not necessarily equate to well dispersed nanoparticles with nanometric dimensions. That is, if the particle agglomerations are much smaller than the sample dimensions and they are uniformly distributed, this may not lead to highly scattered breakdown results.

Comparing the effect of the submicro-hBN in [29] and the micro-silica in [83] reveals that the hBN reduces the T_g more than does the micro-silica. The impediment of reticulation caused by the micro-sized particles might be the reason for reducing the T_g, however the active surface of the silica may form hydrogen bonds with the epoxy which contributes to mitigating the T_g reduction caused by the first factor. For the breakdown strength, the submicro-hBN in [52] achieved higher breakdown strength than both the micro- and nano-silica in [83]. This may return to the difference in the surface chemistry of both of them. The hBN ideally does not have any functional groups on the surface of its platelets, but it has hydroxyl and amine groups on the edge of the platelets [84]. Conversely, it is expected that silica has many more functional groups, mainly hydroxyl groups, on its surface, which may adsorb water and increase the charge mobility. This is enhanced by the study in [53] which investigates the space charge distribution and movement in submicro-hBN epoxy composites and nano-silica epoxy composites, which shows that the space charge movement in silica filled epoxy is more than in the unfilled or hBN filled epoxy. The space charge encouragement has been reported for silica with other base materials like polyethylene in [85, 86]. Moreover, epoxy resin is a polar polymer [87] and the

incorporation of filler material with many hydroxyl groups, such as silica, could interfere with the chemical reactions that occur during the curing process. This is highlighted by [88], which states that the addition of silica to the epoxy is electrically comparable to increasing the hardener stoichiometric ratio. This emphasises the fact that many interrelated factors are operative in these nanocomposites.

Other contradictory findings indicate that the addition of 10 wt% BN leads to a considerable increase in the DC breakdown strength over the unfilled epoxy [89]. The highest improvement occurred for the smallest particle size (70 nm). No data was given about the crystal structure of the BN used. This brings attention to the subtlety of comparing results which are produced in different studies. For instance, the measured breakdown strength is very sensitive to the sample thicknesses and, therefore, comparing the findings of two studies produced using different sample thickness may be not too fair.

It is worth mentioning that all the above studies are based on DGEBA resin.

2.8.2 Epoxy nanocomposites with treated particles

Many studies indicate that modifying or treating the surface of nanoparticles lead to improved electrical properties, such as the breakdown strength and partial discharge resistance, of the resulting nanocomposites. For example, grafting silane coupling agent with epoxy compatible functionalities onto the silica significantly increases the AC breakdown strength of the nanocomposite over the unfilled epoxy [90]. Similar trends are reported for alumina and magnesia nanoparticles [91]. However, it is not clear if this boost in AC breakdown strength is a result of increasing the compatibility, increasing the dispersion, initiating chemical bonds between the particles and the polymer or reducing the charge traps in the surface of the particles.

Another particle treatment route was proposed in [92]. Here, the nano-silica was treated using a “bimodal brush” technique, where the particles where treated with long epoxy compatible molecules and short electroactive molecules. The long brush is used to improve the particles’ dispersion and the short brush electrically to modify the surface of the particles. The results match well with the aims of the treatment. When the particles were treated with the long brush alone, the dispersion improved but the AC breakdown strength was only marginally enhanced. However, when the bimodal brush was used, it significantly increased from 187 kV/mm for the unfilled epoxy to 257 kV/mm for 2 wt% treated silica filled epoxy. The authors state that the short electroactive molecules reduce the potential needed for the particle’s surface to gain electrons, which mean that the short brush on the silica surface may trap electrons in the composite. This study reveals that the nanoparticle dispersion is not the only factor affecting the electrical performance of nanocomposites.

Another study [93] used atmospheric pressure plasma to modify nano-silica, which had previously been treated with dimethyldichlorosilane. The data indicate that this treatment increases the partial discharge inception voltage and the breakdown strength of the subsequently produced nanocomposites. Due to the energetic ions in the plasma, it is expected that many chemical bonds in the surface silane groups will be broken which leads to highly reactive species covering the surface of the particles. This creates stronger interactions between the nanoparticles and the epoxy matrix [93].

2.8.3 Variation in the reported results (possible reasons)

The variation seen in the reported results for the insulation performance of nanocomposites may be associated with many factors, including the variation in the filler characteristics discussed in section 2.7, the storage conditions of the filler and the prepared samples, which can affect the water content of the tested samples, the preparation routes used to prepare the samples and the testing techniques. The influence of water absorption is discussed in the next paragraph.

Storage conditions and water absorption

The large specific surface area of nanoparticles enables them to adsorb water molecules upon contacting water vapour during storing or processing, as stated in section 2.7 for silicon nitride and silica nanopowders. This might be an origin for the variation in the results seen in the literature, where storage periods and/or conditions may affect the amount of the chemically or physically adsorbed water. Water adsorption onto the nanofiller has a bad effect on the insulation properties of the prepared sample. Storing the nanoparticles in a 50% relative humidity environment for one week reduced the breakdown strength and increased the space charge, dielectric loss and conductivity of the produced nanocomposite samples as reported in [94]. The charge can move through hopping the localized conductive states in the water shell around the particles, which may introduce percolation or sub-percolation paths into nanocomposite materials [3].

The prepared nanocomposites samples are found to absorb water more than the unfilled polymer and the amount of absorbed water depends strongly on the nanofiller material. For example, nano-silica filled polyethylene absorbs more water than the nano-silicon nitride based composites [95]. Modifying the surface of the particles can change this and decrease the water absorption [5, 26].

Chapter 3

Characterization and Experimental Techniques

3.1 Glass transition process

At T_g, an amorphous polymer transforms into a flexible rubbery phase where the polymer chains are capable of changing their conformation. As the temperature increases beyond T_g, the amorphous polymer gradually coverts into viscous fluid where the chain translational motion becomes easier. However, the translational motion is not possible for crosslinked polymers, since the chains are connected to each other via covalent bonds. Therefore, the chains can only change their conformation [96]. For a crosslinked polymer, T_g is affected by the following factors.

1- Degree of crosslinking: as the degree of crosslinking increases, the temperature needed to overcome the intermolecular forces also increases and hence the Tg goes higher. In the limiting case, when the distance between two crosslinking points is relatively small, no transition into the rubbery phase could occur before the polymeric chains start chemically to decompose (thermal degradation takes place) [97].

2- The stiffness of the segments between two crosslinking points: the stiffer the polymeric segment is, the more difficult for it to coil or rotate and the higher T_g is needed. Segments that contains parallel bonds or bulky aromatic groups in their backbone are generally stiff and tend to have high T_g, whereas segments that contain ether bonds are generally flexible and tend to have low T_g [96].

3- Free volume: the free volume is the unoccupied space between the polymer segments. Increasing the free volume will decrease T_g since the polymer segments can move inside the free volume more easily without steric hindrance or interaction with other chains. Any factor affecting the percentage of the free volume like the existence of bulky side groups will affect T_g [98].

To measure T_g, the changing in a thermodynamic property with temperature is observed. For example, the heat capacity increases when the polymer goes from the glassy phase into the rubbery phase and, hence, by observing the heat capacity using technique like differential scanning calorimetry (DSC), it is possible to determine the T_g. Unlike the melting process, the glass transition process does not have latent energy. Other method uses the change happened in the electric permittivity when converting from the glassy state into the rubbery state. At the rubbery state, the polymer segments have higher mobility and more dipolar groups have the ability to orientate themselves in response to the applied

electric field. Thus, a relaxation peak can be detected at the glass transition temperature [99].

3.1.1 Differential scanning calorimetry (DSC)

The DSC measures the difference in the heat flow required for a considered sample and a reference sample to increase their temperature at the same rate. Both the considered and the reference samples are, nominally, kept at the same temperature during the whole test. As the considered sample undergoes the glass transition, its heat capacity increases due to the increase in the segments' mobility and, thus, it needs more heat flow. The DSC curves provide the following information about the glass transition:

1- The temperature range over which the glass transition occurs. The width of this range indicates the homogeneity of the sample. A narrow range means that the polymer chains need similar energy to increase their mobility and convert into the rubbery phase. On the other hand, large transition width is referred to the crosslinking and composition heterogeneity of the sample [100]. In this study, Tg is defined as the temperature at which the gradient of the heat capacity is maximum [43].

2- The increase in the heat capacity, which implies the magnitude of the acquired mobility when converting into the rubbery state. The heat energy can be absorbed by the rotational and conformational motions brought by the rubbery state [96]. Hence, a greater increase in the heat capacity reflects a more mobile molecular structure [29].

3- The enthalpy relaxation area. This parameter refers to the amount of energy needed for the segments to go to their equilibrium positions. The origin of this enthalpy relaxation is as follows. During the curing process while the network is in its rubbery state, the polymer segments can move around their equilibrium positions. Upon finishing the curing process, the network converts into a glassy state and the polymer segments stay in their non-equilibrium positions. If the sample temperature rises to around Tg or more, i.e. during a DSC scan, the polymer segments reach a sufficient energy level which enables them to absorb some energy and go to their equilibrium positions. This absorbed energy results in an endothermic energy peak (enthalpy relaxation peak) superimposed on the (first) DSC scan, see Figure 3.1. The relaxation peak does not appear if a second (or any additional) DSC scan performed to the same sample, since the segments are already in their equilibrium positions after the first DSC scan. Thus, the enthalpy relaxation area can be calculated by subtracting a second DSC scan from the first scan as illustrated in Figure 3.1 [101]. This parameter is sensitive to the storage history of the sample being tested, particularly the storage temperature relative to Tg and the storage period. Storing the sample at temperature near its Tg can enable the

polymer chains to move to their equilibrium positions and hence, the enthalpy relaxation area will decrease.

Additionally, the value of the measured T_g depends on the applied temperature rate. The network cannot respond instantaneously to the increase in temperature and it need some time to reach equilibrium. Thus, for a higher heating rate, the observed T_g is expected to be higher.

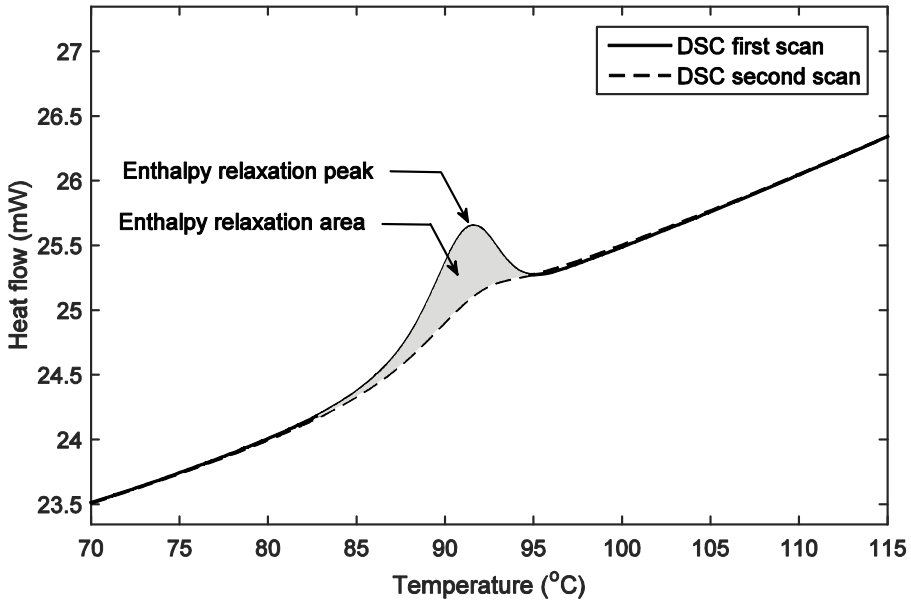

Figure 3.1: Typical DSC first and second scans for a cured epoxy sample, showing the enthalpy relaxation peak.

3.1.2 Measurement settings

The glass transition was observed using a Perkin Elmer DSC 7 differential scanning calorimeter A specimen of ~10 mg in mass was used to perform two consecutive DSC scans at a heating rate of 10 °C/min. The obtained DSC traces were normalized with respect to sample mass after subtracting the filler mass, since the filler does not contribute to the glass transition. The glass transition process was characterized using four parameters: the glass transition temperature (T_g), the glass transition width (ΔT_g), the increase in the heat capacity (ΔC_p) and the enthalpy relaxation area. The first three parameters were extracted from the second DSC scan, in the absence of enthalpy relaxation effects. The enthalpy relaxation area was calculated by subtracting the second DSC scan from the first, as explained above. The equipment was calibrated using indium, which has a known melting temperature of 156.6 °C. The experiment was done under nitrogen environment. For each material, the measurements were repeated three times using different specimens, in order to determine the uncertainties in these measurements.

3.2 Dielectric spectroscopy

Dielectric spectroscopy of a material offers a powerful tool for monitoring the dipole content and mobility and understanding the molecular behaviour of that material. Hence, by observing the dielectric spectra of nanocomposites, one can deduce useful information about the influence of adding nanoparticles on the polar content and on the dynamics of dipolar groups. The desired value of the dielectric constant or relative permittivity (ϵ_r) depends on the considered application. For energy storing applications like capacitors, high value of ϵ_r is desired. However, the high value of ϵ_r should not be at the expense of the breakdown strength since the magnitude of the stored energy increases linearly with ϵ_r and quadratically with the breakdown strength. For power transmission applications like power cables, low value of ϵ_r is desired to reduce the capacitance of the long cables and subsequently reduce the capacitive power which is otherwise needed to charge/discharge the cable during the power transmission. Additionally, low ϵ_r indicates lower probability of relaxation processes and lower dielectric loss.

The value of the dielectric constant is associated with the polarisation occurred due to the applied electric field. The electric polarisation in solid dielectrics can be ascribed to the following sources:

1- Electronic polarisation: The applied electric field will slightly shift the centre of the electronic clouds with respect to their positive nucleus which will generate induced dipoles in the dielectric material. Thus the electronic polarisation is attributed to a slight displacement of the electrons and it is generally independent of the dielectric's temperature.
2- Atomic polarisation: When the molecules of the dielectric contain two or more different atoms unsymmetrically sharing the electrons, the electric field can distort the bonds between these atoms and consequently generate atomic polarisation. Thus, in this type of polarisation, the electric field disturbs the arrangement of the atoms in the molecules or the lattice of the dielectric.
3- Orientation polarisation: In the materials that have permanent diploes, the electric field will try to align these dipoles along its direction. This results in a net polarisation in the direction of the electric field.

These types of polarisation contribute variously to the total polarisation and their contributions depend on the temperature of the material and the frequency of the electric field. The electronic polarisation, which is attributed to the shift of the electrons, can follow the oscillation of the electric field at high frequencies up to the frequencies of visible light. On the other hand, orientation polarisation, which is related to alignment of relatively heavy dipolar groups, cannot follow the alternating of the electric field at high frequencies, therefore, these dipoles will "relax" at these frequencies. As illustrated in Figure 3.2, at constant temperature, the highest possible polarisation (which implies highest ϵ_r) occurs at

low frequencies since the total polarisation is due to the contributions from all possible polarisation types. As the frequency increases, the orientation polarisation will not contribute to the total polarisation and hence the total polarisation will decrease. Similar thing will happen to the atomic polarisation but at higher frequencies.

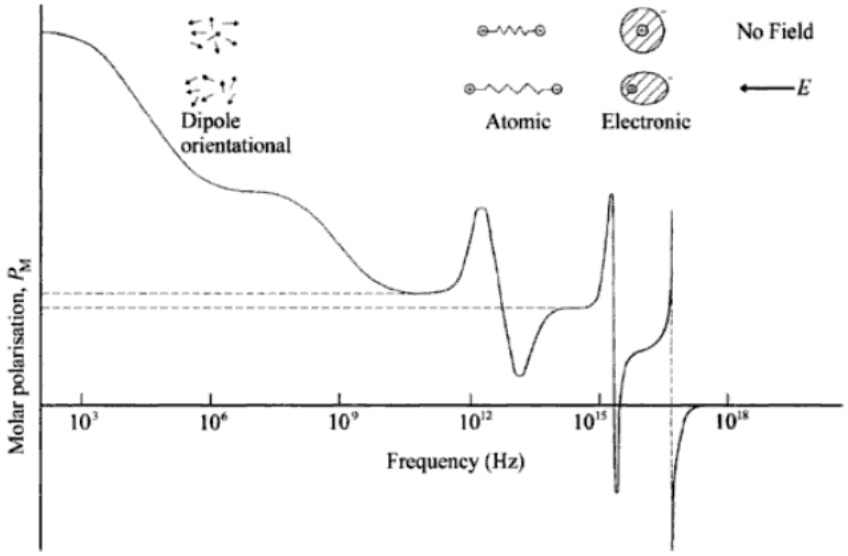

Figure 3.2: The relaxation of different polarisation types as a function of the frequency [99].

All types of polarisation need time to response to the incident electric field. Debye suggested using the term "dielectric relaxation time (τ)" to refer to the time required for the polarisation to reach 63.2 % of its final or equilibrium value. He assumed that the polarisation exponentially approaches its equilibrium value. For high frequencies with cycle time comparable to τ, the polarisation firstly starts to delay behind the electric field and finally becomes out of phase and loses its synchronisation with the electric field. Thus it stops following the electric field and relaxes. This process is called relaxation process. The polarisation and consequently the relative permittivity can be divided into two components, the first one is in phase with the electric field and the other is 90^o lagging the electric field. Mathematically, it is convenient to represent the two component using complex numbers:

$$\epsilon_r^* = \epsilon_r' - i\epsilon_r'' \qquad \text{Eq. 3.1}$$

where ϵ_r' represents the relative permittivity in phase with the electric field, ϵ_r'' represents the relative permittivity 90^o lagging the electric field and ϵ_r^* is the complex relative permittivity. The real permittivity will give displacement current 90^o leading the electric filed (capacitive current) whereas the imaginary permittivity will result in displacement current in phase with the electric field (resistive current) and hence it will represent loss in the dielectric material. The ratio between the resistive component, ϵ_r'', and the capacitive components, ϵ_r', is called loss tangent:

$$tan\,\delta = \frac{\epsilon_r''}{\epsilon_r'} \qquad \text{Eq. 3.2}$$

Every polarisation type has its own relaxation time and hence it will relax at a different frequency as indicated in Figure 3.2. Relying on the relaxation time, many models were suggested to estimate the value of ϵ_r^* over the relaxation process. The first model proposed by Debye is given by:

$$\epsilon_r^* = \epsilon_\infty + \frac{\epsilon_s - \epsilon_\infty}{1 + i\omega\tau} \qquad \text{Eq. 3.3}$$

where ϵ_∞ represents the instantaneous polarisation response (relative to the considered frequencies), ϵ_s is the static or equilibrium response and ω is the frequency. The term $\epsilon_s - \epsilon_\infty$ represents the relaxation strength, i.e. it represents the amount of the polarisation that will be relaxed through this relaxation process. As an example, Figure 3.3 shows a plot for ϵ_r' and ϵ_r'' as a function of ω for τ = 0.001 s, ϵ_∞ = 1 and ϵ_s = 7. The relaxation peak occurs at $\omega = 1/\tau$ = 1000 rad/s in this case. This model describes the frequency dispersion in the dielectric constant caused by one relaxation process. Additional relaxation processes can be described similarly over different frequency ranges. Other empirical equations based on Debye model, like Cole-Cole and Havriliak-Negami equations, were suggested to better fit the experimental results [99].

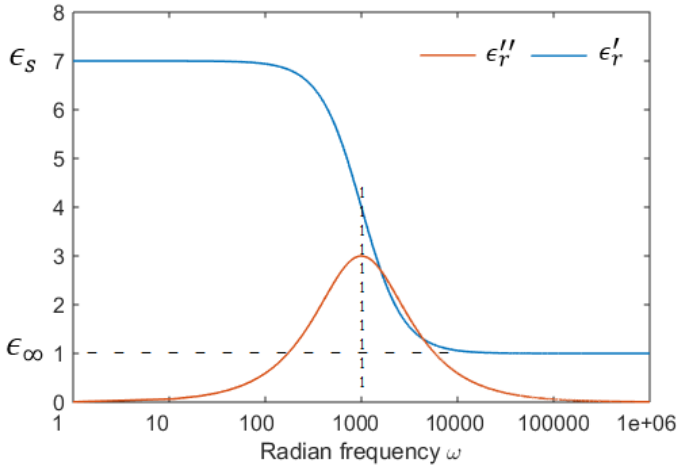

Figure 3.3: The real and imaginary relative permittivity as a function of frequency, based on Debye model.

In solid dielectric like cured epoxy, several relaxation processes are usually found and they are conventionally labelled α, β, and Υ. Traditionally, α relaxation occurs at low frequencies and it is related to the motion of the dipoles caused by large segments. β relaxation takes place at higher frequencies and it is related to the motion of smaller dipolar groups. Υ relaxation is related to the motion of individual groups like amine or epoxy groups and occurs at high frequencies [102].

In addition to the frequency dispersion, dielectric spectroscopy is affected by the temperature of the dielectric material, which leads to thermal dispersion. High temperature supplies the dipolar groups with the activation energy needed for these dipoles to orientate themselves in response to an electric field. As the temperature decreases, the mobility of the polymeric segments decreases, which reduces the polarisation and results in a relaxation process. In a crosslinked epoxy, the glass transition is always accompanied by a relaxation process. At temperatures higher than T_g, polymeric segments are capable of changing their conformation, which enables the rigidly attached dipolar groups to align with the applied electric field. For temperature less than T_g, the polymeric segments are frozen in position which reduces the possible polarisation, see section 3.1. Same labels used for the frequency relaxation are deployed for the thermal relaxation. The relaxation occurred at the glass transition which is related to mobility of large segments is labelled by α. The relaxations that may occurred at lower temperatures and associated with smaller dipolar groups are labelled β, Υ, and so on [99].

3.2.1 Measurement settings

Dielectric spectra were measured using a Solatron 1296 dielectric interface along with a Schlumberger SI 1260 impedance/phase gain analyser. The instrument represents the dielectric sample by a series lumped circuit, where it gives the values of the resistor and the capacitor representing this equivalent circuit. The values of $tan\,\delta$, ϵ_r' and ϵ_r'' are calculated by the accompanying software using the following equations.

$$tan\,\delta = R_s C_s \omega \qquad \text{Eq. 3.4}$$

$$\epsilon_r' = \frac{C_s}{C_o(1+tan^2\delta)} \qquad \text{Eq. 3.5}$$

$$\epsilon_r'' = \frac{R_s \omega C_s^2}{C_o(1+tan^2\delta)} \qquad \text{Eq. 3.6}$$

where R_s is the equivalent series resistor, C_s is the equivalent series capacitor, ω is the frequency in rad/s and C_o is the capacitance with free space between the electrodes.

The thickness of the used samples was 200 ±10 μm. Initially, a thin layer of gold was sputter coated onto both sides of each specimen, in order to improve the contact between the sample and the electrodes of the measurement cell. The measurement cell consists of two circular parallel electrodes with a diameter of 30 mm in addition to guard electrodes to reduce fringing effects and to maintain a uniform electric field between the electrodes. The voltage applied to the electrodes was a sinusoidal wave of 1 V. Data were measured at 5 points per decade. At each point, the measurements were averaged over 10 cycles.

3.3 DC conductivity

Evaluating the DC conductivity of a material can give valuable information about the charge mobility in this material at an electric stress much lower than the electric field at the breakdown. This can help in explaining the electrical behaviour of the considered material, for example, the DC conductivity can affect the dielectric spectra at low frequencies. Also characterising the behaviour of the DC conductivity of a material can show if there is a relation between the charge mobility in that material and its breakdown strength.

Values for the DC conductivity were established by measuring the current passing through a specimen from the material of interest, using a Keithley 6487 picoammeter. The specimen was placed between two opposing circular electrodes, 20 mm in diameter. The thickness of the samples is 200 ±10 μm and they were initially gold sputtered on both sides, to improve sample/electrode contact. For each sample, the measurement continued for at least 2 h at a sampling rate of one measurement per minute. The measurements were performed at an applied electric field of 42.5 V/mm, which is the maximum value that can be obtained from the equipment used and it was chosen to increase the signal to noise ratio of the measurement in order to get more accurate results. During the measurement, the temperature was controlled using a fan oven and the measurement was performed at different temperatures to investigate the temperature dependence of the DC conductivity.

Generally, the measured current is made up of two components, capacitive component and conductive component [49]. The capacitive component is due to the charging or polarisation current and its value falls off with time, where its decay rate depends on the capacitance of the sample between the electrodes (i.e. its geometry and ϵ_r'). The conductive component is a function of the material characteristics and its conditions during the measurement, which include its temperature and water content [49].

3.4 Breakdown strength

For insulation materials, the breakdown strength or dielectric strength is an important parameter. Breakdown could happen through fast mechanisms, known as short term breakdown, or slow ageing or degradation mechanisms, known as long term breakdown. The fast mechanisms include electric, thermal, or electro-mechanical breakdown mechanisms whereas the slow mechanisms include partial discharge and electrical trees, which gradually growing in the insulator until the breakdown takes place. Unfortunately, the processes that lead to the breakdown in solids are not well understood yet [103, 104].

3.4.1 Measurement settings

In this study, the focus is on short term breakdown strength. DC and AC breakdown measurements were performed in accordance with ASTM D3755-14 and ASTM D149

respectively. The sample was placed between two steel ball bearing electrodes, 6.3 mm in diameter, which were changed every 5 measurements to avoid pitting influencing the derived data. The test cell is immersed in silicone oil to prevent any surface flashover. The thickness of all samples used in this test was nominally 70 μm. The voltage ramp rate was 50 V/s for AC breakdown measurements and 100 V/s for DC breakdown measurements, and the testing occurred at room temperature (~23 ^{o}C). Typically, at high ramp rate, the material does not have enough time to develop a breakdown, particularly via the relatively slow mechanism like thermal mechanism and, therefore, it is expected to measure relatively higher breakdown strength when applying higher ramp rate. The effect of the sample thickness on the measured breakdown strength is discussed in the next section.

3.4.2 Sample thickness

The breakdown strength is greatly dependent upon the sample thickness. Experimental data show that it changes inversely as a fractional power of the sample thickness, as indicated by the empirical relationship in Eq. 3.7 [105].

$$E_2 = E_1 * \left(\frac{t_2}{t_1}\right)^n \qquad \text{Eq. 3.7}$$

where t_1 and E_1 are the thickness and the breakdown strength of the first sample and t_2 and E_2 are the thickness and the breakdown strength of the second sample. The value of the power coefficient (n) is also dependent on the thickness range. For sample thickness ranges between 0.5 mm and 3 mm, n was estimated in [106] to be around 0.65 for unfilled or alumina filled epoxy nanocomposites. For thinner samples, n was estimated to have a value of 0.4 [107].

Another study found that for unfilled epoxy with a thickness between 50 and 1000 μm, the breakdown strength follows an exponential relation with the thickness as expressed in Eq. 3.8 [108].

$$E = E_o\, e^{-kt} + E_\infty \qquad \text{Eq. 3.8}$$

where E_o and E_∞ are constants with the values of 172 ±6 and 32 ±5 kV/mm, respectively, and t is the thickness in μm and k is a fitting constant, which has a value of 0.0033.

The underlying mechanisms for this thickness dependent breakdown strength have not been fully understood yet. A common explanation for this phenomenon is that increasing the sample thickness results in an increase in the probability of a defect or impurity being located in the progressive conduction path which leads to breakdown. Other proposed interpretation implies that the surface processes are more significant than the bulk processes during the breakdown [109, 110].

3.4.3 Breakdown data analysis (Weibull distribution)

Electrical breakdown represents a phenomenon where the breakdown occurs randomly whenever there is enough electric stress to create a conductive bath between two electrodes. The most commonly utilized function to analyse the breakdown data is Weibull function. Mathematically, the Weibull cumulative distribution function is given by:

$$F(E,\eta,\beta) = 1 - \exp[-(E/\eta)^{\beta}] \qquad \text{Eq. 3.9}$$

where η is the scale parameter, β is the shape or slope parameter, and E is the electric field. Eq. 3.9 gives the cumulative failure probability (i.e. of a breakdown taking place) when the electric field is $\leq E$. It uses two parameters, η and β, where the Weibull third parameter, the location parameter, is assumed to be zero and that is why it is called two parameter Weibull function. η indicates the range at which the breakdown occurs and literally it gives the value of the electric field where the cumulative probability of the breakdown is $1 - e^{-1}$ or 63.2%. β reflects the scatter in the data, where a high β value means that the breakdown occurs over narrow range and low β value means that the breakdown measurements are scattered over a wide range of electric field. For each set of breakdown measurements, the best fit η and β parameters are calculated using a software program based on the maximum likelihood estimation, like Matlab or the Reliasoft Weibull 7++ software. To visualize the Weibull distribution, normally, an adjusted version of Eq. 3.9 is deployed. Mathematical manipulation of Eq. 3.9 can generate the formula in Eq. 3.10. Using Eq. 3.10, a straight line with a slope of β and x-axis displacement of $\beta \log(\eta)$ can be obtained by plotting $\log\left[-\ln\left(1 - F(E)\right)\right]$ against $\log(E)$. After plotting the straight line the labels of the x-axis and y-axis are mapped to the corresponding electric field and probability of failure, $F(E)$, respectively. This method of visualizing the Weibull function provides easily readable Weibull graphs, where the most important information like the scale and shape parameters can be easily seen from the graph.

$$\log\left[-\ln\left(1 - F(E)\right)\right] = \beta \log(E) - \beta \log(\eta) \qquad \text{Eq. 3.10}$$

In practice, the cumulative failure probability for each experimental breakdown measurement is approximated using Bernard's approximation:

$$F(E_i) = \frac{i - 0.3}{n + 0.4} \qquad \text{Eq. 3.11}$$

where n is the total number of performed breakdown tests, i is the order of the breakdown electric field after ascendingly sorting the measured breakdown data, where the smallest measured breakdown strength takes $i = 1$ and the largest takes $i = n$. The data then are scattered on the plot using Eq. 3.10 [111].

3.5 Scanning electron microscopy

Scanning electron microscopy (SEM) is used to observe the particle dispersion within the epoxy matrix. The SEM image depends on the signals emitting from the specimen when an accelerated beam of electrons impinges on it. The smaller the diameter of the electronic beam, the more resolution is achieved. This is why an SEM with a field emission electron gun gives higher resolution than an SEM with a thermal electron gun. The diameter of the electron beam emitted from a field emission electron gun is on the order of nanometres. The beam accelerating voltage determines the energy of the electron beam. Higher accelerating voltages increase the electron beam current and increase the energy of the electrons incident into the specimen which result in increasing the beam penetration into the specimen [112].

The signals emitted from the specimen when the electron beam is incident upon it include secondary electrons, backscattered electrons and X-rays. The secondary electrons are emitted due to inelastic collisions between the beam electrons and the electrons in the atoms of the specimen. The secondary electrons have low energy (< 50 eV), therefore they only escape from regions which are approximately less than 50 nm under the surface of the sample. Backscattered electrons are beam electrons which elastically collide with the sample's atoms and change their direction to the surface of the sample. These electrons have high energy and can escape from deep regions under the surface of the sample. X-rays are released when the vacancies created due to the emission of the secondary electrons are filled by higher level orbital electrons. The emitted X-ray is a characteristic for each element and can be used to identify the composition of the sample. The X-rays have deeper escape depth than both secondary and backscattered electrons [112].

A JEOL JSM-6500F scanning electron microscope with an accelerating voltage of 15 kV was used in this study. This SEM has a thermally assisted field electron gun. To observe the dispersion in the bulk of the samples, a cryo-fracturing method was used. Plaque samples 2 mm in thickness were cooled in a liquid nitrogen for 15 min before being fractured and, consequently, exposing an internal surface from the material. This method exposes an internal surface from the nanocomposite without deforming or tearing the polymer in a way that might affect structural observation. A very thin layer of gold was sputtered on the samples to prevent charge accumulation during SEM examination.

3.6 Fourier transform infrared spectroscopy

Fourier transform infrared (FTIR) spectroscopy is a technique that can provide information about the chemical composition of a material. It is based on the interactions between infrared (IR) radiation and chemical components of the involved material. Whenever the frequency of the IR radiation matches the characteristic frequency of vibration of a functional group or molecule in the concerned material, IR absorption occurs and, thus,

the intensity of the radiation will decrease. By comparing the radiation intensity, with respect to the frequency, before and after passing through the sample, information about the chemical content of the sample can be deduced.

In the current study, this technique was used to observe the extent of crosslinking reaction and to monitor the concentration of different chemical groups in cured epoxy samples. Additionally, the technique was employed to characterise the surface chemistry of the Si_3N_4 nanopowder.

FTIR spectroscopy measurements were performed using a Perkin Elmer Spectrum GX spectrometer. The FTIR spectrum of each material was collected from 580 cm-1 to 7800 cm^{-1} in transmission mode; 32 scans were performed at 4 cm^{-1} resolution. For cured epoxy, 70 mm thick samples were used without further preparation. For nanopowder, about 1 mg of the considered nanopowder was mixed with 150 mg of ground potassium bromide (KBr) and then the mixture was pressed into a KBr disc.

Chapter 4

Materials Processing and Sample Preparation

4.1 Introduction

The surface chemistry of a nanofiller is a key characteristic that crucially determines its impact on a host matrix. Within the boundary of a nanoparticle, the surface chemistry may affect the characteristics of the particle interphase, as outlined in section 2.4. When the particle is embedded in a polymeric matrix, the surface chemistry governs its interactions with the host polymer and thus affect the characteristics of the polymer interphase. Also, these interactions affect the dispersion of the nanoparticles within the polymer. Furthermore, the surface chemistry of the particles determines their tendency to adsorb water. Therefore, it is of paramount importance to precisely characterise the surface chemistry of a nanofiller before introducing it into a polymer matrix. This chapter is set out to characterise the surface chemistry of Si_3N_4 nanoparticles using FTIR spectroscopy. The chapter also investigate the influence of heat treatment on the surface chemistry of Si_3N_4 nanoparticles. In addition, the experimental procedure used to produce and process nanocomposite samples is illustrated in this chapter.

4.2 Basic materials

The basic materials used in this study are listed below, along with useful information about each of them, as provided by the manufacturers.

1- Silicon nitride: silicon nitride (Si3N4) amorphous nanopowder was utilized as the filler material in all the samples produced in this study. The powder was obtained from Sigma Aldrich (product number 636703); the manufacturer states a spherical shape and a particle size < 50 nm.
2- Silica: although silica nanoparticles did not used in any of the prepared nanocomposite samples in this study, studying its surface chemistry may be useful for understanding the surface chemistry of the Si_3N_4 nanoparticles. As indicated in section 2.7, the surface of Si_3N_4 may be partially oxidised to silica, therefore, comparing the FTIR spectra obtained from both Si_3N_4 and SiO_2 nanopowder and their interaction with water might provide better understanding for the surface chemistry of the Si_3N_4 nanoparticles. Specifically, the powder employed for this purpose was obtained from Sigma Aldrich (product number 637238) with a quoted particle size range of 10 - 20 nm.

3- Epoxy resin: the epoxy resin used in this study was DER 332, DGEBA based resin, obtained from Sigma Aldrich. This resin has a mean molar mass equalling 348 g/mol.
4- Hardener: the hardener used to cure the epoxy resin was Jeffamine D-230, aliphatic diamine hardener obtained from Huntsman.

4.3 Filler heat treatment and surface chemistry

4.3.1 Particle heat treatment at 200 °C

To remove the water molecules, which might be physically adsorbed on the surface, the nanopowder was dried at 200 °C. As discussed in section 2.7, at 200 °C, the surface hydroxyl or amine groups will not be affected [69]. This step was done to eliminate the possibility of forming water shells around the particles and, hence, offset the effect of water absorption. Furthermore; by monitoring the weight, the magnitude of the weight reduction after this heat treatment should provide an indication of the density of the OH groups on the surface of the nanoparticles.

Around one gram of both nano-Si_3N_4 and nano-SiO_2 were heated in a fan oven at 200 °C for one week. Results of mass monitoring (Table 4.1) indicate that the Si_3N_4 nanopowder showed a slight decrease in its weight while the silica nanopowder showed a considerable reduction in its weight. Compared with silica nanopowder, these results suggest that silicon nitride does not absorb a lot of water when it is stored under ambient conditions. This can be ascribed to the surface of silicon nitride being partially covered by amine groups, which are less polar than hydroxyl groups. Further, Fubini *et al.* [69] reported that the hydroxyl groups on silicon nitride have slightly less acidity than the corresponding ones on silica.

Table 4.1: Particles weight reduction due to the heat treatment.

Nanofiller	Weight before heat treatment at 200 °C (mg)	Weight after heat treatment at 200 °C (mg)	Weight reduction percentage (%)
Si_3N_4	1024	1008	1.6
SiO_2	1174	978	16.2

4.3.2 Particle heat treatment at 1050 °C

As proposed by the particle interphase model (section 2.4), the particle interphase may play a fundamental role in nanocomposite electrical behaviour. In order to investigate this proposition, part of the silicon nitride nanopowder was heated at 1050 °C for 10 h in a nitrogen environment, in an attempt to modify the particle interphase of the nanofiller. This heat treatment is expected to remove the active amine and hydroxyl groups, release any

foreign atom on the surface and produce a surface covered by stable siloxane bridges (section 2.7). According to the discussion in section 2.4, this will affect the charge traps and the electronic energy states within the particle interphase. Furthermore, this surface treatment is distinguished from other surface treatment by its simplicity, where it can produce a relatively well-defined surface chemistry. For example, in silane surface treatment, it is impossible to ensure that the silane molecules replace all the surface hydroxyl groups. Additionally, the silane molecules can condense with each other resulting in a complicated surface chemistry.

To discriminate between the two heat treatments, the powder which was dried at 200 ^{o}C is termed SiN, whereas the powder calcinated at 1050 ^{o}C is termed SiN-C.

4.3.3 Nanofiller surface chemistry

FTIR spectra obtained from the both the dried and calcinated Si_3N_4 nanoparticles are presented in Figure 2.1.

The FTIR spectra of dried nanoparticle confirm the existence of both the amine (NH) and hydroxyl (OH) groups. The absorption peak centred at 3422 cm^{-1} is related to the OH vibrations and the overlapping band with a spike centred at 3140 cm^{-1} is assigned to the NH vibrations [76, 113, 114]. The broadening of both of these peaks is an indicator of hydrogen bonded amine and hydroxyl groups, which also implies a high density for the presence of these groups [113, 114]. The sharp peak at 1400 cm^{-1} corresponds to the Si_2-NH deformation mode [76]. The absorption at 1633 cm^{-1} can be attributed to molecule water [115], the intensity of this peak does not decrease after heating the particles at 1050 ^{o}C indicating no physically adsorbed water was still present on SiN. The absorption between 750 cm^{-1} and 1150 cm^{-1} is due to two overlapping peaks, one at 965 cm^{-1}, which is attributed to the backbone vibration of Si-N-Si bonds, and the other at 1075 cm^{-1}, which is associated with the stretching vibration of Si-O-Si bonds (siloxane bridges) [76, 116]. The existence of Si-O-Si is indicative of part of the particle surface being oxidised to silica [75, 76]. The weak absorption between 2800 cm^{-1} and 2900 cm^{-1} can be assigned to C-H stretching. A similar C-H absorption was reported by Li *et al.* [75], who referred the existence of this bond to the reaction between SiN_2H and CO_2 absorbed from air. In conclusion, the FTIR spectra of the dried Si_3N_4 nanopowder indicate a complex surface chemistry characterized mainly by the presence of NH and OH groups, and impurities.

Heating the powder at 1050 ^{o}C (SiN-C) results in remarkably different spectra. The disappearance of the peaks at 3140 cm^{-1} and 1400 cm^{-1} evidently mark the removal of the NH groups. Furthermore, the peak at 1075 cm^{-1} becomes stronger, whereas the peak at 965 cm^{-1} becomes very weak. This implies a higher Si-O-Si concentration accompanied by depletion of some of the Si-N-Si bonds [75]. The weakness of Si-N-Si absorption and

the absence of the amine groups implies that this absorption originates from the Si-N-Si in the bulk of the particles, rather than on the surface, particularly since the spectra were collected in transmission mode [75]. Therefore, the spectra of calcinated Si_3N_4 particles suggest that the surface of the particles is covered by a silica layer. Additionally, the presence of a peak at 813 cm^{-1}, assigned to siloxane bridges, and the absence of any peak at ~951 cm^{-1}, which is normally observed for silica and assigned to Si-OH groups [115], suggest that the silica layer on the particles surface is terminated with siloxane bridges rather than silanol groups. The same conclusions about the surface chemistry of silicon nitride powder upon heating at > 1000 ^oC have been reported elsewhere [75]. To further confirm this above, FTIR spectra of a silica powder which was subjected to the same heat treatment (SiO-C), is collected and shown in Figure 4.2. Comparing the spectra of SiN-C and SiO-C shows that they are similar apart from two differences. The first one is that the Si-O-Si peak at 813 cm^{-1} are stronger in case of SiO-C, which is expected, since the Si-O-Si bonds exist in the bulk and on the surface of these silica particles. The other difference is the absence of any absorption around 965 cm^{-1} in case of SiO-C, which is due to the existence of this bond in the bulk of the silicon nitride powder and its absence in the bulk of the silica powder.

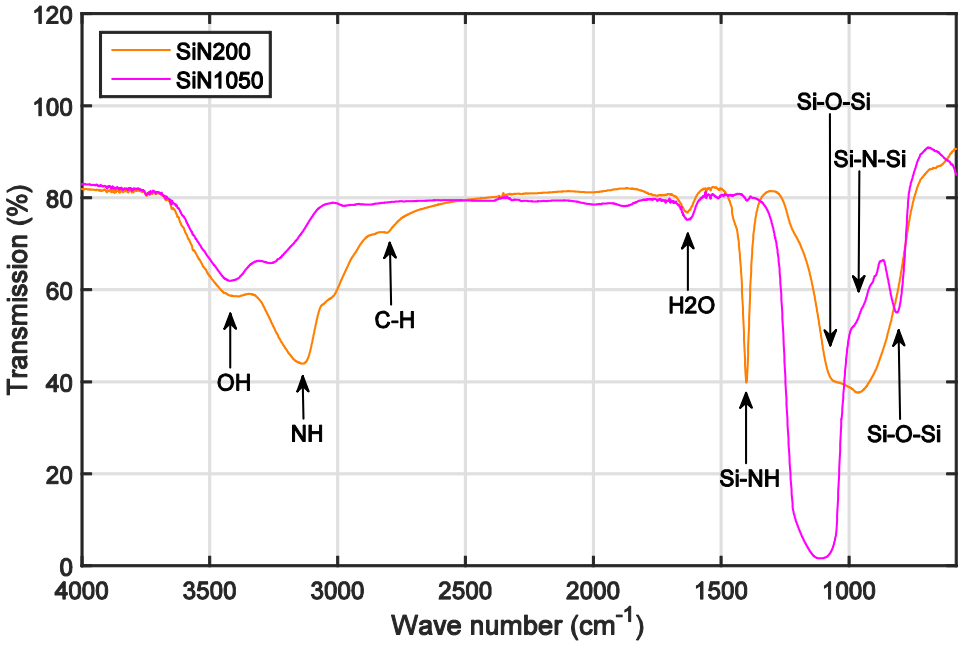

Figure 4.1: FTIR spectra for SiN and SiN-C nanoparticles.

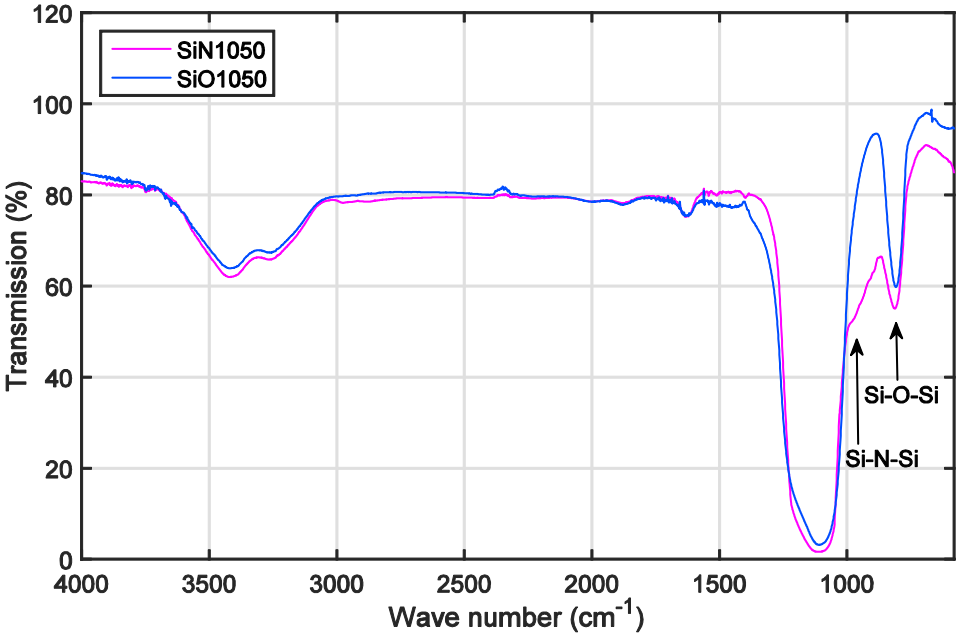

Figure 4.2: FTIR spectra for SiN-C and SiO-C nanoparticles.

4.4 Nanocomposite sample preparation

Initially, the required mass of the epoxy resin was weighed and degassed at 50 ºC at full vacuum. This step is done to purify the resin from any absorbed water or solvent, and to warm the resin so as to reduce its viscosity and enable easier processing. To prepare a nanocomposite sample, the required mass of the nanofiller was added to the resin, according to the targeted filler loading ratio. It is worth mentioning that the filler loading ratio is defined as the weight of the added nanofiller as a percentage of the weight of the whole sample (the weight of the resin + the weight of the hardener + the weight of the filler). The nanofiller was manually mixed with the resin, and then a probe sonicator was used for 45 min to further disperse the particles. The selection of this method for dispersing the nanoparticles in the epoxy resin based upon the studies reported in [33, 108], which compared between different mixing regimes and found that using sonication can effectively disperse nanoparticles in an epoxy matrix. The duration of the sonication depended on the work of Yeung [117] who studied the impact of changing the sonication period on particle dispersion using SEM microscopy.

Subsequently, the hardener was added and thoroughly mixed with the resin using a magnetic stirrer for 15 min at room temperature. Once the hardener is added, the curing process will start, therefore, a care was taken not to allow the processing temperature to be greater than 40 ºC in order to slow down the crosslinking reaction and increase the pot life of the mixture. After that, the mixture was degassed at 35 ºC to for 20 min, before casting it into a steel mould, with a specified thick spacer, for curing. Based on the manufacturer's instructions, the curing was performed in a fan oven for 2 h at 80 ºC followed by 3 h of post-curing at 125 ºC. After the curing process, the sample was left to slowly cool down

for 12 h before taking it for further processing and examination. Each material type was produced in two thicknesses: 70 ± 5 µm for dielectric breakdown measurements and infrared spectroscopy, and 200 ± 10 µm for dielectric spectroscopy and DC conductivity measurements.

The above described preparation steps are summarised in the flowchart shown in Figure 4.3. Most of these steps are in accordance with epoxy nanocomposite preparation methods developed by a number of authors [33, 83, 108, 117, 118], and thus more information about different preparation methods can be found in these references.

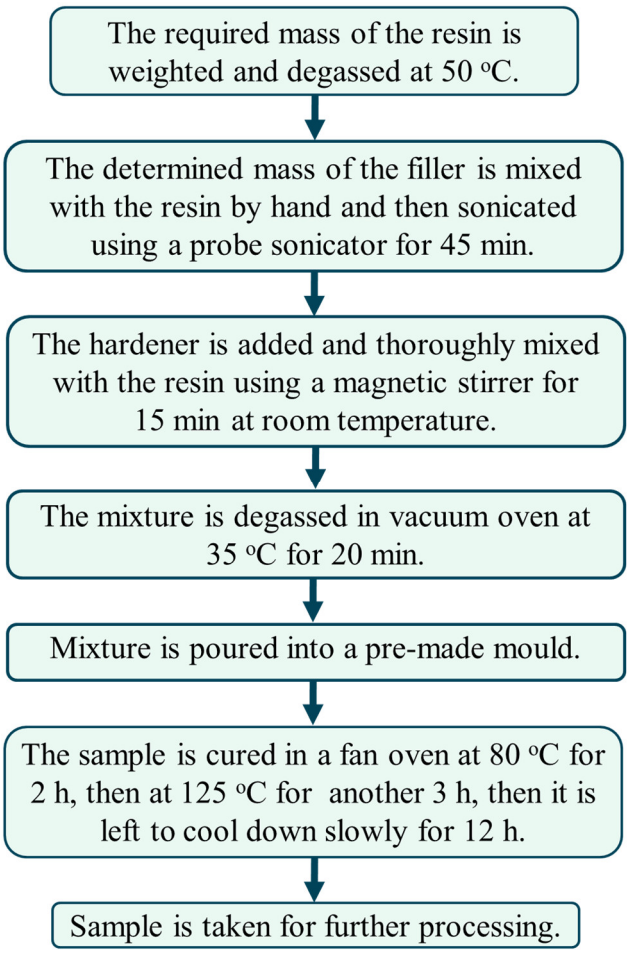

Figure 4.3: A flowchart showing the experimental procedure used for sample preparation.

4.4.1 Resin : hardener mass ratio

a) Stoichiometric formulation:

The stoichiometric resin : hardener mass ratio can be achieved when each epoxy group has one counterpart active hydrogen atom in the amine group of the hardener. This ratio should give the maximum degree of crosslinking, where no epoxy or amine groups are left unreacted. Theoretically, this ratio can be calculated using the following equation [83]:

$$Hardener\ mass = \frac{Amine\ hydrogen\ equivalent\ molar\ mass}{Epoxy\ equivalent\ molar\ mass} \times Resin\ mass \qquad \text{Eq. 4.1}$$

In this equation, the epoxy equivalent molar mass is the mass of the epoxy resin which gives one mole of epoxide group and the amine hydrogen equivalent molar mass is the mass of the hardener which gives one mole of active amine hydrogen. According to the manufacturers, the epoxy equivalent molar mass for DER 332 = 174 g/mol and the amine hydrogen equivalent molar mass for Jeffamine D-230 = 60 g/mol, thus, the optimum resin/hardener mass ratio is 1000/344.

Empirically, the stoichiometric ratio or the maximum degree of crosslinking is, in most cases, associated with the highest T_g of the cured epoxy. Consequently, the optimum stoichiometric ratio can be obtained by changing the hardener/resin ratio and monitoring the T_g of the cured product [119]. The empirical method should give a more accurate ratio, since it considers the actual work conditions. According to the manufacturer, the empirical stoichiometric ratio is very similar to the calculated one [65], hence the theoretical resin/hardener ratio of (1000/344) is taken as a reference and termed the stoichiometric or optimum ratio.

b) Non-stoichiometric formulations

The FTIR spectra has revealed the presence of amine groups on the surface of the Si_3N_4 nanoparticles, which can react with the epoxy groups in the resin. Therefore, the addition of Si_3N_4 nanoparticles may reduce the epoxy groups available for reaction with the hardener's amine groups and, thus, affect the effective resin/hardener stoichiometry. Exploring this possibility necessitates firstly investigating the impact of changing the resin/hardener stoichiometry on the properties of the unfilled epoxy system, which is the subject of chapter 5, and then studying if there is a correlation between the addition of the nanofiller and changing the resin/hardener stoichiometry; if such correlation can be demonstrated, then this may be considered as an evidence for the expected effect of the nanofiller on the network stoichiometry. Therefore, the study will employ different resin/hardener ratios other than the stoichiometric ratio. At this point, it is convenient to define a new parameter, the hardener percentage (*HP*), to distinguish between different resin/hardener formulations. This parameter is defined by Eq. 4.2,

$$HP = \frac{mass\ of\ the\ hardener\ used}{hardener\ stoichoimetric\ mass}\ \% \qquad \text{Eq. 4.2}$$

where the hardener stoichiometric mass equals 0.344 of the resin mass. Based on this definition, formulations with $HP > 100$ % contain excess amine groups and are termed amine rich samples. Analogously, formulations with $HP < 100$ % are called epoxy rich samples.

4.4.2 Sample processing

After the curing process, the produced samples were directly stored in a vacuum oven with dried silica gel at room temperature for at least 14 days, in order to remove any water absorbed during the preparation process. At the end of this period, the mass of each sample was monitored and considered as the dry sample mass. At this point, the samples were split into two groups, dry samples and wet samples. The dry samples were kept in vacuum until performing the required measurements. The wet samples were exposed to controlled environment with a relative humidity (RH) of ~60 % and a temperature of 22.5 ^{o}C, and their masses were periodically monitored over a period of 14 days. After this period, the wet samples were subject to different characterisations to investigate the impact of water absorption on the considered properties. The selection of 60 % RH and 22.5 ^{o}C for the conditioning environment is because these conditions are similar to the lab ambient conditions, which reduces the change in the water content of the wet samples during their characterisation processes. If the difference between the two conditions is too big, then the considered sample may lose or gain water during its property characterisation process, depending on the lab conditions with respect to the chosen conditions.

4.4.3 Sample coding

The samples prepared in this study can be identified by two parameters, the employed resin/hardener formulation, which is represented by the *HP*, and the nanofiller used and its loading ratio. Accordingly, each sample was given a code which consists of two parts, the first part refers to the *HP* used in the samples and the other part refers to the filler loading. For example, E/100H/0 refers to an epoxy cured with 100 % hardener percentage (stoichiometric ratio) without any filler, this sample is taken as a reference for all other samples; 80HP/5SiN refers to an epoxy cured with 80 % hardener percentage (i.e. epoxy rich sample) and containing 5 wt% of dried silicon nitride nanoparticles; 110HP/2SiN-C refers to an epoxy cured with 110 % and filled with 2 wt% of calcinated silicon nitride nanoparticles.

Chapter 5

Effect of Resin/Hardener Stoichiometry on Electrical Behaviour of Unfilled Epoxy

5.1 Introduction

As was indicated in the previous chapter, it is suspected that the amine groups existing on the surface of Si_3N_4 particles chemically react with the resin's epoxy groups. This implies that the particles could affect the resin/hardener stoichiometry, where incorporating Si_3N_4 nanoparticles might increase the active amine content. To investigate this hypothesis, the effect of changing the resin/hardener stoichiometry of the unfilled matrix is firstly investigated in this chapter. This provides background information for the next chapter, which investigates if there is any correlation between the effects of changing the resin/hardener stoichiometry and adding Si_3N_4 nanoparticles. Hence, this chapter emphasises investigating the effect of changing the stoichiometry on the molecular relaxation processes and the electrical properties of the unfilled epoxy. Changing the resin/hardener ratio results in changes in the crosslinking density and, consequently, the network structure of the cured epoxy. In addition, this will also affect the functional groups that are retained within the network: for example, in amine-cured systems, using formulations with excess hardener will increase the residual amine group content, whereas using formulations with excess resin will likely lead to an increase in epoxy group content. Furthermore, changing the crosslinking density will affect the concentration of hydroxyl groups that result from the reaction between epoxy and amine groups. Therefore, analysing the effect of resin/hardener stoichiometry on the electrical properties can give insights on how the network structure and the chemical composition each affect the electrical behaviour of the bulk material. Table 5.1 lists the samples prepared for this purpose along with the formulations used in each sample. The hardener percentage (*HP*) ranges from 60 % to 140 % of the hardener stoichiometric mass.

Table 5.1: Samples prepared for studing the stoichiometry effect.

Sample code	Resin : Hardener mass ratio	Hardener percentage (*HP*) $\left(\frac{mass\ of\ the\ hardener}{hardener\ stoichiometric\ mass}\ \%\right)$
60HP/0	1000 : 206	60%
70HP/0	1000 : 240	70%
80HP/0	1000 : 275	80%
90HP/0	1000 : 309	90%
100HP/0	1000 : 344	100%
110HP/0	1000 : 378	110%
120HP/0	1000 : 413	120%
125HP/0	1000 : 430	125%
130HP/0	1000 : 447	130%
140HP/0	1000 : 482	140%

5.2 Glass transition process and network structure

The glass transition temperature for each of the samples in Table 5.1 is shown in Figure 5.1. As would be expected, the theoretical stoichiometric ratio (*HP* = 100 %) leads to the highest T_g. Deviating from the stoichiometric ratio, T_g decreases but not in a symmetric way: T_g decreases more sharply for the epoxy rich samples. Comparable variations in T_g have been reported previously [63, 120] for similar resin and hardener systems.

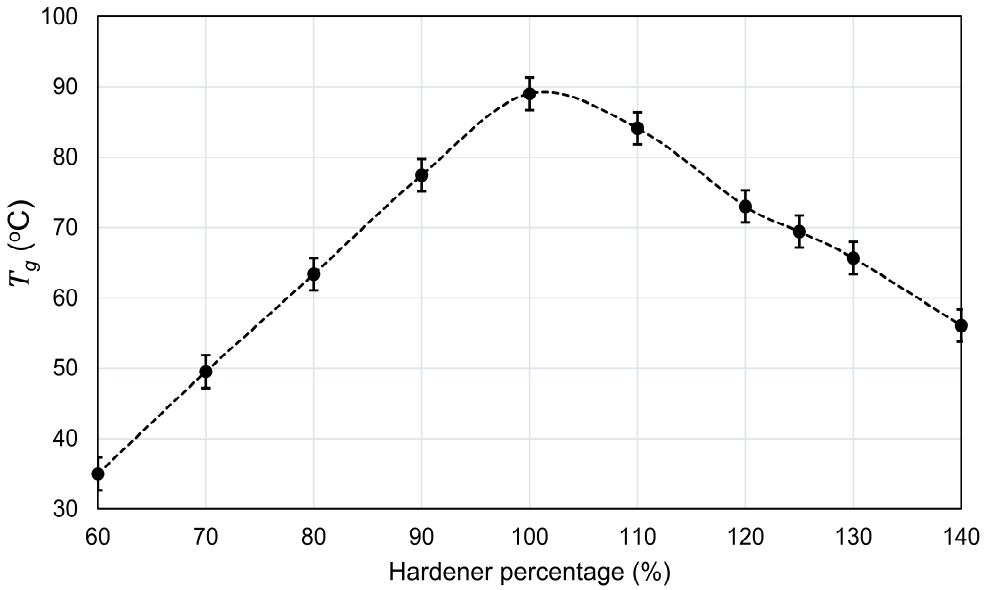

Figure 5.1: The glass transition temperature for all formulations.

As reviewed in section 3.1, for crosslinked polymers, T_g can be affected by the stiffness of the segments between crosslinking points, the free volume content and the crosslinking density. Considering first the rigidity of the segments between the crosslinking joints, the polyether diamine molecules in the Jeffamine D-230 are more flexible than the DGEPA

molecules in the DER-332, which would suggest that samples containing an excess of epoxy molecules should exhibit a higher T_g. However, the results presented above demonstrate the reverse, which implies that the segment rigidity is not the dominant factor.

The free volume content depends on the regularity of the polymer chains and their ability to pack efficiently [121]. Both the resin and the hardener used in this study are linear aliphatic molecules, which does not enable easy correlation between the regularity of the polymer chains and the free volume content of the system. However, previous work has concluded that crosslinking imposes steric restrictions on the polymer segments near the crosslink junctions, which reduces the packing efficiency and consequently increases the local free volume content [121, 122]. Indeed, for a similar resin and hardener system to the one used here, Morgan *et al*. [120] reported that the cured epoxy corresponding to the stoichiometric formulation had a *minimum* in the macroscopic density, compared with other formulations. This would suggest that the system with $HP = 100$ % contains more free volume. However, at temperatures near T_g, crosslinking can limit the divergence of chain segments, which consequently reduces the thermally induced free volume within the system [122]. As a consequence, the influence of free volume content on T_g is dominated by the crosslinking density and, therefore, we suggest it is this factor that largely determines the form of the data shown in Figure 5.1. This assertion is supported by dynamic mechanical characterization data reported elsewhere [120] for the same resin, albeit cured with a similar, but different, amine hardener (Jeffamine T-403). This study showed that the crosslinking density and T_g are well correlated and follow similar trends; both decrease more sharply for formulations containing excess epoxy. The asymmetry in the derived crosslinking density might be related to the fact that each hardener molecules in the Jeffamine D-230 is terminated with primary amine group and thus can react with two resin molecules, whereas each molecule in the DEGBA resin is terminated with one epoxy group and thus can react with one hardener molecule. Therefore, when there is an excess of the amine groups, some of the amine groups may react with one epoxy group and convert into a secondary amine. This can slightly affect the crosslinking degree since the hardener molecule is still connected. For the case of excess epoxy groups, each unreacted epoxy group leads to unconnected terminal of one resin molecule and, consequently, have relatively more impact on the crosslinking density.

FTIR spectra obtained from specimens prepared from different stoichiometric ratios are presented in Figure 5.2. For samples where $HP < 100$ %, an absorption peak is evident near 915 cm^{-1}, which is assigned to the resin's epoxy groups [123]; the intensity of this increases monotonically with decreasing *HP* in this composition range. For samples with the stoichiometric formulation or with an excess of hardener ($HP > 100$ %), this peak disappears. Thus, we conclude that for epoxy rich samples, a fraction of the epoxy groups is left unreacted while, in the amine-rich systems, all are consumed during curing. Other key FTIR feature is located in the wavenumber range 3150 to 3650 cm^{-1}. For epoxy rich

samples, this feature is related to the hydroxyl groups, generated from the crosslinking reaction, which result in a broad absorbance peak centred at ~3420 cm^{-1} [124]. For amine rich samples, additional overlapping absorption centred at ~3300 cm^{-1} occurs, which is associated with residual amine groups; the appearance of this as a single peak at a relatively low wave number is indicative of the presence of secondary (rather than primary) amine groups [124]. This peak is evident only in amine rich formulations, where its intensity increases monotonically with increasing *HP* above 100 %, thereby indicating the presence of retained N-H groups (i.e. unreacted secondary amines) in these formulations. Compared with the stoichiometric formulation, the FTIR spectra show that the breadth and strength of the hydroxyl peak decrease for all other formulations, with a more pronounced decrease for formulations with *HP* < 100 %. Hence, the FTIR spectra indicate that the concentration of the hydroxyl group decreases for all non-stoichiometric formulations, particularly for epoxy rich formulations. The hydroxyl concentration will be revisited in the next section. The increase in absorption in the range 2500 - 2800 cm^{-1} as a function of *HP* is attributed to an increase of the aliphatic C-H bonds present in the hardener, even though absorption around 2900 cm^{-1} is saturated [125, 126].

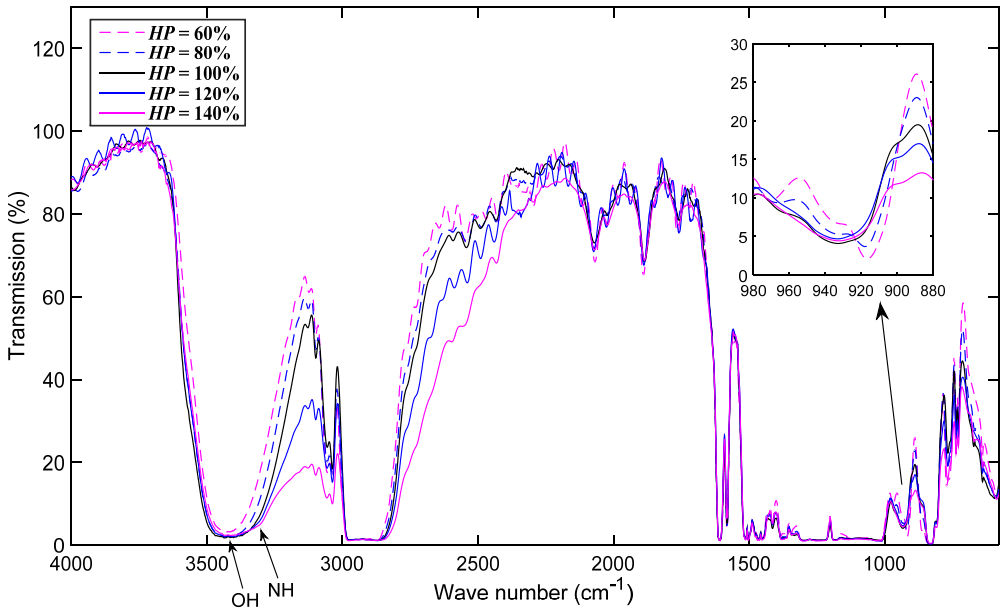

Figure 5.2: FTIR spectra for selected samples.

On the basis of the spectral data presented above, it is possible to represent, schematically, the effect of resin stoichiometry on network structure. Figure 5.3 does this for a number of *HP* values in the range 50 % to 200 % and is based on the DER-332 resin behaving as a bifunction monomer, being terminated with an epoxide group at either end, while the hardener is a quarto-functional moiety. It is assumed that the reaction rate of the primary amine is higher than that of the secondary amine, as evinced by the FTIR data shown above and also reported by Morgan *et al*. [120], and that no epoxy group is left unreacted while there is an available amine group and vice versa (i.e. complete reaction). For formulations containing excess epoxy (*HP* < 100 %), all the primary and secondary amines will react,

leaving a fraction of unreacted epoxy groups within the network, as terminal end groups or unreacted resin (see Figure 5.3a). In the case of formulations that contain an excess of hardener, the primary amine hydrogens will react first and, thus, in the case of *HP* = 150 % (see Figure 5.3c), all primary amine hydrogen will react, while only one third of the secondary amine hydrogen will be consumed. Based on the above assumptions, the average molecular mass between crosslinks (M_c) is calculated and shown in the same figure.

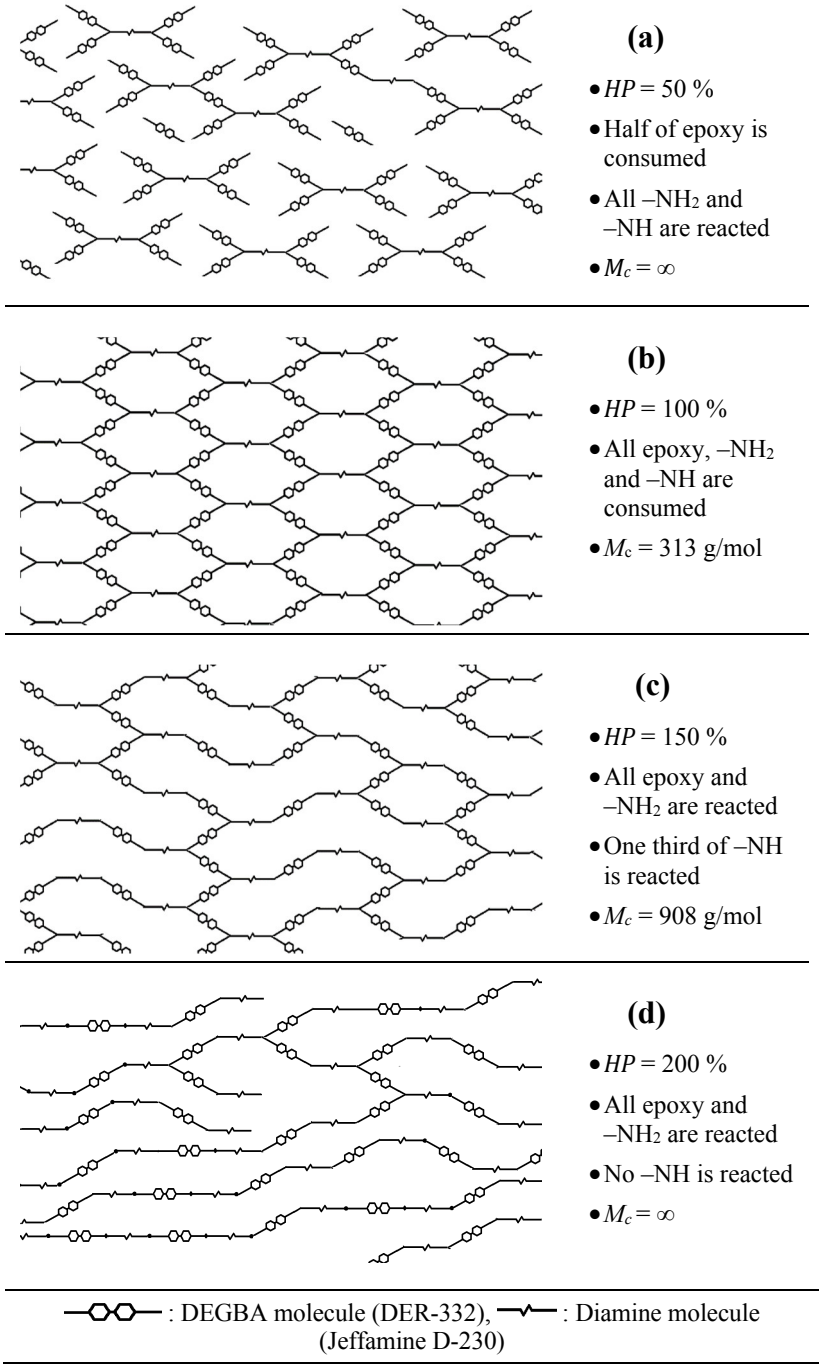

Figure 5.3: A schematic representation of the network structure as a function of hardener percentage.

Many studies have indicated that, in addition to epoxy/amine reaction, additional chemical processes can also occur during the curing process. For example, the hydroxyl groups

generated by the epoxy/amine reaction may react with epoxy groups in the resin to form ether bonds, or the epoxy groups may react with each other (homopolymerization), particularly at high temperature [27, 28]. However, the FTIR data presented above provide no evidence for this. Also, the dependence of T_g on amine/epoxy stoichiometry discussed above does not imply that the extent of such reactions is significant since, particularly for epoxy rich systems, the existence of such reactions would lead to additional crosslinking processes that would tend to hinder the acute decrease in T_g observed with decreasing *HP*. Nevertheless, to investigate this hypothesis further, selected samples were postcured at 160 ^{o}C for 3 h in a nitrogen environment. The results (Figure 5.4) indicate that the post-curing results in a slight increase in T_g (<2.5 ^{o}C), which is within the experimental uncertainties of the measurements. Furthermore, this slight increase is not specific to the epoxy rich samples, which implies that none of the above mentioned side reactions plays a significant role in the crosslinking process under the range of conditions considered here. The same conclusion was drawn by Bell [127], for a DGEBA resin cured with an aromatic diamine, and by Kolar and Svitilova [128], neither of whom reported extensive reactions between the hydroxyl and epoxy groups. Consequently, this signifies that the dominant crosslinking reaction is associated with the amine/epoxy reaction.

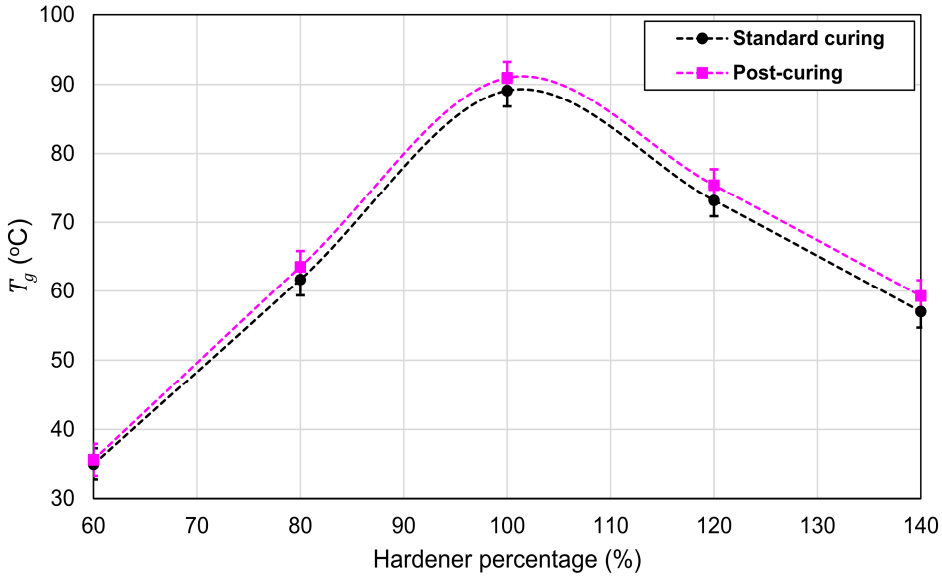

Figure 5.4: Effect of post-curing on T_g of selected samples.

The increase in the heat capacity (ΔC_p) across the glass transition is shown in Figure 5.5 as a function of *HP*. For amine rich samples, ΔC_p increases monotonically with increasing *HP*. This trend might be attributed to the flexibility of the hardener molecules compared with the resin molecules; the latter contain bulky epoxy and phenol groups. At high *HP*, some of the amine groups react with only one of their hydrogen atoms, see Figure 5.3c, which produces relatively flexible linear reaction points. This increases rotational and conformational motions brought by the rubbery state in amine rich formulations. For the same ER system, other workers [121, 129] observed an increase in ΔC_p when increasing the length of the hardener molecules, i.e. increasing the number of the oxypropylene units

in Figure 2.9a, which is in line with the trend obtained here for amine rich formulations. For resin rich samples, ΔC_p appears to increase slightly at HP = 90 % before decreasing at HP = 80 %, albeit that these variations are within the uncertainties shown. Thereafter, ΔC_p decreases sharply at HP = 70 %. The data are not shown for HP = 60 %, since the DSC used cannot give reliable information near room temperature. The initially slight increase in ΔC_p for HP = 90 % might be a reflection of a marked reduction in the crosslinking density at this formulation. However, on further reducing HP, the network will mainly consist of relatively rigid resin molecules, which allows less segmental motion upon entering the rubbery state. A comparable relation between ΔC_p and hardener ratio was reported by Calventus *et al*. [130] for DEGBA epoxy cured with a similar polyether amine hardener.

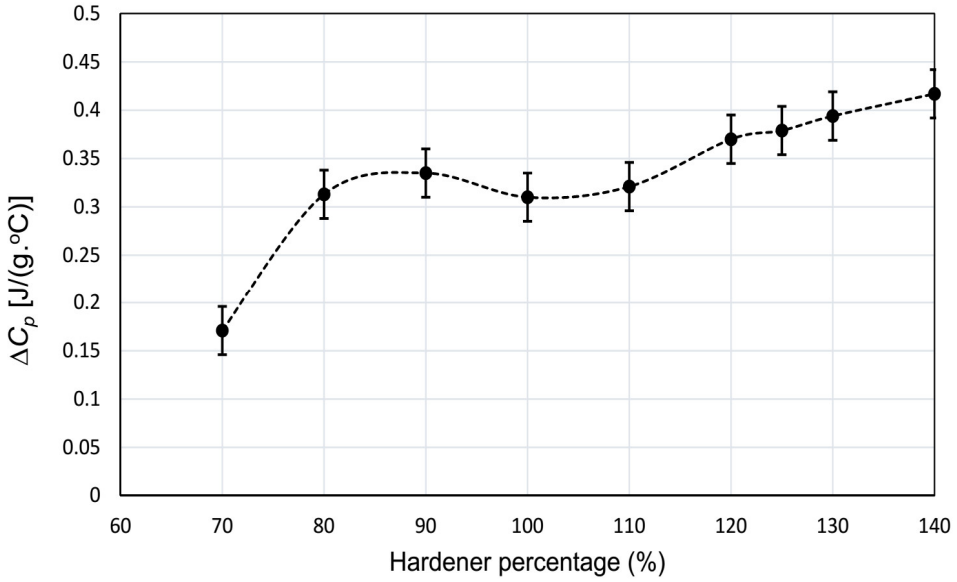

Figure 5.5: The change in the heat capacity over the glass transition process as a function of HP.

The glass transition width, ΔT_g, for all formulations is displayed in Figure 5.6. The transition width increases for the formulations with hardener percentage far away from 100 % on both sides. This reflects increasing heterogeneity in networks with either excess epoxy or excess amine. For excess amine formulations, this heterogeneity can be detected from the illustrations in Figure 5.3c and d, where the distance between neighbouring network nodes may be as short as one molecule or as long as a sequence of resin and hardener molecules. A comparable explanation can be proposed when 80 % < HP < 100 %, where competition for the available amine moieties leads to local variations in crosslinking density. A similar general form of behaviour to that described above was reported by Gupta *et al*. [131]. In this case, the glass transition process was examined using dynamic mechanical analysis and found to broadening, notably for hardener rich samples. However, for HP = 70 %, Figure 5.6 reveals a sharp decrease in ΔT_g, which implies the formation of a more homogenous molecular structure or, more likely, that as the crosslink density drops (see Figure 5.3a), so the system is able to act in

a more cooperative manner. That is, the observed glass transition is influenced by both structural and dynamical factors.

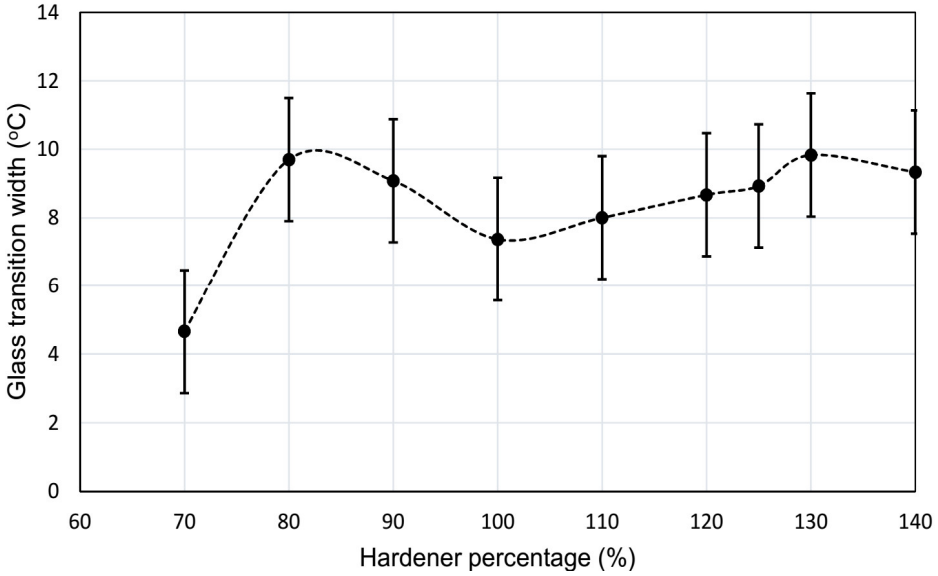

Figure 5.6: The width of the glass transition as a function of *HP*.

The enthalpy relaxation area for all samples is shown in Figure 5.7 as a function of *HP*. Comparing these data with the T_g results shown in Figure 5.1 reveals that the variation in enthalpy relaxation is the inverse of the variation in T_g and, correspondingly, in the crosslinking density. Similar trends have also been reported by other workers [101, 130]. In the rubbery state (i.e. prior to vitrification during curing), the polymer segments have sufficient energy to move away from their equilibrium positions and, consequently, the lower the crosslinking density, the further the segments can be displaced. Consequently, at low crosslinking densities, the polymer segments need more energy to return to their equilibrium positions, which explains the trend observed in Figure 5.7.

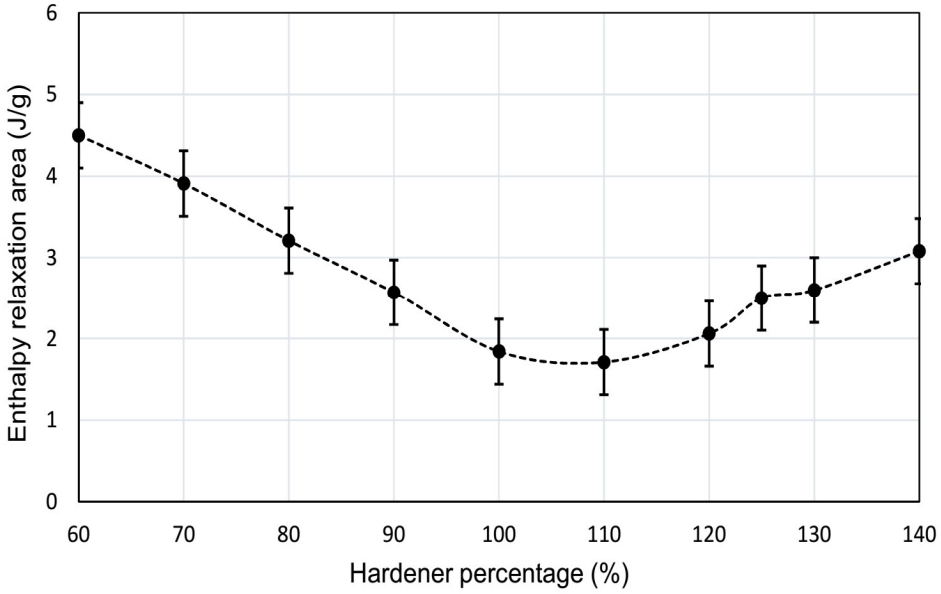

Figure 5.7: The enthalpy relaxation area as a function of *HP*.

5.3 Dielectric spectra

The effect of changing the stoichiometry on the dielectric spectrum is shown in Figure 5.8 for epoxy rich samples at room temperature. For the sample corresponding to the theoretically ideal stoichiometric formulation, *HP* = 100 %, a broad β relaxation process can be observed starting at frequencies higher than 1 MHz and extending down to frequencies around 10 Hz. The breadth of this relaxation suggests that it is related to a distribution of segmental motions with different activation energies, where the motions with low activation energy are responsible for the high-frequency part of the relaxation and the motions with high activation energy are responsible for the low-frequency part [132]. The peak of this relaxation is at approximately 4×10^4 Hz and its strength is ~0.6 (evaluated by calculating the increase in ϵ_r' between 1 MHz and 10 Hz). The β relaxation also appears in the epoxy rich samples, albeit that both its strength and breadth monotonically decrease with reducing amount of hardener, as shown in Figure 5.8b. Additionally, the peak of this relaxation moves slightly to higher frequencies. Comparable trends for the relaxation strength and breadth have been reported for similar epoxy/amine systems when reducing the crosslinking density [133, 134]. Many studies have claimed that the β relaxation in such systems is associated with the crankshaft rotation of the hydroxyether group (–CH(OH)–CH_2–O–) that is generated at each crosslink point due to the reaction between the epoxy and amine groups [133-135]. Based on this assumption, the β relaxation strength should have a direct relation with the crosslinking density. Thus, at *HP* = 100 %, the β relaxation should have the highest strength, which agrees with the results presented in Figure 5.8b. From the analysis conducted to produce Figure 5.3, the number of crosslinking junctions (epoxy/amine reactions) per unit volume of the cured sample was estimated as a function of *HP* and presented in Figure 5.9 after normalizing it to its maximum at *HP* = 100 %. Also illustrated in Figure 5.9, the strength of the β relaxation, which is derived from the measured spectrum for each formulation. The strength of the β relaxation correlates with the density of epoxy/amine reaction for epoxy rich samples. However, the reduction in the β relaxation strength is sharper than that predicted by the concentration of the crosslinking nodes. This might be caused by the reduction of the activation energy of some of the segmental motions that contribute to this relaxation with reducing the crosslinking density [132], which suggests that part of the relaxation moves to higher frequencies. Two consequences of this explanation would be expected. First, the strength of the low-frequency component of the relaxation should decrease with decreasing crosslinking density, which is the case in Figure 5.8. Second, part of the relaxation should move to higher frequencies and might manifest itself as a new relaxation process or as an extension of the existing β relaxation to higher frequencies, i.e. beyond the range accessible here. Indeed mechanical spectroscopy results described in [121] indicate the emergence of a new relaxation peak beside the β relaxation at a lower temperature for loosely crosslinked systems. This explanation is also in line with the

gradual increase in the real relative permittivity at 1 MHz from around 3.6 for *HP* = 100 % to around 4 for *HP* = 60 %.

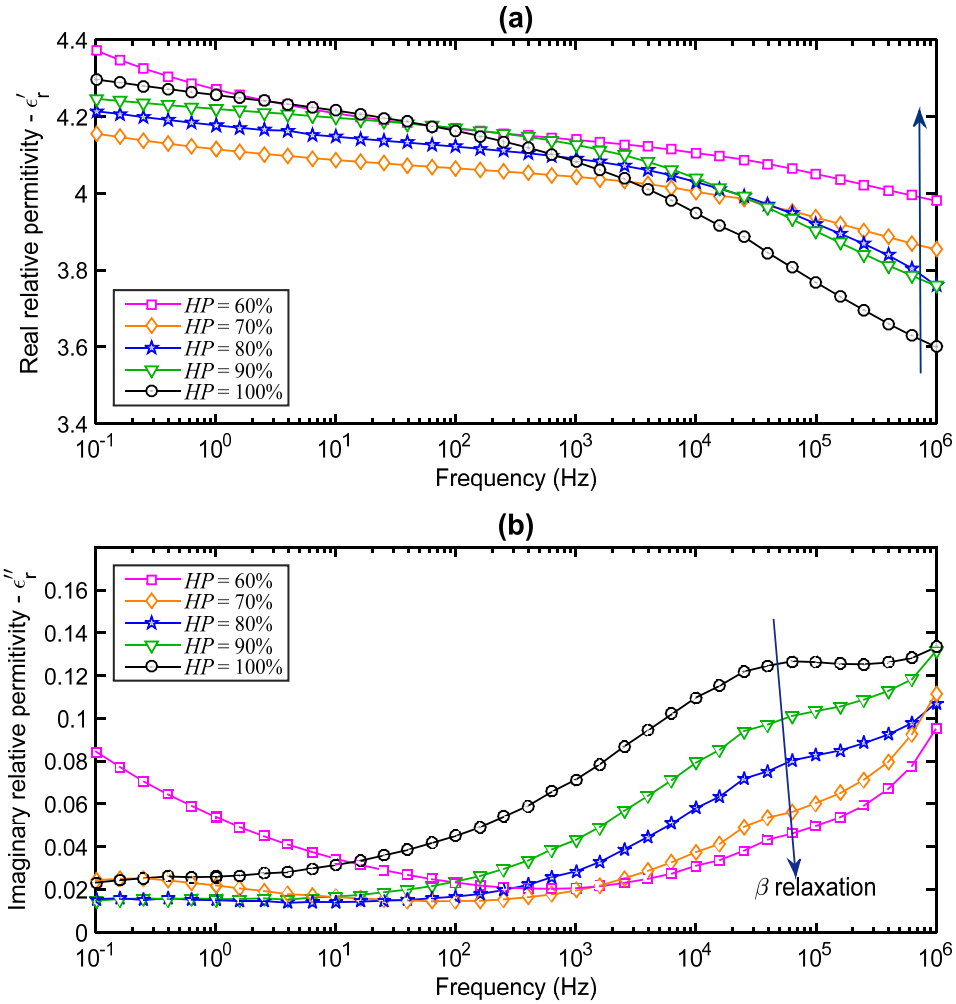

Figure 5.8: The dielectric spectra for epoxy rich samples at room temperature.

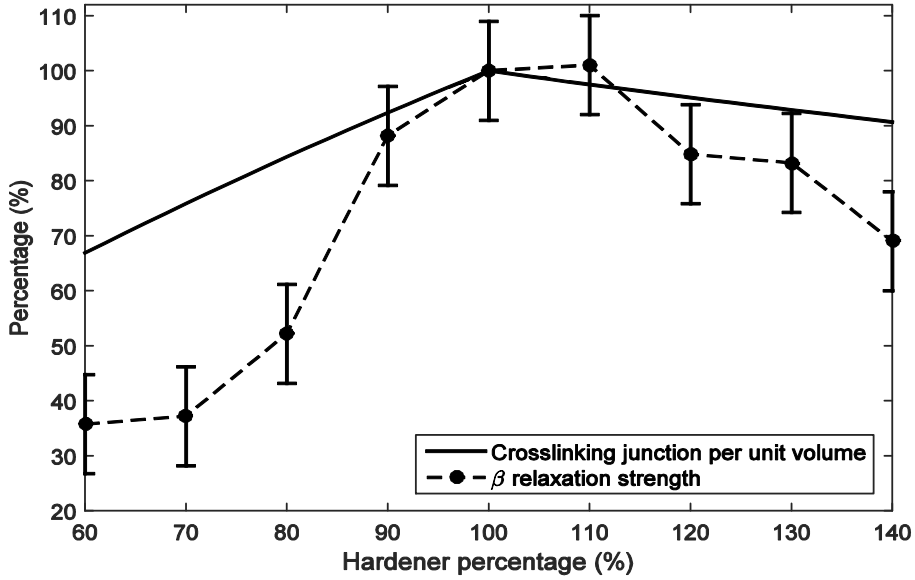

Figure 5.9: The number of the crosslinking junctions per unit volume and the β relaxation strength normalized to their maximum at *HP* = 100 %.

Another relaxation process starts appearing for *HP* = 70 % and is clearly visible for *HP* = 60 % in Figure 5.8b. The T_g for these two samples is close to the spectroscopy measurement temperature (~23 °C), which indicates that this relaxation process is associated with the main relaxation process occurring at the glass transition, the α relaxation.

Concerning the real part of the permittivity (ϵ_r'), at low frequencies, it decreases as *HP* falls from 100 % to 70 %, as shown in Figure 5.8a. This reduction can be ascribed to the reduction in the density of hydroxyether groups, as discussed earlier. Hence, decreasing *HP* from 100 % to 70 % results in a reduction in the β relaxation strength and, correspondingly, the magnitude of ϵ_r' of the resulting network. However, at *HP* = 60 %, ϵ_r' increases to around the same values as for the sample where *HP* = 100 %. This might be a result of the enhancement of the contributions from other moieties enabled by the dramatic reduction in the crosslinking, particularly since, at the measurement temperature, the network is not far from its rubbery state for *HP* = 60 %. This could be deduced from the appearance of the α relaxation for *HP* = 60 %.

Dielectric spectra for amine rich samples are shown in Figure 5.10. As can be predicted from the trends discussed above in connection with Figure 5.9, the β relaxation strength smoothly decreases as *HP* increases from 100 % to 140 %, due to the consequent reduction in the hydroxyether group density. Similar to what was stated for epoxy rich samples, the decrease in the β relaxation strength is sharper than would be expected by estimating the hydroxyether group density. This can again be explained by a displacement of part of the β relaxation to higher frequencies for loosely crosslinked networks. No α relaxation process is observed for the amine rich samples, since none of these samples is close to its T_g during these measurements.

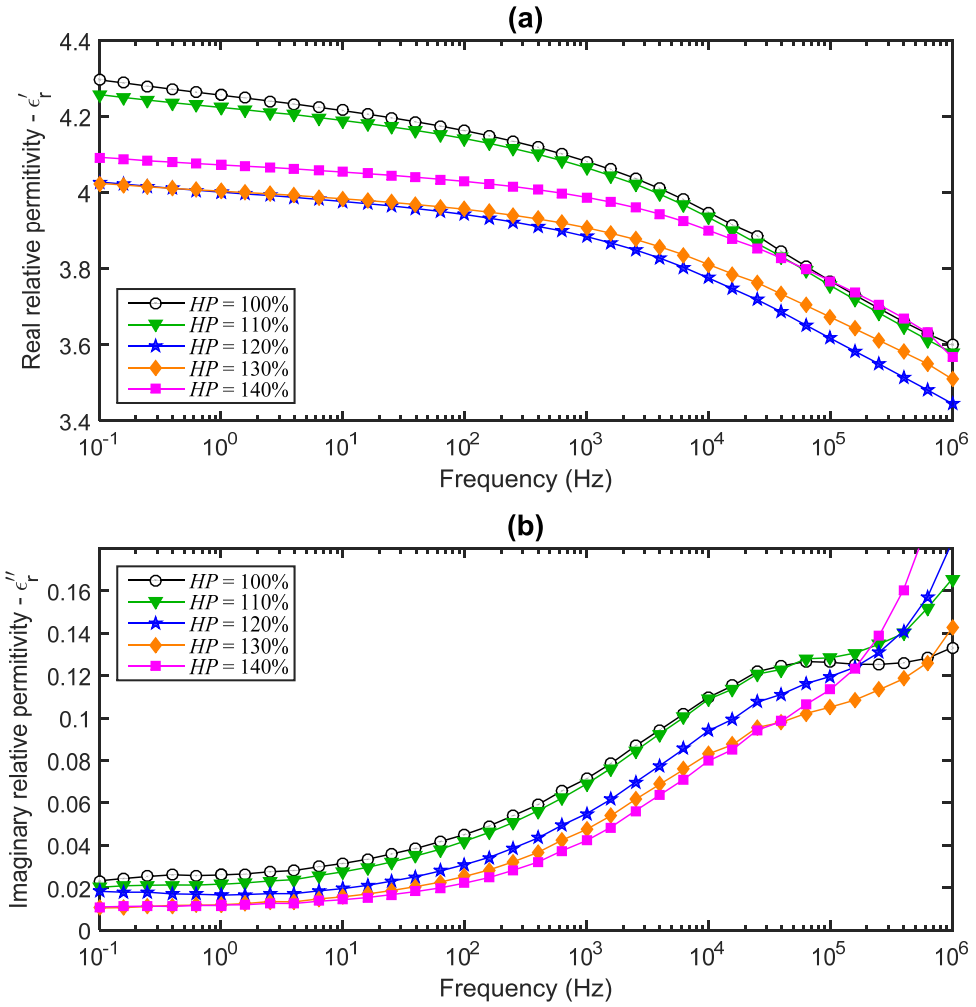

Figure 5.10: The dielectric spectra for amine rich samples at room temperature.

5.4 DC conductivity

The effect of stoichiometry on charge transport was characterised by measuring the DC conductivity at an applied field of 42 kV/mm at temperatures up to 60 °C. Before starting the measurements, each sample was put inside the measurement cell at the specified temperature for around 10 min so as to stabilize its temperature. All samples were stored under dry conditions in a vacuum desiccator until starting the measurement. However, there was no control over the humidity level during the measurement process itself.

Figure 5.11 presents the DC conductivity results obtained from all samples at a temperature of 30 °C. For the epoxy rich samples (Figure 5.11a), apart from sample 60HP/0, the DC conductivity of all other samples is comparable. The high scatter in the results indicates a low signal to noise ratio. This implies that for specimens with a conductivity around 10^{-17} S/cm or lower the facilities used to measure the DC conductivity give noisy results, which might be caused by reaching the lower limit of the sensitivity of the picoammeter used. Therefore, the results obtained from the samples with 70 % < *HP* < 100 % cannot reveal whether the reduction in the amine content leads to a decrease in the DC conductivity, albeit it is clear that it does not cause a significant rise in the DC conductivity.

For sample 60HP/0, unlike the other samples, a noticeable increase in the DC conductivity can be observed. At temperature of 30 ºC, this sample is very close to its T_g, see section 5.2, and it might enter into its rubbery state gradually. Thus, the rise in the DC conductivity of sample 60HP/0 is a consequence of its being in rubbery state during the measurement, rather than being related to a change in the sample's chemical composition or network architecture. This explanation is based on the DC conductivity of the same sample at different temperatures as will be detailed below, see Figure 5.13. For the amine rich samples, the data in Figure 5.11b obviously reveal that the DC conductivity increases steadily with rising the hardener percentage, *HP*. The gradual increase in the DC conductivity versus time in Figure 5.11 might be related to water absorption by the regarded samples during the measurement period. Water absorption is discussed in section 5.6.

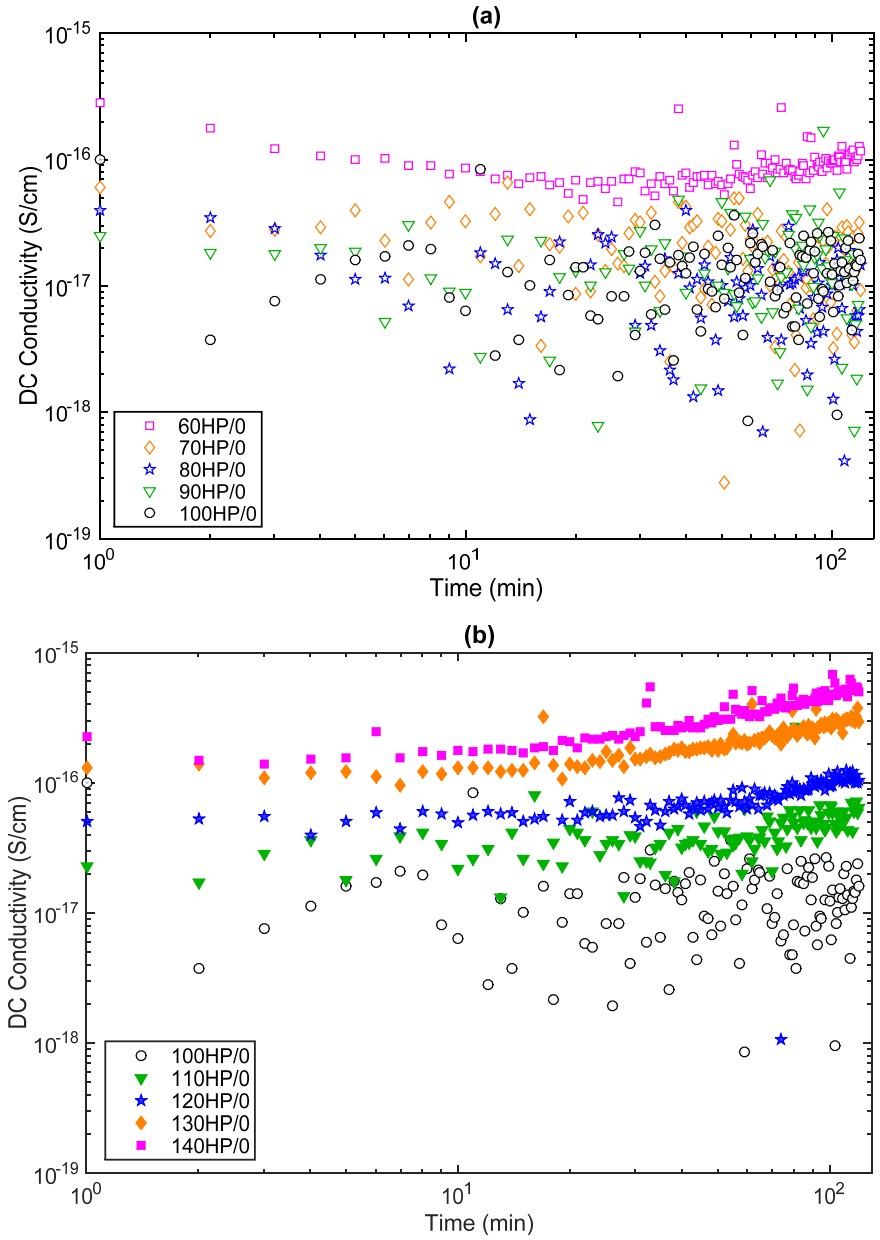

Figure 5.11: DC conductivity at 30 ºC and applied field of 42 kV/mm for (a) epoxy rich samples and (b) amine rich samples.

To examine the time dependence of the DC conductivity over longer time periods, one sample (90HP/0) was tested for 12 hours and the result is shown in Figure 5.12. From this, the DC conductivity appears to increase slightly with time, which can be related to water absorption from the ambient environment during the measurement process, as will be discussed in section 5.6. However, no dramatic change in the DC conductivity could be observed. Hence the DC conductivity measurements were performed for two hours for most of the samples.

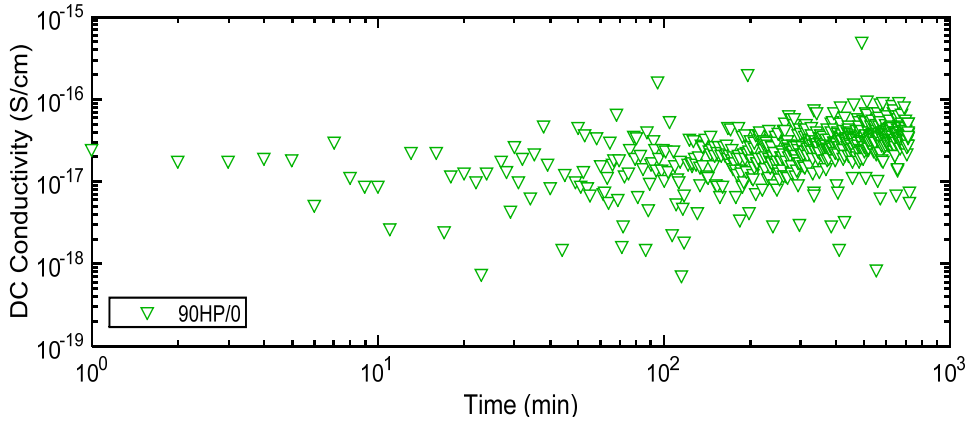

Figure 5.12: DC conductivity for sample 90HP/0 at 30 °C and 42 kV/mm throughout 12 h of testing.

Measurements comparable to those conducted at 30 °C were performed at room temperature (23 °C), 45 °C and 60 °C and the resulting data were averaged at each temperature and presented in Figure 5.13. These data show that increasing the temperature results in an increase in the DC conductivity, but that the relation is not linear. As the temperature approaches T_g for the particular sample, the DC conductivity increases much more sharply. Being close to the rubbery state enhances the movement of any ionic residues available within the network, such as Na^+ and Cl^- ions which are generated as by-products during the synthesis process of many commercial DGEBA resins [136]. Hence, as the material enters its rubbery state, the contribution from ionic conductivity increases and, consequently, the whole DC conductivity increases.

At room temperature, when all samples are well in their glassy state, these data indicate that the DC conductivity increases steadily with increasing *HP*. Such behaviour may be associated with either or both of two factors that are affected by changing *HP*: the network structure; the chemical constituents of the network. As established earlier, increasing or decreasing *HP* beyond the stoichiometric ratio (i.e. *HP* =100 %) results in a less crosslinked network with enhanced segmental dynamics at a given temperature, which means that the network structure does not monotonically change with *HP*. Since the measured DC conductivity increased monotonically with increasing *HP* from 60 % to 140 %, it cannot be correlated with the variation that occurs in the network dynamics or architecture. Therefore, in the glassy state, the DC conductivity of the epoxy networks should be

primarily related to their chemical content. Virtanen *et al*. [92] studied the impact of introducing electroactive groups (i.e. modifying the chemical content) into an epoxy matrix by adding two types of surface modified silica nanoparticles. Particles functionalized with long epoxy compatible molecules resulted in improved particle dispersion, but had only a marginal effect on electrical behaviour. Treating the same particles with short electroactive molecules, namely oligothiophene and ferrocene, produced a substantial beneficial influence on dielectric performance. The authors argued that the electroactive molecules offer new energy states that could trap electrons and, thus, affect charge transport dynamics within the system. A similar conclusion was drawn by Siddabattuni *et al*. [137], who found that the inclusion of nanoparticles functionalized with electron-withdrawing functional groups led to a nanocomposite with reduced DC conductivity, whereas the inclusion of electron-donating functional groups, such as amine groups, resulted in increased DC conductivity. These studies suggest that the electrical behaviour of a material is sensitive to the electroactivity of the system. In the systems investigated here, the main electroactive groups, which are affected by modifying *HP*, are the hydroxyl and the amine groups. The concentration of hydroxyl groups was discussed and shown in Figure 5.9 as a function of *HP*. The amine groups mainly exist in the amine rich formulations and their concentration increases with increasing *HP*. Consequently, the slight decrease in the DC conductivity for epoxy rich samples may be associated with the lower concentration of hydroxyl group. For amine rich samples, since the hydroxyl content decreases as *HP* increases, the significant rise in the DC conductivity might be related to the increase in the amine group concentration in these samples.

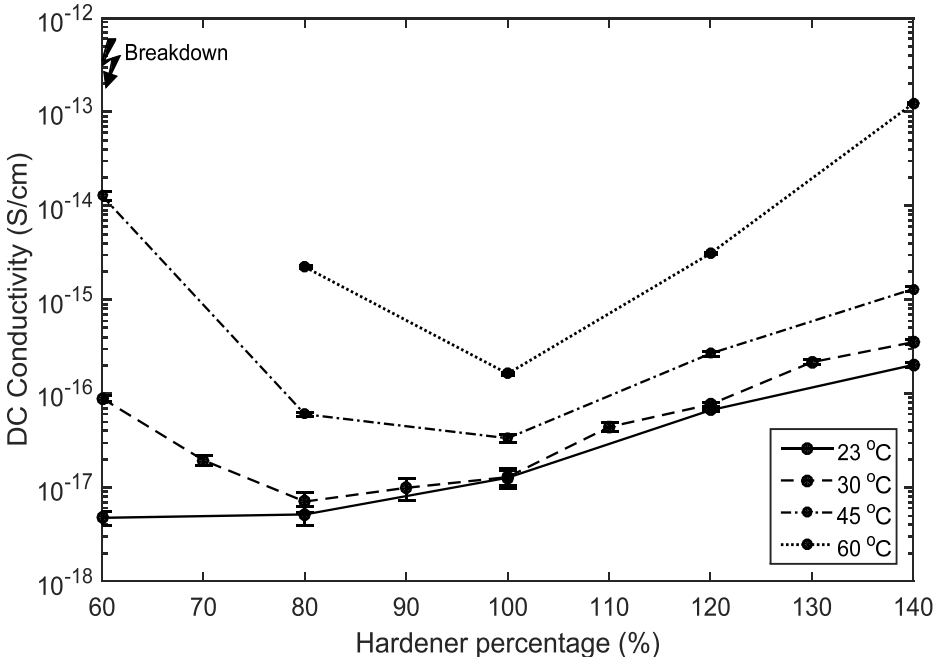

Figure 5.13: DC conductivity averaged over two hours at different temperatures and applied field of 42 kV/mm, breakdown occurred at 60 °C for *HP* = 60 %.

Considering the DC conductivity and dielectric spectroscopy results in concert suggests that while the polar amine groups do not obviously affect the dielectric constant of the material, they do significantly influence charge transport. Being part of the backbone chains that make up the network, the amine groups will possess limited rotational/conformational mobility and, consequently, it will be difficult for them to reorient in response to the electric field. This, therefore, limits their contribution to the orientation polarization and, hence, to the permittivity. Conversely, the electroactive character of the amine and hydroxyl groups might alter the local density of states [138] in a way that increases the electronic conductivity without the need for any rotational or conformational motions. This again emphasizes that the dielectric performance is more sensitive to the electroactive character of the network constituents rather than to its segmental dynamics.

5.5 DC and AC breakdown strength

DC breakdown data obtained from selected samples are plotted assuming a two-parameter Weibull distribution in Figure 5.14. Derived Weibull scale and shape parameters for these samples at the 63.2 percentile with error bars that represent the 95 % confidence bounds are shown in Figure 5.15. For $HP > 100$ %, the DC breakdown strength decreases monotonically with increasing amine content while, for samples with $HP < 100$ %, the Weibull scale parameter increases slightly with decreasing HP up to 80 % before decreasing for $HP = 60$ %, albeit that these latter variations are not statistically significant. These results broadly correlate with the DC conductivity values measured at room temperature, as breakdown testing was also performed at room temperature. Being well below T_g, the DC conductivity and, consequently, the DC breakdown strength are mainly affected by the hydroxyl and amine content, this is applicable to samples with $HP \geq 80$ %. However, on approaching the rubbery state, the DC conductivity might be enhanced by other mechanisms such as enabling more ionic conduction as could be revealed from the results at $HP = 60$ %.

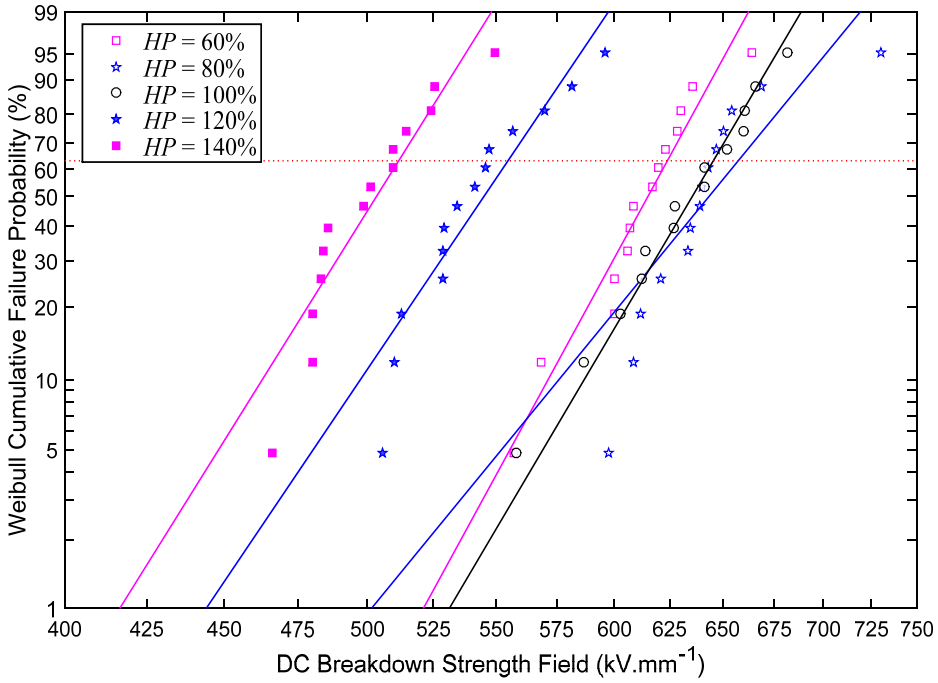

Figure 5.14: Weibull plot of DC breakdown strength for selected samples.

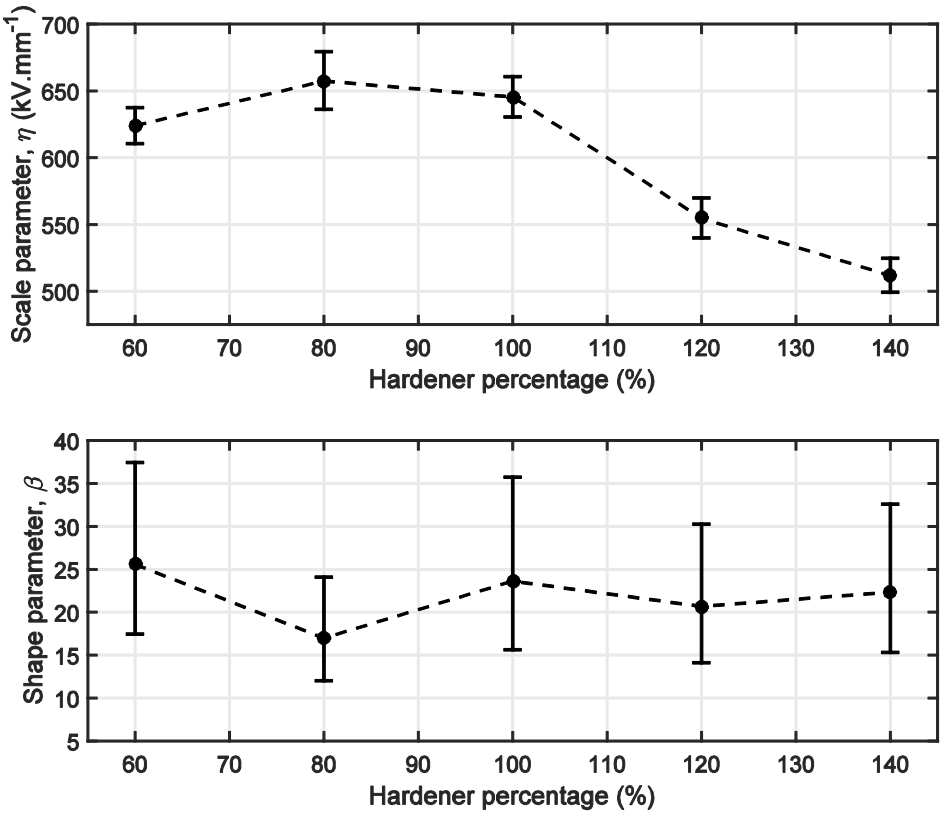

Figure 5.15: DC Weibull scale parameter (top) and shape parameter (bottom) as a function of *HP*, the error bars indicate the 95 % confidence bounds.

The effect of changing the hardener percentage on the AC breakdown strength is shown in Figure 5.16 and the Weibull parameters for all samples are presented in Figure 5.17 with error bars that indicate the 95 % confidence bounds. There are no significant changes to

the Weibull scale parameters of the measured samples, which range between 210 and 226 kV/mm with overlapping confidence bounds. Thus, these results do not support any correlation between the AC breakdown strength and the material formulation within the composition range considered here. Unlike the DC breakdown strength, which broadly correlates with the DC conductivity, the AC breakdown strength seems to be unaffected by variations in the DC conductivity, which implies that the AC and DC breakdown strengths are controlled by different mechanisms. This conclusion is in line with other experimental findings [22, 139-141], which also show that the AC breakdown strength does not correlate with variations in DC conductivity or DC breakdown strength. Grzybowski [139] studied the impact of water absorption on AC and DC breakdown strengths of polyethylene terephthalate and found that, compared with the sharp reduction in the DC breakdown strength, the AC breakdown strength only showed a relatively slight reduction due to water absorption. This implies that the uniform distribution of water molecules inside the insulation material has a more detrimental effect on DC breakdown than on AC breakdown. Huang [22] reported that adding surface treated nanoparticles into a polyethylene matrix reduced the AC breakdown strength, even though it reduced the value of DC conductivity to below that of the unfilled matrix. The authors attributed this behaviour to the defects and free volume that were introduced by the addition of the nanoparticles. This is in accordance with the finding in [140], which indicated that the AC breakdown strength is more sensitive to the presence of defects or deficiencies in insulation materials. In the systems investigated here, since the amine and hydroxyl groups, which affect the conductivity, are uniformly distributed throughout the material, they should not produce defects and, thus, should not severely affect the AC breakdown strength.

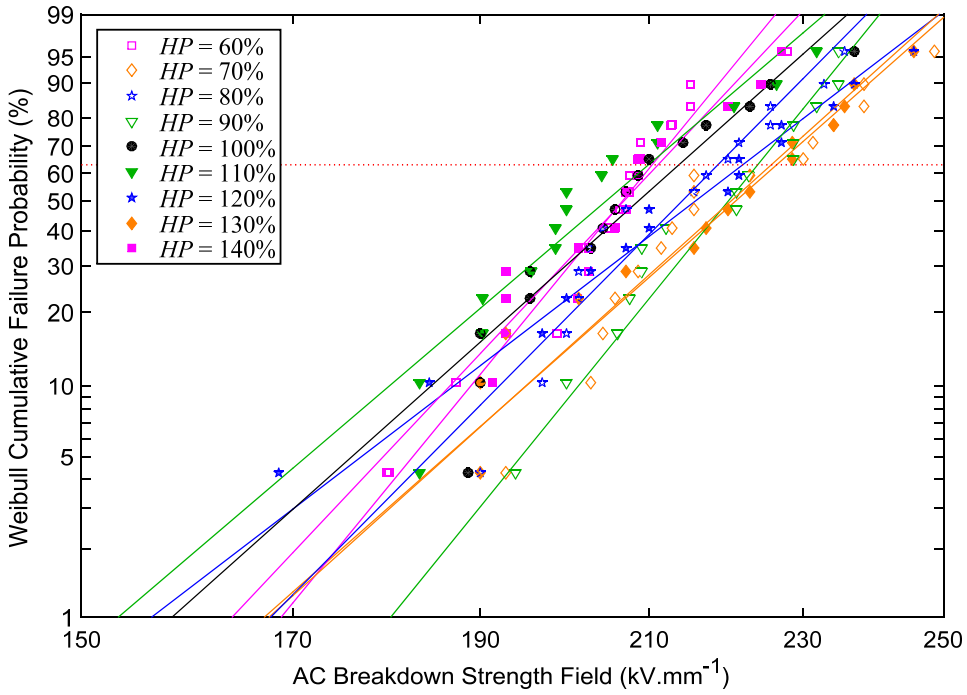

Figure 5.16: Weibull plot of AC breakdown strength for all samples.

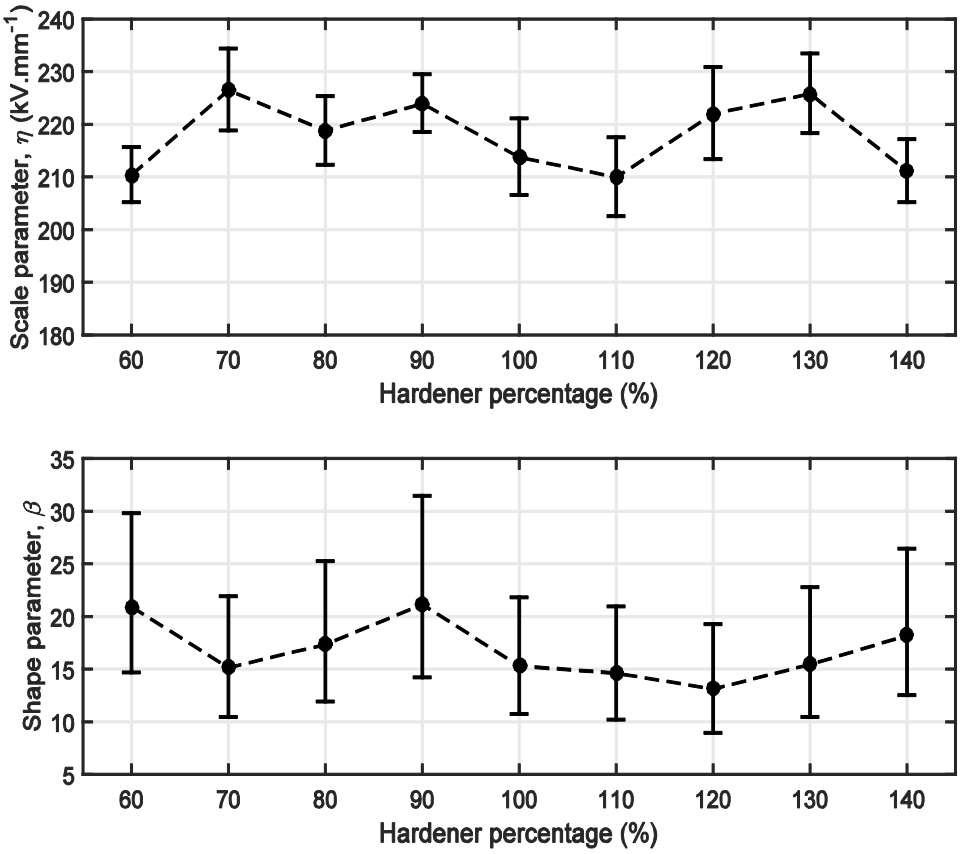

Figure 5.17: Weibull scale parameter (top) and shape parameter (bottom) versus hardener percentage, the error pars are based on 95 % confidence bounds.

5.6 Moisture absorption and its effect on electrical properties

The water uptake for all samples was observed by exposing them to a controlled environment with a temperature of 22.5 ºC and relative humidity of ~60 % and monitoring their masses regularly over a period of 14 days. Water absorption curves as a function of exposure time for selected samples are plotted in Figure 5.18, assuming Fickian water diffusion. The presented curves are based on mass measurements obtained from 70 µm thick specimens. Initially, water uptake increases linearly with the square root of time, which indicates that water diffuses in the samples according to a Fickian mechanism. The data show that the slope of the linear part of the curves and, consequently the diffusion coefficient, progressively increases with increasing amine content, or *HP*. Similar behaviour has been reported elsewhere [142]. The data indicate that for 70 µm thick specimens, the water uptake reaches around 40 % of its saturation value within 30 min. No significant increase in the water uptake occurred after one day of exposure to the conditioning atmosphere, which indicates that all samples are effectively saturated by this point. Since the conditioning environment is similar to laboratory ambient conditions (21 – 25 ºC, 40 – 60 % RH), these figures suggest that moisture absorption can substantially affect the data obtained from different characterization measurements. For example, if a

dry sample, i.e. taken from a vacuum oven or a desiccator, is exposed to ambient laboratory conditions for a few minutes during the measurement process, then it would absorb a relatively significant amount of water, such that the sample should no longer be considered dry. The consequences of this were observed in the DC conductivity results presented in section 5.4, where the DC conductivity of dry samples was found to increase gradually with time during the measurement period of 2 h. Consequently, this factor should be carefully identified and taken into account when analysing experimentally obtained results.

Regarding equilibrium water uptake values, Figure 5.19 shows these values for all samples as a percentage of their dry mass. Apart from the formulation with *HP* = 60 %, water uptake increases with increasing *HP*. Water absorption depends on two factors, the concentration of polar sites within the system and the free volume content [122]. The latter factor is affected by the temperature, particularly when it is near or higher than T_g of the relevant sample. Furthermore, the free volume content can result in a considerable effect on the water absorption only when the polar content factor is offset [133]. In the systems considered here, the polar content is related to two polar groups: the hydroxyl group, generated from the reaction between the epoxy and amine groups; residual amine groups from the hardener [143]. As was detailed in section 5.3, the concentration of the hydroxyl groups increases sharply on increasing *HP* from 60 % up to 100 %, where it reaches its maximum, and then it decreases slightly on further increasing *HP* from 100 % to 140 %. Consequently, both the hydroxyl and amine group concentrations increase with increasing *HP* up to 100 %. Increasing *HP* beyond 100 % leads to a slight reduction in the OH concentration, while the total OH and amine content continues to increase for *HP* > 100 % as a consequence of increasing the hardener percentage. Accordingly, the polar content is proportional to *HP*. Therefore, the increase in equilibrium water uptake with increasing *HP* correlates well with the increase in the polar site concentration and, thus, the results obtained here are consistent with the conclusion drawn by Soles [133], who suggested that the network water uptake is predominantly controlled by the concentration of included polar sites, rather than the network structure itself.

For *HP* = 60 % (sample 60HP/0), although its polar content is supposed to decrease, the data indicate that its water uptake does not decrease. Such behaviour might be explained by the effect of the other factor, the free volume content. At the conditioning temperature (~22.5 °C), this sample, which has T_g < 35 °C, is very near to its rubbery state. According to Soles [133], the broad segmental motion that accompanies entering into the rubbery state leads to a significant increase in water uptake by generating more rooms (free volume) for water molecules to be absorbed and packed inside the polymer network. This might explain the slight increase in the water uptake seen in this sample.

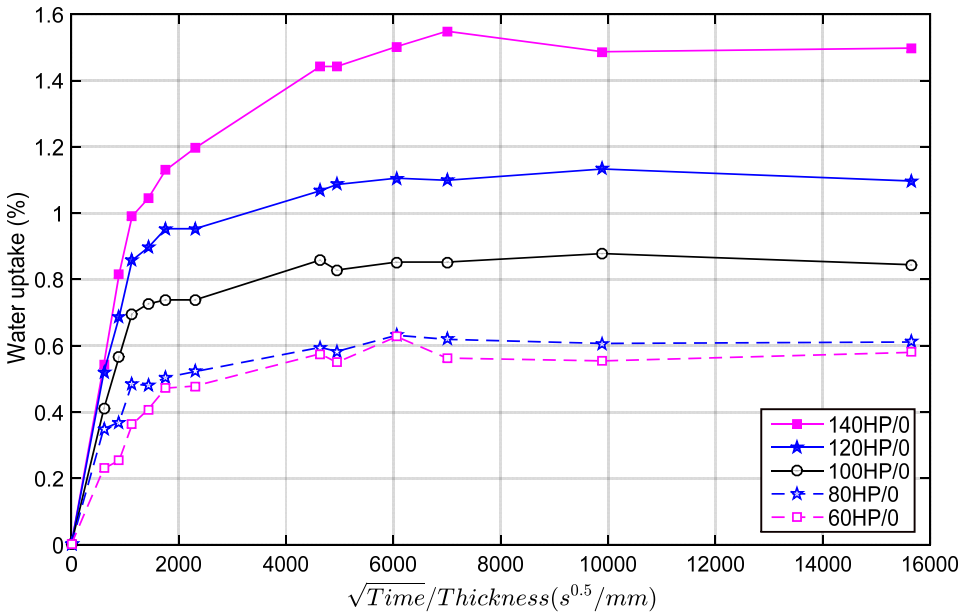

Figure 5.18: Water uptake as a function of time, obtained from 70 µm thick specimens.

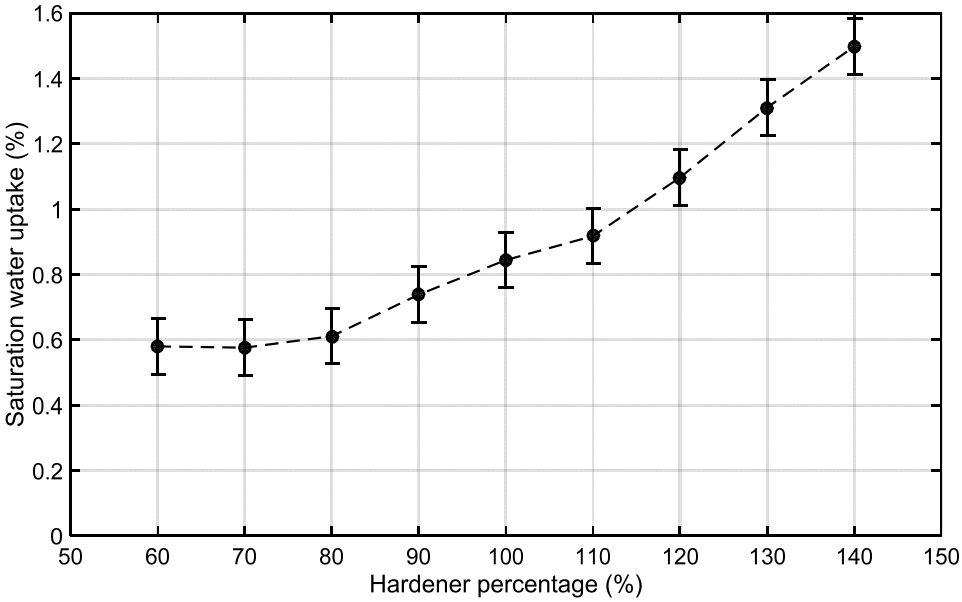

Figure 5.19: Saturation water uptake as a function of hardener percentage.

The absorbed water molecules may form hydrogen bonds with the polar sites within the epoxy network. Additionally, the water molecules may chemically react with the epoxy network, which would lead to an irreversible absorption of water. To examine the reversibility of the water absorption, the same selected samples were dried under vacuum at room temperature (22.5 ºC) and their masses were monitored regularly as illustrated in Figure 5.20. These data show that the samples rapidly lose more than 80 % of the absorbed water within 2 h and return to their dry mass after 1 day of vacuum drying. Thus, the results indicate that the water molecules diffuse into the epoxy matrix forming only hydrogen bonds, such that water absorption is reversible.

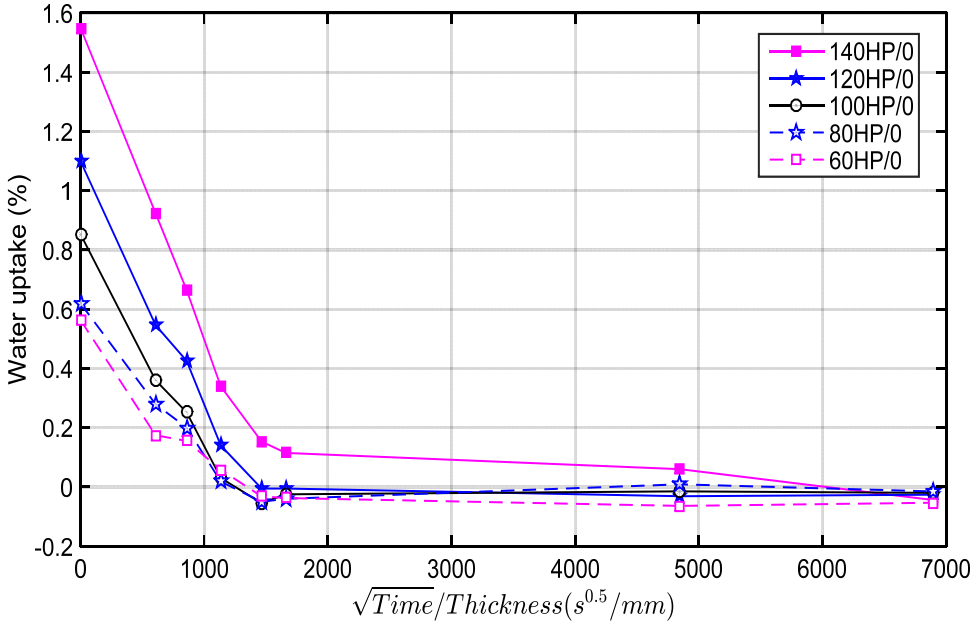

Figure 5.20: Vacuum drying for selected samples after being exposed to the conditioning atmosphere for 14 days.

In the following subsections, the samples which are exposed to the conditioning atmosphere for around 14 days are called 'wet samples'.

5.6.1 Moisture absorption effect on T_g

The absorbed water molecules can form hydrogen bonds with the network polar sites, replacing other inter- or intra-segmental hydrogen bonds as illustrated in Figure 5.21. This results in more flexible polymeric segments, reduces the rigidity between the crosslinking junctions and consequently reduces T_g of the network. Figure 5.22 clearly shows this effect on T_g where the water absorption reduces T_g and the reduction in T_g is broadly proportional to the water uptake. The data indicate that each 1 wt% of absorbed water causes on average around 9.5 ^{o}C reduction in T_g. Comparable values for the impact of water absorption on T_g were reported in [144, 145] for similar amine/epoxy systems. From the dielectric performance perspectives, reducing the T_g will enable more ionic conduction and, thus, moisture uptake will reduce the working temperature range of epoxy networks.

Figure 5.22 does not show the T_g for HP = 60 % since the DSC used here cannot give useful information in low temperature range, around 30 ^{o}C, where the T_g of this formulation is expected to lie.

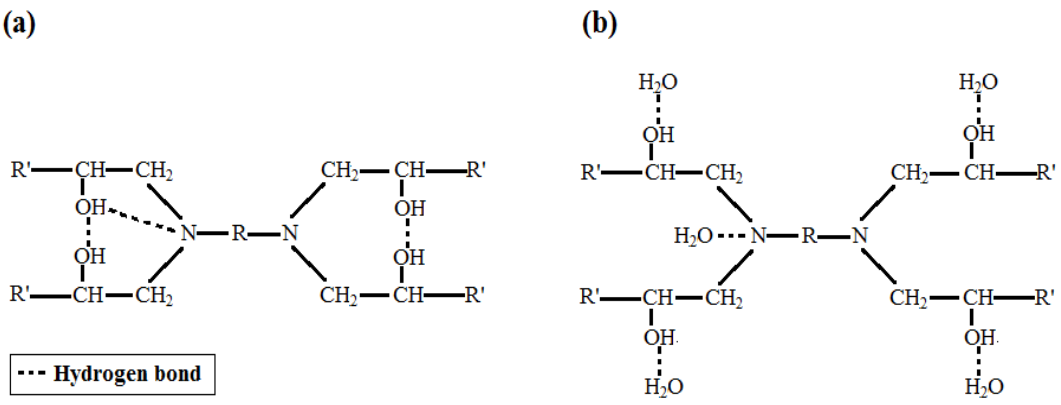

Figure 5.21: (a) possible inter- or intra-segmental hydrogen bonds in dry network, (b) possible hydrogen bonds between water molecules and polar sites in wet network.

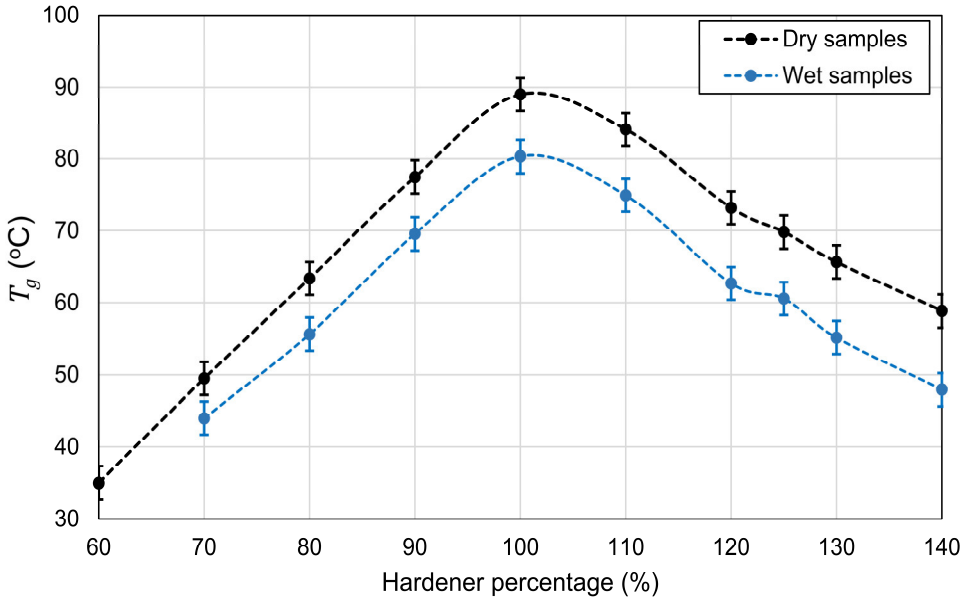

Figure 5.22: The effect of water absorption on T_g.

5.6.2 Moisture absorption effect on the dielectric spectra

Dielectric spectra obtained from all the wet samples are shown in Figure 5.23, for epoxy rich samples, and Figure 5.24, for amine rich samples. The water molecules increase the polar content within the material, which leads to a higher relative permittivity. The dielectric spectra show that ϵ_r' increased in reasonable agreement with the water uptake. These data also show that the absorbed water affects the imaginary part of the relative permittivity (ϵ_r''). Bulk water exhibits a main relaxation process at a very high frequency (~20 GHz at 20 °C) and other relaxations that take place at even higher frequencies [146]. However, it has been shown that water molecules relax at lower frequencies when they are bounded to other polar moieties within a matrix [147, 148]. Furthermore, the bound water relaxation is affected by the dynamics of the moieties to which the water molecules are

bound and, in many cases, the bound water molecules have been found to relax in phase with these moieties [27, 149]. Indeed, the dielectric spectra obtained here indicate that a significant part of the absorbed water manifests itself as a relaxation process similar to the β relaxation observed in the dry samples and, thus, strengthens the existing β relaxation, as can be seen by comparing the spectra of the dry and wet samples; this is shown in Figure 5.25 for selected samples. This suggests that a fraction of the absorbed water is bound to the polar content that is responsible for the β relaxation in the epoxy network, which is in line with the impact of the absorbed water on T_g, where the bounded water masks the network polar groups from forming intra- or inter-segmental hydrogen bonds (see Figure 5.21). The other part of the absorbed water may be bound to other polar moieties that relax at frequencies higher than the range accessible here (i.e. at frequencies > 1 MHz) and/or may represent unbound or isotropically mobile water clustered within the free volume inside the epoxy matrix and, thus, relax at much higher frequencies [143, 150, 151].

Many authors have tried to evaluate the ratio of the bound and unbounded water, by observing the increase in the value of ϵ_r' at different frequencies that results from the absorbed water, [142, 143]. As stated above, in the current investigation, the absorbed water can be divided into two parts: the first part represents the water that relaxes at frequencies > 1 MHz and can be evaluated by calculating the increase in ϵ_r' at 1 MHz between the wet and dry samples, and the other part represents the water that relaxes in phase with the β relaxation (i.e. from 1 MHz to 10 Hz) and can be evaluated by calculating the increase in the strength of the β relaxation due to the absorbed water. Figure 5.26 shows the increase in ϵ_r' due to each of these parts for all samples. This estimation shows that on average about 60 % of the absorbed water relaxes between 1 MHz and 10 Hz, which suggests that ~60 % of the absorbed water is bound to the polar groups that result in the β relaxation. Similar figures have been reported in [142, 143]. One thing that should be highlighted concerning the methodology used in the above estimation is that it assumes that the effective permittivity of the bound and less confined or free water are comparable. Since the less confined or free water might have a higher permittivity, taking this into account would lead to an increase in the estimated fraction of bound water and, therefore, does not affect the conclusion that a significant fraction of the absorbed water relaxes in phase with the β relaxation. Consequently, the fact that the absorbed water relaxes in synchrony with the polar components of the network renders dielectric spectroscopy a powerful tool to probe these polar components and to study the interactions between them and the absorbed water. This may be useful for the characterization of more complex systems, such as nanocomposites, as will be explored in the next chapter.

At low frequencies (< 1 Hz), ϵ_r'' starts increasing gradually on going to lower frequencies, particularly for amine rich samples (Figure 5.24). This phenomenon is caused by the higher DC conductivity of these samples, as will be discussed in the next subsection.

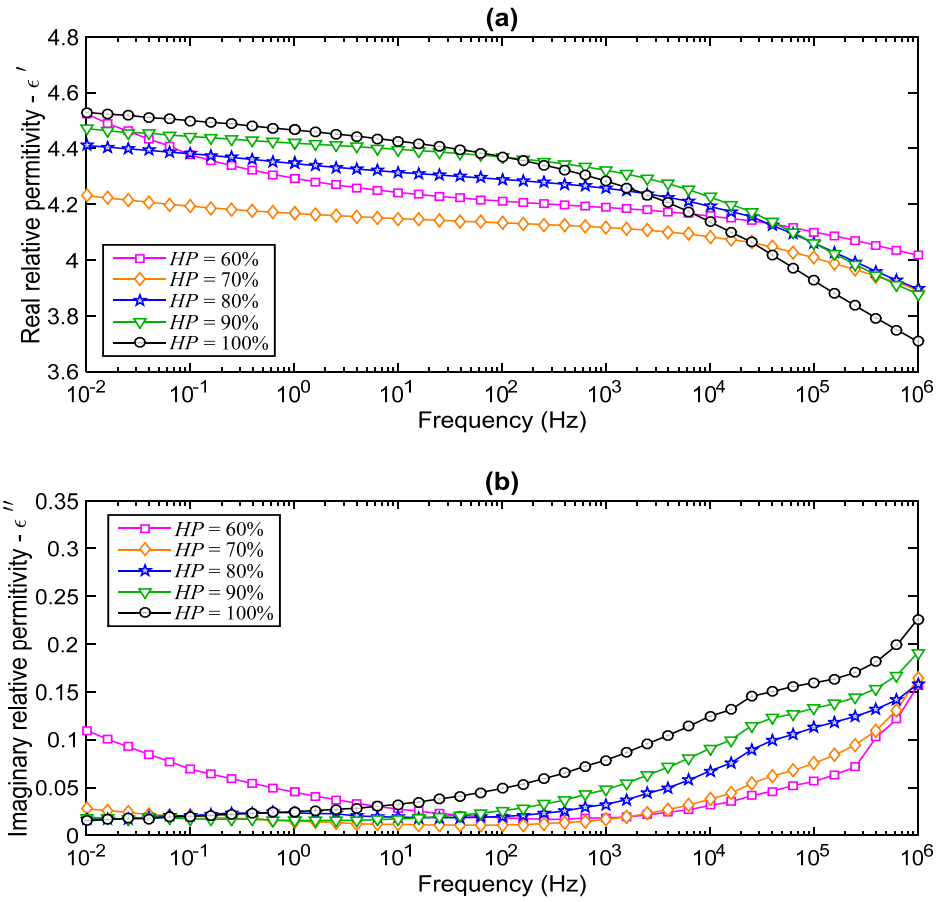

Figure 5.23: Dielectric spectra for epoxy rich wet samples at room temperature.

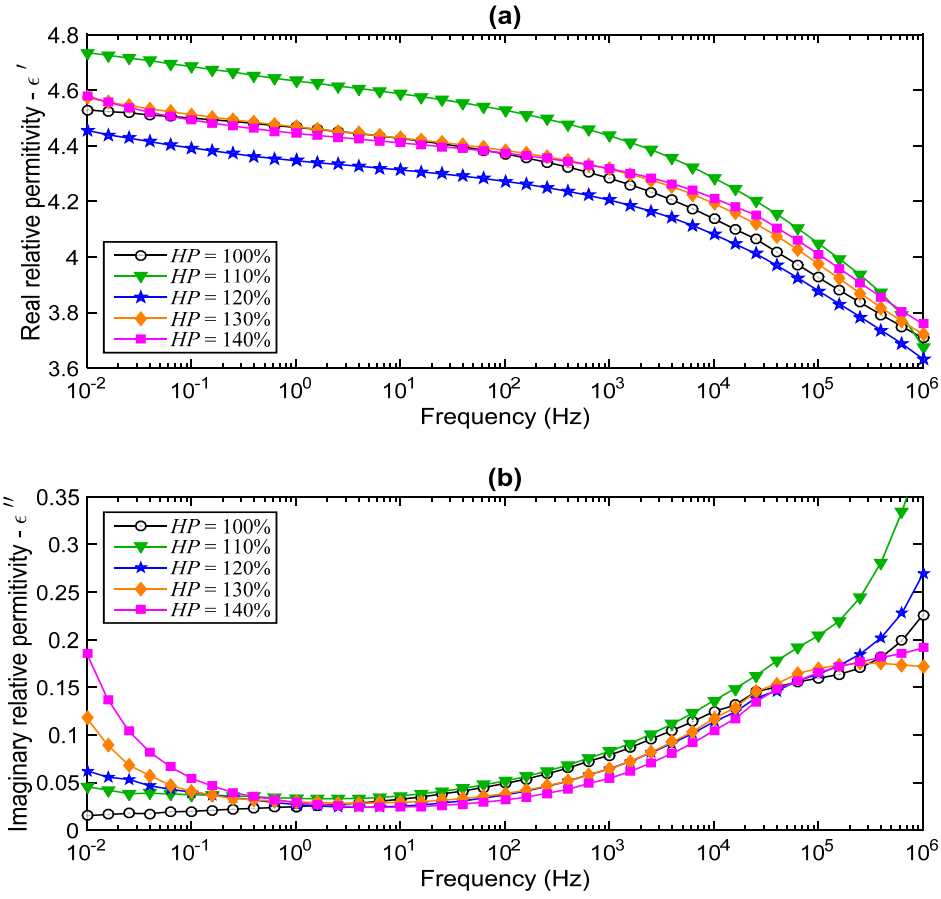

Figure 5.24: Dielectric spectra for amine rich wet samples at room temperature.

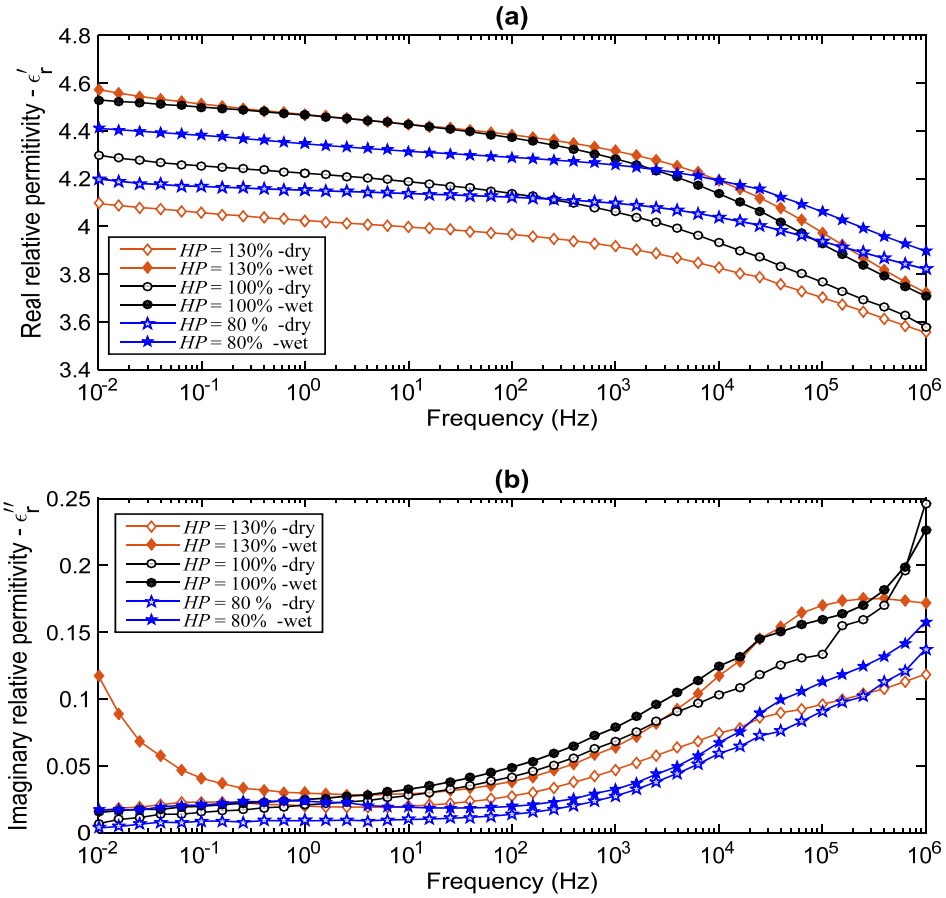

Figure 5.25: Dielectric spectra for selected wet samples compared with their dry counterparts, at room temperature.

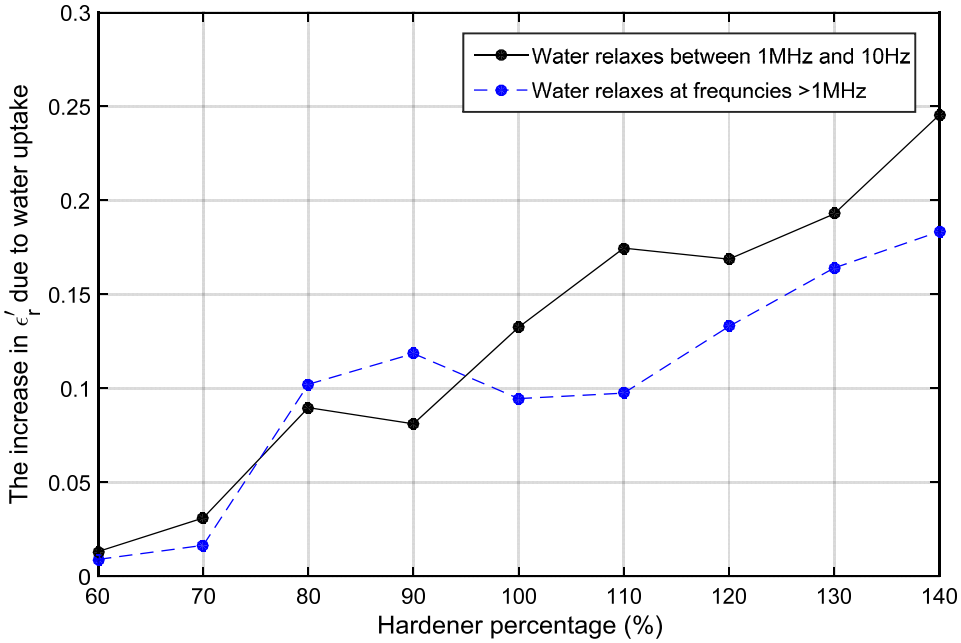

Figure 5.26: The increase in ϵ_r' due to water absorption.

5.6.3 Moisture absorption effect on the DC conductivity

Figure 5.27 presents the DC conductivity results for all wet samples obtained at a temperature of 30 ºC and an applied electric field of 42 kV/mm. Comparing these results

with the DC conductivity of the dry samples, shown earlier in section 5.4, indicates that the absorbed water leads to an increase in the DC conductivity and this increase is in a realizable agreement with the water uptake for all samples, except the case of *HP* = 60 % (sample 60HP/0). As *HP* and, consequently, the water uptake increase, the DC conductivity increases more greatly. This explains the rise in ϵ_r'' observed at low frequencies in the dielectric spectra of the amine rich samples. The increasing of DC conductivity due to water inclusion is reported in the literature [152-154]. Water molecules are highly polar and can be auto-ionized (i.e. producing OH^- and H_3O^+ ions), leading to higher charge transport [27, 155]. Marx [156] suggested that charge transport can take place via proton (H^+) transfer along hydrogen bonded water networks.

For sample 60HP/0, Figure 5.27 shows that the increase in the DC conductivity of this sample is greater than would be expected based only on its water uptake. The glass transition temperature of this sample in its dry state is 35 °C and, with water absorption, this value is expected to decrease further. Hence, this sample is relatively well within its rubbery state at a measurement temperature of 30 °C, which is possibly equal to its expected T_g. Therefore, the marked increase in the DC conductivity of this sample may be primarily caused by it being in a rubbery state at the measurement temperature, as will be explored below.

The data shown in Figure 5.27 indicate that the DC conductivity slightly decreases with time, particularly for the samples with high water uptake. This may indicate that these samples lose some of their absorbed water during the measurement process, which was carried out at a higher temperature and lower RH than the conditioning environment (22.5 °C and 60 % RH).

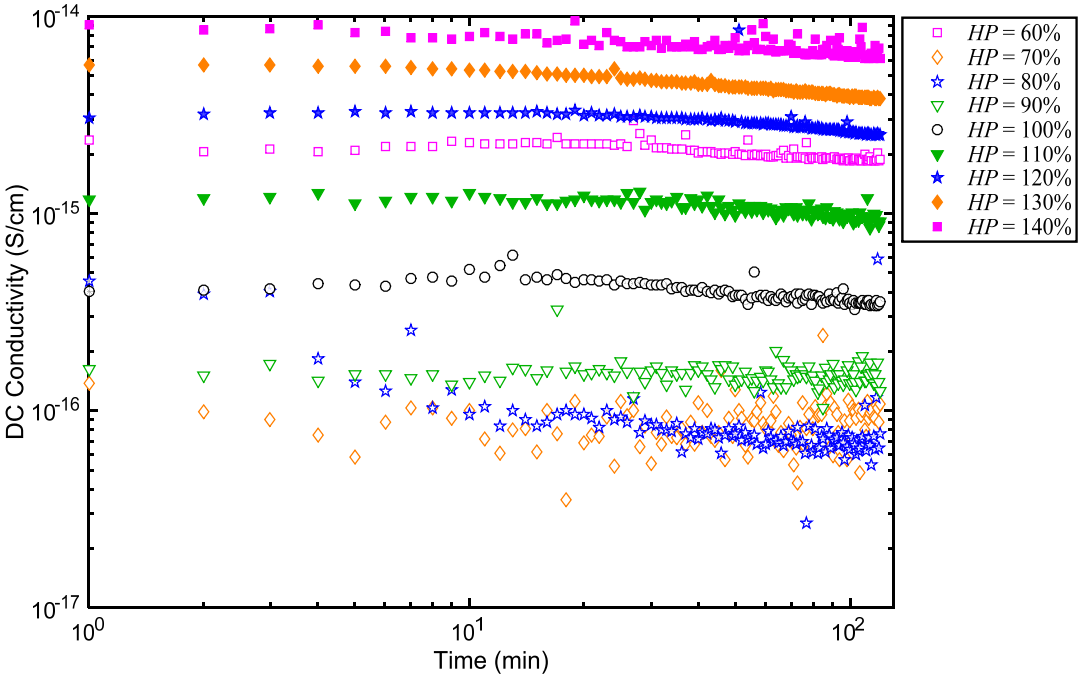

Figure 5.27: DC conductivity for all wet samples at 30 °C and applied field of 42 kV/mm.

In a trail to offset the effect of the rubbery state, the DC conductivity for some samples was measured at room temperature and the results are illustrated in Figure 5.28. The data imply that by measuring the DC conductivity at room temperature, the DC conductivity of the samples that are deeply in their glassy state at 30 °C decreases marginally, whereas the DC conductivity of the samples that are near their rubbery state at 30 °C decreases considerably. Sample 60HP/0 is the most affected, whereby its DC conductivity decreases by more than one order of magnitude when it is measured at ~23 °C rather than 30 °C. Therefore, this confirms that the relatively high DC conductivity observed for this sample at 30 °C is not exclusively due to a direct impact of water absorption but, instead, it is chiefly caused by its being in a rubbery state at 30 °C.

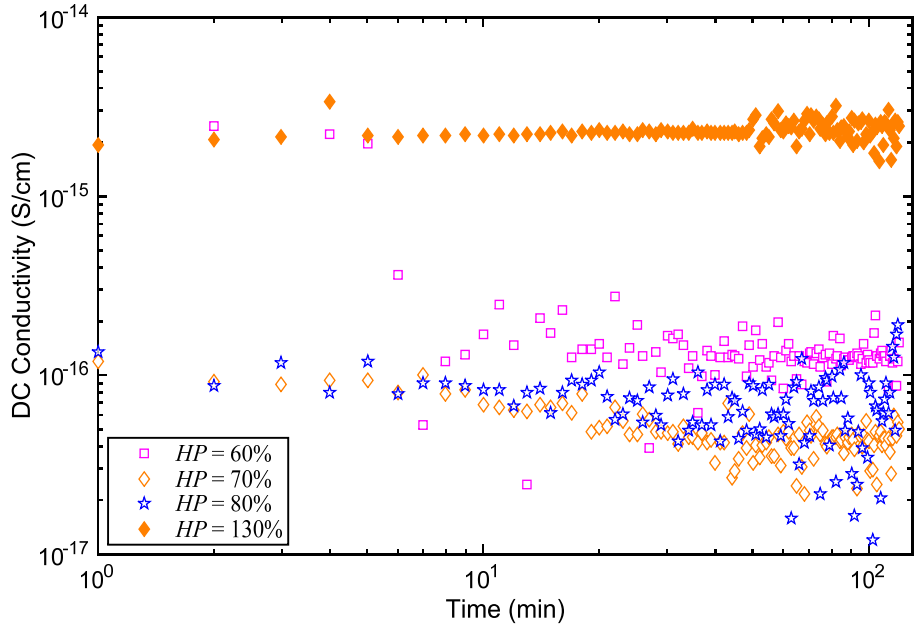

Figure 5.28: DC conductivity for some wet samples at room temperature and applied field of 42 kV/mm.

5.6.4 Moisture absorption effect on the DC breakdown strength

DC breakdown results for selected wet samples are shown in Figure 5.29 and the Weibull parameters for these samples are presented in Figure 5.30. The data reveal that the water uptake has a detrimental impact on the DC breakdown strength, which is similar to its effect on the DC conductivity. The reduction in the DC breakdown strength is directly proportional to the water uptake and, in turn, to the *HP*. This suggest that for using this material for HVDC applications, a care should be taken to reduce its moisture uptake.

Considering the water content of the wet samples (Figure 5.19), the DC breakdown data (Figure 5.30) suggest that 1 wt% of water uptake result in a reduction in the DC breakdown strength of around 35 %, which indicates the extreme sensitivity of DC breakdown strength to the water content of the material. The detrimental impact of water absorption on DC

breakdown strength has been reported elsewhere in the literature. Grzybowski [139] found that water uptake causes a sharp reduction in DC breakdown strength of polyethylene terephthalate. Fabiani *et al*. [94] showed that adding hydrophilic nanoparticles into a polymeric matrix without pre-drying them results in a DC breakdown strength that is significantly lower than that obtained when the same particles were dried before introducing them into the polymer matrix. Unfortunately, in both of these studies, the exact amount of water content was not mentioned. Hosier *et al*. [4, 28] reported that the addition of 10 wt% silica nanofiller significantly increases the water uptake of an otherwise hydrophobic polyethylene matrix. Their data showed that the absorption of 1 wt% of water causes at least a 60 % reduction in the DC breakdown strength of the nanocomposite. This figure is even greater than what is observed in the current study. A possible explanation for this might be associated with the distribution of the absorbed water in both cases. In the current study, the water molecules are homogeneously distributed throughout the material, i.e. there are no local zones that have more water content than the rest of the material, whereas in Hosier's study, the absorbed water was shown to form water shells around the nanoparticles and, consequently, these shells may form percolation paths and, thus, severely reduce the DC breakdown strength [26, 27]. This speculation will be further discussed in section 6.7, in connection with the effect of water uptake in Si_3N_4 filled samples.

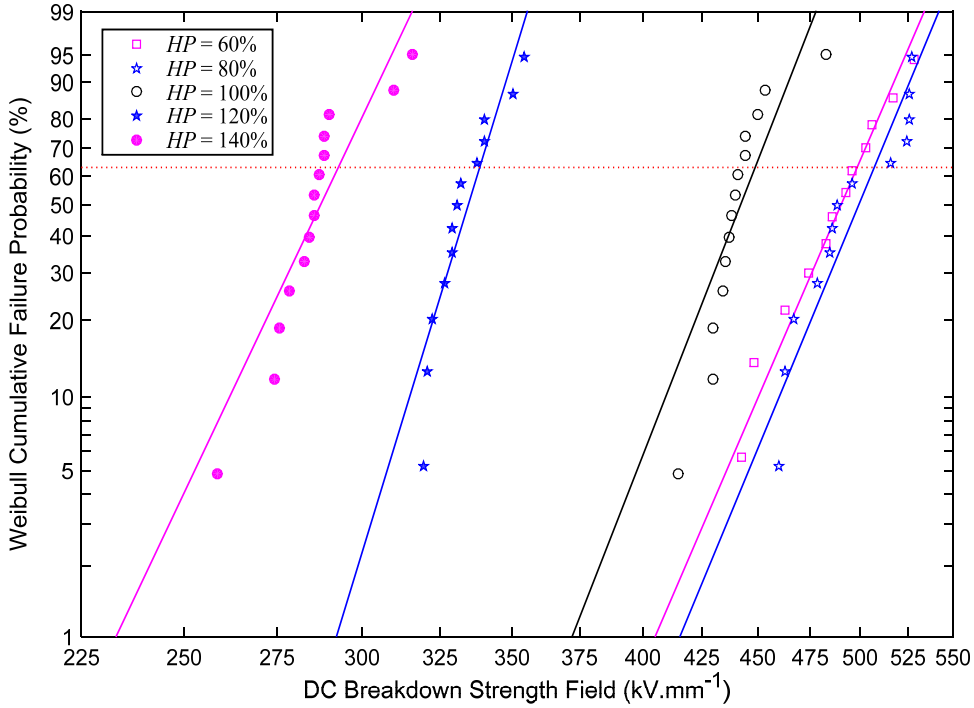

Figure 5.29: DC breakdown results for selected wet samples.

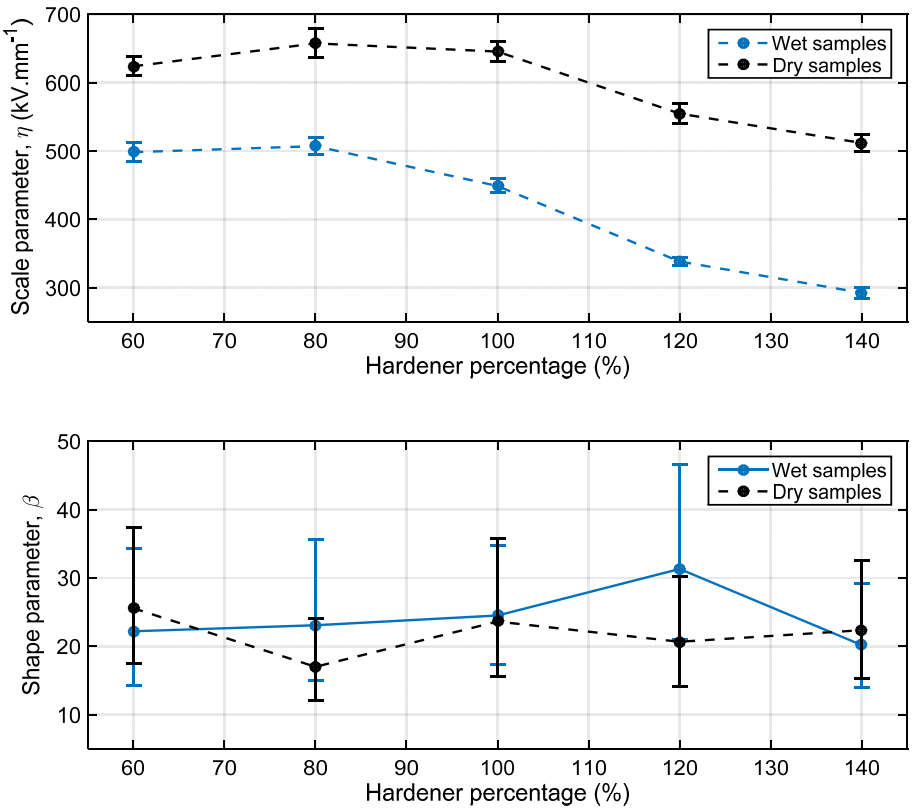

Figure 5.30: DC breakdown Weibull parameters for selected wet samples.

5.6.5 Moisture absorption effect on the AC breakdown strength

Figure 5.31 presents a Weibull plot for AC breakdown measurements obtained from selected wet samples and Figure 5.32 compares the Weibull parameters of these samples with the corresponding parameters of the dry samples. The data show that the AC breakdown strength decreases slightly by the effect of water absorption. The 95 % confidence bounds of wet and dry samples are overlapped, which indicates that this reduction is not significant and it is within the experimental error. This behaviour is similar to that reported by Grzybowski [139] who found that, compared with the sharp reduction in the breakdown strength, the AC breakdown strength only showed a relatively slight reduction due to water absorption.

These results suggest that the noticeable increase in the DC conductivity which caused by water absorption does not lead to an equivalent change in the short term AC breakdown strength. Thus, the effect of the absorbed water seems to be similar to the effect of the excess amine in the dry samples, in that both factors cause a significant rise in the DC conductivity but have a marginal effect on the AC breakdown strength. As was discussed in section 5.5, the AC breakdown strength is more sensitive to the presence of defects or inhomogeneities in the material. In the current systems, the absorbed water is supposed to be uniformly distributed with the epoxy matrix, which is similar to the distribution of amine content, therefore, it should not produce defects in the wet sample. Consequently, water absorption should not severely affect the AC breakdown strength.

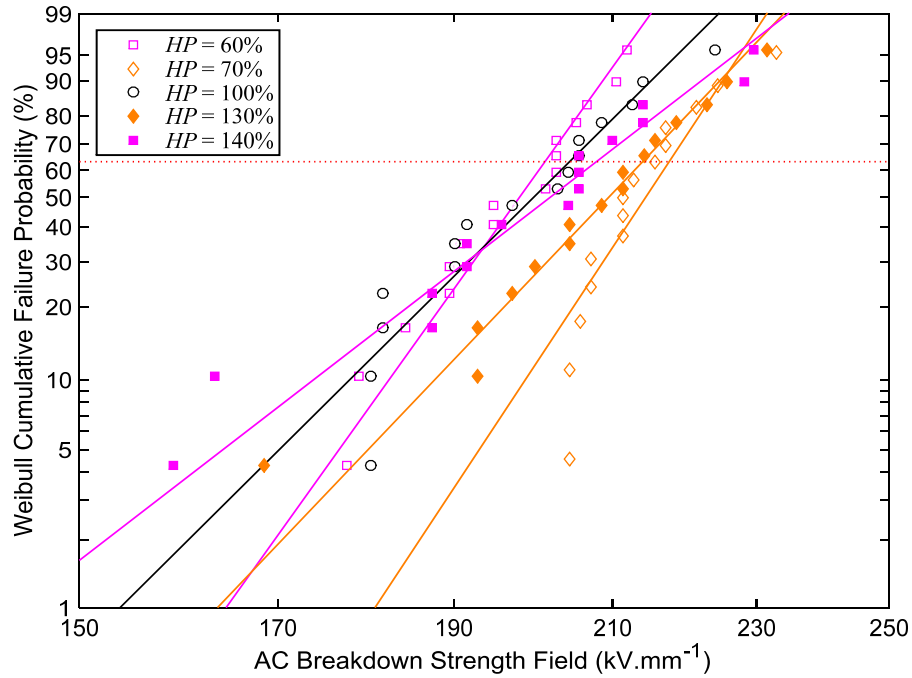

Figure 5.31: AC breakdown results for selected wet samples.

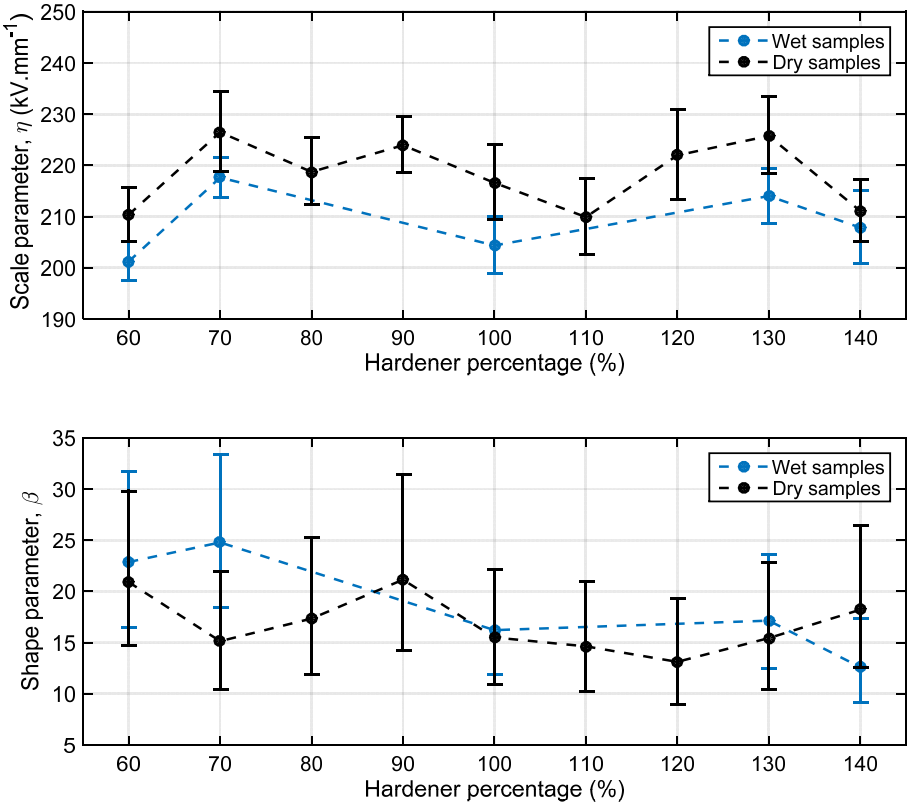

Figure 5.32: AC breakdown Weibull parameters for selected wet samples compared with the parameters of the dry samples, the error pars are based on 95 % confidence bounds.

5.7 Chapter summary

By changing the ratio of resin to hardener, a series of epoxy resin samples has been produced with differing network structures and different retained chemical functionalities.

Differential scanning calorimetry showed that the glass transition temperature is primarily determined by the crosslinking density and indicated that, under the range of conditions employed here, side reactions, such as etherification or homopolarization, are negligible.

Electrical characterisation data showed that, unlike the glass transition temperature, the electrical properties do not correlate directly with the network structure and crosslinking density. Instead, the electrical behaviour is mainly related to the chemical content, represented by the amine and hydroxyl groups, of the cured epoxy. Increasing the hardener (amine) content beyond the optimal stoichiometry has a detrimental effect on electrical properties like DC conductivity and DC breakdown strength. On the other hand, decreasing the amine content has some beneficial electrical consequences, such as reduced DC conductivity and increased DC breakdown strength, particularly when the material is well within its glassy state. However, consequent changes to the network structure will affect T_g and, as the temperature approaches the T_g of the material, increased ionic conduction will play an increasingly important role.

Unlike the DC breakdown strength, which correlates with the DC conductivity, the AC breakdown strength is not significantly influenced by the change in the DC conductivity, which implies that a *homogenous* increase in the DC charge transport does not necessarily lead to a noticeable change in the short-term AC breakdown strength.

The changes occurring in the dielectric spectra are chiefly ascribed to the change in the hydroxyl group content accompanied by changing the hardener (amine) percentage. Although the amine group is a polar one, increasing the amine content does not have a discernible effect on the dielectric spectra. This might be attributed to the limited rotational/conformational mobility of the amine groups inside the network. In the cured epoxy, the amine group is part of the main chains that constitute the network. Therefore, it is difficult for the amine groups to reorient in response to an electric field, which limits their contribution to the orientation polarisation and to the permittivity. Conversely, the OH groups in the hydroxyether groups represent side groups and they can rotate more easily.

Water uptake is proportional to the polar content, which is ultimately related to the amine content. The absorbed water forms hydrogen bonds with the polar sites replacing other inter- or intra-segmental hydrogen bonds and leading to a proportional reduction in T_g. In terms of the dielectric spectra, the absorbed water increases the polar content of the matrix and thus increases its relative permittivity. Part of the absorbed water interacts with the polar sites in the network and, therefore, its dielectric relaxation is related to the relaxation of the moieties to which this fraction of the water is bound. For the DC conductivity and DC breakdown strength, the absorbed water causes a significant rise in the DC conductivity which is reflected into an analogous reduction in the DC breakdown strength. However, its effect on the AC breakdown strength is marginal.

Chapter 6

Effect of Resin/Hardener Stoichiometry on Electrical Behaviour of Si_3N_4 Epoxy Nanocomposites

6.1 Introduction

One of the key aspects of a nanofiller is its large specific surface area, which will result in a large interfacial area between the nanofiller and the encapsulating polymer. Different chemical [1], physical [2] or electrical [3] interactions can occur between the two phases, depending on the characteristics of the matrix and the nanofiller. For epoxy based nanocomposites, nanoparticles are incorporated into the resin in its liquid state before the curing process, which allows better particle dispersion and also enables the particles to interact with the reactive resin and hardener. These interactions might include chemical reactions between the nanofiller surface functionalities and the active groups, either in the resin (epoxy groups) or in the hardener (amine groups in this study). Such reactions may modify the effective resin/hardener stoichiometry and change the structure of the resulting network after curing. As established in the previous chapter, modifying the resin/hardener ratio significantly influences the electrical properties of the resulting epoxy network. Accordingly, the influence of nanofiller addition into an epoxy matrix might be related to a commensurate change in the resin/hardener stoichiometry, rather than directly associated with the presence of the nanofiller. Therefore, this parameter, which usually receives little attention, should be considered when analysing the electrical performance of epoxy based nanocomposites.

As the FTIR spectra revealed (section 4.3.3), the surface chemistry of Si_3N_4 is characterised by the existence of amine and, to a lesser extent, hydroxyl groups. Both of these groups, particularly the amine groups, can react with the epoxy groups in the resin and therefore this surface chemistry makes Si_3N_4 intrinsically compatible with an epoxy matrix. In principle, the reactivity between the amine groups on the silicon nitride surface and the resin's epoxy groups is expected to be similar to the reactivity between the latter groups and the hardener's amine groups. Hence, the inclusion of a Si_3N_4 nanofiller within an epoxy matrix may consume a fraction of the epoxy groups, which would otherwise be expected to crosslink with the hardener, and consequently, may change the effective resin/hardener stoichiometry throughout the whole matrix.

While detecting a nanofiller stoichiometric influence can help in analysing the performance of epoxy-based nanocomposites, it also offers an opportunity to investigate

and verify many of the hypotheses that have been proposed in the literature for describing the behaviour of nanodielectrics. For example, a direct chemical reaction between the nanoparticles and the epoxy resin in its liquid state should lead to an excellent dispersion of the as prepared nanofiller. Nanoparticle dispersion usually imposes a challenge for obtaining actual nanodielectric systems (the applicability of nanodielectric systems), where the nanoparticles, due to their large specific surface area and surface tension forces, tend to agglomerate, producing a sub-microcomposites [7, 8]. Many researchers have tried to overcome this by treating the nanofiller with matrix-compatible functionalities [9-11]. However, this treatment brings other parameters into play, such as changing the particle surface chemistry and water absorption, and thus complicates the analysis of the influence of particle dispersion.

Furthermore, many studies have claimed that interactions between nanoparticles and the polymer host matrix may result in an interfacial zone or interphase layer with modified polymeric chain dynamics [12], alignment [13, 14], or morphology [15]. Commonly, these models or proposals were proposed to interpret the unexpectedly significant effect of adding a small amount of nanofiller on one or more of the properties of the resulting composites, where two-component effective medium theories cannot explain such effect, and some workers term it a nanoeffect [16]. For example, the dielectric permittivity of epoxy nanocomposites was found to be lower than that of both the filler and polymer materials in [17, 18]. Therefore, the above proposals suggest the formation of an interphase layer and, consequently, define nanocomposites by a tertiary system that consist of filler, matrix and interphase layer around the particles. The thickness for such an interphase has been postulated to range from 5-50 nm for different models, based on the experimental results concerned. Identifying a stoichiometric effect for the addition of Si_3N_4 nanofiller implies the presence of chemical reactions between the epoxy matrix and the nanofiller which, according to the above suggestions, should result in an interphase layer around the nanoparticles with distinct molecular dynamics. Therefore, this chapter will firstly investigate the impact of filler/matrix interactions between an epoxy matrix and inherently compatible Si_3N_4 nanoparticles on resin/hardener stoichiometry, particle dispersion, and molecular dynamics of silicon nitride epoxy nanocomposites. After that, the consequences of these interactions for the electrical properties of the generated nanocomposites will be explored. Table 6.1 lists the samples which were prepared for this purpose. These samples can be divided into two series, the first one is filled with 2 wt% Si_3N_4 at three different *HP*s whereas the other series is filled with 5 wt% at the same *HP*s used in the first series. As stated above, the incorporation of Si_3N_4 nanofiller will increase the overall amine content of the system, therefore, the emphasis here is on preparing nanocomposite samples with $HP < 100$ % to observe if the added filler will compensate the lack of hardener amine groups. Furthermore, the effect of changing *HP* on the filled samples will be compared

with its effect on unfilled samples. The reference for each sample will be its correspondent from the unfilled samples, studied in chapter 5.

Table 6.1: Proposed formulations to study the stoichiometric effect of Si_3N_4.

Sample code	Resin : Hardener mass ratio (*HP* (%))	Si_3N_4 filler loading (wt%)
80HP/2SiN	1000 : 275 (60 %)	2
90HP/2SiN	1000 : 309 (70 %)	2
100HP/2SiN	1000 : 344 (80 %)	2
80HP/5SiN	1000 : 275 (80 %)	5
90HP/5SiN	1000 : 309 (90 %)	5
100HP/5SiN	1000 : 344 (100 %)	5

6.2 Glass transition and molecular dynamics

6.2.1 Glass transition temperature

Variations in the glass transition temperature of the 2 wt% and 5 wt% filled samples are presented in Figure 6.1 and Figure 6.2, respectively. T_g of the unfilled samples are also included in these figures, for comparison. For the unfilled epoxy, as stated in chapter 5, T_g is predominantly controlled by the crosslinking density, which is a function of the resin/hardener stoichiometry. Conversely, both the 2 and 5 wt% filled samples apparently exhibit different trends. For the 2 wt% filled samples, reducing the *HP* to 90 % does not lead to a significant reduction in T_g, as for the unfilled counterpart sample. Reducing the *HP* further from 90 % to 80 % results in a considerable decrease in T_g, comparable to the decrease in the unfilled samples when decreasing *HP* by 10 %. This indicates that the 2 wt% filled samples follow the trend of the unfilled samples when *HP* was reduced from 90 % to 80 %. For the 5 wt% filled samples, the addition of Si_3N_4 to the stoichiometric formulation results in a significant decrease in T_g when compared with the stoichiometric unfilled sample. Decreasing the *HP* to 90 % results in a significant increase in T_g and this increase continues when *HP* decreases to 80 %, which is in total contrast to the trend seen in the unfilled samples.

This substantial variation between the effect of changing the stoichiometry on T_g of the filled and unfilled samples, might be a physical or chemical consequence of the presence of the Si_3N_4 nanofiller. In the former case, the presence of the nanoparticles may impose a geometric confinement on the polymer molecules, alter the morphology of the matrix, or affect the dynamics of the surrounding polymer chains depending on the attraction strength between the polymer and the particle surface [157-159]. These effects would modify the dynamics or the free volume content of the host polymer, which correspondingly influences T_g. For the chemical case, the nanoparticles chemically interact with the active functionalities in the resin or the hardener, which might then change the crosslinking

mechanism or modify the stoichiometry of the active groups in the system. Bignotti [160] compared the effect of changing the resin/hardener ratio on unfilled and clay filled amine/epoxy matrix and found that the nanofiller affects neither the crosslinking density, deduced via measuring the elastic modulus, nor the T_g, extracted from DSC measurements. Similar finding has been reported by Nguyen [88] for anhydride epoxy system, where the incorporation of naonsilica affects neither the curing mechanism nor the T_g. Yeung [19] recently has reported that the addition of untreated silica has no significant influence on the T_g of the same epoxy matrix considered here. Other studies [44, 161] which considered non-crosslinking polymers also reported a slight influence on T_g even when the nanoparticles affect the polymer dynamics by inducing a rigid layer, which does not exhibit a glass transition. These findings suggest that as long as the nanoparticles do not chemically interfere with the curing process, their physical presence has a marginal impact on T_g. Nevertheless, a number of studies have claimed that nanofiller inclusion may increase the free volume in polymeric matrix [137] or it may act as an obstacle that disrupts polymer chain crosslinking [162, 163], which in both cases leads to lower T_g. Conversely, other studies have indicated that strong filler/matrix interactions might reduce polymer chain mobility and thus yield a more rigid polymer with higher T_g [157, 164, 165]. In the current investigation, if any of the physically induced effects is dominant, then the variations in T_g should be a function of the filler loading not the *HP*. Clearly this is not applicable, where, for example at 5 wt% Si_3N_4 loading, the nanofiller decreases T_g by 17 ^oC at *HP* of 100 % and increases it by 24 ^oC at *HP* of 80 % (here each filled sample was compared with the unfilled sample that has the same *HP*, as shown in Figure 6.2). Therefore, the behaviour of T_g should be predominantly governed by the stoichiometric effect of the nanofiller. Since the surface of Si_3N_4 is covered by amine groups, it would be expected to increase the effective amine content and, thus, result in an effective *HP* that is higher than the nominal *HP*. Indeed, as shown in Figure 6.1, at 2 wt% the particles compensate for part of the amine groups as evinced by lowering the sharp reduction in T_g when the nominal $HP < 100$ %. Similarly, at 5 wt% loading, the particles increase the amine content, which produces an amine-rich matrix at a nominal *HP* of 100 % and compensates for a considerable part of the amine content at a nominal *HP* of 80 %. In order quantitatively to estimate the influence of the filler on the stoichiometry, the *HP* of the nanocomposites was modified until T_g of the filled samples best matches T_g of the unfilled samples. According to its definition in Eq. 4.2, the *HP* is calculated as a ratio of the resin and, therefore, if the amine groups on the surface of the Si_3N_4 particles have consumed a percentage x of the epoxy groups in the resin, then the effective hardener percentage (HP_{eff}) can be calculated by:

$$HP_{eff} = \frac{HP}{(100 - x)} \qquad \text{Eq. 6.1}$$

where *HP* is the nominal hardener percentage as defined in Eq. 4.2. Depending on curve fitting between the filled and unfilled samples, it was estimated that x is ~6.5 and ~18 for

the 2 wt% and 5 wt% nanocomposite series, respectively. Hence, 2 wt% of Si_3N_4 reacts with ~ 6.5 % of the epoxy groups and 5 wt% of Si_3N_4 consumes ~ 18 % of the resin epoxy groups. Figure 6.3 shows T_g results for all samples as a function of HP_{eff}, i.e. after adjusting the *HP* of nanocomposite samples following Eq. 6.1. Here, it is worth mentioning that *HP* and HP_{eff} are equivalent for unfilled samples, since $x = 0$. Evidently, T_g of filled and unfilled samples exhibit similar trends and this was for both 2 and 5 wt% filled samples. The ratio between the resin consumed in 2 wt% filled samples and 5 wt% filled samples according to the above estimation is 18/6.5 (2.77), which is close to the nominal ratio of 5/2*98/95 (2.58), (the factor 95/98 is to account for the resin replaced by the 5 and 2 wt% filler content). This provides substance to the hypothesis that the added filler reacted with 6.5 % and 18 % of the epoxy groups at 2 wt% and 5 wt%, respectively.

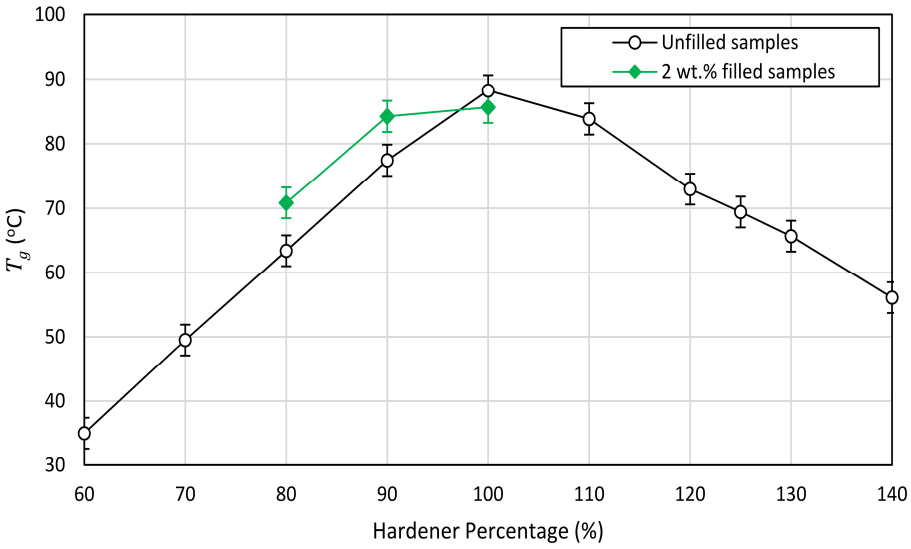

Figure 6.1: A comparison between T_g of 2 wt% filled nanocomposites and unfilled samples.

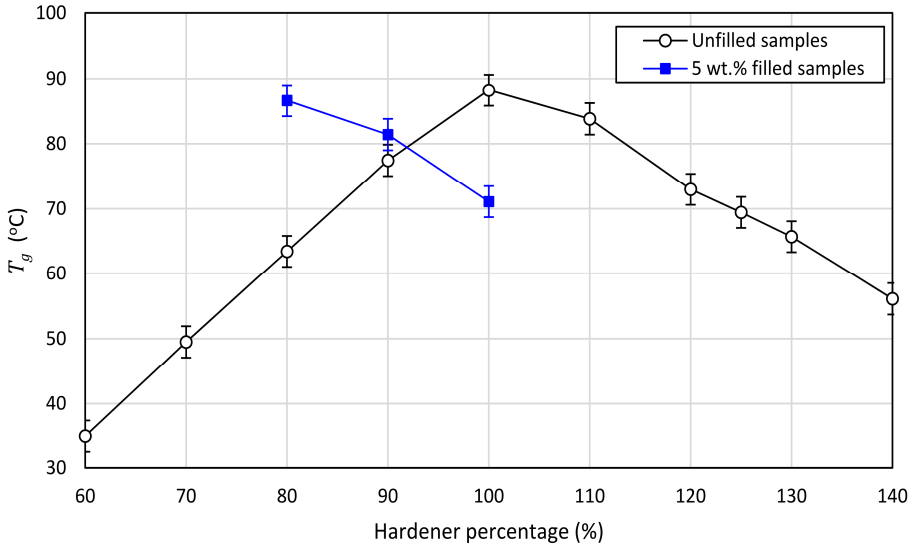

Figure 6.2: A comparison between T_g of 5 wt% filled nanocomposites and unfilled samples.

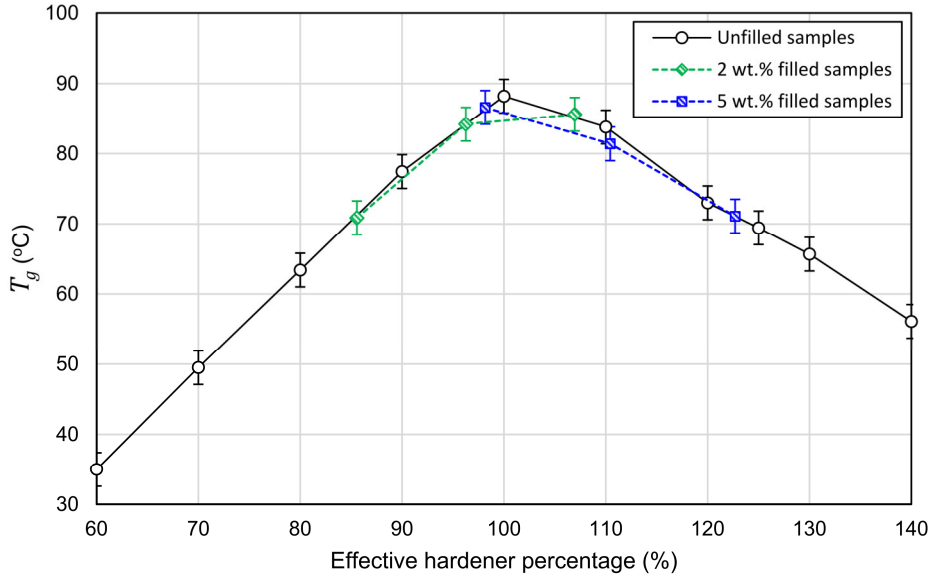

Figure 6.3: T_g of all samples as a function of effective hardener percentage.

6.2.2 Molecular dynamics over the glass transition

As the stoichiometric effect described above provides clear evidence of chemical reaction between the Si_3N_4 particles and the polymer, the next step is to see how this bonding affects the molecular dynamics over the glass transition. Figure 6.4a illustrates ΔC_p of the 2 wt% filled, 5 wt% filled and unfilled samples. The data show that ΔC_p of the nanocomposite samples does not line up with their counterparts from the unfilled samples. However, when the *HP* of the nanocomposites is adjusted in the same way as was done for the T_g results, ΔC_p for both nanocomposite series nicely matches the results obtained from the unfilled samples (see Figure 6.4b). Such agreement reinforces the above conclusion about the Si_3N_4 filler's stoichiometric effect and also implies that anchoring of the epoxy molecules on the surface of the particles does not appreciably modify the segmental dynamics of the epoxy network. Harton [43] and Sargsyan [44] reported that strong hydrogen bonding interactions between silica nanoparticles and polymeric matrices result in an immobilised layer around the particles that does not take part in the glass transition relaxation and, consequently, the ΔC_p of the nanocomposites was found to decrease proportionally with the filler loading. In both of these studies, experimental ΔC_p values obtained from the nanocomposite samples could be statistically discriminated from ΔC_p values of the corresponding pure polymers only when the filler loading was > 20 vol% (filler size < 25 nm in both investigations). Consequently, the authors estimated the thickness of the immobilised layer to be ~1 nm in [43] and ~2 nm in [44]. Since the maximum filler loading used in this study is much less than 20 vol%, one can easily conclude that the existence of such immobilised layer cannot be differentiated from experimental uncertainties. However, relying on filler size and loading when comparing different studies might be insufficient, since there is another factor that needs to be included, particle dispersion; however this is difficult to quantify. As an alternative, in this study, we can rely on the estimate that around 18 % of the epoxy

groups crosslink with the particle surfaces at 5 wt% filler loading to explore the possibility of any constrained layer. Assuming that for each attached epoxy group, the dynamics of its corresponding DGEBA molecule is confined and forms an immobilised segment. This implies that the thickness of the postulated immobilised layer is one DGEBA molecule or 2.6 nm [166], which is in the range of the thicknesses proposed by the above studies. This would result in an immobilised mass fraction that equals 18 *2 *1000/1344 or ~27% of the whole polymeric matrix; assuming that each DGEBA molecule can react with the particles with only one of its two epoxy groups and considering the mass of the hardener at *HP* = 100 %. A mass fraction of 27 % is well out of the experimental uncertainties shown in Figure 6.4 and, therefore, it should be detectable. Since this is not the case, the thickness of any possible immobilised layer should be less than one DGEBA molecule length. Based on 95 % uncertainty boundaries, which is around ±7.5 % of the average of ΔC_p, an immobilized layer that represents more than 7.5 % of the sample polymer mass should be experimentally detectable. Consequently, the thickness of any immobilized layer should be < 0.8 nm. Investigating the chemical structure of DGBEA shows that the epoxy group is connected to the rest of the molecule through an ether functional group. This connection is structurally flexible as the conformation of C–O–C has low energy and steric barriers. The existence of such a flexible bond might limit the effect of any dynamic confinement, due to the bonding to the particle, to the few atoms next to the epoxy/particle bond and, therefore, this will bring the thickness of any affected layer to a few angstroms.

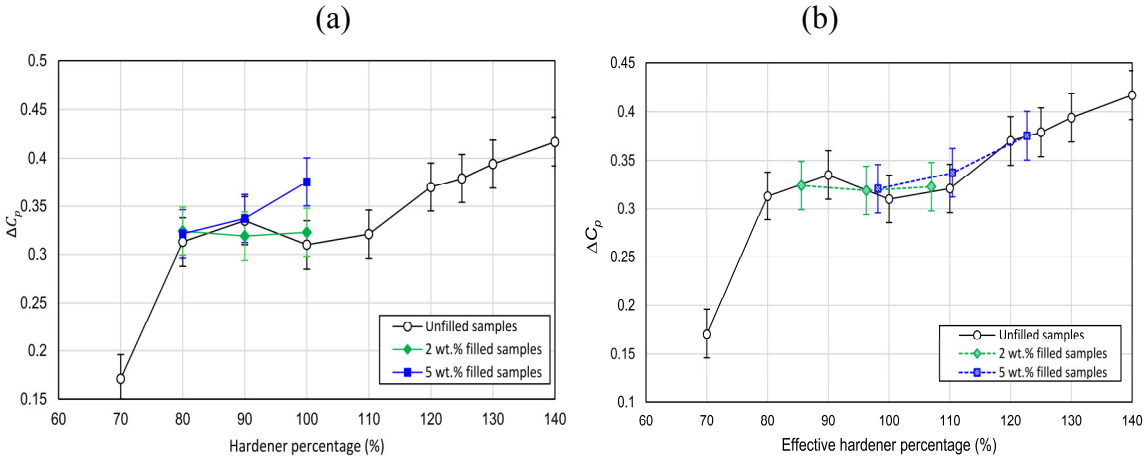

Figure 6.4: The change in the heat capacity over the glass transition process: (a) as a function of nominal hardener percentage and (b) as a function of effective hardener percentage.

6.2.3 Network homogeneity

Instead of forming a completely rigid layer that does not contribute to the glass transition, other studies have claimed that strong filler/polymer interactions cause a broadening of the glass transition to higher temperatures [45, 46, 167], or result in additional glass transition step at different temperature [45, 46, 167, 168]. Therefore, the polymer/filler attachment

might cause a restriction for the segmental dynamics of the surrounding polymer and this effect gradually decreases with the distance from the particle surface. Such an effect would reduce the homogeneity of the polymeric matrix and, as a result, increase the glass transition width (ΔT_g). Alternatively, the affected polymeric fraction may relax at a distinct temperature range, which would be reflected as a second glass transition step in DSC traces. To investigate these possibilities, Figure 6.5 presents representative DSC traces obtained from some of the filled and the reference samples and Figure 6.6 compares ΔT_g of the nanocomposite samples (after adjusting their *HP*) with ΔT_g of the unfilled samples. Both of these figures do not show any sign of significant glass transition broadening nor additional glass transition process in the nanocomposite samples. This again suggests that the thickness of any affected polymeric layer is too small to result in a discernible influence on the cooperative dynamics of the epoxy network or, in the limit, this might imply the absence of any impact on the segmental dynamics, as was concluded in other studies [41, 42].

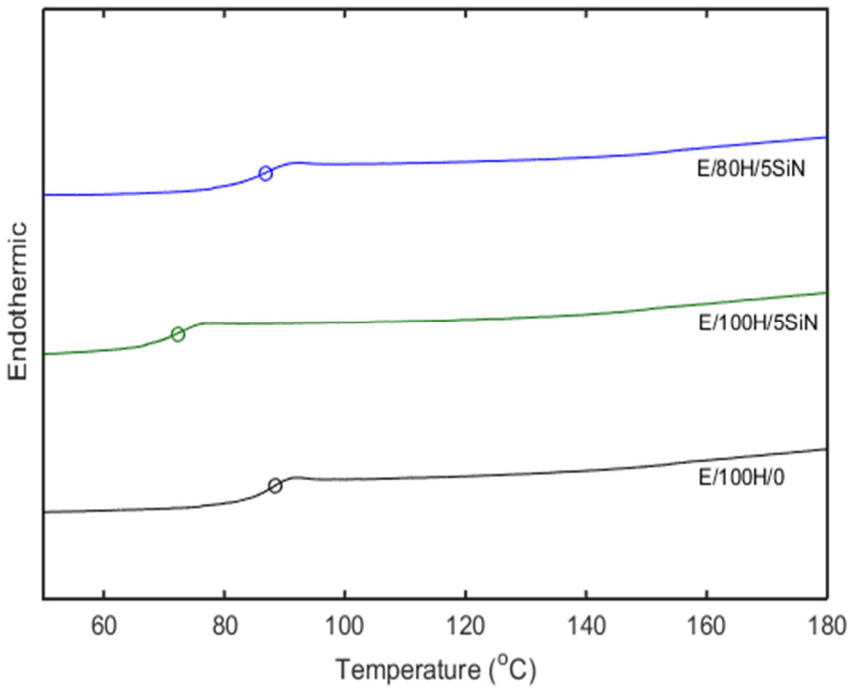

Figure 6.5: DSC traces obtained from the refernce sample and some of the filled samples; the circles superimposed on the curves indicate T_g.

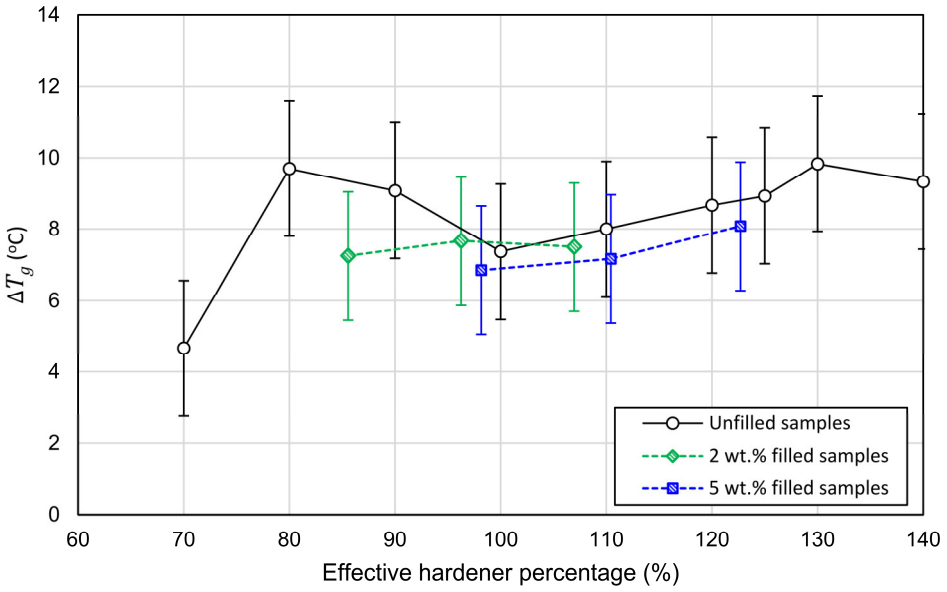

Figure 6.6: Glass transition width as a function of effective hardener percentage for all samples.

6.3 Dielectric spectra

Dielectric spectra obtained from the two nanocomposite series along with the reference sample are presented in Figure 6.7 and Figure 6.8. A broad β relaxation process that peaks at ~4 × 10^4 Hz and extends from 1 MHz down to low frequencies around 10 Hz is pronounced in all samples. However, its strength varies from one sample to another. As established in section 5.3, this relaxation is generally attributed to the rotation of the hydroxyether groups that are generated due to the crosslinking reaction between the epoxy and amine groups and its strength should therefore be related to the crosslinking density of the epoxy network. For the 2 wt% filled nanocomposites, the strength of the β relaxation for samples 100HP/2SiN and 90HP/2SiN is not significantly different from that of the reference sample, since the crosslinking density in these samples, deduced from T_g, is not markedly affected. For sample 80HP/2SiN, Figure 6.7b indicates that the strength of the β relaxation is noticeably reduced and, consequently, the real part of the relative permittivity (ϵ_r') is increased at high frequencies. This behaviour was also seen in unfilled samples when *HP* is less than 100 %, see section 5.3. Part of the β relaxation reduction is attributed to the lower concentration of hydroxyether groups (as evinced by the lower T_g) and another part is related to its partial displacement to higher frequencies, which results in the uplift in the values of ϵ_r' at high frequencies. For the 5 wt% filled samples, the β relaxation smoothly increases by decreasing the nominal *HP* from 100 % to 80 %, which correlates with the behaviour of T_g of these samples and also implies that the effective crosslinking density and HP_{eff} are anti-correlated with the nominal *HP*. Furthermore, such smooth variations in the β relaxation is in accordance with its behaviour for amine rich unfilled

samples (section 5.3). Therefore, these variations in the β relaxation lead to the same conclusions derived from the DSC results about the crosslinking density and the stoichiometric influence of the Si_3N_4 filler. To consolidate further the above description of the β relaxation, its strength was estimated by evaluating the difference in ϵ_r' between 1 MHz and 10 Hz for each sample and the results are presented in Figure 6.9 as a function of HP_{eff} (based on T_g analysis) for all samples. This approach of evaluating the relaxation strength, rather than depending on absolute values of ϵ_r'', has the advantage of eliminating some of the experimental errors. Although the data in Figure 6.9 could be influenced by the experimental errors as could be seen by the overlapping of the error bars, the data reveal that both the unfilled and filled epoxy matrices exhibit analogous β relaxation with respect to their nominal and effective *HP*, respectively.

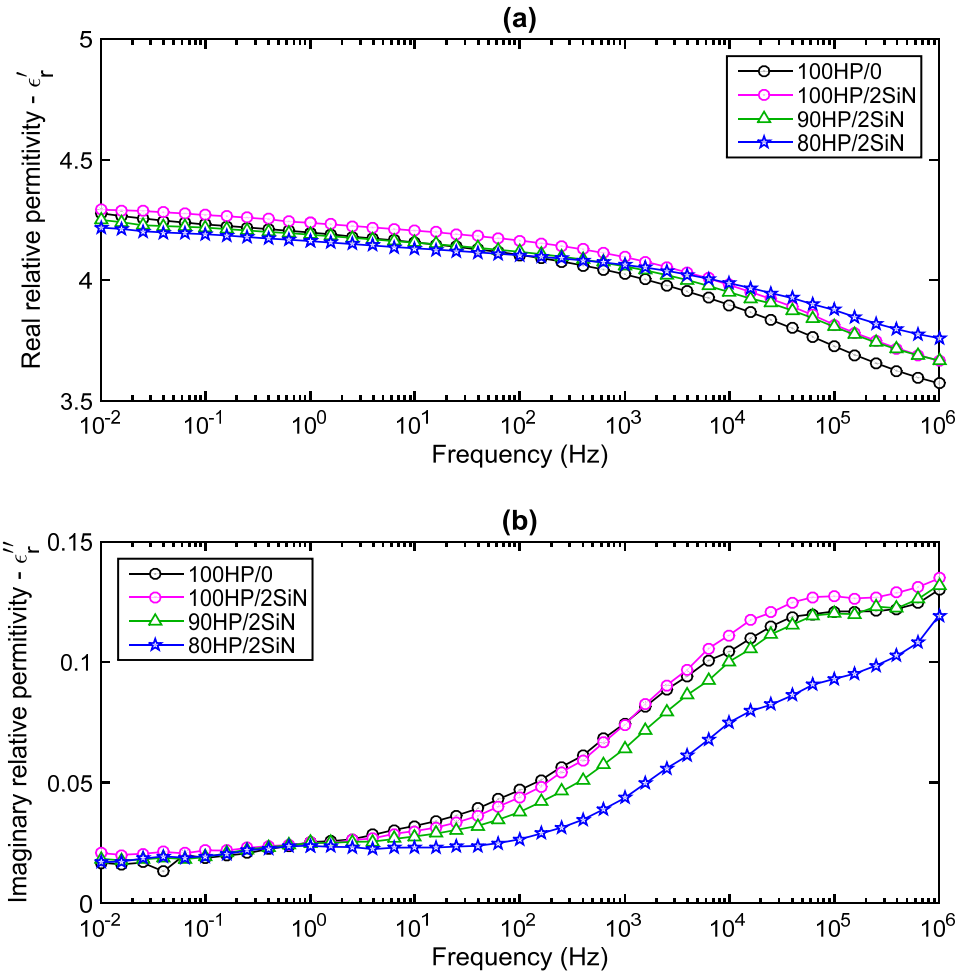

Figure 6.7: Dielectric spectra for 2 wt% filled nanocomposites compared with the reference sample, (a) real permittivity and (b) imaginary permittivity.

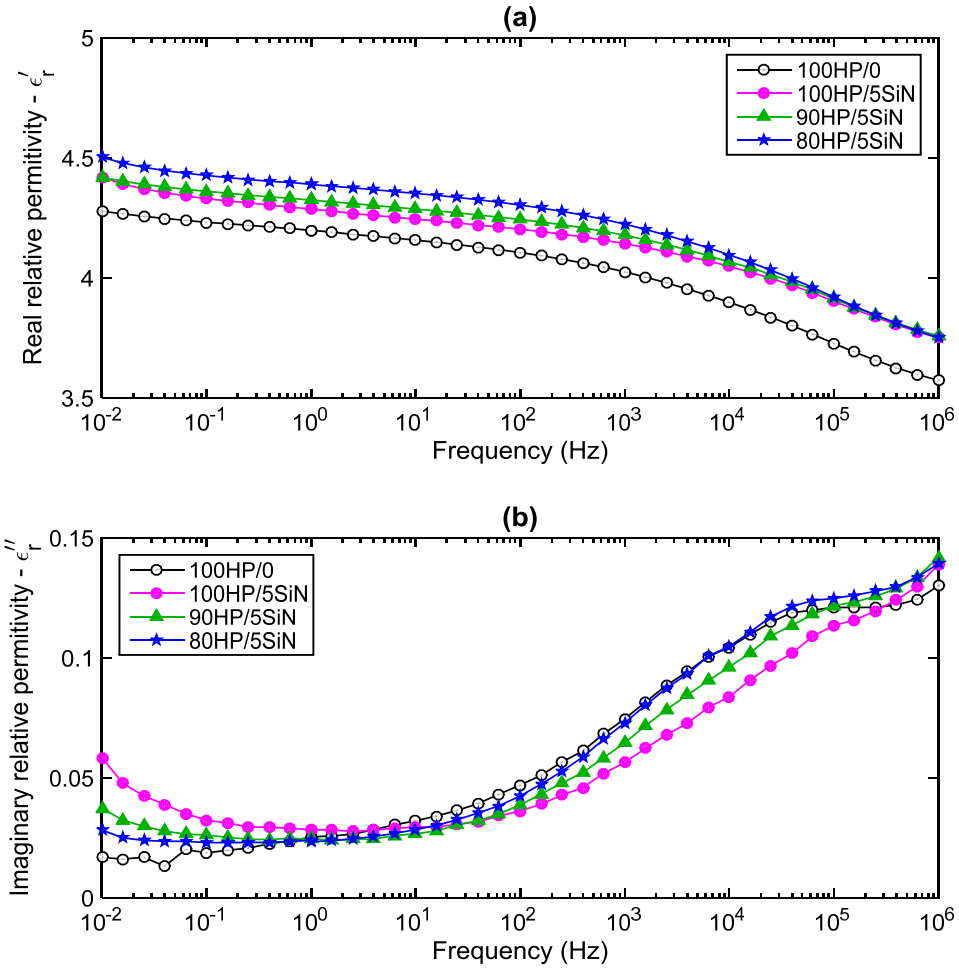

Figure 6.8: Dielectric spectra for 5 wt% filled nanocomposites compared with the reference sample, (a) real permittivity and (b) imaginary permittivity.

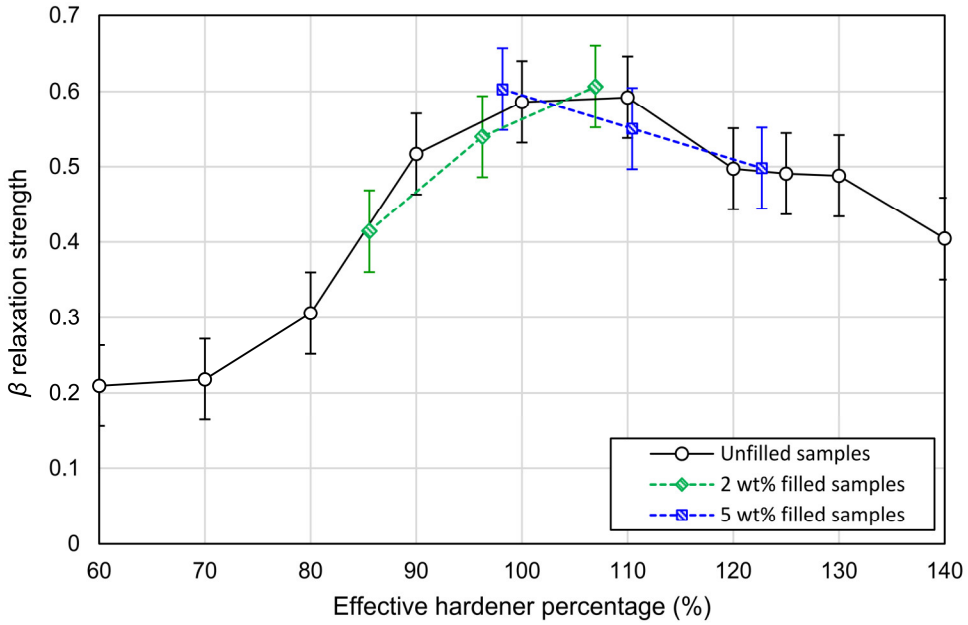

Figure 6.9: The strength of the β relaxation for all samples as a function of HP_{eff} (based on T_g analysis).

Another feature that appeared only in the spectra of the 5 wt% filled series at frequencies < 1 Hz, is that ϵ_r'' starts increasing gradually with decreasing frequency (Figure 6.8). This increase in ϵ_r'' at low frequencies might be due to a higher DC conductivity of these samples or might be the high frequency tail of a relaxation that peaks at a frequency below our accessible range. Many studies have shown that the addition of nanoparticles imparts a new mid- or low-frequency relaxation peak that moves to higher frequencies with higher temperatures [19, 169, 170] or with absorbed water [27, 29, 95]. Related to the materials considered here, Hosier [4] has recently reported that the addition of Si_3N_4 nanoparticles into a polyethylene matrix causes a new relaxation that shifts to higher frequency with higher water uptake; Yeung [19] has also observed a similar feature that peaks at higher frequencies for higher temperatures, for the same epoxy matrix when filled with nanosilica. This phenomenon is attributed to the polar functionalities on the nanoparticles' surface and the water molecules which associate with these groups. Consequently, if the behaviour observed here is due nanoparticle related relaxation, it should be a function in the nanoparticle content. While this may rationalize the absence of this feature in the 2 wt% filled series, it is not consistent with the variations seen between the different 5 wt% filled samples (which have same particle content) and, thereby, this eliminates the attribution to particle related relaxation. Nevertheless, to corroborate the above conclusion, dielectric spectra of sample 100HP/5SiN was obtained at higher temperatures (Figure 6.10a) and after exposing it to ambient condition, which allows it to absorb water (Figure 6.10b). As is evident from these spectra, in none of these cases does this feature develop into a relaxation peak that moves to higher frequencies. Instead, ϵ_r'' continues to further increase at low frequencies, which is a typical behaviour that results from higher DC conductivity at higher temperature [171] or higher water content [172]. Therefore, this behaviour should be a result of increased DC conductivity in these samples. As will be shown in section 6.5, the DC conductivity of these samples is markedly greater than that of other samples and its value decreases from sample 100HP/5SiN to sample 80HP/5SiN, which correlates with the values of ϵ_r'' at low frequencies in Figure 6.8b. Another inference relating to the above discussion, is that the absence of any particle related relaxation in the systems investigated here implies that most of the polar content on the surface of the particles is removed. This suggests that most of the particles' amine groups have reacted with the resin's epoxy groups which results in hydroxyether groups, as is the case when the resin reacts with the hardener. This again reinforces the effect of Si_3N_4 filler on the stoichiometry.

Regarding to variations seen in the absolute values of ϵ_r', notwithstanding that most of these variations are within experimental uncertainties, one trend can be observed. That is, within each nanocomposite series, ϵ_r' decreases in proportional with the decrease in the β relaxation strength. For example, at 10 Hz, ϵ_r' slightly decreases from sample 100HP/2SiN to sample 80HP/2SiN, which has ϵ_r' even less than the reference sample. This trend can be

explained by the decline in hydroxyether group concentration (polar content), which is a consequence of the reduction in the crosslinking density.

In conclusion, apart from the feature caused by the apparent increase in DC conductivity, the dielectric spectra of the filled samples and their unfilled counterparts are analogous, when the filler stoichiometric effect is taken into account. That is, the nanofiller does not appreciably affect the polar content or the dynamics of the already existed polar groups. Rationally, since the DSC data analysis demonstrated that the filler does not markedly modify the cooperative α relaxation at the glass transition, it is expected that the more localized β relaxation is not affected as well. Even in studies that have reported a nanofiller effect on the glass transition, the smaller scale β relaxation was not perturbed [43, 44]. On the other hand, other studies [32, 33, 173], which investigated the effect of nanofiller on dielectric response of epoxy matrices, claimed that nanofiller inclusion led to ϵ_r' that is lower than ϵ_r' of both the filler and the host matrix. These studies justified this reduction by postulating a layer of restricted polymer chain mobility around the nanoparticles, however no experimental exploration has been attempted to validate this proposition. As discussed above, changing the resin/hardener stoichiometry results in decreasing the β relaxation strength and, to less extent, ϵ_r'. Therefore, the reduction in ϵ_r' seen in these studies might be related to nanofiller-induced stoichiometry variations, particularly this attitude only observed when the particles were coated with an epoxy-terminated silane coupling agent. Although, in both studies the behaviour of T_g was not reported to confirm any stoichiometric effect, yet, in both of these studies, there are signs that may support this rationalisation. In [32] the reduction in ϵ_r' was accompanied by a reduction in the β relaxation, which may imply a reduction in crosslinking density. In the other study [33], the ϵ_r' reduction was more pronounced in the samples prepared following a specific route that included mixing the particles with the resin for 12 h. In this preparation route, any possible reaction between the particles and the components of the epoxy matrix is maximised, due to the long period of mixing, which may affect the stoichiometry of the network.

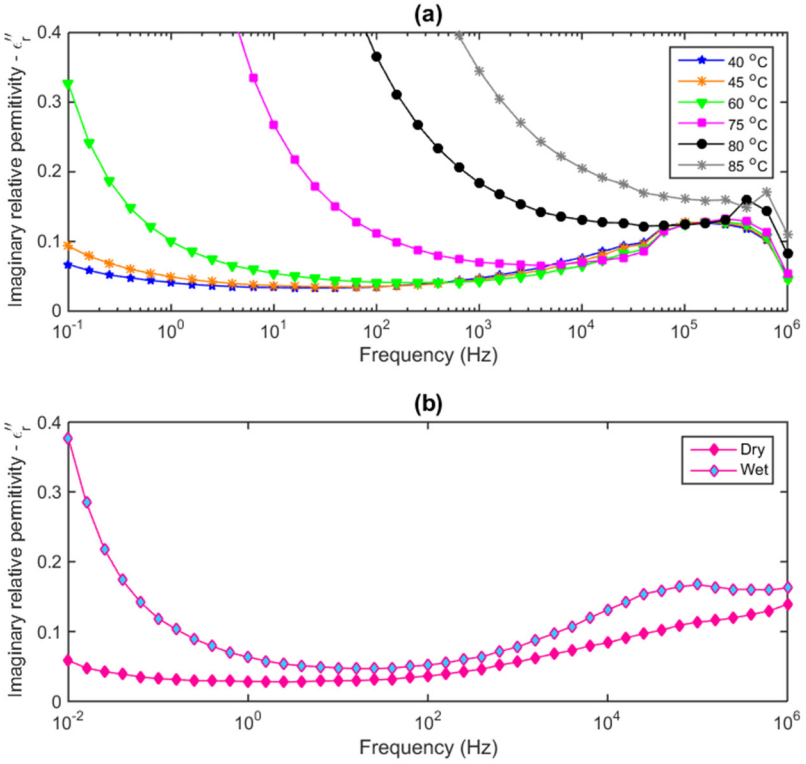

Figure 6.10: Imaginary relative permittivity of sample 100HP/5SiN at: (a) different temperatures, and (b) different water content.

6.4 Nanoparticle dispersion

Figure 6.11 presents representative SEM images obtained from unfilled and filled samples. The image of the unfilled sample, Figure 6.11a, shows a typical featureless one phase morphology, in accordance with the amorphous single phase structure of epoxy networks. Similar SEM images have been reported elsewhere [88, 174]. For the filled samples, Figure 6.11b shows well dispersed nanoparticles throughout the network. The higher magnification image shown in Figure 6.11c indicates that individual particles, with size comparable to that is quoted by the supplier (< 50 nm), are uniformly distributed within the matrix. Nonetheless, Figure 6.11c also shows the presence of occasional small agglomerations, less than ~300 nm in size, where a few particles are clustered beside each other. Compared with some other nanofiller types, the dispersion state shown here for Si_3N_4 is much better. For example, the introduction of untreated silica, which is polar and thus can be considered compatible with the polar epoxy matrix, has been reported to produce particle agglomerations that reach the microscale size [170, 175]. Even for silica which was treated with a silane coupling agent terminating with an epoxy group, microscale particle agglomerations have been observed [19]. Furthermore, the same Si_3N_4 nanofiller investigated in this study, showed an inferior dispersion state when it was added into polyethylene [95] or polypropylene [176] matrices. Therefore, the superior particle dispersion in the systems investigated here should be related to strong interactions between the surface amine groups of the Si_3N_4 and the epoxy groups in the resin.

(a)

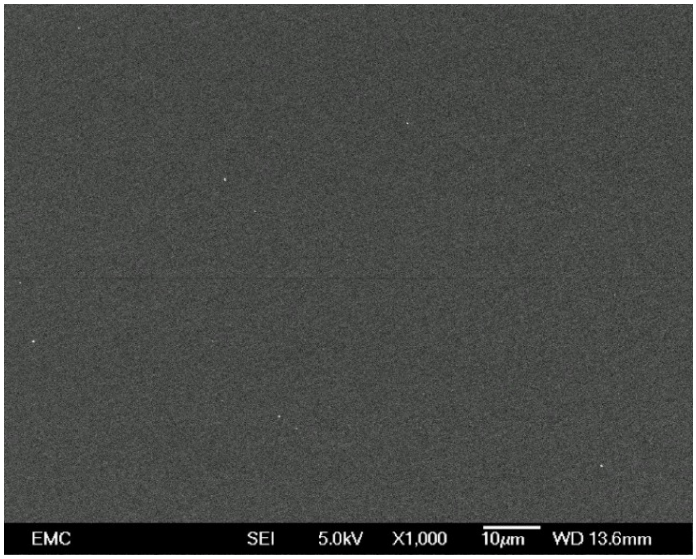

(b)

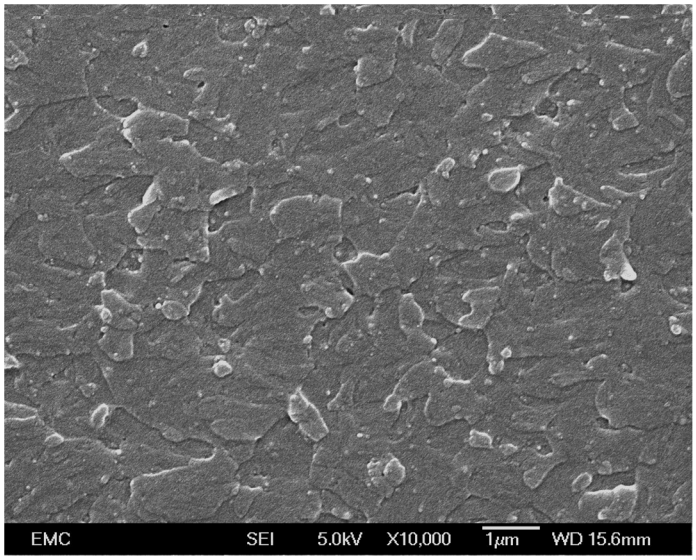

(c)

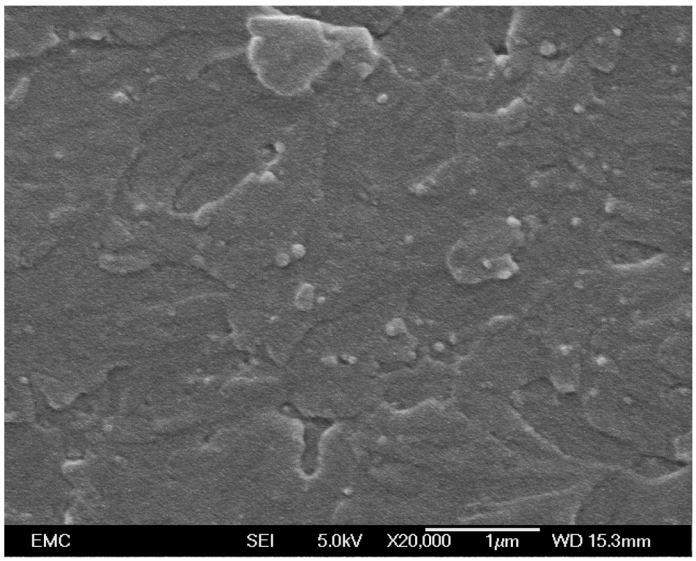

Figure 6.11: Representative SEM images for (a) unfilled epoxy, (b) 5 wt% Si_3N_4 filled epoxy, and (c) 5 wt% Si_3N_4 filled epoxy (higher magnification).

6.5 DC conductivity

The effect of the Si_3N_4 nanofiller on charge transport was investigated by measuring the DC conductivity at an applied electric field of 42 kV/mm. Figure 6.12 presents the data obtained at 30 ^oC for all nanocomposite samples, along with the reference sample (HP100/0). Comparable measurements were performed at room temperature (23 ^oC) and 45 ^oC and the resulting data were averaged to give a mean conductivity value for each system at each temperature and the resulting values are presented in Figure 6.13. The emphasis here is to compare the charge transport of all the samples in their glassy state, in order to offset the glassy/rubbery state factor, discussed in section 5.4. Therefore, the three measurement temperatures were chosen to be well below the T_g of all samples. At the three temperatures, the data show the same pattern for the values of the DC conductivity of all samples, which confirms the validity of the obtained results.

Following the same approach used to analyse the behaviour of the glass transition and the dielectric response, the effect of the Si_3N_4 nanoparticles on DC conductivity can be associated with the particles themselves and/or can be related to the impact of the particles on the matrix stoichiometry. The effect of the former factor should be exclusively a function of the filler content, whereas the effect of the other factor can be highlighted by observing the impact of changing the *HP* on DC conductivity and comparing this effect between the filled and unfilled samples. Figure 6.12 and Figure 6.13 show that for both the 2 wt%- and 5 wt%-filled nanocomposite series, the DC conductivity decreases with reducing the *HP* from 100 % to 80 %, which is in line with the behaviour of the unfilled samples (section 5.4), where the DC conductivity was found to decrease with decreasing *HP*. However, in both nanocomposite series, the DC conductivity remained higher than that of the reference sample, which is unexpected for those samples where HP_{eff} is lower than 100 %. For example, samples HP90/2SiN and HP80/2SiN have $HP_{eff} < 100$ %, according to the conclusions derived from the DSC and dielectric spectroscopy results, and thus, they would be expected to exhibit a slightly lower DC conductivity than the reference sample, based on the behaviour of the unfilled samples. Likewise, sample HP80/5SiN should have a DC conductivity that is around the DC conductivity of the reference sample. Consequently, this signifies that the stoichiometric impact of the Si_3N_4 nanofiller cannot fully account for the variations seen in the DC conductivity of the nanocomposite samples.

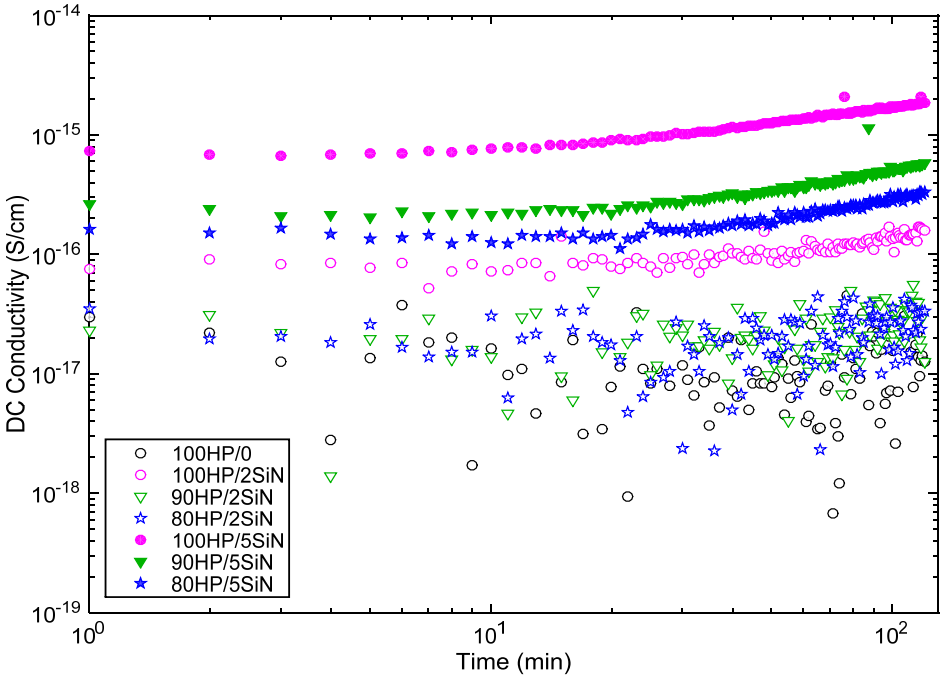

Figure 6.12: DC conductivity measurements at 30 ºC and electric field of 42 kV/mm.

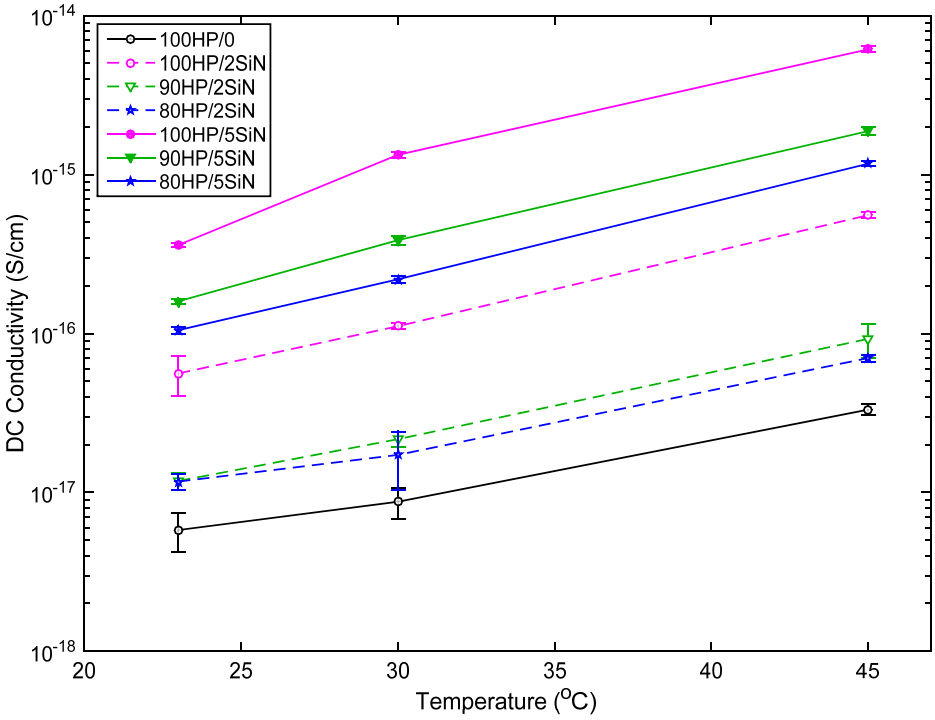

Figure 6.13: Average of DC conductivity for all samples at different temperatures and electric field of 42 kV/mm, the error bars indicate the 95 % confidence bounds of the average.

In order properly to visualize the influence of the nanoparticles on the DC conductivity, the filled samples should be compared with equivalent unfilled samples, where the HP_{eff} and HP of the filled and unfilled samples should be equivalent. This has been done in Figure 6.14, which reveals that the DC conductivity of the filled and unfilled samples

changes with respect to HP_{eff} in a similar fashion. However, there is a shift to higher DC conductivity for the filled samples and this shift seems to be a function of the filler loading. This implies that the variation seen in the DC conductivity of the filled samples is a result of a superposition of the effect of the particles on the network stoichiometry and other factors that are associated with the presence of the particles. The effect of the stoichiometry on the DC conductivity was discussed in section 5.4 and will not therefore be discussed further here.

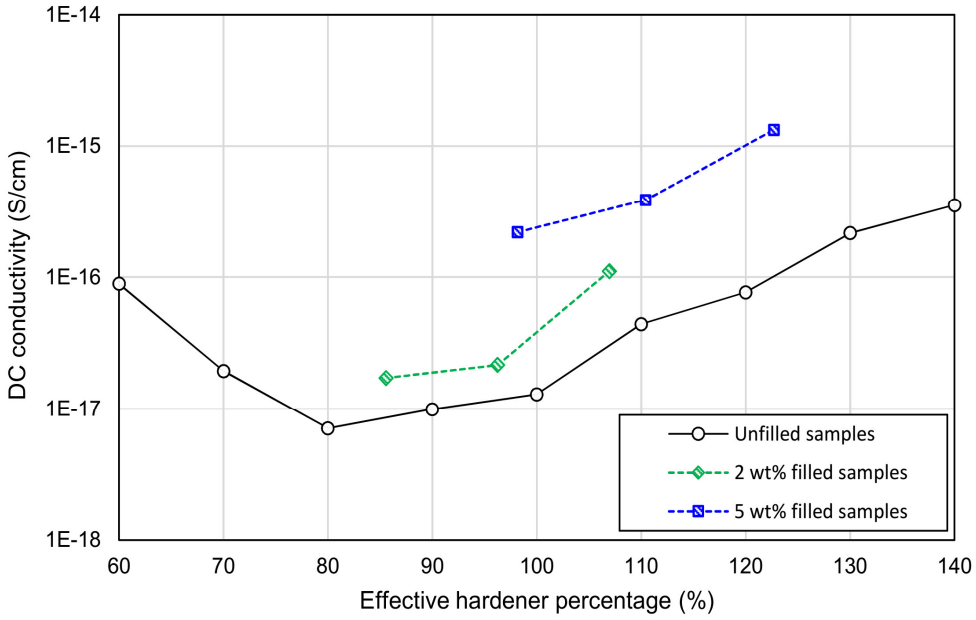

Figure 6.14: DC conductivity at 30 °C and 42 kV/mm of the filled and unfilled samples as a function of HP_{eff}.

Regarding the effect of nanoparticles, as detailed in chapter 2, there are many mechanisms that have been proposed in the literature to explain the influence of nanofillers on electrical properties. Among these mechanisms, many researchers have suggested that nanoparticles affect the polymeric layer around them, which results in the formation of an interphase layer (polymer interphase according to the definition in section 2.1) with different properties from the rest of the polymer matrix. Many authors have tried to connect the formation of a polymer interphase layer and the electrical performance of nanodielectrics. For example, Tanaka *et al*. [37], in their multicore model, suggested that strong interactions between the particles and the encapsulating polymer may restrict the polymer chain dynamics around the particles. Subsequently it was suggested that the charge carriers may have lower mobility in the tightly bound layer around the particles [177]. Correspondingly, Siddabattuni *et al*. [178] claimed that interfacial covalent bonding between the polymer and the nanoparticles leads to increasing nanocomposite resistance to charge flow and to electrical breakdown. Similarly, Andritsch *et al*. [179-181] suspected that strong filler/matrix interfacial interactions and the implications of these interactions on the matrix structure are one of the key reasons for the improvements observed in the dielectric

performance of epoxy based nanocomposites. Furthermore, Singha *et al*. [182] and Kosmidou *et al*. [135] pointed out a correlation between the volume electrical resistivity and T_g of epoxy based nanocomposites. In the systems investigated here, although the stoichiometric effect of the Si_3N_4 nanofiller implies a strong filler/matrix interaction, this does not appreciably influence the polymeric segmental dynamics, neither at a cooperative level nor at lower scale level, as revealed by DSC and dielectric spectroscopy, respectively. After all, the above cited studies advise that such strong interactions (including chemical bonding) would lead to improved dielectric properties, contrary to the obtained results. Beyond that, chapter 5 showed that changing the segmental dynamics and the network structure by changing the crosslinking density in the epoxy matrix did not correlate with the dielectric performance. Therefore, the influence of the nanoparticles cannot be explained by this mechanism. Other workers [135, 137, 183, 184] speculated that nanoparticles may increase the free volume content in the polymer interphase layer, particularly if the surface chemistry of the nanoparticles is not compatible with the polymeric chains (i.e. the polymeric chains do not effectively wet the surface of the particles) [158, 159]. Increasing the free volume content can degrade the insulation properties of solid insulators [185]. However, Nelson *et al*. [47] have recently experimentally demonstrated that the incorporation of nanoparticles exerts only a little influence on free volume content of an epoxy matrix and such a marginal effect cannot account for the significant variations seen in the electrical properties of nanodielectrics. The Same finding has been reported in [186]. Furthermore, in the system investigated here, analysis of the glass transition results implies that the resin molecules are chemically bonded to the surface of the particles, which indicates that the nanoparticles are compatible with the matrix. Such compatibility is also evident from the good dispersion of the nanoparticles within the matrix (Figure 6.11). Consequently, the effect of the Si_3N_4 nanofiller on the DC conductivity is unlikely to be attributable to its impact on the matrix dynamics or the formation of polymer interphase region with different properties and significant volume fraction.

Nanoparticle agglomeration [20, 21, 187, 188] and water absorption [3, 26-28] are other factors that are usually cited in the literature as reasons for degrading the electrical performance of nanocomposites. As the SEM images show (Figure 6.11), the nanoparticles are well dispersed throughout the matrix, such that no large agglomerations can be seen. Hence, this factor is not expected to cause a significant deterioration in electrical performance. Concerning water absorption, the FTIR spectra of the particles (section 4.3.3) did indicate the existence of polar groups (amine and, to a lesser extent, hydroxyl groups) on the surface of the particles, which can absorb water once it is available. Indeed, Hosier *et al*. [4] reported that the addition of the same nanofiller to a polyethylene matrix increases the water uptake. In the current investigation, however, a care was taken to remove any absorbed water before performing any testing, by drying the prepared samples under

vacuum for > 14 days. Secondly, as was deduced from analysing the dielectric spectroscopy results, most of the particles' amine groups have reacted with the resin's epoxy groups. Therefore, any potentially absorbed water will not be concentrated around the particles and, consequently, its effect on the filled and unfilled samples should be comparable. This inference will be further supported in section 6.7. Thirdly, the increase in the DC conductivity is correlated with a significant decrease in the AC breakdown strength as will be shown in the next section, in contrast with the impact of water absorption, which does not cause a significant change to the AC breakdown strength, as shown in section 5.6 for unfilled epoxy and will be shown in section 6.7 for filled samples. Based on these reasons, nanoparticle water absorption cannot account for this increase in the DC conductivity.

Returning to the FTIR results, the surface of the Si_3N_4 particles has complex chemistry, is partially oxidised to silica, and contains many defects as indicated by detecting carbon and hydrogen atoms. Beside the amorphous structure of the particles, this surface chemistry suggests a disordered band gap in the particle interphase with a high concentration of localised electronic states. As was discussed earlier, such particle interphase might increase the charge transport as was illustrated by Figure 2.6. This hypothesis will be investigated in chapter 7.

6.6 DC and AC breakdown strength

The DC breakdown data obtained from all the nanocomposite samples, along with results from the unfilled reference sample, are plotted assuming a two-parameter Weibull distribution in Figure 6.15. A comparison between the Weibull scale parameter of the filled and unfilled samples, with respect to HP_{eff}, is shown in Figure 6.16. These results broadly anti-correlate with the DC conductivity results shown in Figure 6.14, where the systems with higher DC conductivity have lower breakdown strength and vice versa. As was shown in the previous section, the DC conductivity in the filled samples is affected by both the resin/hardener stoichiometry and the filler loading ratio. Therefore, such an anti-correlation between the DC breakdown strength and the overall DC conductivity suggests that the DC breakdown strength is affected by the DC conductivity, regardless of the mechanism that controls it.

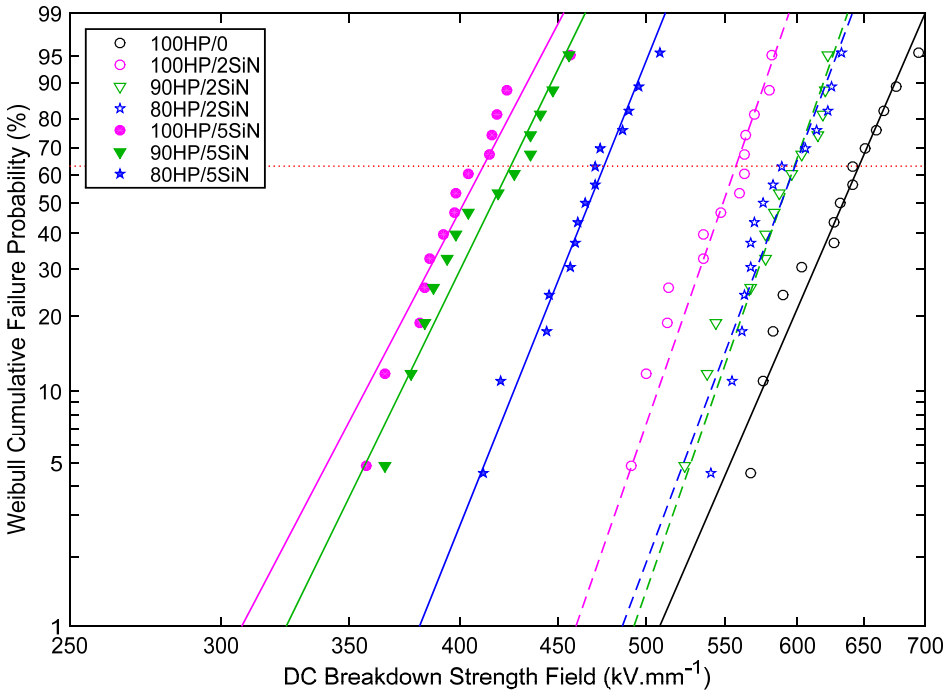

Figure 6.15: Weibull plot of DC breakdown measurements for all the nanocomposite samples and the reference sample.

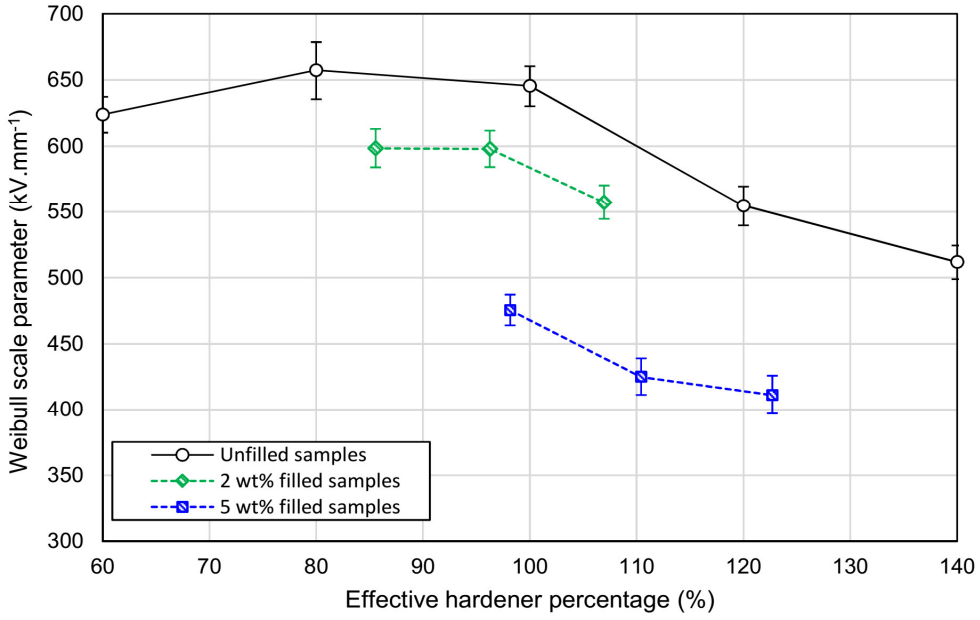

Figure 6.16: DC Weibull scale parameter of the filled and unfilled samples as a function of HP_{eff}, the error bars indicate the 95 % confidence bounds.

The effect of the Si_3N_4 nanofiller on the AC breakdown strength is shown in Figure 6.17 and the Weibull scale parameter for all samples is presented Figure 6.18 with error bars that indicate the 95 % confidence bounds. The data clearly show that the AC breakdown strength is not affected by the changing the *HP* for both nanocomposite series. This is in

accordance with the behaviour of the unfilled samples. On the other hand, the results indicate that the AC breakdown strength decreases with increasing the filler loading. Therefore, unlike the DC conductivity and breakdown strength, which are affected by both the presence of the particles and their impact on the network stoichiometry, the AC breakdown strength is only influenced by the particles themselves. The insensitivity of the AC breakdown strength to the variations in the DC conductivity that are induced by changing the network stoichiometry was analysed in chapter 5, where it was suggested that a homogeneous change in the charge transport is not expected to produce defects in the material and, thus, does not significantly affect the AC breakdown strength. Conversely, the addition of the Si_3N_4 particles will increase the charge transport locally within the particle interphase, as was proposed in the previous section and will be demonstrated in the next chapter. Such a local increase in the charge transport in a small volume within the dielectric material may form defects in this material and thus affect the AC breakdown strength.

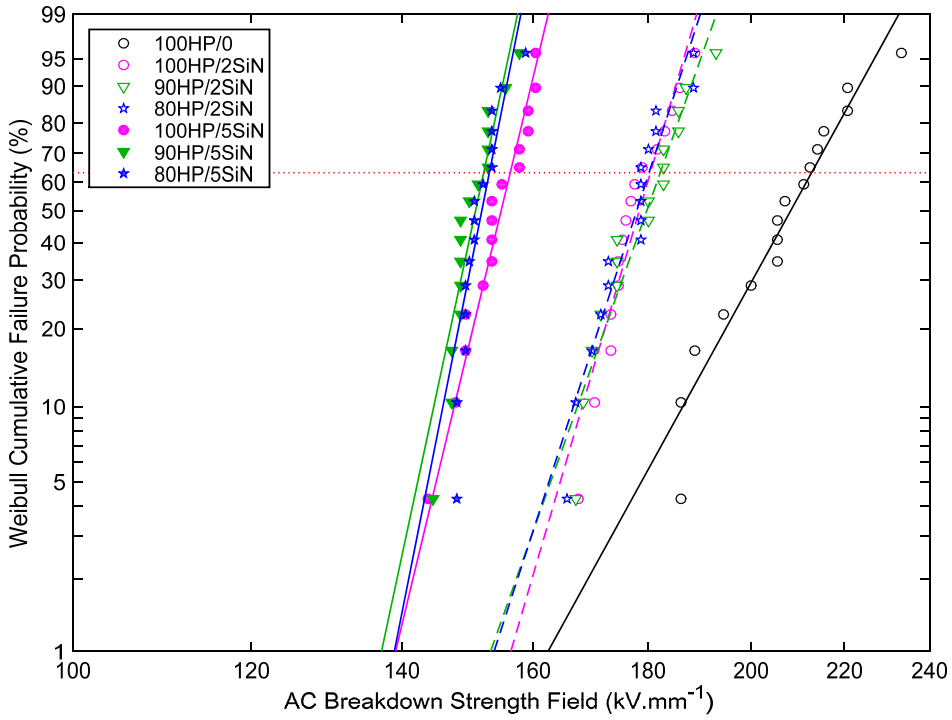

Figure 6.17: Weibull plot of AC breakdown measurements for Si_3N_4 epoxy nanocomposites and the reference sample.

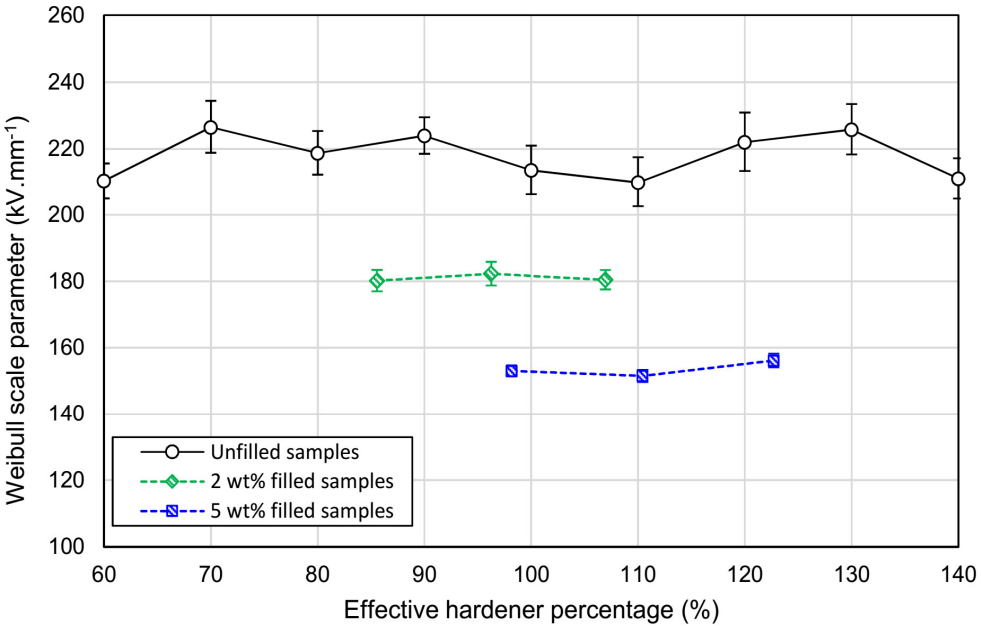

Figure 6.18: AC Weibull scale parameter of the filled and unfilled samples as a function of HP_{eff}, the error bars indicate the 95 % confidence bounds.

6.7 Moisture absorption and its effect on electrical properties

It is known that water absorption can have a detrimental influence on the dielectric properties of insulation materials. For nanodielectrics, many studies have reported that the addition of nanofillers increases the water uptake and, thus, degrades the dielectric performance of the resulting systems [3, 26-28]. This effect originates from the fact that these nanofillers have a large surface area which is, in many cases, covered by polar functionalities such as hydroxyl groups. This might result in the formation of water shells around the nanoparticles and, consequently, the impact of such particle-associated water can be different from the water that is homogeneously dispersed throughout unfilled systems. For example, many investigations have reported that water uptake in silica nanocomposites results in a dielectric relaxation that does not appear in the corresponding unfilled systems [4, 19, 29]. Exposure to water is inevitable and, therefore, its effects should be considered when exploring the potential of nanodielectrics. Furthermore, water content should be identified and taken into account as an important parameter in order better to analyse the electrical behaviour of nanocomposites and to discriminate between the impact of the particles themselves and the water that is absorbed around them. For example, based on the results in this section, the water was excluded from being a cause for the increase in DC conductivity of the filled samples, discussed in section 6.5.

This section investigates the effect of the presence of Si_3N_4 nanoparticles on moisture uptake and the consequences for this on the dielectric behaviour of nanocomposite samples. As FTIR spectroscopy (section 4.3.3) has revealed, the Si_3N_4 nanopowder has a surface chemistry that is characterized by the presence of amine and, to a lesser extent,

hydroxyl groups. Hosier *et al*. [4] investigated the effect of adding the same nanofiller on water uptake in hydrophobic polyethylene and found that it caused an increase in the water uptake of the resulting composite compared with the equivalent unfilled system. However, for the current epoxy matrix, as the stoichiometric effect implies, the surface amine groups on the Si_3N_4 particles can chemically react with the epoxy groups in the resin, which will change the surface chemistry of the Si_3N_4 inside the epoxy matrix. In this case, analysing the effect of the nanofiller on water uptake will serve as a tool to probe the surface chemistry of the Si_3N_4 nanoparticles inside the polymer.

6.7.1 Moisture uptake

To monitor moisture absorption, specimens with different formulations were exposed to the conditioning environment and their masses were periodically measured over a period of two weeks. Water uptake was calculated from these measurements. The data obtained from 70 µm thick specimens are plotted in Figure 6.19a and the data obtained from 200 µm thick specimens are shown in Figure 6.19b. Evidently, both the 70 µm and 200 µm thick samples produce superimposable curves when water uptake is plotted versus $\sqrt{t}/d$ (t is the exposure time and d is sample thickness), which is a feature of Fickian behaviour [142]. Therefore, water diffuses into the nanocomposite samples following a Fickian mechanism, which is similar to its behaviour in the unfilled samples. Regarding the rate of diffusion of the water inside the materials, the obtained data suggest that the addition of Si_3N_4 does not significantly affect the rate of water diffusion, as can be deduced by comparing the slope of the linear part of the water absorption curves for the nanocomposites and the reference sample. Approximately, Figure 6.19 indicates that for the 70 µm thick specimens, the water uptake reaches around 40 % of its saturation value within ~30 min, whereas for 200 µm thick specimens, this period increases to ~200 min.

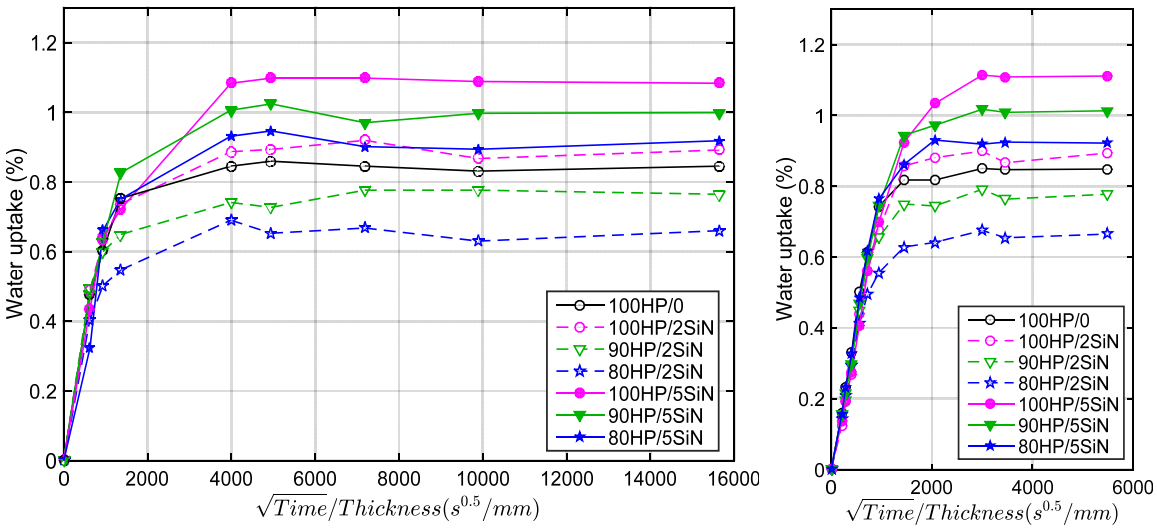

Figure 6.19: Water absorption curves as a function of time, obtained from (a) 70 µm thick specimens and (b) 200 µm thick specimens.

Comparing the saturation water uptake for different samples, Figure 6.19 shows that decreasing the *HP* from 100 % to 80 % leads to lower water uptake levels for both the nanocomposite series, which is consistent with the trend observed for the unfilled samples in chapter 5. However, at the same *HP*, the data show that the 5 wt% filled samples absorb a significantly greater amount of water than the 2 wt% filled samples which, in turn, absorb more than the unfilled samples that have same *HP*. Compare, for example, samples 100HP/5SiN, 100HP/2SiN and 100HP/0. This behaviour is expected, as the incorporation of Si_3N_4 results in a higher HP_{eff}. To check if considering the stoichiometric effect of the nanofiller can account for this increase in water uptake, Figure 6.20 presents the saturation water uptake for the unfilled and the nanocomposite samples as a function of HP_{eff}. The illustration reveals that with respect to their HP_{eff}, both the filled and unfilled samples absorb comparable amount of water. This finding suggests that water absorption in the nanocomposite samples is almost exclusively a function of the effective matrix stoichiometry. Consequently, this means that the nanoparticles impart no significant polar content to each system, apart from the amine groups that react with the resins' epoxy groups and are responsible for the stoichiometric effect. Since FTIR spectroscopy has demonstrated that the surface of the particles is covered by amine and, to less extent, hydroxyl groups, two inferences may be drawn from this conclusion:

1- Most of the particle amine groups have reacted with the resin and, hence, they only affect water absorption through the stoichiometric effect.
2- The number of the unreacted amine groups that remain on the surface and the number of the hydroxyl groups are not significant. Otherwise, the particles would lead to higher water uptake than would be expected based on the HP_{eff} value for the samples. Such effect would appear in Figure 6.20 as a shift to higher water uptake values for the filled samples and this shift should be only related to the nanofiller loading. Closer examination of Figure 6.20 does show that the filled samples absorb slightly more than the unfilled samples, which may be due to a small amount of unreacted amine and hydroxyl groups on the particles, nevertheless, this effect is within experimental uncertainties.

To sum up, the above findings are in line with and, therefore, support the conclusions drawn from analysis of the dielectric spectra of these samples.

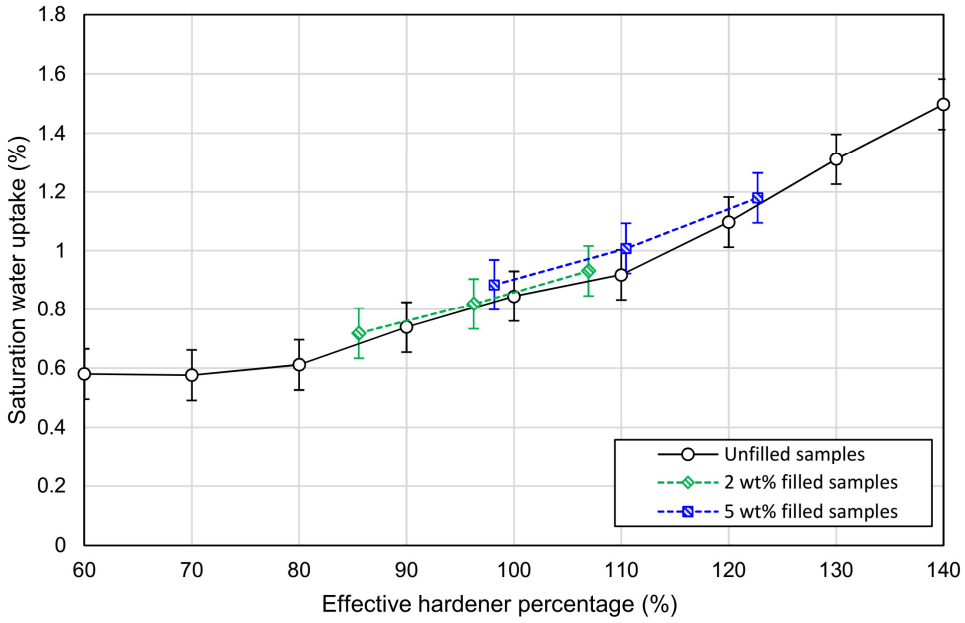

Figure 6.20: Saturation water uptake for the unfilled and the nanocomposite samples as a function of HP_{eff}.

6.7.2 Reversibility of water absorption

The reversibility of water absorption was examined by placing the same specimens exposed to the humid conditioning in a vacuum oven at room temperature and regularly monitoring their mass. The measurements (Figure 6.21) show that the samples lose the absorbed water and return to their dry mass. This process took around one day for 70 µm thick specimens and around 3 days for 200 µm thick specimens. Consequently, the inclusion of Si_3N_4 does not affect the reversibility of the water absorption process, where it is reversible for both the filled and unfilled samples. Additionally, these data indicate the minimum period of time should be used to dry samples after being exposed to ambient conditions.

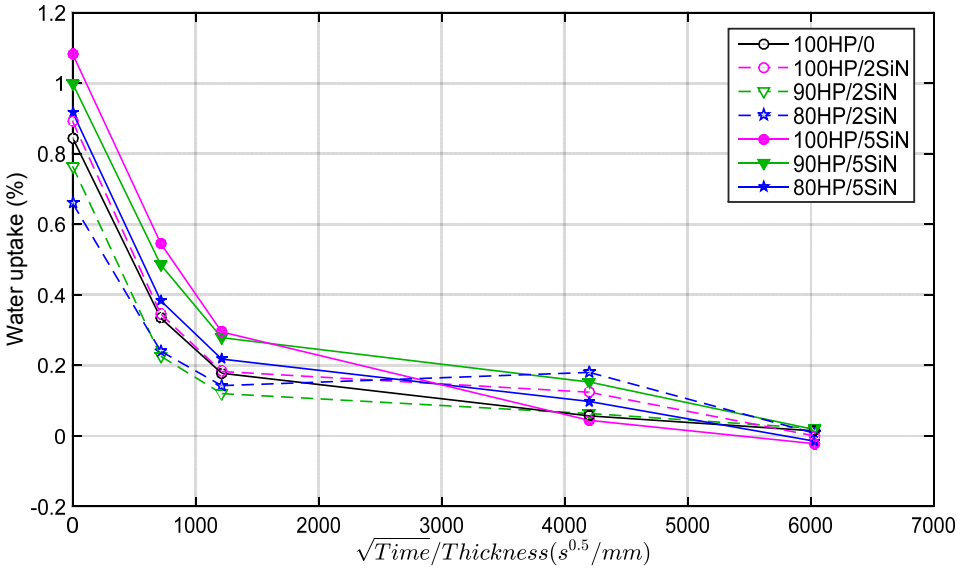

Figure 6.21: Vacuum drying for wet samples as a function of time.

6.7.3 Moisture absorption effect on the dielectric spectra

Dielectric spectra obtained from all the nanocomposite samples along with the reference sample are shown in Figure 6.22. As expected, the absorbed water increases the polar content in the samples and thus increases ϵ_r'. With regard to ϵ_r'', the absorbed water increases the strength of the β relaxation, which is consistent with its impact on the unfilled samples. An additional feature that is only pronounced in the spectra obtained from the 5% filled samples is that the absorbed water increased the values of ϵ_r'' at low frequencies. As was concluded in section 6.3, this feature is due to an increased higher DC conductivity of these samples, rather than due to a relaxation of absorbed water molecules. Furthermore, similar behaviour has been observed in the spectra of unfilled amine-rich samples containing absorbed water (see section 5.6.2), which further confirms that this feature is not caused by a direct effect of the particles on the relaxation of the absorbed water, instead it is related to higher DC conductivity values for the 5 wt% filled samples. Consequently, apart from this increase in ϵ_r'' at low frequencies, the impact of the absorbed water on the spectra of the neat and nanocomposite samples is analogous. This suggests that the absorbed water exhibits similar relaxation in both the filled and unfilled samples. Based on the discussion in section 5.6.2, this similarity implies that the distribution and interactions of the absorbed water in both cases are similar. As established in that section, the water absorbed in the unfilled samples can be divided into two parts, the first part represents the water that relaxes at frequencies > 1MHz and the other part represents the water that relaxes in phase with the β relaxation (i.e. from 1 MHz to 10 Hz). Figure 6.23 estimates the ratios of each of these parts, following the same methodology used to produce Figure 5.26, for all filled and unfilled samples. This estimation confirms the above qualitative description that the interactions of the absorbed water with the polar components of the filled and unfilled samples are comparable and, consequently, signifies that the addition of Si_3N_4 nanoparticles does not introduce distinctive polar moieties where water molecules can be attached and, thus, exhibit distinctive relaxations, as was observed in other studies [4, 19, 189]. This is consistent with the conclusion drawn from water uptake results that most of the polar content on the Si_3N_4 particles have reacted with the resin epoxy groups and, hence, produced hydroxyether groups that have the same dielectric spectra as the rest of the matrix. Dependently, the water attached to these groups will exhibit a relaxation similar to the water attached to the rest of the matrix [147, 148].

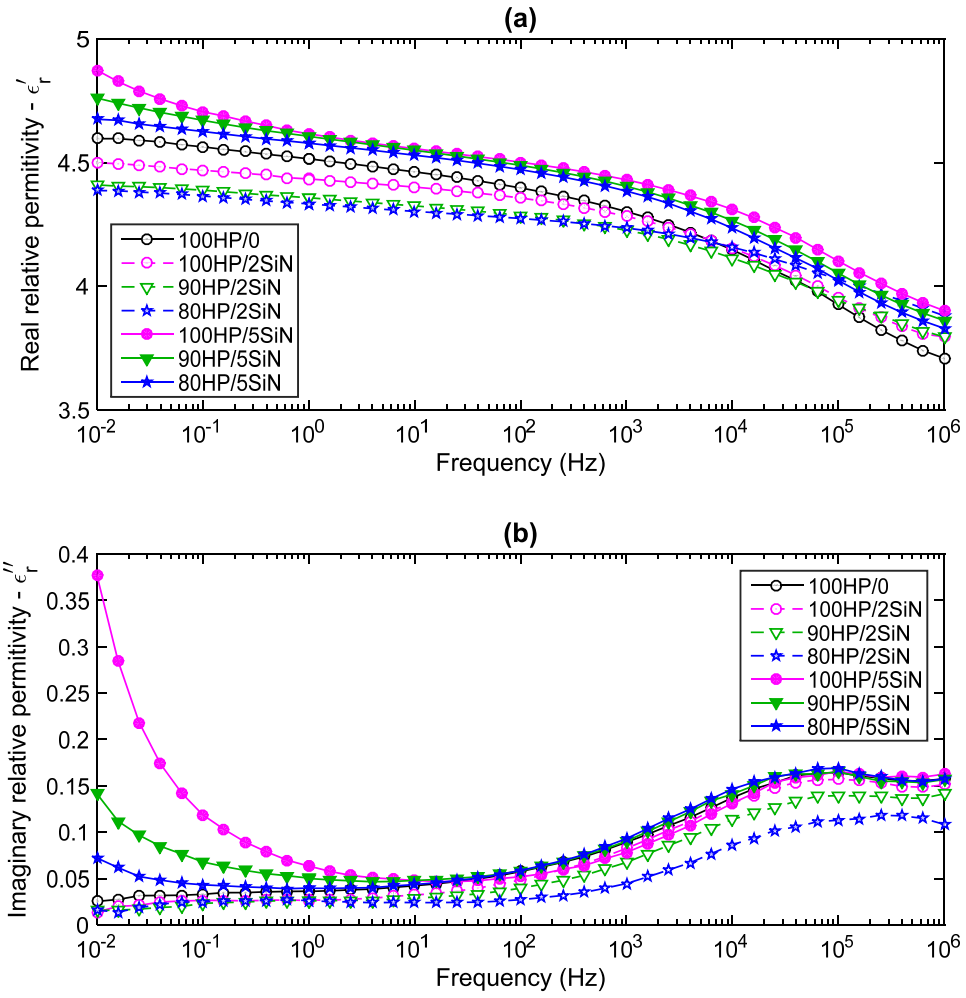

Figure 6.22: Dielectric spectra obtained from all the nanocomposite samples along with the reference sample, wet samples.

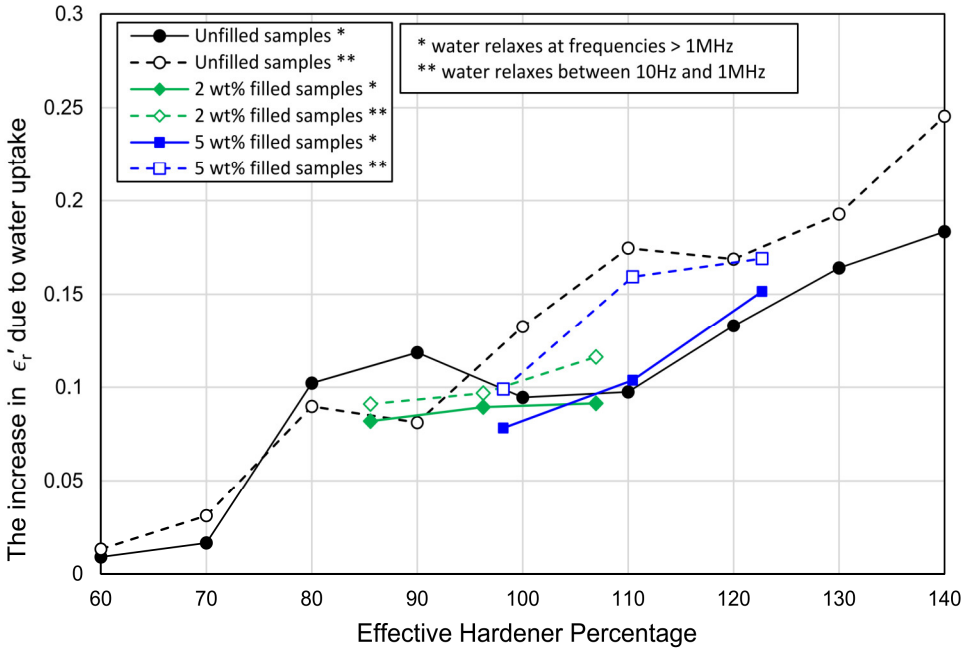

Figure 6.23: The increase in ϵ_r' due to water absorption for all filled and unfilled samples.

6.7.4 Moisture absorption effect on the DC conductivity

Figure 6.24 shows DC conductivity measurements obtained from all the nanocomposite samples along with an unfilled reference sample at room temperature and an applied electric field of 42 kV/mm. Comparing these results with the DC conductivity of the dry samples (Figure 6.12) indicates that the absorbed water leads to a marked increase in the DC conductivity and that this increase is broadly proportional to the water uptake. For example, the DC conductivity increases by almost two orders of magnitude for sample 100HP/5SiN and by around one and half order of magnitude for sample 80HP/5SiN, in line with amount of water absorbed by these samples. Furthermore, compared with the behaviour of the unfilled samples, these results indicate that the impact of water absorption on DC conductivity of the filled and unfilled samples is comparable.

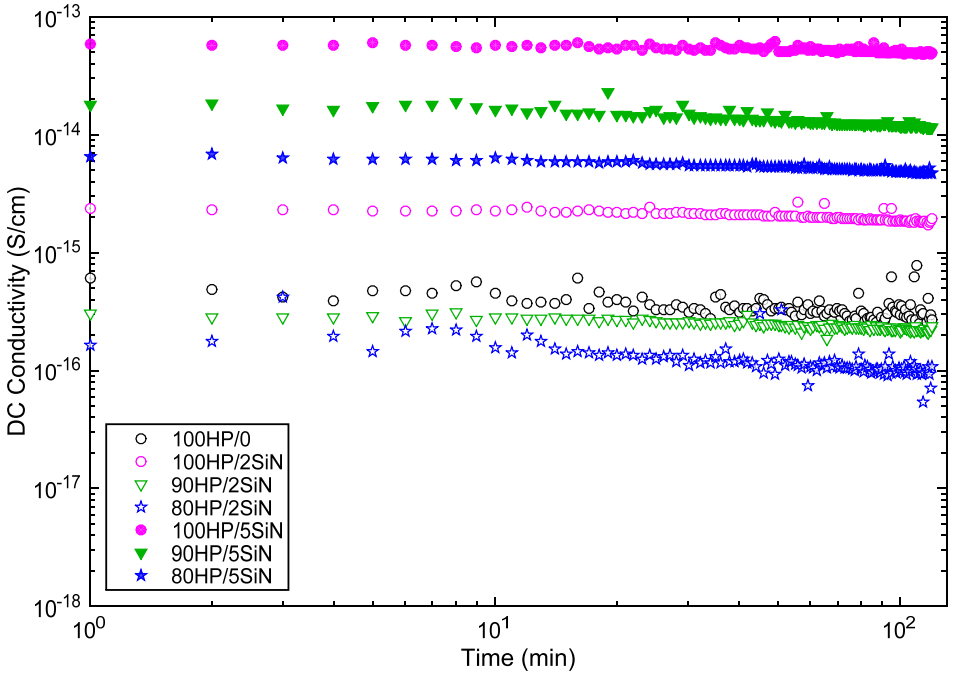

Figure 6.24: DC conductivity measurements for all wet nanocomposite samples at 23 ºC and 42.5 kV/mm.

6.7.5 Moisture absorption effect on the DC breakdown strength

Figure 6.25 presents a Weibull plot of DC breakdown data obtained from all the nanocomposite samples along with an unfilled reference sample (wet samples). As expected, water absorption leads to a significant reduction in the DC breakdown strength, which aligns with the variations seen in the DC conductivity. Additionally, this behaviour is consistent with the behaviour of the unfilled samples upon absorbing water. In order quantitively to compare the influence of moisture absorption on filled and unfilled samples, Figure 6.26 illustrates the impact of water absorption on Weibull scale parameter of the filled and unfilled samples as a function of HP_{eff}. As shown in section 6.7.1, at the same HP_{eff}, the water content in the nanocomposite samples is comparable to that of the unfilled

samples. Therefore, if the absorbed water affects the DC breakdown strength of the nanocomposite and the neat samples in an equivalent manner, one would expect that the reduction in the DC breakdown strength with respect to HP_{eff} should be comparable in both cases. Indeed, Figure 6.26 shows that the reduction in the DC breakdown strength with respect to HP_{eff} is roughly equivalent for the filled and unfilled samples. Consequently, this suggests that the impact of water absorption is comparable for the filled and unfilled samples.

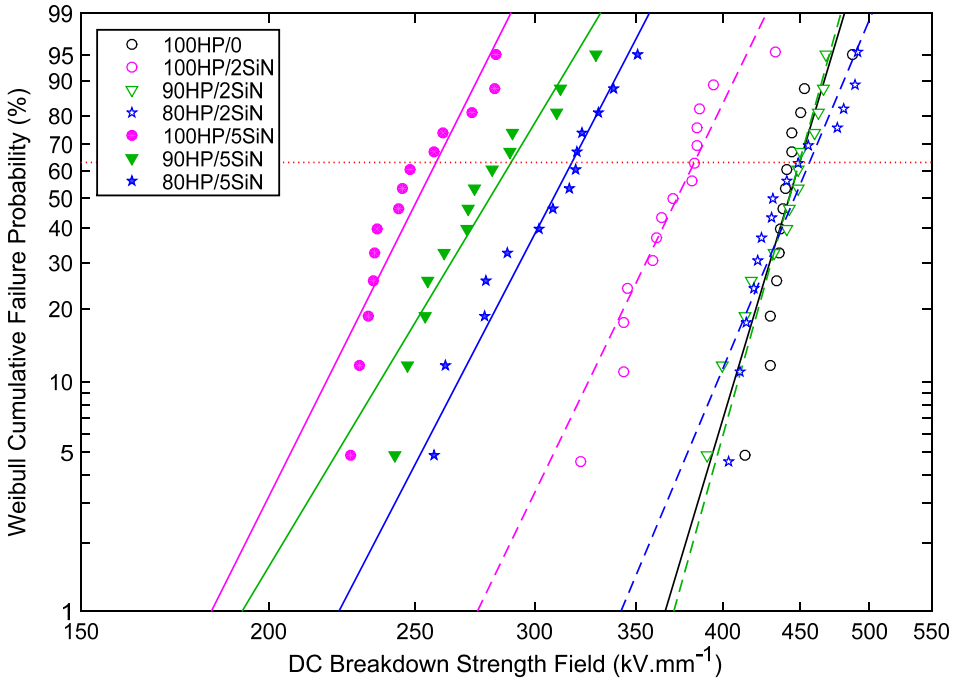

Figure 6.25: DC breakdown measurements obtained from all the nanocomposite samples along with the reference sample (wet samples).

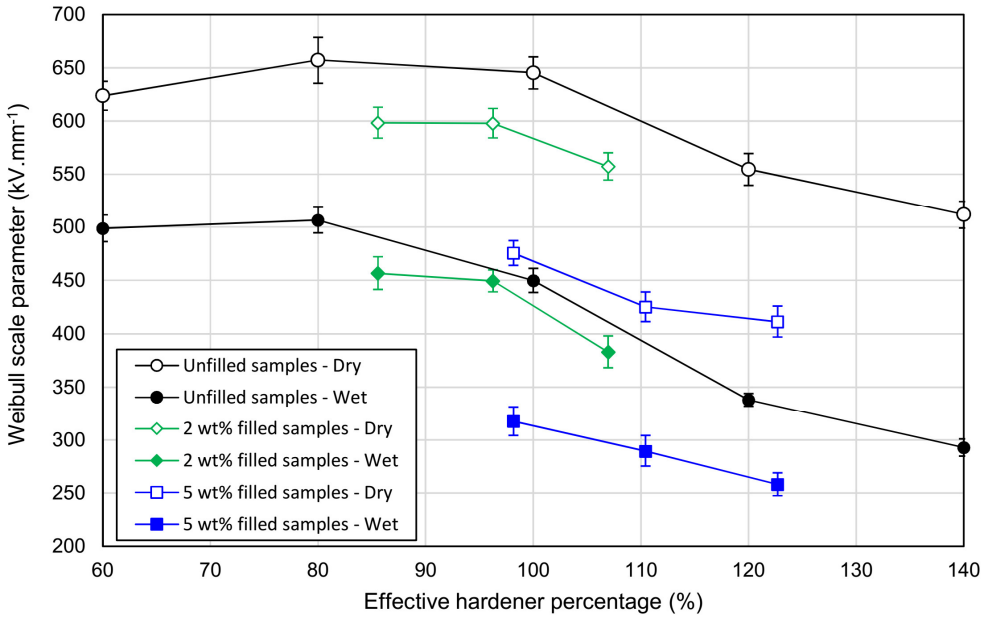

Figure 6.26: A comparison between the impact of water absorption on DC breakdown strength of the nanocomposite and neat samples.

Figure 6.27 presents Weibull plots of AC breakdown measurements obtained from all the nanocomposite samples, along with the reference sample (wet samples), while Figure 6.28 compares the impact of water absorption on the Weibull scale parameter of the filled and unfilled samples. These data show that the absorbed water does not significantly affect the AC breakdown strength of both nanocomposite series, which is in accordance with the behaviour of the unfilled samples. This behaviour clearly indicates that the decrease in the AC breakdown strength observed in the dry nanocomposite samples cannot be linked to water shells around the particles, (see the discussion in section 6.5).

From the above discussion, the impact of water uptake on the electrical properties of the nanocomposite samples is comparable to its impact on the unfilled, neat epoxy samples. While this behaviour corroborates the conclusions drawn from the mass monitoring and dielectric spectroscopy results, it also suggests that a similar distribution of water molecules occurs within the filled and unfilled samples which leads to a similar impact on the measured electrical properties. However, is the reverse correct? That is, if two materials absorb identical amount of water but the absorbed water distributes differently in the two materials (e.g. the addition of hydrophilic particles may result in a concentration of the absorbed water around them), will the impact on electrical properties be different? This question is suggested for future work in chapter 8.

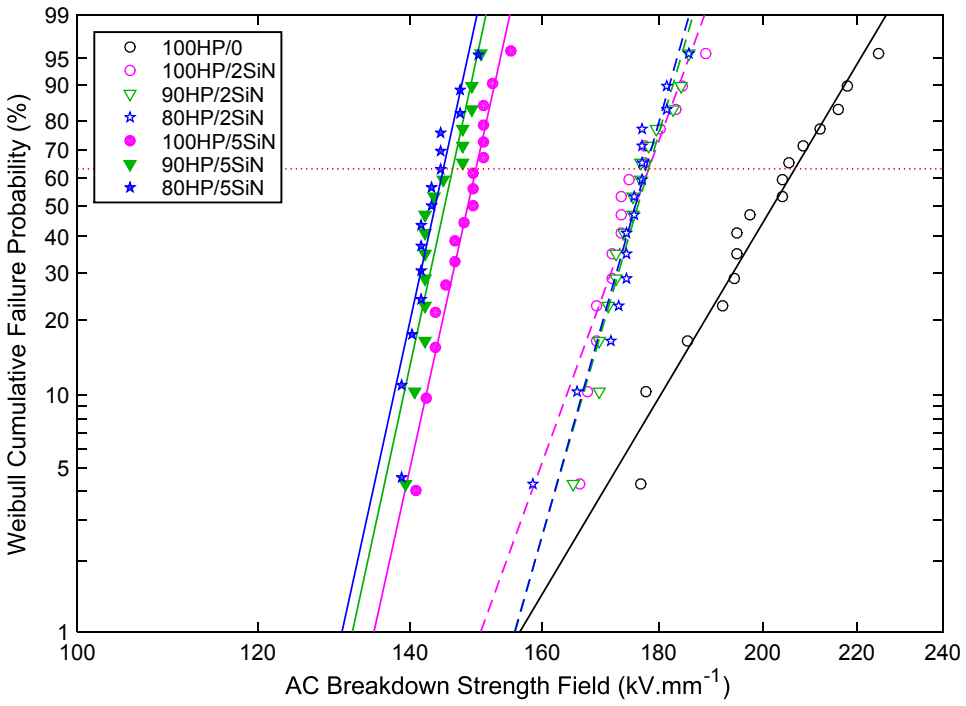

Figure 6.27: AC breakdown measurements obtained from all the nanocomposite samples along with the reference sample (wet samples).

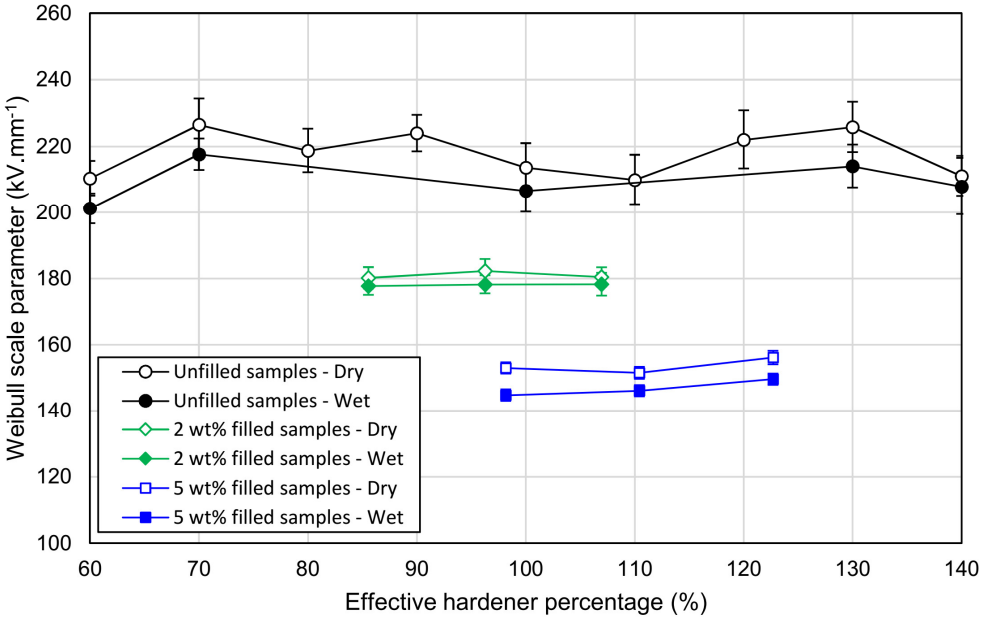

Figure 6.28: A comparison between the impact of water absorption on AC breakdown strength of the nanocomposite and neat samples.

6.8 Chapter summary

The addition of nanofillers can have a significant influence on the resin stoichiometry of thermosetting polymer systems. In the amine/epoxy system considered here, the Si_3N_4 nanofiller can react with a considerable fraction of the epoxy groups in the system and, consequently, affect the resin/hardener stoichiometry and the resulting network structure. Based on DSC result analysis, it was estimated that the inclusion of 2 wt% and 5 wt% of silicon nitride nanofiller displaces the resin/hardener stoichiometry by 6.5 % and 18 %, respectively. Dielectric spectroscopy results further confirmed the above finding, where the spectra of the nanocomposite samples were found to be equivalent to the spectra of unfilled samples when the above stoichiometric effect is taken into account. Therefore, this chapter renders conclusive evidence that nanofillers can directly and significantly affect the curing process of an epoxy network and, therefore, this parameter should be always considered when introducing nanofillers into thermosetting matrices. Such finding implies the presence of covalent bonding between the nanoparticles and the surrounding polymer and, therefore, offered an opportunity to question what is usually conjectured in the literature that strong filler/polymer interactions can affect or confine the molecular dynamics of the polymer layer around the particles and also lead to better particle dispersion. SEM images indicated that this chemical bonding leads to a good nanoparticle dispersion. However, DSC and dielectric spectroscopy results suggest that this strong filler/matrix interaction does not have an appreciable influence on the segmental dynamics of the polymer. This signifies either the absence of any affected polymeric layer around the particles or the thickness of such layer is too small to be distinguished from

experimental uncertainties, i.e. < 0.8 nm, according to the uncertainties of the experimental technique used here.

Electrical characterisation showed that considering the impact of the Si_3N_4 nanoparticles on the resin/hardener stoichiometry and the implications of this on the electrical properties cannot account alone for the electrical behaviour of the nanocomposite samples. A comparison of the electrical behaviour of the filled and the unfilled samples, with respect to HP_{eff}, indicated that there is an additional effect, which is exclusively a function of the nanofiller loading, superimposes on the former effect in influencing the electrical behaviour. Several possibilities were explored to explain this additional effect. Extensive analysis demonstrated that this effect cannot be attributed to particle agglomeration, water shells around the particles or to the influence of the particles on the matrix dynamics, structure or free volume content of polymer interphase. It was proposed that it is the particle interphase which has critical impact on the electrical properties; this proposal will be investigated in the next chapter.

Water absorption results reveal that the nanocomposite samples absorb a comparable amount of moisture to that absorbed by the unfilled samples at same HP_{eff}. Furthermore, the impact of water inclusion on the characterised electrical properties is roughly equivalent for the filled and unfilled samples. This suggests that the distribution of the absorbed water molecules is identical in both cases and therefore implies the reaction of most of the polar amine groups on the surface of the Si_3N_4 particles, giving further credence to the stoichiometric effect of these particles.

Chapter 7

Effect of Particle Interphase on Electrical Behaviour of Si_3N_4 Epoxy Nanodielectrics

7.1 Introduction

As was proposed in the previous chapter, the particle interphase of Si_3N_4 nanoparticles may have a critical impact on the electrical behaviour of the considered nanocomposites, since other factors, such as particle dispersion, water absorption and the influence of the particles on the network stoichiometry or segmental dynamics, could not completely explain the obtained results. This chapter will investigate this hypothesis by studying the impact of modifying the particle interphase of the Si_3N_4 nanoparticles on the electrical behaviour of the resulting epoxy nanocomposites. The particle interphase was modified by heating the particles at 1050 ^oC before introducing them into the polymer matrix. The details of the heat treatment and its impact on the surface chemistry of the particles was elaborated in section 4.3, where the FTIR spectra indicated that this treatment results in removing the surface NH & OH groups, releasing any foreign atom on the particle surface and producing a surface covered by stable siloxane bridges. According to the particle interphase model (section 2.4), such substantial change in the surface chemistry is expected to modify the particle interphase, and if such modification of the particle interphase has an impact on the electrical behaviour, this will appear when comparing the electrical properties of nanocomposites filled with the particles before and after the particle calcination process. The materials prepared for this purpose can be divided into three types (summarised in Table 7.1):

1- Unfilled epoxy: the resin and the hardener were mixed following the theoretical resin : hardener stoichiometric ratio, 1000 : 344 by mass. This sample acts as a reference for the others.
2- Nanocomposite containing 5 wt% of dried Si_3N_4 (SiN): as the focus in this chapter is on the influence of the particle interphase, the effect of the particles on the matrix stoichiometry was negated by adjusting the resin : hardener ratio employed in this sample. According to chapter 6, at 5 wt%, it was estimated that the dried Si_3N_4 powder displaces the resin/hardener stoichiometric ratio by ~18 wt%. Therefore, the resin/hardener ratio was adjusted to 1000: 282 (344* 0.82) in this sample.
3- Nanocomposite containing 5 wt% of calcinated Si_3N_4 (SiN-C): since the heat treatment at 1050 ^oC is expected to remove the active amine groups on the surface of the powder, the resin/hardener ratio followed for this sample is 1000 : 344.

Table 7.1: A summary of the investigated materials and their details.

Sample code	Resin : Hardener mass ratio (*HP* (%))	Filler loading (wt%)	Comments
100HP/0	1000 : 344 (100 %)	0	Neat epoxy (reference)
82HP/5SiN	1000 : 282 (82 %)	5	Filled with dried Si_3N_4
100HP/5SiN-C	1000 : 344 (100 %)	5	Filled with calcinated Si_3N_4

7.2 Particle dispersion

Representative SEM images of the nanocomposite samples are shown in Figure 7.1. As expected based on the data in the previous chapter, the image of sample 82HP/5SiN, (Figure 7.1a), shows well dispersed nanoparticles throughout the matrix, where no large agglomerations can be observed. For the sample filled with calcinated particles, sample 100HP/5SiN-C, Figure 7.1b illustrates that the particle dispersion is worse than in the case of sample 82HP/5SiN, where the particles form a higher number of clusters of a larger size, reaching 1 μm. As the FTIR spectra showed, the dried nanoparticles have a high

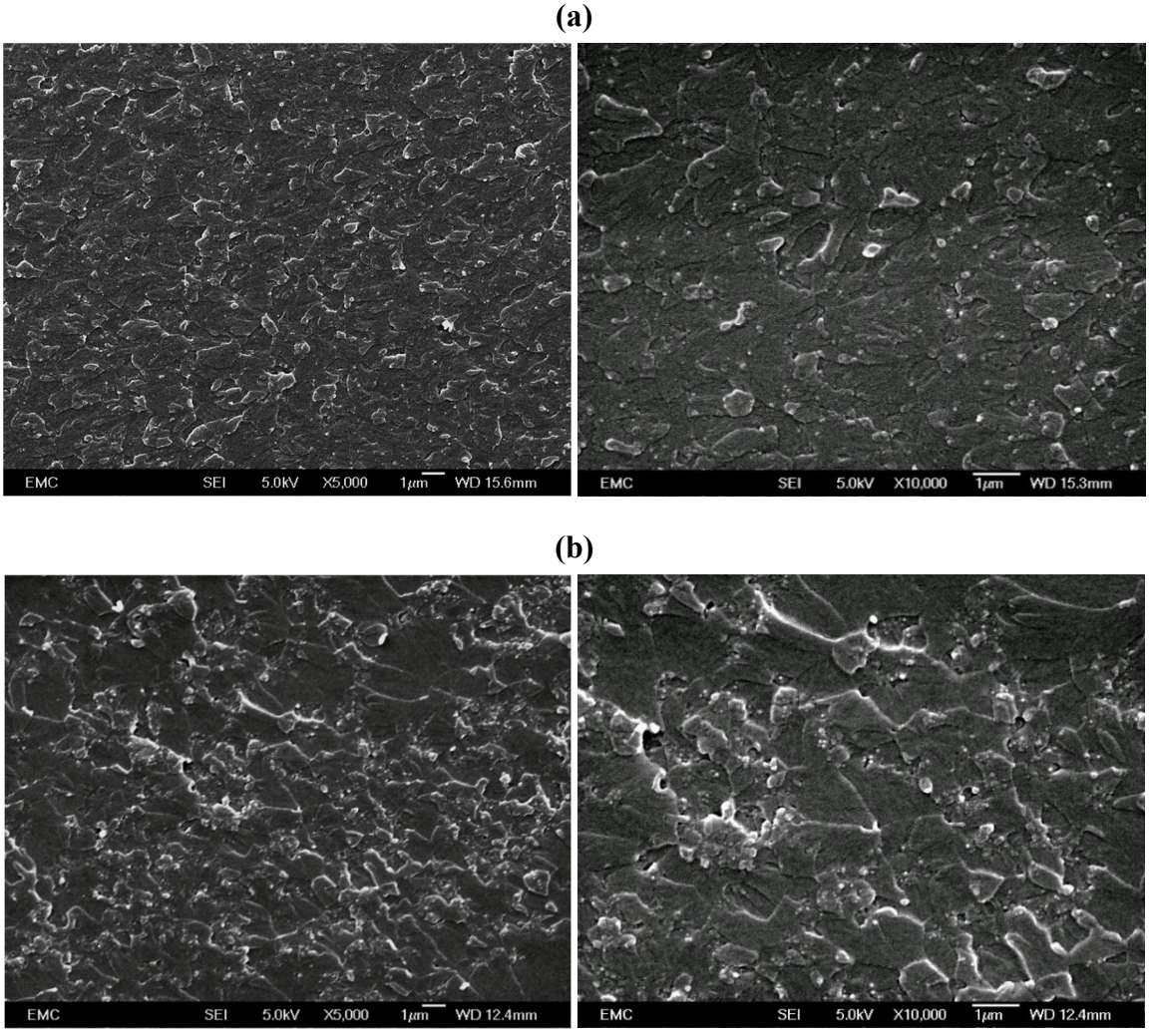

Figure 7.1: SEM images for (a) sample 82HP/5SiN and (b) sample 100HP/5SiN-C, low magnification (left), high magnification images (right).

concentration of surface amine groups, which can form strong interactions with the epoxy matrix, whereas the calcinated nanoparticles are covered with siloxane bridges, which cannot form such strong interactions with the polar epoxy matrix. This reasoning is in line with the theory of solubility between two phases, which implies that the interactions between the particles and the matrix molecules should be stronger than the cohesive forces between the particles themselves in order for them to be efficiently dispersed in the matrix [14-16].

7.3 Glass transition and molecular dynamics

Typical DSC traces for all the samples are plotted in Figure 7.2 and the derived parameters are summarised in Table 7.2.

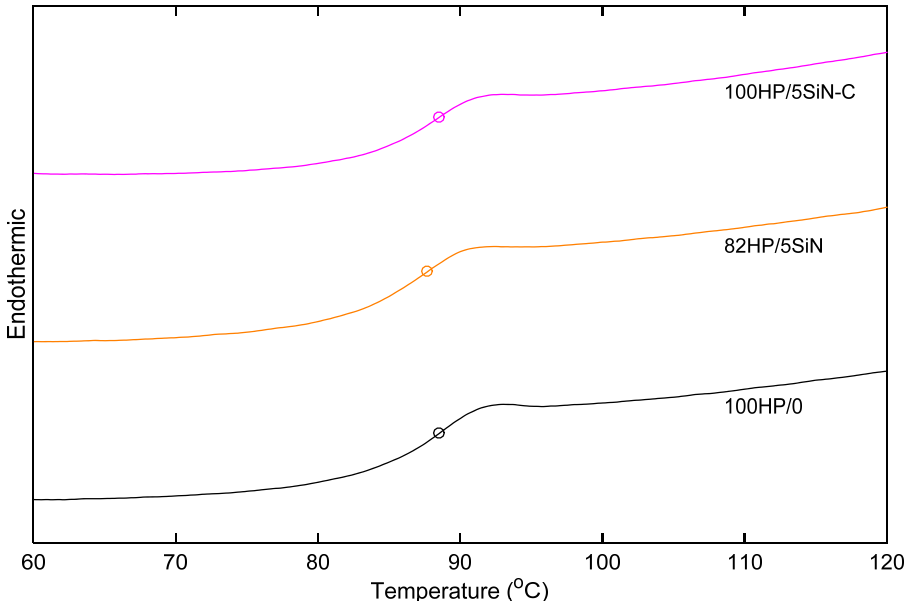

Figure 7.2: DSC traces for the three samples; the circles superimposed on the curves indicate T_g.

Table 7.2: Glass transition parameters for the three samples.

Sample code	T_g [°C]	ΔC_p [J/(g.°C)]	ΔT_g [°C]
100HP/0	88.2 ±2.4	0.31 ±0.026	7.66 ±1.8
82HP/5SiN	87.5 ±2.4	0.316 ±0.026	7.1 ±1.8
100HP/5SiN-C	88.5 ±2.4	0.309 ±0.026	6.79 ±1.8

The above data indicate that within the experimental uncertainties the three systems exhibit identical glass transition processes. That is, the cooperative segmental dynamics of the polymeric matrix in all of these samples are very similar, so that no variations can be detected by this characterisation method. For the sample filled with SiN, the data demonstrate that the stoichiometric effect of the filler is successfully accounted for. For

SiN-C filled sample, the obtained data indicate that the calcinated particles do not affect the glass transition of the host epoxy network. This is expected based on the surface chemistry of the calcinated particles, which revealed the absence of any surface functional groups that can chemically interfere with the curing reaction and, consequently, affect the crosslinking density of the network. This behaviour of the sample filled with the calcinated particles substantially supports the conclusion drawn in section 6.2 that as long as the nanoparticles do not chemically interact with the network, their physical presence as solid entities inside the epoxy matrix does not have an appreciable influence on the glass transition. Furthermore, the data obtained from samples 82HP/5SiN and 100HP/5SiN-C suggest that in both cases, whether the nanoparticles interact or do not interact with the epoxy, the nanofiller does not induce an observable confined or loose layer around themselves. This, in turn, implies either the absence of such layers, as was reported by [41], or that the thickness of such layers is too thin (< ~1 nm) to be distinguished from experimental uncertainties at the considered filler loading (5 wt% or 1.65 vol%) [43].

In addition to the glass transition, dielectric spectroscopy was used to probe any change in the segmental dynamics or the polar content brought by the nanofiller. Dielectric spectra obtained from the three sample types are presented in Figure 7.3, which show that the real part of the permittivity (ϵ_r') is comparable in all the three systems. The slight scaling up or down in ϵ_r' are within the experimental uncertainties which could be due to experimental errors in assessing the samples thickness or in producing exactly 30 mm gold layers on both sides of the samples. The data of the imaginary part of the relative permittivity (Figure 7.3b) show that the strength of the β relaxation is very similar in the three systems. Since the strength of this relaxation is proportional to the crosslinking density, established in the previous two chapters, these spectra indicate a similar crosslinking density in the three samples, which is in line with the DSC glass transition results. In fact, the comparable strength of the relaxation provides another evident that the stoichiometric effect of the SiN filler was properly accounted for, otherwise, the lower hardener content used in sample 82HP/5SiN should result in a sharp reduction in its β relaxation as was seen in unfilled systems (chapter 5). Furthermore, the presence of both the dried and the calcinated Si_3N_4 nanoparticles does not impart any distinctive relaxation in the obtained dielectric spectra. For the SiN filled system, the implications of this was discussed in section 6.3, where the absence of any additional relaxation, despite the presence of polar functional groups on the surface of the nanoparticles, was attributed to the reaction of these polar groups with the resin's epoxy groups. For the SiN-C filled system, this is expected, since the calcination treatment resulted in the removal of the polar groups on the particle surface.

Both the above DSC and dielectric spectroscopy data suggest that the segmental dynamics, at both a cooperative level and a more localised level, and the polar content of the epoxy matrix in the three systems are comparable.

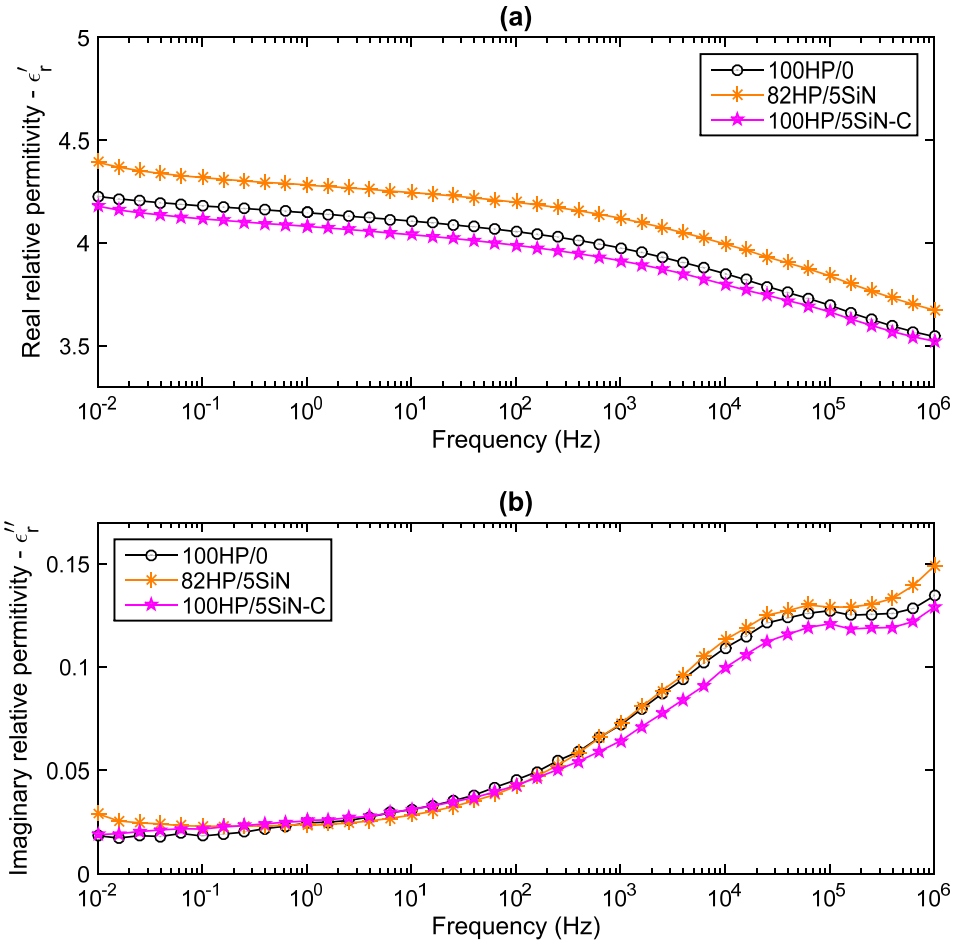

Figure 7.3: Dielectric response, (a) real part of the relative permittivity and (b) imaginary part of the permittivity.

7.4 DC conductivity and breakdown strength

7.4.1 Results

The DC conductivity of all the three samples at 45 °C is illustrated in Figure 7.4. The less scattering in the data obtained from sample 82HP/5SiN compared with the data of the other samples indicates higher signal to noise ratio since the DC conductivity and the current passes through this sample is considerably higher. The data show that the DC conductivity slightly increases as a function of time, however no dramatic change could be observed. The slight increase can be ascribed to the water absorption where the measurements were performed in a fan oven without moisture control and the samples start absorbing water after being exposed to ambient (see sections 5.6 and 6.7). Same DC conductivity measurements were conducted at other temperatures and the resulting data were statistically manipulated and presented in Figure 7.5. The results obviously indicate that the SiN filled sample has a significantly higher DC conductivity, whilst the SiN-C filled epoxy has a slightly lower DC conductivity than the unfilled epoxy sample. This trend in the DC conductivity distinctly correlates with the DC breakdown results shown in Figure 7.6a, where sample 82HP/5SiN has significantly lower DC breakdown strength and sample

100HP/5SiN-C has comparable breakdown strength to that of the unfilled refence epoxy. The AC breakdown results (Figure 7.6b) also show that the heat treatment at 1050 oC significantly increases the AC breakdown strength to be comparable to that of the refence sample. Table 7.3 summarises the Weibull parameters derived from the DC and AC breakdown measurements of the three systems.

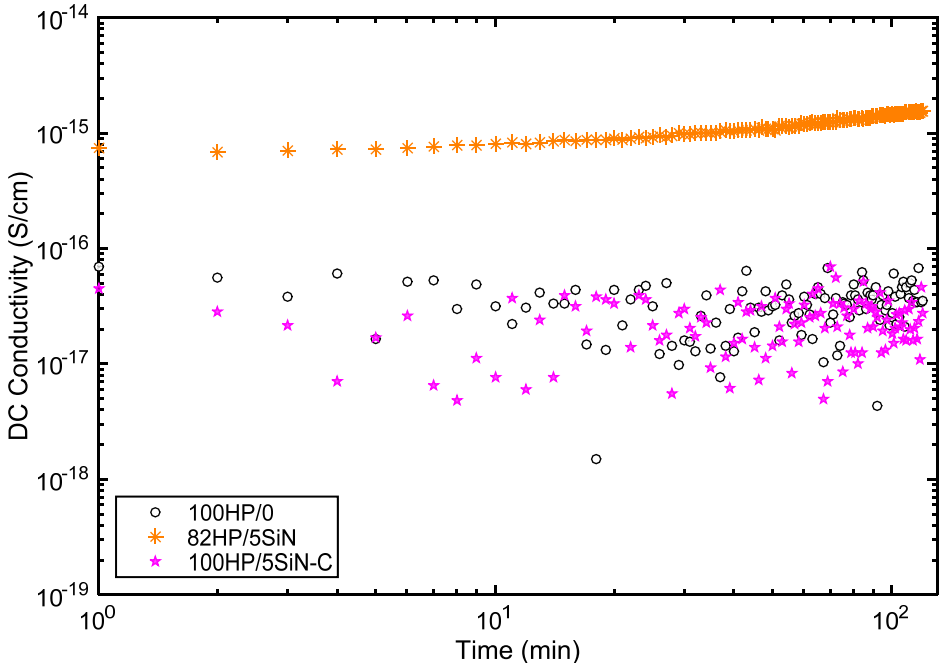

Figure 7.4: DC conductivity measurements at 45 °C and electric field of 42 kV/mm.

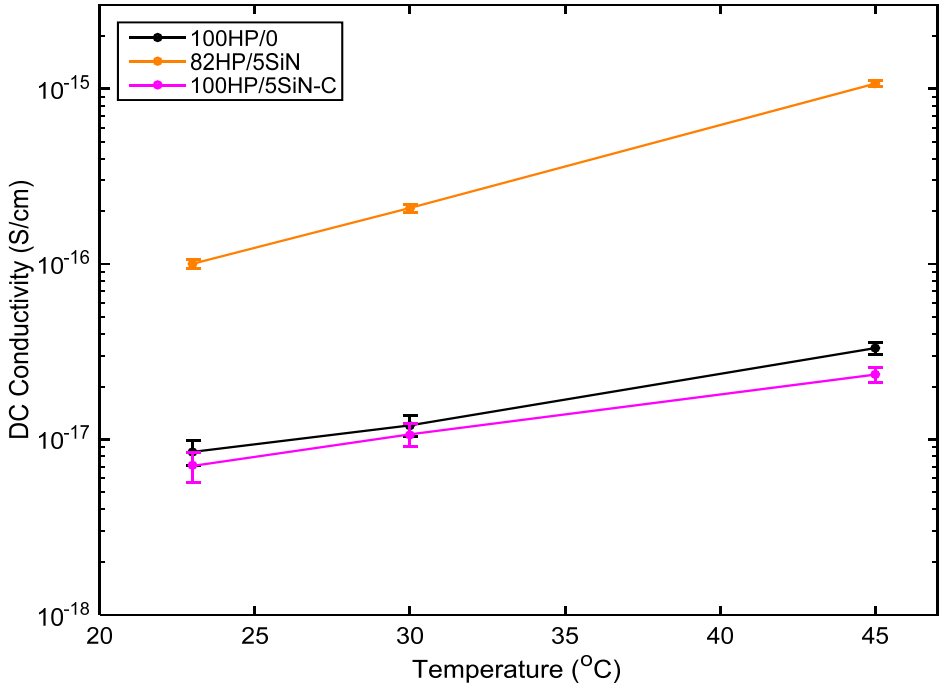

Figure 7.5: Average of DC conductivity for all samples at different temperatures and electric field of 42 kV/mm, the error bars indicate the 95 % confidence bounds of the average.

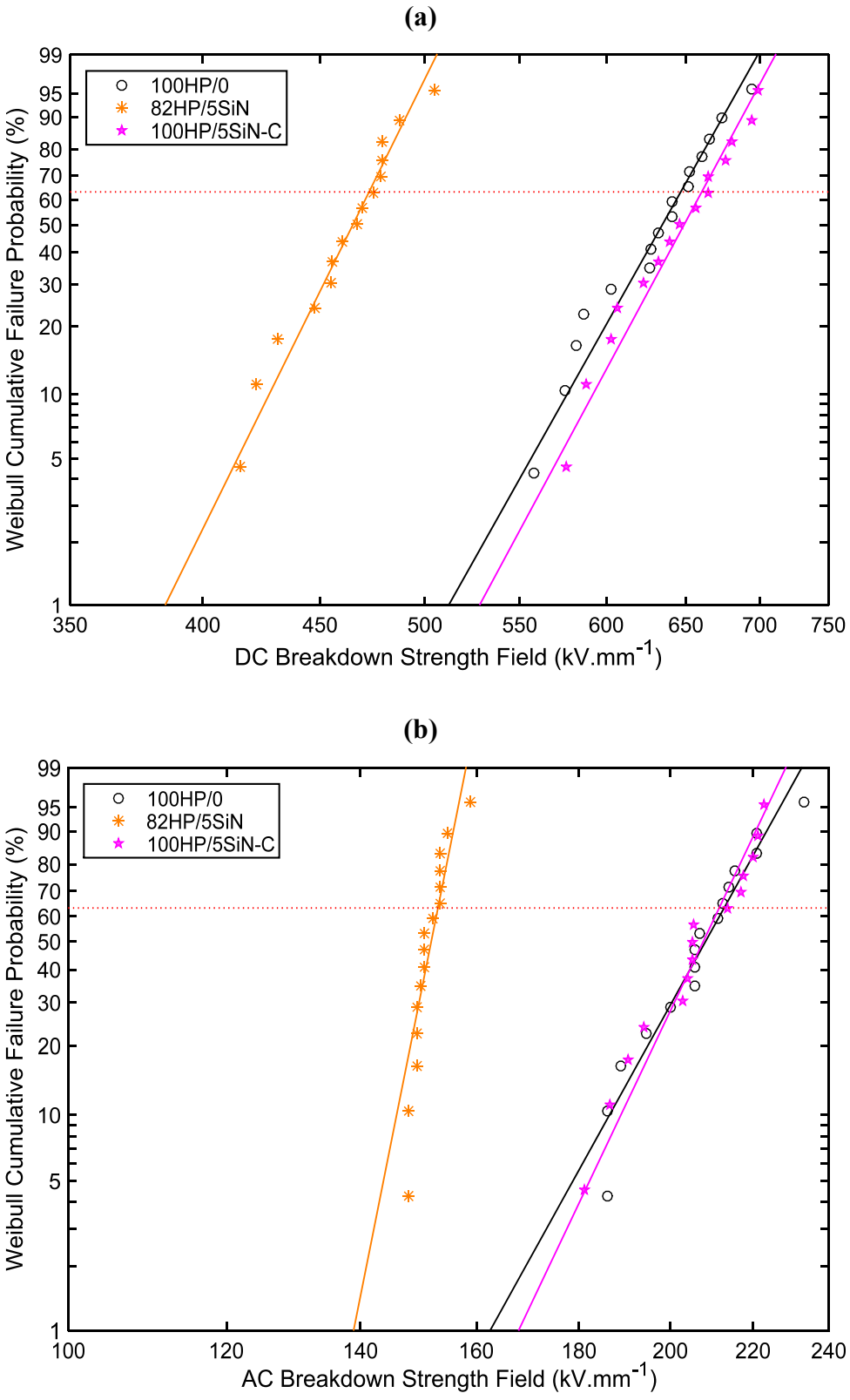

Figure 7.6: Breakdown measurements at room temperature for the three systems, (a) DC, and (b) AC.

Table 7.3: Weibull parameters derived from the DC and AC breakdown measurements for all samples, the uncertainties are based on the 95 % confidence bounds.

Sample code	DC breakdown Weibull parameters		AC breakdown Weibull parameters	
	η (kV.mm^{-1})	β	η (kV.mm^{-1})	β
100HP/0	646 ±18	19 ±6	212 ±7	17 ±6
82HP/5SiN	472 ±12	22 ±7	153 ±2	46 ±13
100HP/5SiN-C	660 ±17	20 ±6.8	211 ±5	20 ±8

7.4.2 Discussion

The above results clearly show that calcinating the particles at 1050 ^{o}C significantly affects the electrical performance of the resulting nanocomposite material. The fact that this effect includes a significant variation in the AC breakdown strength signifies that this behaviour is not associated with the matrix stoichiometry, as modifying the resin/hardener ratio in chapter 5 does not affect the AC breakdown strength. Furthermore, since the polymer matrix in the three investigated materials does not exhibit any other significant variations, as demonstrated by the glass transition results and the dielectric response, these variations in the DC conductivity and breakdown strength must be associated with the nanoparticles. Regarding the particle dispersion, the SiN dispersion is much better than the SiN-C dispersion and, hence, the dispersion factor would advise that the system filled with SiN has a better electric performance, which is not the case. Accordingly, the particle dispersion is not a decisive factor in determining the charge transport dynamics in these systems. Praeger *et al.* [190] studied the effect of calcinating a silica nanofiller at 1050 ^{o}C, before introducing it into a polyethylene matrix. They found that the calcinated silica resulted in a considerable increase in the DC breakdown strength, while the as-delivered silica, without any heat treatment, caused a substantial reduction in the DC breakdown strength; no other heat treatment was tried. The authors attributed this behaviour to the water shells that surround the hydrophilic as-delivered silica and evaporate upon heating the particles at 1050 ^{o}C. Water molecules are highly polar and can be auto-ionized (i.e. producing OH^{-} and H_3O^{+} ions), leading to higher charge transport [27, 155]. In the current investigation, a care was taken to remove such water layers by heating the particles at 200 ^{o}C and drying the samples at vacuum for > 14 days. Additionally, this possibility was ruled out in chapter 6 by studying the impact of water absorption on the electrical behaviour of the considered nanocomposites. Returning to the FTIR results, the surface of SiN particles has complex chemistry, is partially oxidised to silica, and contains many defects as indicated by detecting carbon and hydrogen atoms. Beside the amorphous structure of the particles, this surface chemistry suggests disordered band gap in the particle interphase with a high concentration of localised electronic states. As was discussed earlier, such particle interphase might increase the charge transport as was illustrated by Figure 2.6. On the other

hand, the SiN-C is covered by a silica layer terminating with stable siloxane bridges without NH or OH groups. Such surface chemistry indicates particle interphase with a lower concentration of localised electronic states. Indeed, Sameshima *et al.* found that changing the surface chemistry of silica films into Si-O-Si network significantly reduces the density of trap states [191]. Furthermore, it is known that the silica has a considerable larger band gap than the silicon nitride [192], which implies a particle interphase with wider band gap. Consequently, the particle interphase might, in this case, work as an energy barrier for the charge movement as proposed by Figure 2.7.

7.5 Chapter summary

This chapter showed that removing the surface amine groups by heating the particles at 1050 ^{o}C results in a worse particle dispersion, which is in line with the generally accepted rule that weak nanofiller/matrix interactions lead to a bad filler dispersion and vice versa. The obtained DSC results demonstrated that the inclusion of calcinated Si_3N_4 nanoparticles does not affect the glass transition process of the matrix, which supports the conclusion drawn in chapter 6 that nanoparticles do not affect the glass transition of an epoxy network unless they interfere with the curing process of the network (at least for the considered filler loading and for the specific epoxy matrix considered here).

The electrical property characterisation has demonstrated the critical impact of the particle interphase on the electrical performance of nanodielectrics. Although calcinating the Si_3N_4 particles should lead to much weaker filler/matrix interactions, as evinced by worsening the particle dispersion within the matrix, this results in a positive impact on the dielectric properties of the produced nanocomposites, in a striking contrast to what is conventionally claimed in the literature that strong filler/matrix interaction is one of the key factors that leads to a better dielectric performance in nanodielectrics [177-181]. This suggests that the particle interphase may have a more profound impact on the electrical properties than any variation in the polymer interphase that may be induced by the interacting with the incorporated nanoparticles.

Chapter 8

Conclusions and Future Work

8.1 Conclusions

Investigating the electrical behaviour of nanocomposites imposes challenges that may vary depending on the considered filler & host materials and the interactions between them. For the considered thermosetting system, the potential interference of the incorporated nanofiller with the network curing process is a major challenge that needs to be addressed to better understand the behaviour of these nanocomposites. Such interference may affect the resin/hardener stoichiometry and, consequently, the structure of the resulting network. Therefore, the study was initially concerned with the impact of changing the resin/hardener stoichiometry, before investigating the electrical behaviour of the Si_3N_4/epoxy nanocomposites. This methodology offers a great opportunity to understand the main mechanisms that control glass transition, dielectric spectra, DC conductivity and AC&DC breakdown strength of the base material. For example, by changing the resin/hardener ratio, it could be deduced that the crosslinking density, and consequently, T_g are primarily determined by the epoxy/amine group ratio, where side reactions, such as etherification or homopolarization, are negligible. Regarding electrical properties, it was found that the DC conductivity and the DC breakdown strength are sensitive to the chemical content of the epoxy network rather than to the network structure or dynamics. Specifically, increasing the hardener (amine) content beyond the optimum stoichiometric ratio, i.e. the $HP > 100$ %, has a detrimental impact on these properties whereas, reducing the hardener content has some benefits to the DC dielectric properties. On the other hand, the AC breakdown strength is not significantly influence by changing the resin/hardener stoichiometry. This may imply that a homogenous variation in the DC charge transport does not necessarily lead to a noticeable change in the short-term AC breakdown strength.

For the nanocomposite systems, the study has revealed that the addition of Si_3N_4 nanoparticles into the considered epoxy/amine network directly and significantly affects the resin/hardener stoichiometry. Analysis of data obtained from DSC measurements revealed that the addition of 2 and 5 wt% of Si_3N_4 nanofiller displaces the resin/hardener stoichiometry by 6.5 and 18 wt%, respectively. These figures were confirmed using other experimental techniques, dielectric spectroscopy and water uptake measurements. Therefore, this study demonstrate that nanofillers, due to their large surface area which may be covered by reactive chemical groups, can chemically interact with the reactive groups in the liquid resin and hardener and, thus, influence the networking process of

thermosetting systems. Hence, this parameter should always be considered when introducing nanofillers into thermosetting polymers.

Many of the models that aimed to explain the behaviour of nanocomposites refer to the formation of an interphase region, in which the polymer chains dynamics is different from the rest of the matrix. Although, in the system investigated here, there is a chemical bonding (i.e. strong interaction) between the polymer and the particles, DSC and dielectric spectroscopy results did not reveal any appreciable mark for such interphase region. This signifies that the thickness of any affected polymeric layer around the particles might be too small to be distinguished from experimental uncertainties and, accordingly, makes those models (which are based on this effect) no applicable to the investigated systems.

Water uptake monitoring showed that for thin samples, absorption of relatively significant amount of water occurs within few tens of minutes of exposure to ambient conditions. This was reflected on the DC conductivity results, which showed that water uptake during the measurement process can significantly affect the obtained data. Therefore, this factor should be carefully identified and taken into account when analysing experimentally obtained results. For the saturation water uptake, the obtained data indicated that the saturation water uptake is proportional to the polar content of the network, which correlates with the *HP* in the unfilled systems and HP_{eff} in the filled systems. Dielectric spectroscopy results revealed that part of the absorbed water forms hydrogen bonds with the polar sites in the network and, therefore, its dielectric relaxation is related to the relaxation of the moieties to which this fraction of the water is bound. Consequently, analysis of the dielectric spectra of the wet samples can give information about the polar content of the network and the interactions between these polar groups and the absorbed water. For the systems considered in this study, the results showed that the impact of water inclusion on the dielectric spectra is roughly equivalent for the filled and unfilled samples. This suggests that the distribution of the absorbed water molecules is identical in both cases and, therefore, implies the reaction of most of the polar amine groups on the surface of the Si_3N_4 nanoparticles, giving further credence to the stoichiometric effect of these particles. Electrical characterisation suggested that water absorption leads to a sharp increase in the DC conductivity, a sharp decrease in the DC breakdown strength, but a marginal impact on the AC breakdown strength. Therefore, more attention should be paid to water absorption in case of DC dielectric applications.

While most work reported in the literature has concentrated on investigating the characteristics of the polymer interphase, this study proposed an interphase region within the boundaries of the particles, which was called the particle interphase. The experimental investigation in chapter 7 has demonstrated that the particle interphase has a critical influence on the electrical properties of nanodielectrics, which could be more crucial than any variations may take place in the polymer interphase. This may be attributed to that the

particle material has higher density and, consequently, any perturbations in the particle interphase will lead to modifying the electronic density of states and, therefore, affect the electronic dynamics in this region. Due to its small molecules, the particle interphase is expected to be very thin and have insignificant impact on other properties such as mechanical properties. On the other hand, the polymers have long molecules, which may interact and form hydrogen or chemical bonds with the particle surface, which can affect the fracture or mechanical performance of nanocomposites. Hence, the interactions that occur in the polymer interphase may have more pronounce influence on the mechanical properties of the nanocomposites.

The electrical properties are essentially affected by the dynamics of charge carriers, which could be as small as electrons, and therefore, the behaviour of these properties is not necessarily correlated with the dynamics of larger constituents, i.e. dynamics of the polymeric segments or chains. The experimental results obtained in this study clearly support such conclusion, where, for example, no correlation has been detected between the network segmental dynamics, and the electrical performance of the samples investigated in chapter 5. Furthermore, all the samples investigated in chapter 7 exhibit similar molecular dynamics but significantly different charge dynamics and, consequently, electrical performance.

Designing nanodielectrics needs a more analytical approach than the currently empirically-dominated approach. Such approach should consider the relative location of the conduction and valence energy levels between the filler and matrix materials. These levels can be engineered by properly selecting the suitable filler/matrix combinations. Furthermore, the variations that may occur in these levels in the interphase regions can lead to a critical impact on the dielectric performance. As was proposed, the particle interphase may offer conduction paths or represent an energy barrier for electronic mobility. For this purpose, computer modelling can be a very useful tool, where simulation of the charge transport and distribution within the filler, matrix and interphase regions can provide a fundamental base for such approach.

Finally, this investigation demonstrates how a systematic methodology to analyse electrical behaviour of nanocomposites can lead to conclusive information. This methodology should start from a thorough characterisation of the key characteristics of both the filler and base materials. Additionally, such methodology includes critically understanding the main mechanisms that affect electrical properties of the base polymer before beginning to analyse the impact of the nanofiller incorporation. Without this understanding, it would be impossible to reach many of the findings reported in this thesis. For example, the conclusion that the reduction of the AC breakdown strength observed in the nanocomposite samples cannot be attributed to the impact of the nanofiller on the

network structure or stoichiometry is chiefly based on the behaviour of the AC breakdown strength of the unfilled epoxy upon changing the network stoichiometry.

8.2 Future work

Based on the findings presented in this study, the following paragraphs outline some of the topics that are suggested for future investigations.

- Thermal conductivity: improving thermal conductivity of polymers by filling them with nanoparticles that have considerably higher thermal conductivity is beneficial for many applications. For example, as electrical insulation materials, higher thermal conductivity increases the dissipation rate of the heat generated from the insulated equipment and, thus, allows higher power ratings to be applied. Many studies have indicated that the thermal conductivity of polymeric nanocomposites is affected by the thermal conductivity of both the filler and matrix materials and the interactions in the interphase between the filler and the polymer. The existence of covalent bonds between the polymeric matrix and the ceramic filler can reduce the phonon scattering at the interface and, consequently, enhance the overall phonon transport in the composite. A recent study [193] suggested an empirical proportional relation between the thermal transport over the interface between two phases, and the strength of the bonding between them. Therefore, it would be worth to investigate the role of the interactions and the surface chemistry of silicon nitride nanofiller on the thermal conductivity of the resulting silicon nitride/epoxy nanocomposites.

4- Water influence on electrical properties: it has been shown in this study that the impact of water absorption on electrical properties of Si_3N_4/epoxy nanocomposites is comparable to its impact on unfilled epoxy systems. This was connected to that the distribution of the absorbed water is comparable in both cases. It would be interesting to explore if different water distribution would lead to different implications on electrical properties. This can be examined by filling an epoxy matrix with a polar nanofiller, like silica, where the absorbed water is expected to be more concentrated around the particles. Consequently, by performing the same characterisation performed in this study, the influence of the distribution of absorbed water can be highlighted.

5- Mechanical properties and erosion resistance: the fact that Si_3N_4 particles can crosslink with epoxy may suggest that this filler may enhance mechanical and erosion properties of Si_3N_4/epoxy nanocomposites. Therefore, it would be worth to investigate the impact of Si_3N_4 particles on mechanical properties and erosion resistance of Si_3N_4/epoxy based nanocomposites.

Appendix A

Polymer Properties

A.1 Crystallinity of polymers

The arrangement of the polymeric chains and their ability to form crystalline regions depend on the regularity of these chains. For example, in case of linear polymer chains with small side groups, the chains can arrange themselves to form crystalline regions. However, due to the complicated structure and different length of the polymeric chains, a 100 % crystalline polymer seems to be not possible. Always, there are amorphous regions that lie between the crystalline regions and the degree of crystallinity therefore depends on the regularity of the polymeric chains. Linear polymer chains containing bulky side groups, branched polymer chains or crosslinked polymer chains cannot form crystalline regions easily and the degree of crystallinity may reach zero for these polymers, i.e. completely amorphous polymer [194].

A.2 Transparency of polymers

The band gap of most polymers is more than the photon energy of visible light and therefore, these materials should be transparent if there are no other determining factors. This generally applies to amorphous polymer, where the material is considered to be one phase.

Crystalline polymers, however, contain both crystalline and amorphous regions. The crystalline structures are usually denser and thus have higher refractive indices than amorphous regions. Therefore, crystalline polymers contain two phases and if the dimensions of these phases are similar or larger than the wavelength of the visible light, then the light will experience refraction and scattering each time it passes from one phase to the other. By repeating this process many times, most of the light will be scattered and the material will appear translucent or opaque.

Introducing nanoparticles into a polymeric matrix has a similar effect on the transparency of the material, where the nanoparticles are considered one phase and the polymeric matrix is considered another phase. For well dispersed nanoparticles, the dimensions of the nanoparticles phase should be less than 100 nm, specifically for spherical nanoparticles, which is less than the wavelength of visible light (400 - 700 nm). Therefore, well dispersed nanoparticles inside a polymeric matrix would not be expected greatly to affect the transparency of an otherwise transparent polymer. The opposite is true where, if the

nanoparticles agglomerate to form regions with dimensions equal or more than the wavelength of light, then the otherwise transparent polymer could appear opaque [92].

A.3 Solubility of polymers

Many nanocomposite preparation methods involve the use of solvents in one or more of the processing stages and, therefore, understanding the interaction between polymers and solvents is important. A solvent can dissolve a polymer if it initiates new bonds with the polymer chains, replacing the existed intermolecular bonds. When a suitable solvent is mixed with a polymer, the solvent molecules can diffuse between the long polymer chains and form new bonds, which replace the intermolecular bonds and finally dissolve the polymer into its constituent chains. However, the polymer chains are very long compared with the solvent molecules and there are many bonds connecting the chains together, which result in slowing down the dissolution process taking up to several days. This is particularly relevant for crystalline polymers, where the polymeric chains are well backed and have denser number of bonds to be overcome by the solvent [14].

In a crosslinked polymer, the solvent cannot replace the covalent bonds between the polymer chains and, thus, crosslinked polymers cannot be dissolved. However, crosslinked polymers can be swollen by solvent molecules, which diffuse into the free spaces within the polymeric network. Figure A.1 shows a cured epoxy sample after immersing it in acetone for several days.

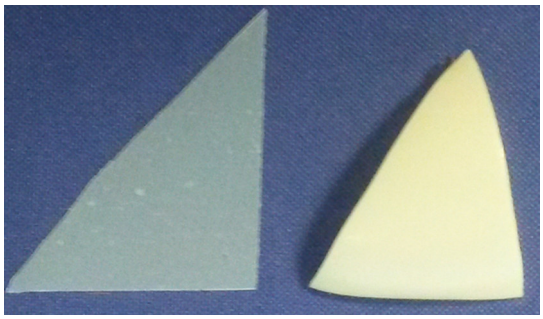

Figure A.1: Effect of solvent on cured epoxy nanocomposite, the sample on left is the original one and the sample on the right is after being in acetone for more than 10 days.

A.4 Thermal effect on polymers

Due to their long molecules and the entanglements between these molecules, the thermal effect on the polymers is more complicated than on other materials of low molecular mass.

In amorphous polymers, the chains are randomly connected and entangled together, therefore, there is no definite temperature where the thermal energy can exceed the intermolecular bonds and the polymer flows as a simple liquid. Even if the thermal energy

is sufficient to overcome these bonds, the random entanglements between the long chains do not allow the polymer to flow easily. Instead, amorphous polymers convert from a rigid glassy phase into a flexible rubbery phase. The temperature that differentiates between the glassy phase and the rubbery phase is known as glass transition temperature (T_g). In reality, T_g corresponds to a narrow range of temperatures instead of being a definite temperature. Below T_g, the material is hard and glassy, where the polymeric chain motion is restricted to vibrations of the atoms about equilibrium positions or motions of a few atoms along the main chain. Above T_g, the material is soft and rubbery, where polymeric chains have more freedom to move.

In crystalline polymers, the chains are connected together regularly and, therefore, at a sufficient temperature, the melting temperature (T_m), the crystalline regions can melt and the polymeric chains can flow. However, since the crystalline regions are not all of the same size, they melt at slightly different temperatures. Accordingly, the melting temperature might be a range of temperatures rather than single temperature. Additionally, the crystalline polymers have both crystalline and amorphous regions, thereby, they have both T_m and T_g.

References

[1] T. J. Lewis, "Nanometric dielectrics," *IEEE Transactions on Dielectrics and Electrical Insulation,* vol. 1, pp. 812-825, 1994.

[2] J. K. Nelson, J. C. Fothergill, L. A. Dissado, and W. Peasgood, "Towards an understanding of nanometric dielectrics," *2002 IEEE Conference on Electrical Insulation and Dielectric Phenomena* pp. 295-298, 2002.

[3] D. Fabiani, G. C. Montanari, and L. Testa, "Effect of aspect ratio and water contamination on the electric properties of nanostructured insulating materials," *IEEE Transactions on Dielectrics and Electrical Insulation,* vol. 17, pp. 221-230, 2010.

[4] I. L. Hosier, M. Praeger, A. S. Vaughan, and S. G. Swingler, "The Effects of Water on the Dielectric Properties of Silicon-Based Nanocomposites," *IEEE Transactions on Nanotechnology,* vol. 16, pp. 169-179, 2017.

[5] M. Praeger, I. L. Hosier, A. S. Vaughan, and S. G. Swingler, "The effects of surface hydroxyl groups in polyethylene-silica nanocomposites," *IEEE 2015 Electrical Insulation Conference (EIC),* pp. 201-204, 2015.

[6] J. K. Nelson, "Nanodielectrics - the first decade and beyond," *IEEE Proceedings of 2014 International Symposium on Electrical Insulating Materials (ISEIM 2014),* pp. 1-11, 2014.

[7] T. J. Lewis, "Interfaces are the dominant feature of dielectrics at the nanometric level," *IEEE Transactions on Dielectrics and Electrical Insulation,* vol. 11, pp. 739-753, Oct 2004.

[8] K. J. Klabunde, *Nanoscale materials in chemistry*: John Wiley & Sons, Inc., 2001.

[9] M. Supova, G. S. Martynkova, and K. Barabaszova, "Effect of nanofillers dispersion in polymer matrices: a review," *Science of Advanced Materials,* vol. 3, pp. 1-25, 2011.

[10] T. J. Lewis, "Interfaces: nanometric dielectrics," *Journal of Physics D-Applied Physics,* vol. 38, pp. 202-212, Jan 21 2005.

[11] J. K. Nelson, "Overview of nanodielectrics: Insulating materials of the future," *IEEE 2007 Electrical Insulation Conference and Electrical Manufacturing Expo,* pp. 229-235, 2007.

[12] C. W. Reed, "Self-Assembly of Polymer Nanocomposites for Dielectries and HV Insulation," *2007 IEEE International Conference on Solid Dielectrics, Vols 1 and 2,* pp. 397-400, 2007.

[13] J. K. Nelson, *Dielectric Polymer Nanocomposites*. USA: Springer, 2010.

[14] Christopher S. Brazel and S. L. Rosen, *Fundamental Principles of Polymeric Materials*, 3 edition ed.: Wiley, 2012.

[15] C. M. Hansen, "The three dimensional solubility parameter and solvent diffusion coefficient," PhD Thesis, Danish Technical Press, Copenhagen, 1967.

[16] F. W. Starr, J. F. Douglas, and S. C. Glotzer, "Origin of particle clustering in a simulated polymer nanocomposite and its impact on rheology," *Journal of Chemical Physics,* vol. 119, pp. 1777-1788, 2003.

[17] L. He, W. Chuang, G. Zihao, W. Haoran, Z. Yuxuan, H. Rui*, et al.*, "Effects of silane coupling agents on the electrical properties of silica/epoxy nanocomposites," *2016 IEEE International Conference on Dielectrics (ICD),* vol. 2, pp. 1036-1039, 2016.

[18] D. L. Ma, R. W. Siegel, J. I. Hong, L. S. Schadler, E. Martensson, and C. Onneby, "Influence of nanoparticle surfaces on the electrical breakdown strength of nanoparticle-filled low-density polyethylene," *Journal of Materials Research,* vol. 19, pp. 857-863, 2004.

[19] C. Yeung and A. S. Vaughan, "On the effect of nanoparticle surface chemistry on the electrical characteristics of epoxy-based nanocomposites," *Polymers,* vol. 8, 2016.

[20] D. L. Ma, T. A. Hugener, R. W. Siegel, A. Christerson, E. Martensson, C. Onneby*, et al.*, "Influence of nanoparticle surface modification on the electrical behaviour of polyethylene nanocomposites," *Nanotechnology,* vol. 16, pp. 724-731, 2005.

[21] X. Y. Huang, Z. S. Ma, Y. Q. Wang, P. K. Jiang, Y. Yin, and Z. Li, "Polyethylene/aluminum nanocomposites: improvement of dielectric strength by nanoparticle surface modification," *Journal of Applied Polymer Science,* vol. 113, pp. 3577-3584, 2009.

[22] X. Y. Huang, F. Liu, and P. K. Jiang, "Effect of nanoparticle surface treatment on morphology, electrical and water treeing behavior of LLDPE composites," *IEEE Transactions on Dielectrics and Electrical Insulation,* vol. 17, pp. 1697-1704, 2010.

[23] I. L. Hosier, M. Praeger, A. F. Holt, A. S. Vaughan, and S. G. Swingler, "On the effect of functionaliser chain length and water content in polyethylene/silica nanocomposites: Part I – dielectric properties and breakdown strength," *IEEE Transactions on Dielectrics and Electrical Insulation,* 2015.

[24] I. L. Hosier, A. S. Vaughan, and S. G. Swingler, "On the effects of morphology and molecular composition on the electrical strength of polyethylene blends," *Journal of Polymer Science Part B-Polymer Physics,* vol. 38, pp. 2309-2322, 2000.

[25] Y. Wang, D. MacKernan, D. Cubero, D. F. Coker, and N. Quirke, "Single electron states in polyethylene," *Journal of Chemical Physics,* vol. 140, 2014.

[26] C. Zou, J. C. Fothergill, and S. W. Rowe, "The effect of water absorption on the dielectric properties of epoxy nanocomposites," *IEEE Transactions on Dielectrics and Electrical Insulation,* vol. 15, pp. 106-17, 2008.

[27] L. Hui, L. S. Schadler, and J. K. Nelson, "The influence of moisture on the electrical properties of crosslinked polyethylene/silica nanocomposites," *IEEE Transactions on Dielectrics and Electrical Insulation,* vol. 20, pp. 641-653, 2013.

[28] I. L. Hosier, M. Praeger, A. F. Holt, A. S. Vaughan, and S. G. Swingler, "Effect of water absorption on dielectric properties of nano-silica/polyethylene composites," in *2014 IEEE Conference on Electrical Insulation and Dielectric Phenomena*, ed, 2014, pp. 651-654.

[29] H. Couderc, M. Frechette, S. Savoie, M. Reading, and A. S. Vaughan, "Dielectric and Thermal Properties of Boron Nitride and Silica Epoxy Composites," *Conference Record of the 2012 IEEE International Symposium on Electrical Insulation (Isei),* pp. 64-68, 2012 2012.

[30] M. Roy, J. K. Nelson, R. K. MacCrone, L. S. Schadler, C. W. Reed, R. Keefe*, et al.*, "Polymer nanocomposite dielectrics - The role of the interface," *IEEE Transactions on Dielectrics and Electrical Insulation,* vol. 12, pp. 629-643, 2005.

[31] P. Morshuis, "Interfaces: To be avoided or to be treasured? What do we think we know?," *2013 IEEE International Conference on Solid Dielectrics (ICSD),* pp. 1-9, 2013.

[32] R. Kochetov, T. Andritsch, P. H. F. Morshuis, and J. J. Smit, "Anomalous behaviour of the dielectric spectroscopy response of nanocomposites," *IEEE Transactions on Dielectrics and Electrical Insulation,* vol. 19, pp. 107-117, 2012.

[33] M. Kurimoto, H. Okubo, K. Kato, M. Hanai, Y. Hoshina, M. Takei*, et al.*, "Permittivity characteristics of epoxy/alumina nanocomposite with high particle dispersibility by combining ultrasonic wave and centrifugal force," *IEEE Transactions on Dielectrics and Electrical Insulation,* vol. 17, pp. 1268-1275, 2010.

[34] W. Zhou and D. Yu, "Fabrication, thermal, and dielectric properties of self-passivated Al/epoxy nanocomposites," *Journal of Materials Science,* vol. 48, pp. 7960-7968, 2013.

[35] M. Praeger, I. L. Hosier, A. F. Holt, A. S. Vaughan, and S. G. Swingler, "On the effect of functionaliser chain length and water content in polyethylene/silica nanocomposites: Part II – charge transport," *IEEE Transactions on Dielectrics and Electrical Insulation,* 2015.

[36] G. Cao, *Nanostructures & Nanomaterials: Synthesis, Properties & Applications*. London, UK: Imperial College Press, 2004.

[37] T. Tanaka, M. Kozako, N. Fuse, and Y. Ohki, "Proposal of a multi-core model for polymer nanocomposite dielectrics," *IEEE Transactions on Dielectrics and Electrical Insulation,* vol. 12, pp. 669-681, 2005.

[38] A. S. Vaughan, "Nano at nineteen," *IEEE International Conference on Solid Dielectrics (ICSD 2013),* vol. 1 and 2, pp. 706-709, 2013.

[39] R. Xu, *Particle Characterization: Light Scattering Methods*: Kluwer Academic Publishers, 2002.

[40] Y. Miwa, A. R. Drews, and S. Schlick, "Detection of the direct effect of clay on polymer dynamics: The case of spin-labeled poly(methyl acrylate)/clay nanocomposites studied by ESR, XRD, and DSC," *Macromolecules,* vol. 39, pp. 3304-3311, 2006.

[41] R. B. Bogoslovov, C. M. Roland, A. R. Ellis, A. M. Randall, and C. G. Robertson, "Effect of silica nanoparticles on the local segmental dynamics in poly(vinyl acetate)," *Macromolecules,* vol. 41, pp. 1289-1296, 2008.

[42] C. G. Robertson, C. J. Lin, M. Rackaitis, and C. M. Roland, "Influence of particle size and polymer-filler coupling on viscoelastic glass transition of particle-reinforced polymers," *Macromolecules,* vol. 41, pp. 2727-2731, 2008.
[43] S. E. Harton, S. K. Kumar, H. C. Yang, T. Koga, K. Hicks, E. Lee*, et al.*, "Immobilized polymer layers on spherical nanoparticles," *Macromolecules,* vol. 43, pp. 3415-3421, 2010.
[44] A. Sargsyan, A. Tonoyan, S. Davtyan, and C. Schick, "The amount of immobilized polymer in PMMA SiO2 nanocomposites determined from calorimetric data," *European Polymer Journal,* vol. 43, pp. 3113-3127, 2007.
[45] A. P. Holt, P. J. Griffin, V. Bocharova, A. L. Agapov, A. E. Imel, M. D. Dadmun*, et al.*, "Dynamics at the polymer/nanoparticle interface in poly(2-vinylpyridine)/silica nanocomposites," *Macromolecules,* vol. 47, pp. 1837-1843, 2014.
[46] V. Bershtein, V. Gun'ko, L. Egorova, N. Guzenko, E. Pakhlov, V. Ryzhov*, et al.*, "Well-defined silica core-poly(vinyl pyrrolidone) shell nanoparticles: Interactions and multi-modal glass transition dynamics at interfaces," *Polymer,* vol. 50, pp. 860-871, 2009.
[47] J. K. Nelson, Y. H. Huang, T. M. Krentz, L. S. Schadler, J. Dryzek, B. C. Benicewicz*, et al.*, "Free Volume in Nanodielectrics," *2015 IEEE 11th International Conference on the Properties and Applications of Dielectric Materials,* pp. 40-43, 2015.
[48] J. A. Anta, G. Marcelli, M. Meunier, and N. Quirke, "Models of electron trapping and transport in polyethylene: Current-voltage characteristics," *Journal of Applied Physics,* vol. 92, pp. 1002-1008, 2002.
[49] L. A. Dissado and J. C. Fothergill, *Electrical degradation and breakdown in polymers*: Institution of Engineering and Technology, 1992.
[50] R. C. Smith, C. Liang, M. Landry, J. K. Nelson, and L. S. Schadler, "The mechanisms leading to the useful electrical properties of polymer nanodielectrics," *IEEE Transactions on Dielectrics and Electrical Insulation,* vol. 15, pp. 187-196, 2008.
[51] S. Le Roy, G. Teyssedre, C. Laurent, G. C. Montanari, and F. Palmieri, "Description of charge transport in polyethylene using a fluid model with a constant mobility: fitting model and experiments," *Journal of Physics D-Applied Physics,* vol. 39, pp. 1427-1436, 2006.
[52] M. Reading, A. S. Vaughan, and P. L. Lewin, "An investigation into improving the breakdown strength and thermal conduction of an epoxy system using boron nitride," *2011 IEEE Conference on Electrical Insulation and Dielectric Phenomena,* pp. 636-9, 2011.
[53] Z. Xu, M. Reading, A. S. Vaughan, and P. L. Lewin, "Space charge distribution in filled epoxy composites containing micro and nano fillers," *2011 14th International Symposium on Electrets (ISE),* pp. 117-118, 2011.
[54] K. Y. Lau, A. S. Vaughan, G. Chen, I. L. Hosier, A. F. Holt, and K. Y. Ching, "On the space charge and DC breakdown behavior of polyethylene/silica nanocomposites," *IEEE Transactions on Dielectrics and Electrical Insulation,* vol. 21, pp. 340-351, 2014.
[55] E. Kubyshkina, B. L. G. Jonsson, and M. Unge, "Electronic properties of magnesium oxide - polyethylene interface," *2016 IEEE International Conference on Dielectrics (ICD),* vol. 2, pp. 788-791, 2016.
[56] C. May, *Epoxy Resins: Chemistry and Technology*, Second Edition ed.: CRC Press, 1987.
[57] B. Ellis, *Chemistry and Technology of Epoxy Resins* 1ed.: Springer, 1993.
[58] P. Dufton, *Lightweight Thermoset Composites: Materials in Use, Their Processing and Applications*: Rapra Technology Ltd, 1999.
[59] Edith Turi, *Thermal Characterization of Polymeric Materials*: Academic Press, 1981.
[60] S. G. Prolongo, A. Salazar, A. Urena, and J. Rodriguez, "Effect of hydroxyl content on the morphology and properties of epoxy/poly(styrene-co-allylalcohol) blends," *Polymer Engineering and Science,* vol. 47, pp. 1580-1588, Oct 2007.
[61] M. F. Grenierloustalot and P. Grenier, "The role of impurities in the mechanisms and kinetics of epoxy-resins and their effects on final resin properties," *British Polymer Journal,* vol. 22, pp. 303-313, 1990.
[62] X. R. Wang and J. K. Gillham, "Analysis of crosslinking in amine-cured epoxy systems: the one-to-one relationship between Tg and conversion," *Journal of Applied Polymer Science,* vol. 45, pp. 2127-2143, Aug 1992.

[63] F. Meyer, G. Sanz, A. Eceiza, I. Mondragon, and J. Mijovic, "The effect of stoichiometry and thermal history during cure on structure and properties of epoxy networks," *Polymer,* vol. 36, pp. 1407-1414, Mar 1995.

[64] V. Nguyen, A. S. Vaughan, P. L. Lewin, and A. Krivda, "On the Stoichiometry with Space Charge and Breakdown Behaviour of an Epoxy Based System with Nano-Sized And Micro-Sized Fillers," *2012 Annual Report Conference on Electrical Insulation and Dielectric Phenomena (CEIDP),* pp. 287-290, 2012.

[65] B. Burton;, D. Alexander;, H. Klein;, A. Garibay-Vasquez;, A. Pekarik;, and C. Henkee;, "Epoxy formulations using Jeffamine® polyetheramines," ed: Huntsman, 2005.

[66] H. Lim, J. Lee, J. Jeong, S. Oh, and S. Lee, "Comparative Study of Various Preparation Methods of Colloidal Silica," *Engineering,* vol. 2, pp. 998-1005, 2010.

[67] F. K. Vandijen, A. Kerber, U. Vogt, W. Pfeiffer, and M. Schulze, "Comparative study of three silicon nitride powders, obtained by three different syntheses," *Key Engineering Materials,* vol. 89-91, pp. 19-27, 1994.

[68] M. Praeger, A. S. Vaughan, and S. G. Swingler, "The breakdown strength and localised structure of polystyrene as a function of nano silica fill-fraction," *Proceedings of the 2013 IEEE International Conference on Solid Dielectrics,* pp. 863-866, 2013.

[69] B. Fubini, M. Volante, V. Bolis, and E. Giamello, "Reactivity towards water of silicon nitride: energy of interaction and hydration dehydration mechanism " *Journal of Materials Science,* vol. 24, pp. 549-556, 1989.

[70] G. Busca, V. Lorenzelli, M. I. Baraton, P. Quintard, and R. Marchand, "FT-IR characterization of silicon nitride Si3N4 and silicon oxynitride SI2ON2 surfaces," *Journal of Molecular Structure,* vol. 143, pp. 525-528, Mar 1986.

[71] K. Bula, T. Jesionowski, A. Krysztafkiewicz, and J. Janik, "The effect of filler surface modification and processing conditions on distribution behaviour of silica nanofillers in polyesters," *Colloid and Polymer Science,* vol. 285, pp. 1267-1273, Aug 2007.

[72] G. Cheng, J. Qian, Z. Tang, G. Ding, and J. Zhu, "Dispersion stability of Si3N4 nano-particles modified by gamma-methacryloxypropyl trimethoxy silane (MAPTMS) in organic solvent," *Ceramics International,* vol. 41, pp. 1879-1884, Jan 2015.

[73] L. S. Cerovic, S. K. Milonjic, D. Bahloul-Hourlier, and B. Doucey, "Surface properties of silicon nitride powders," *Colloids and Surfaces A: Physicochemical and Engineering Aspects,* vol. 197, pp. 147-156, Feb 2002.

[74] C. M. Wang, X. Pan, M. Ruhle, F. L. Riley, and M. Mitomo, "Silicon nitride crystal structure and observations of lattice defects," *Journal of Materials Science,* vol. 31, pp. 5281-98, Oct. 1996.

[75] Y. L. Li, Y. Liang, F. Zheng, K. Xiao, Z. Q. Hu, and T. Shun, "Fourier transformation infrared investigation of surface oxidation of ultrafine Si3N4 powders," *Journal of Materials Science Letters,* vol. 14, pp. 713-715, 1995.

[76] J. Szepvolgyi, I. Mohai, and J. Gubicza, "Atmospheric ageing of nanosized silicon nitride powders," *Journal of Materials Chemistry,* vol. 11, pp. 859-863, 2004.

[77] J. Szepvolgyi, I. Mohai, and J. Gubicza, "Studies on atmospheric ageing of nanosized silicon nitride powders," *Key Engineering Materials,* vol. 264-268, pp. 2311-2314, 2004.

[78] B. V. Zhmud, J. Sonnefeld, and L. Bergstrom, "Influence of chemical pretreatment on the surface properties of silicon nitride powder," *Colloids and Surfaces a-Physicochemical and Engineering Aspects,* vol. 158, pp. 327-341, Nov 1999.

[79] W. Liwu, W. Sigmund, and F. Aldinger, "Systematic approach for dispersion of silicon nitride powder in organic media. I. Surface chemistry of the powder," *Journal of the American Ceramic Society,* vol. 83, pp. 691-6, April 2000.

[80] L. T. Zhuravlev, "Concentration of hydroxyl-groups on the surface of amorphous silicas," *Langmuir,* vol. 3, pp. 316-318, Jun 1987.

[81] L. T. Zhuravlev, "The surface chemistry of amorphous silica. Zhuravlev model," *Colloids and Surfaces A: Physicochemical and Engineering Aspects,* vol. 173, pp. 1-38, Nov 2000.

[82] W. Zhou, J. Zuo, X. Zhang, and A. Zhou, "Thermal, electrical, and mechanical properties of hexagonal boron nitride-reinforced epoxy composites," *Journal of Composite Materials,* vol. 48, pp. 2517-2526, 2014.

[83] M. Reading, Z. Xu, A. S. Vaughan, and P. L. Lewin, "The thermal and electrical properties of nano-silicon dioxide filled epoxy systems for use in high voltage insulation," *2011 Electrical Insulation Conference (EIC),* pp. 493-497, 2011.
[84] K. Sato, H. Horibe, T. Shirai, Y. Hotta, H. Nakano, H. Nagai*, et al.*, "Thermally conductive composite films of hexagonal boron nitride and polyimide with affinity-enhanced interfaces," *Journal of Materials Chemistry,* vol. 20, pp. 2749-2752, 2010.
[85] K. Y. Lau, A. S. Vaughan, G. Chen, and I. L. Hosieri, "Space Charge Dynamics in Silica-based Polyethylene Nanocomposites," *Proceedings of the 2013 IEEE International Conference on Solid Dielectrics (ICSD 2013), Vols 1 and 2,* pp. 880-883, 2013.
[86] K. Y. Lau, A. S. Vaughan, G. Chen, and I. L. Hosier, "Polyethylene Nanodielectrics: The Effect of Nanosilica and its Surface Treatment on Electrical Breakdown Strength," *2012 Annual Report Conference on Electrical Insulation and Dielectric Phenomena (CEIDP),* pp. 21-24, 2012.
[87] Z. Chao and G. C. Stevens, "The dielectric response of polar and non-polar nanodielectrics," *IEEE Transactions on Dielectrics and Electrical Insulation,* vol. 15, pp. 606-17, 2008.
[88] V. T. Nguyen, A. S. Vaughan, P. L. Lewin, and A. Krivda, "The Effect of Resin Stoichiometry and Nanoparticle Addition on Epoxy/Silica Nanodielectrics," *IEEE Transactions on Dielectrics and Electrical Insulation,* vol. 22, pp. 895-905, 2015.
[89] T. Andritsch, R. Kochetov, Y. T. Gebrekiros, P. H. F. Morshuis, and J. J. Smit, "Short term DC breakdown strength in epoxy based BN nano- and microcomposites," *Proceedings of the 2010 10th IEEE International Conference on Solid Dielectrics,* pp. 4 pp.-4 pp., 2010.
[90] C. Yeung, A. S. Vaughan, and Ieee, "A study of how varying degrees of functionalised nanofiller have an effect on nanodielectrics," *2012 Annual Report Conference on Electrical Insulation and Dielectric Phenomena (Ceidp),* pp. 319-322, 2012 2012.
[91] R. Kochetov, T. Andritsch, P. H. F. Morshuis, and J. J. Smit, "Evaluation of the influence of various nanofillers on the AC breakdown strength of epoxy-based nanocomposites," *2011 International Conference on Electrical Insulating Materials,* pp. 383-6, 2011.
[92] S. Virtanen, T. M. Krentz, J. K. Nelson, L. S. Schadler, M. Bell, B. Benicewicz*, et al.*, "Dielectric breakdown strength of epoxy bimodal-polymer-brush-grafted core functionalized silica nanocomposites," *IEEE Transactions on Dielectrics and Electrical Insulation,* vol. 21, pp. 563-570, Apr 2014.
[93] W. Yan, Z. J. Han, B. T. Phung, and K. Ostrikov, "Silica Nanoparticles Treated by Cold Atmospheric-Pressure Plasmas Improve the Dielectric Performance of Organic-Inorganic Nanocomposites," *ACS Applied Materials & Interfaces,* vol. 4, pp. 2637-2642, May 2012.
[94] D. Fabiani, G. C. Montanari, L. Testa, R. Schifani, F. Guastavino, F. Bellucci*, et al.*, "Effect of water adsorption on the dielectric properties of polymer nanocomposites," *2008 International Symposium on Electrical Insulating Materials,* pp. 510-13, 2008.
[95] I. L. Hosier, M. Praeger, A. S. Vaughan, and S. G. Swingler, "Electrical properties of polymer nano-composites based on oxide and nitride fillers," *IEEE 2015 Electrical Insulation Conference (EIC),* pp. 438-441, 2015.
[96] R. O. Ebewele, *Polymer Science and Technology*: CRC Press 2000.
[97] A. A. Askadskii, *Analysis of the Structure and Properties of High-Crosslinked Polymer Networks*: Harwood Academic Publisher GmbH, 1992.
[98] C. A. Daniels, *Polymers: Structure and Properties*, 1st ed.: CRC Press, 1989.
[99] A. R. Blythe and D. Bloor, *Electrical Properties of Polymers*, second ed.: Cambridge University Press, 2005.
[100] N. M. Alves, J. L. G. Ribelles, and J. F. Mano, "Enthalpy relaxation studies in polymethyl methacrylate networks with different crosslinking degrees," *Polymer,* vol. 46, pp. 491-504, Jan 2005.
[101] J. M. Morancho and J. M. Salla, "Relaxation in partially cured samples of an epoxy resin and of the same resin modified with a carboxyl-terminated rubber," *Polymer,* vol. 40, pp. 2821-2828, 1999.
[102] L. M. Zong, S. J. Zhou, N. Sgriccia, M. C. Hawley, R. S. Sun, and L. C. Kempel, "Dielectric properties of an epoxy-amine system at a high microwave frequency," *Polymer Engineering and Science,* vol. 45, pp. 1576-1580, Dec 2005.

[103] E. Kuffel, W. S. Zaengl, and J. Kuffel, *High Voltage Engineering Fundamentals*, 2 ed.: Newnes, 2000.
[104] L. Shengtao, Y. Guilai, G. Chen, L. Jianying, B. Suna, Z. Lisheng*, et al.*, "Short-term breakdown and long-term failure in nanodielectrics: a review," *IEEE Transactions on Dielectrics and Electrical Insulation,* vol. 17, pp. 1523-35, Oct. 2010.
[105] "ASTM D 149-97a, Standard Test Method for Dielectric Breakdown Voltage and Dielectric Strength of Solid Electrical Insulating Materials at Commercial Power Frequencies," *American Society for Testing and Materials, 100 Barr Harbor Drive, West Conshohocken, PA 19428, United States,* 2004.
[106] P. Preetha and M. J. Thomas, "AC Breakdown Characteristics of Epoxy Nanocomposites," *IEEE Transactions on Dielectrics and Electrical Insulation,* vol. 18, pp. 1526-1534, Oct 2011.
[107] M. Takala, H. Ranta, P. Nevalainen, P. Pakonen, J. Pelto, M. Karttunen*, et al.*, "Dielectric Properties and Partial Discharge Endurance of Polypropylene-Silica Nanocomposite," *IEEE Transactions on Dielectrics and Electrical Insulation,* vol. 17, pp. 1259-1267, Aug 2010.
[108] M. Reading, Z. Xu, A. S. Vaughan, and P. L. Lewin, "On sample preparation and dielectric breakdown in nanostructured epoxy resins," *Journal of Physics: Conference Series,* vol. 310, 2011.
[109] M. Reading, Z. Xu, A. Vaughan, and P. Lewin, "The effect of sample thickness on the relative breakdown strength of epoxy systems," *At Dielectrics 2011, The University of Kent, Canterbury, UK,* 13 - 15 Apr 2011.
[110] G. Chen, J. Zhao, S. Li, and L. Zhong, "Origin of thickness dependent dc electrical breakdown in dielectrics," *Applied Physics Letters,* vol. 100, May 28 2012.
[111] J. C. Fothergill, "Estimating the cumulative probability of failure data points to be plotted on Weibull and other probability paper," *IEEE Transactions on Electrical Insulation,* vol. 25, pp. 489-492, Jun 1990.
[112] J. Goldstein, D. E. Newbury, D. C. Joy, C. E. Lyman, P. Echlin, E. Lifshin*, et al.*, *Scanning Electron Microscopy and X-ray Microanalysis*, Third ed.: Springer US, 2003.
[113] Y. L. Tai, J. S. Qian, J. B. Miao, R. Xia, Y. C. Zhang, and Z. G. Yang, "Preparation and characterization of Si3N4/SBR nanocomposites with high performance," *Materials & Design,* vol. 34, pp. 522-527, Feb 2012.
[114] L. G. Wade, *Organic Chemistry*, 8 ed.: Pearson Education, 2013.
[115] X. J. Chen, J. G. Jiang, F. Yan, S. C. Tian, and K. M. Li, "A novel low temperature vapor phase hydrolysis method for the production of nano-structured silica materials using silicon tetrachloride," *RSC Advances,* vol. 4, pp. 8703-8710, 2014.
[116] A. M. Pourrahimi, L. K. H. Pallon, D. Liu, T. A. Hoang, S. Gubanski, M. S. Hedenqvist*, et al.*, "Polyethylene Nanocomposites for the Next Generation of Ultralow-Transmission-Loss HVDC Cables: Insulation Containing Moisture-Resistant MgO Nanoparticles," *ACS Applied Materials & Interfaces,* vol. 8, pp. 14824-14835, 2016.
[117] C. Yeung, "Spectroscopic Analysis of Nanodielectric Interfaces," PhD Thesis, University of Southampton, 2013.
[118] V. T. Nguyen, "Nanodielectrics for Machine Insulation," PhD thesis, University of Southampton, 2013.
[119] N. A. Stjohn and G. A. George, "Diglycidyl amine-epoxy resin networks: kinetics and mechanisms of cure," *Progress in Polymer Science,* vol. 19, pp. 755-795, 1994.
[120] R. J. Morgan, F.-M. Kong, and C. M. Walkup, "Structure-property relations of polyethertriamine-cured bisphenol-a-diglycidyl ether epoxies," *Polymer,* vol. 25, pp. 375-386, 1984.
[121] P. N. Patil, S. K. Rath, S. K. Sharma, K. Sudarshan, P. Maheshwari, M. Patri*, et al.*, "Free volumes and structural relaxations in diglycidyl ether of bisphenol-A based epoxy-polyether amine networks," *Soft Matter,* vol. 9, pp. 3589-3599, 2013.
[122] C. L. Soles, F. T. Chang, B. A. Bolan, H. A. Hristov, D. W. Gidley, and A. F. Yee, "Contributions of the nanovoid structure to the moisture absorption properties of epoxy resins," *Journal of Polymer Science Part B-Polymer Physics,* vol. 36, pp. 3035-3048, Dec 1998.

[123] G. Nikolic, S. Zlatkovic, M. Cakic, S. Cakic, C. Lacnjevac, and Z. Rajic, "Fast Fourier Transform IR Characterization of Epoxy GY Systems Crosslinked with Aliphatic and Cycloaliphatic EH Polyamine Adducts," *Sensors,* vol. 10, pp. 684-696, Jan 2010.
[124] D. L. Pavia, G. M. Lampman, G. S. Kriz, and J. R. Vyvyan, *Introduction to Spectroscopy*, 5 ed.: Cengage Learning, 2013.
[125] C. Sisbandini, D. Brandell, T. Gustafsson, and L. Nyholm, "The Mechanism of Capacity Enhancement in LiFePO4 Cathodes Through Polyetheramine Coating," *Journal of the Electrochemical Society,* vol. 156, pp. A720-A725, 2009.
[126] T. Y. Lo, Y. J. Wang, D. M. Liu, and W. T. Whang, "Surface characteristics and biofunctionality of a novel high-performance, hydrophilic Jeffamine-added fluoro-containing polyimide for biomedical applications," *Journal of Polymer Research,* vol. 22, 2015.
[127] J. P. Bell, "Structure of a typical amine-cured epoxy resin," *Journal of Polymer Science Part A-2-Polymer Physics,* vol. 8, pp. 417-436, 1970.
[128] F. Kolar and J. Svitilova, "Kinetics and mechanism of curing epoxy/anhydride systems," *Acta Geodynamica Et Geomaterialia,* vol. 4, pp. 85-92, 2007.
[129] S. Montserrat, P. Cortes, Y. Calventus, and J. M. Hutchinson, "Effect of crosslink length on the enthalpy relaxation of fully cured epoxy-diamine resins," *Journal of Polymer Science Part B-Polymer Physics,* vol. 38, pp. 456-468, 2000.
[130] Y. Calventus, S. Montserrat, and J. M. Hutchinson, "Enthalpy relaxation of non-stoichiometric epoxy-amine resins," *Polymer,* vol. 42, pp. 7081-7093, Jul 2001.
[131] A. P. Gupta, S. Ahmad, and A. Dev, "Development of Novel Bio-Based Soybean Oil Epoxy Resins as a Function of Hardener Stoichiometry," *Polymer-Plastics Technology and Engineering,* vol. 49, pp. 657-661, 2010.
[132] L. Heux, J. L. Halary, F. Laupretre, and L. Monnerie, "Dynamic mechanical and C-13 nmr investigations of molecular motions involved in the beta relaxation of epoxy networks based on DGEBA and aliphatic amines," *Polymer,* vol. 38, pp. 1767-1778, Apr 1997.
[133] C. L. Soles and A. F. Yee, "A discussion of the molecular mechanisms of moisture transport in epoxy resins," *Journal of Polymer Science Part B-Polymer Physics,* vol. 38, pp. 792-802, Mar 1 2000.
[134] C. Jordan, J. Galy, and J. P. Pascault, "Measurement of the extent of reaction of an epoxy-cycloaliphatic amine system and influence of the extent of reaction on its dynamic and static mechanical-properties," *Journal of Applied Polymer Science,* vol. 46, pp. 859-871, Oct 15 1992.
[135] T. V. Kosmidou, A. S. Vatalis, C. G. Delides, E. Logakis, P. Pissis, and G. C. Papanicolaou, "Structural, mechanical and electrical characterization of epoxy-amine/carbon black nanocomposites," *Express Polymer Letters,* vol. 2, pp. 364-372, May 2008.
[136] H. Kim and K. Char, "Dielectric changes during the curing of epoxy resin based on the diglycidyl ether of bisphenol A (DGEBA) with diamine," *Bulletin of the Korean Chemical Society,* vol. 20, pp. 1329-1334, Nov 1999.
[137] S. Siddabattuni, T. P. Schuman, and F. Dogan, "Dielectric Properties of Polymer–Particle Nanocomposites Influenced by Electronic Nature of Filler Surfaces," *ACS Applied Materials & Interfaces,* vol. 5, pp. 1917-1927, 2013.
[138] M. Meunier, N. Quirke, and A. Aslanides, "Molecular modeling of electron traps in polymer insulators: Chemical defects and impurities," *Journal of Chemical Physics,* vol. 115, pp. 2876-2881, 2001.
[139] S. Grzybowski, E. A. Feilat, P. Knight, and L. Doriott, "Breakdown voltage behavior of PET thermoplastics at DC and AC voltages," *IEEE Southeastcon '99, Proceedings,* pp. 284-287, 1999.
[140] B. K. Gupta, "Use of AC and DC hipot tests to assess condition of stator insulation," *Proceedings: Electrical Electronics Insulation Conference and Electrical Manufacturing & Coil Winding Conference, IEEE,* pp. 605-608, 1995.
[141] G. Iyer, R. S. Gorur, R. Richert, A. Krivda, and L. E. Schmidt, "Dielectric Properties of Epoxy based Nanocomposites for High Voltage Insulation," *IEEE Transactions on Dielectrics and Electrical Insulation,* vol. 18, pp. 659-666, 2011.

[142] C. Grave, I. McEwan, and R. A. Pethrick, "Influence of stoichiometric ratio on water absorption in epoxy resins," *Journal of Applied Polymer Science,* vol. 69, pp. 2369-2376, Sep 1998.
[143] J. Mijovic and H. Zhang, "Local dynamics and molecular origin of polymer network-water interactions as studied by broadband dielectric relaxation spectroscopy, FTIR, and molecular simulations," *Macromolecules,* vol. 36, pp. 1279-1288, Feb 2003.
[144] I. Merdas, F. Thominette, A. Tcharkhtchi, and J. Verdu, "Factors governing water absorption by composite matrices," *Composites Science and Technology,* vol. 62, pp. 487-492, 2002.
[145] F. X. Perrin, M. H. Nguyen, and J. L. Vernet, "Water transport in epoxy–aliphatic amine networks – Influence of curing cycles," *European Polymer Journal,* vol. 45, pp. 1524-1534, 2009.
[146] H. Yada, M. Nagai, and K. Tanaka, "The intermolecular stretching vibration mode in water isotopes investigated with broadband terahertz time-domain spectroscopy," *Chemical Physics Letters,* vol. 473, pp. 279-283, May 2009.
[147] P. D. Aldrich, S. K. Thurow, M. J. McKennon, and M. E. Lyssy, "Dielectric relaxation due to absorbed water in various thermosets," *Polymer,* vol. 28, pp. 2289-2296, Dec 1987.
[148] L. Garden and R. A. Pethrick, "A dielectric study of water uptake in epoxy resin systems," *Journal of Applied Polymer Science,* vol. 134, Apr 2017.
[149] J. D. Reid, W. H. Lawrence, and R. P. Buck, "Dielectric properties of an epoxy resin and its composite I. Moisture effects on dipole relaxation," *Journal of Applied Polymer Science,* vol. 31, pp. 1771-1784, May 1986.
[150] D. Hayward, E. Hollins, P. Johncock, I. McEwan, R. A. Pethrick, and E. A. Pollock, "The cure and diffusion of water in halogen containing epoxy/amine thermosets," *Polymer,* vol. 38, pp. 1151-1168, Mar 1997.
[151] I. D. Maxwell and R. A. Pethrick, "Dielectric Studies of Water in Epoxy Resins," *Journal of Applied Polymer Science,* vol. 28, pp. 2363-2379, 1983.
[152] B. Lutz and J. Kindersberger, "Influence of Absorbed Water on Volume Resistivity of Epoxy Resin Insulators," presented at the Proceedings of the 2010 IEEE International Conference on Solid Dielectrics, 2010.
[153] S. Fujita, Y. Kamei, and K. Tanaka, "Effect of water absorption in polimide on electrical properties," *Proceedings of the 2001 IEEE 7th International Conference on Solid Dielectrics,* pp. 183-186, 2001.
[154] B. X. Du, Z. Y. He, Q. Du, and Y. G. Guo, "Effects of Water Absorption on Surface Charge and Dielectric Breakdown of Polyimide/Al2O3 Nanocomposite Films," *IEEE Transactions on Dielectrics and Electrical Insulation,* vol. 23, pp. 134-141, 2016.
[155] S. Cukierman, "Et tu, Grotthuss! and other unfinished stories," *Biochimica Et Biophysica Acta-Bioenergetics,* vol. 1757, pp. 876-885, Aug 2006.
[156] D. Marx, "Proton transfer 200 years after von Grotthuss: Insights from ab initio simulations," *Chemphyschem,* vol. 7, pp. 1848-1870, 2006.
[157] P. Rittigstein and J. M. Torkelson, "Polymer-nanoparticle interfacial interactions in polymer nanocomposites: Confinement effects on glass transition temperature and suppression of physical aging," *Journal of Polymer Science Part B-Polymer Physics,* vol. 44, pp. 2935-2943, 2006.
[158] N. Simone, G. Emmanouil, and B. T. Nicholas, "Glass transition of polymers in bulk, confined geometries, and near interfaces," *Reports on Progress in Physics,* vol. 80, p. 036602, 2017.
[159] A. Bansal, H. C. Yang, C. Z. Li, K. W. Cho, B. C. Benicewicz, S. K. Kumar*, et al.*, "Quantitative equivalence between polymer nanocomposites and thin polymer films," *Nature Materials,* vol. 4, pp. 693-698, 2005.
[160] F. Bignotti, S. Pandini, F. Baldi, and R. De Santis, "Effect of the Resin/Hardener Ratio on Curing, Structure and Glass Transition Temperature of Nanofilled Epoxies," *Polymer Composites,* vol. 32, pp. 1034-1048, Jul 2011.
[161] J. Moll and S. K. Kumar, "Glass Transitions in Highly Attractive Highly Filled Polymer Nanocomposites," *Macromolecules,* vol. 45, pp. 1131-1135, 2012.
[162] M. Preghenella, A. Pegoretti, and C. Migliaresi, "Thermo-mechanical characterization of fumed silica-epoxy nanocomposites," *Polymer,* vol. 46, pp. 12065-12072, Dec 2005.

[163] M. K. Umboh, T. Adachi, K. Oishi, M. Higuchi, and Z. Major, "Mechanical properties of nano-silica particulate-reinforced epoxy composites considered in terms of crosslinking effect in matrix resins," *Journal of Materials Science,* vol. 48, pp. 5148-5156, Aug 2013.

[164] F. D. Blum, W.-Y. Lin, and C. E. Porter, "Dynamics of adsorbed poly(methyl acrylate) and poly(methyl methacrylate) on silica," *Colloid and Polymer Science,* vol. 281, pp. 197-202, 2003.

[165] F. W. Starr, T. B. Schrøder, and S. C. Glotzer, "Molecular Dynamics Simulation of a Polymer Melt with a Nanoscopic Particle," *Macromolecules,* vol. 35, pp. 4481-4492, 2002.

[166] A. Prasad, T. Grover, and S. Basu, "Coarse–grained molecular dynamics simulation of cross–linking of DGEBA epoxy resin and estimation of the adhesive strength," *International Journal of Engineering, Science and Technology,* vol. 2, pp. 17-30, 2010.

[167] L. Chen, K. Zheng, X. Y. Tian, K. Hu, R. X. Wang, C. Liu*, et al.*, "Double Glass Transitions and Interfacial Immobilized Layer in in-Situ-Synthesized Poly(vinyl alcohol)/Silica Nanocomposites," *Macromolecules,* vol. 43, pp. 1076-1082, Jan 2010.

[168] D. K. Chouhan, S. K. Rath, A. Kumar, P. S. Alegaonkar, S. Kumar, G. Harikrishnan*, et al.*, "Structure-reinforcement correlation and chain dynamics in graphene oxide and Laponite-filled epoxy nanocomposites," *Journal of Materials Science,* vol. 50, pp. 7458-7472, 2015.

[169] D. M. Panaitescu, Z. Vuluga, P. V. Notingher, and C. Nicolae, "The Effect of Poly styrene-b-(ethylene-co-butylene)-b-styrene on Dielectric, Thermal, and Morphological Characteristics of Polypropylene/Silica Nanocomposites," *Polymer Engineering and Science,* vol. 53, pp. 2081-2092, Oct 2013.

[170] P. Marx, A. Wanner, Z. Zhang, H. Jin, I.-A. Tsekmes, J. Smit*, et al.*, "Effect of Interfacial Polarization and Water Absorption on the Dielectric Properties of Epoxy-Nanocomposites," *Polymers,* vol. 9, p. 195, 2017.

[171] F. N. Alhabill, R. Ayoob, T. Andritsch, and A. S. Vaughan, "Effect of resin/hardener stoichiometry on electrical behavior of epoxy networks," *IEEE Transactions on Dielectrics and Electrical Insulation,* submitted 2017.

[172] F. N. Alhabill, T. Andritsch, and A. S. Vaughan, "Moisture Absorption Behavior in Silicon Nitride Epoxy Nanocomposites," *IEEE Electrical Insulation Conference (EIC),* 2017.

[173] I. A. Tsekmes, R. Kochetov, P. H. F. Morshuis, and J. J. Smit, "A unified model for the permittivity and thermal conductivity of epoxy based composites," *Journal of Physics D-Applied Physics,* vol. 47, Oct 2014.

[174] D. K. Shukla and V. Parameswaran, "Epoxy composites with 200 nm thick alumina platelets as reinforcements," *Journal of Materials Science,* vol. 42, pp. 5964-5972, 2007.

[175] D. Qiang, M. He, G. Chen, and T. Andritsch, "Influence of nano-SiO2 and BN on space charge and AC/DC performance of epoxy nanocomposites," *IEEE Electrical Insulation Conference (EIC),* pp. 492-495, 2015.

[176] G. C. Xu, J. Wang, X. L. Ji, J. Y. Xiong, and F. Li, "Effect of Nano-silicon Nitride on the Mechanical and Electric Properties of Polypropylene Nanocomposite," *Journal of Composite Materials,* vol. 41, pp. 2213-2223, 2007.

[177] Q. Wang and G. Chen, "Effect of pre-treatment of nanofillers on the dielectric properties of epoxy nanocomposites," *IEEE Transactions on Dielectrics and Electrical Insulation,* vol. 21, pp. 1809-1816, 2014.

[178] S. Siddabattuni, T. P. Schuman, and F. Dogan, "Improved polymer nanocomposite dielectric breakdown performance through barium titanate to epoxy interface control," *Materials Science and Engineering B-Advanced Functional Solid-State Materials,* vol. 176, pp. 1422-1429, Nov 2011.

[179] T. Andritsch, R. Kochetov, Y. T. Gebrekiros, P. H. F. Morshuis, and J. J. Smit, "Short term DC breakdown strength in epoxy based BN nano- and microcomposites," *10th IEEE International Conference on Solid Dielectrics,* pp. 1-4, 2010.

[180] T. Andritsch, R. Kochetov, P. H. F. Morshuis, and J. J. Smit, "Proposal of the polymer chain alignment model," in *2011 Annual Report Conference on Electrical Insulation and Dielectric Phenomena*, 2011, pp. 624-627.

[181] T. Andritsch, R. Kochetov, Y. T. Gebrekiros, U. Lafont, P. H. F. Morshuis, and J. J. Smit, "Synthesis and dielectric properties of epoxy based nanocomposites," *IEEE Conference on Electrical Insulation and Dielectric Phenomena,* pp. 523-526, 2009.

[182] S. Singha and M. J. Thomas, "Dielectric properties of epoxy nanocomposites," *IEEE Transactions on Dielectrics and Electrical Insulation,* vol. 15, pp. 12-23, 2008.
[183] T. P. Schuman, S. Siddabattuni, O. Cox, and F. Dogan, "Improved Dielectric Breakdown Strength of Covalently-Bonded Interface Polymer-Particle Nanocomposites," *Composite Interfaces,* vol. 17, pp. 719-731, 2010.
[184] T. Tanaka, "Interpretation of several key phenomena peculiar to nano dielectrics in terms of a multi-core model," *IEEE Conference on Electrical Insulation and Dielectric Phenomena,* pp. 298-301, 2006.
[185] J. Artbauer, "Electric strength of polymers," *Journal of Physics D-Applied Physics,* vol. 29, pp. 446-456, 1996.
[186] E. do Nascimento, A. Ramos, D. Windmoller, P. R. Rodrigo, R. T. Juanes, A. R. Greus*, et al.*, "Breakdown, free-volume and dielectric behavior of the nanodielectric coatings based on epoxy/metal oxides," *Journal of Materials Science-Materials in Electronics,* vol. 27, pp. 9240-9254, Sep 2016.
[187] W. Li, H. Hillborg, and U. W. Gedde, "Influence of Process Conditions and Particle Dispersion on the AC Breakdown Strength of Polyethylene-aluminium Oxide Nanocomposites," *IEEE Transactions on Dielectrics and Electrical Insulation,* vol. 22, pp. 3536-3542, Dec 2015.
[188] C. Calebrese, L. Hui, L. S. Schadler, and J. K. Nelson, "A Review on the Importance of Nanocomposite Processing to Enhance Electrical Insulation," *IEEE Transactions on Dielectrics and Electrical Insulation,* vol. 18, pp. 938-945, Aug 2011.
[189] D. Qiang, G. Chen, and T. Andritsch, "Influence of Water Absorption on Dielectric Properties of Epoxy SiO2 and BN Nanocomposites," presented at the 2015 IEEE Conference on Electrical Insulation and Dielectric Phenomena, 2015.
[190] M. Praeger, I. L. Hosier, A. S. Vaughan, and S. G. Swingler, "Calcined silica for enhanced polyethylene nano composites," *Applied Physics Letters,* pp. pp. 1-4, 2016 (submitted).
[191] T. Sameshima, K. Sakamoto, Y. Tsunoda, and T. Saitoh, "Improvement of SiO2 properties and silicon surface passivation by heat treatment with high-pressure H2O vapor," *Japanese Journal of Applied Physics Part 2-Letters,* vol. 37, pp. L1452-L1454, 1998.
[192] H. R. Philipp, "Optical properties of silicon nitride," *Journal of the Electrochemical Society,* vol. 120, pp. 295-300, 1973.
[193] P. J. O'Brien, S. Shenogin, J. Liu, P. K. Chow, D. Laurencin, P. H. Mutin*, et al.*, "Bonding-induced thermal conductance enhancement at inorganic heterointerfaces using nanomolecular monolayers," *Nature Materials,* vol. 12, pp. 118-122, 2013.
[194] U. W. Gedde, *Polymer physics*: Champman & Hall, 1995.